DYNAMICS OF THE ANTARCTIC MESOSPHERE

by

R.I.MacLeod.   B.App.Sc., B.Sc(Hons).

A thesis presented

for the degree of

DOCTOR OF PHILOSOPHY

in the

UNIVERSITY OF ADELAIDE

(Mawson Institute for Antarctic Research)

December 1986

And I tell you, if you have the desire for knowledge

and the power to give it physical expression, go out and explore.

If you are a brave man you will do nothing: if you are fearful

you may do much, for none but cowards have need to prove their

bravery. Some will tell you that you are mad, and nearly all

will say, "What is the use?" For we are a nation of shopkeepers,

and no shopkeeper will look at research which does not promise

him a financial return within a year. And so you will sledge

nearly alone, but those with whom you sledge will not be

shopkeepers: that is worth a good deal. If you march your

Winter Journeys you will have your reward, so long as all you

want is a penguin's egg.

(From "The Worst Journey in the World" by Apsley Cherry-Garrard)

CONTENTS

SUMMARY

The main topic discussed in this thesis is the dynamical behaviour of the Antarctic summer Mesosphere, with emphasis on the prevailing winds and diurnal and semidiurnal tidal oscillations. The results were taken at Mawson (68°S) during the 1981/1982 summer using the spaced antenna method and recording partial radio reflections. The installation of the system was undertaken by the author.

The experimental equipment was taken to Antarctica from Townsville, a low latitude (19°S) site. Because of the nature of the site, some difficulties were experienced in establishing the system at Mawson and the resulting data were of a somewhat poorer quality than those obtained at Townsville. This difficulty was partially overcome by the application of data analysis techniques described in the thesis.

The most significant results were obtained in the 80 to 100 km range, where the data were continuous for seven weeks. Observations from lower heights, and some effects of increased geomagnetic activity are noted and discussed. Prevailing winds and tidal oscillations are compared with the relatively few recent results from similar latitudes and from models.

In addition to the Antarctic results, the results obtained by the author in Townsville and those obtained concurrently at Adelaide during 1980 are compared and contrasted.

PREFACE

To the best of the author's knowledge, this thesis contains
no material previously published or written by another
person, except where due reference is made in the text. It
contains no material which has been submitted or accepted
for the award of any other degree or diploma in any
University.

(R.I. MacLeod)

ACKNOWLEDGEMENTS

Finally, thanks must go to the author's wife Linda, who managed to keep her sense of humour through it all.

1 INTRODUCTION.

Wind measurements in the mesosphere and lower thermosphere have been made at a number of sites for many years now, but there are severe shortcomings in the spatial distribution of these results, as most observations are confined to mid-latitudes. In particular, although some attempts have been made, no definitive studies of the large-scale dynamics of these regions in the Antarctic have ever been made. The purpose of this thesis is to help rectify that deficiency.

For the purposes of global modelling, measurements well-placed in time and space are important. For the prevailing circulation, global coverage is necessary to investigate latitudinal and longitudinal changes and possible hemispheric differences in order to produce a consistent model for the whole atmosphere.

As tides in the mesosphere and lower thermosphere have amplitudes comparable to those of the prevailing circulation, their contribution to the dynamic wind fields are at least as important as that from the prevailing wind system. Moreover, tidal theory predicts that the modal composition of atmospheric tides will change with latitude. In the case of the propagating diurnal tide, it is predicted to be dominant near the equator and much weaker at higher latitudes, where evanescent diurnal modes are expected to prevail. The identification of which tidal modes are acting locally, can only be accomplished at present by observing the concurrent tidal structure at an alternate site, ideally, in the same hemisphere, at the same longitude, and sufficiently well-spaced latitudinally to allow identification of the individual modes.

Observations at high latitudes are necessary to determine, for example, the modal composition at mid-latitudes, where, for the diurnal tide, there is a mixture of evanescent and propagating modes.

Regular wind measurements have been carried out for many years at Molodezhnaya (68°S, 45°E) (Lysenko et al., 1979), but these have been made using the meteor technique with no height finding equipment and the results are referred to a mean height of 94 km. Elford and Murray (1960) carried out meteor wind measurements during 1957-1959, but their results were restricted by low data rates. More recently, Fraser (1984a) presented the first wind observations made with a spaced antenna system at Scott Base (78°S, 168°E), showing the prevailing zonal and meridional winds in the 70 to 100 km height range during December 1982. MacLeod and Vincent (1985) have presented zonal and meridional wind profiles from 60 to 100 km and average diurnal and semidiurnal tidal structure from 70 to 100 km, for the December 1981 - January 1982 period at Mawson.

Free electrons, in sufficient concentrations to affect the passage of radio waves, are present in the atmosphere above about 60 km. Irregularities in refractive index occur throughout the atmosphere due to fluctuations in neutral air density, but in the mesosphere and lower thermosphere, changes in refractive index are accentuated by the presence of free electrons. The observation of partial reflections from naturally occurring irregularities in the presence of ionization forms the basis of the spaced antenna method. For consistency, and in order to avoid any ambiguity, the equipment used in this thesis will be referred to as a Partial Reflection Winds (PRW) system.

The PRW system used in this work was previously installed at Townsville (19°40'S, 146°,54'E). As the author was to install, operate and maintain this equipment at Mawson (67°37'S 62°52'E) in the Antarctic, its operation in Townsville yielded not only valuable low latitude results, but also necessary experience. These results from Townsville are particularly useful, because concurrent results from Adelaide (34°38'S, 138°37'E) were obtained also. The prevailing circulation and tidal structure observed at these low, mid- and high latitude sites is discussed in detail in chapter 4 of this thesis.

1.1 The Mesosphere and Lower Thermosphere.

Figure 1.1 shows the typical variation of atmospheric temperature with altitude below 200 km at mid-latitudes. The approximate boundaries of atmospheric subregions which will be referred to in the text are indicated.

If the temperature of the atmosphere decreases with increasing altitude at a rate less than the adiabatic lapse rate ($\sim 10°K$ km^{-1}), a rising parcel of air will encounter a region warmer than itself and fall. Such opposition to vertical motion will reinforce the stable stratification of the atmosphere. For an atmospheric region whose temperature decreases at a rate greater than the adiabatic lapse rate, vertical motion will be supported and the region will tend to be unstable. Examination of figure 1.1 shows that the mesosphere has a negative vertical temperature gradient and is therefore an intrinsically less stable region than the lower thermosphere which has a positive vertical temperature gradient.

The interaction of atmospheric tidal oscillations with the earth's magnetic field and charged particles in the upper atmosphere causes
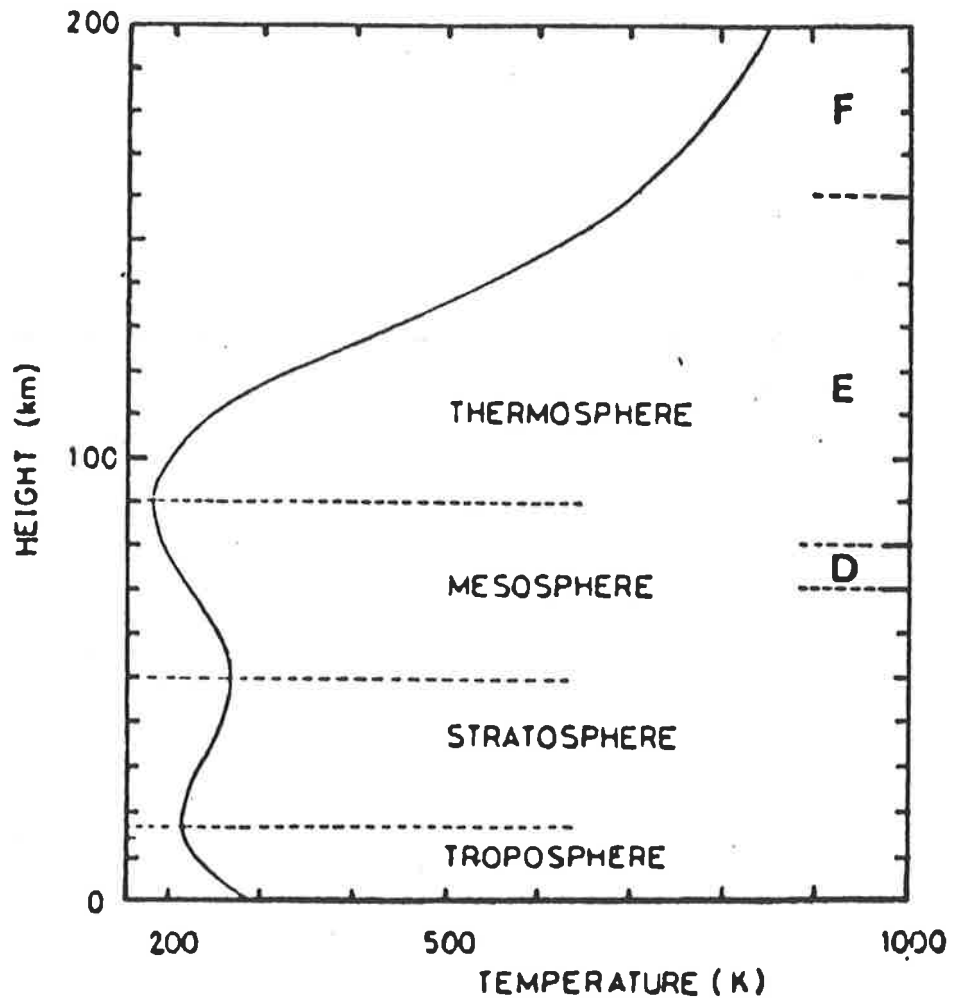
Figure 1.1   Vertical temperature distribution and approximate
position of atmospheric and ionospheric subregions.

electric currents to flow. This is the atmospheric dynamo and its effects maximize near 110 km. At non-polar latitudes, geomagnetic variations due to this current system, observed on the ground, are reasonably represented by a thermally induced component and a weaker gravitationally induced component. Near the geomagnetic equator, the current flow is larger than that observed at mid latitudes because the effective conductivity is enhanced due to the horizontal geomagnetic field. This current flow is the equatorial electrojet.

In polar regions, there is an additional solar variation, which is driven by processes arising in the magnetosphere. During disturbed geomagnetic conditions, the increased conductivity due to particle precipitation, in conjunction with increased magnetospheric electric fields, gives rise to the auroral electrojet. In a recent study of the relative importance of Joule heating and particle precipitation, Brekke (1983) concluded that Joule heating appeared to be the more important heat source at high latitudes, because it is a more permanent feature and is distributed over a much larger area.

Apart from the relatively small contribution to the energy budget from particle precipitation and Joule heating at high latitudes, differential solar heating of the atmosphere provides the overall drive for the prevailing circulation.

A good approximation to the observed prevailing zonal flow is obtained if the motion is assumed to result from the balance between the latitudinal pressure gradient and the Coriolis force. This is the geostrophic approximation and is valid at non-equatorial latitudes.

In addition to prevailing winds, the most important forms of motion which contribute to the total dynamic field of the atmosphere in and below the mesosphere and lower thermosphere are: planetary waves, tides and gravity waves, and turbulence.

Planetary waves result from the variation of the Coriolis force with latitude; they are global in extent, and have periods greater than one day. Quasi-stationary planetary waves are strongly excited in the troposphere. During winter, the vertical propagation of these waves gives rise to the sudden stratospheric warmings observed in the northern hemisphere, and to significant variability of zonal winds in the mesosphere. In summer, the vertical propagation of these waves is severely attenuated by the westward flow which prevails in the stratosphere during that season.

Nevertheless, planetary wave activity in the mesosphere and lower thermosphere has been found to maximize in summer (Craig and Elford, 1981; Manson et al., 1982; Vincent, 1984b). It is generally assumed that these oscillations are caused by Rossby gravity normal modes forced in the lower atmosphere. At higher levels, these modes are evanescent except in certain regions where the prevailing winds and meridional temperature gradients may cause them to be locally propagating (Vincent, 1985). The background wind and temperature structures of the stratosphere and mesosphere during solstice conditions are such that there is a magnified vertical growth in the amplitudes of these modes in the summer hemisphere (Salby, 1981, 1984). Hemispheric differences have been noted for the quasi 2-day wave (Rodgers and Prata, 1981), with results from the southern

hemisphere (Craig et al., 1980) indicating that the amplitude of the meridional component is approximately twice as large as that observed in the northern hemisphere.

In a stably stratified isothermal atmosphere, displacement of a parcel of air in the vertical direction is accompanied by an oppositely directed buoyancy force. The subsequent oscillation of the air parcel around its mean position gives rise to internal gravity waves. The generation of tides will be discussed shortly, but they are essentially forced large-scale gravity waves, which are influenced by the Coriolis force, and whose periods are submultiples of the solar or lunar day. After generation, in the absence of dissipation, gravity wave and tidal oscillations grow exponentially as they propagate vertically upwards in order to maintain a constant energy flux density.

In the context of this work, the most important property of gravity waves is their ability to transport horizontal momentum vertically from their source (normally the troposphere) to the mesosphere and lower thermosphere. This has profound effects on the prevailing circulation and will be discussed in the next section.

The characteristics and behaviour of atmospheric tides are major themes of this thesis and therefore warrant a more than cursory discussion. This will be undertaken presently, after the prevailing circulation has been discussed.

Turbulence is too random to be treated as an ordered phenomenon. Below the turbopause, which occurs at altitudes near 100 km, the atmosphere

is always potentially turbulent, as wind shears or unstable temperature profiles can often generate turbulence. Important processes which occur in the lower atmosphere as a result of turbulence are: the mixing of atmospheric constituents (this is largely responsible for the homogeneous composition of the atmosphere below the turbopause), the deposition of mechanical energy into the atmosphere as heat, and increased rates of diffusion. Above the turbopause, momentum, constituent, and heat transport take place by molecular rather than turbulent processes. Turbulence probably plays an important role in the production of the partially reflecting irregularities observed in this experiment, and in that context it will be discussed in chapter 3.

1.2 The Prevailing Circulation.

The way in which the important elements of the prevailing circulation knit together can be effectively illustrated by examining the features of simple model results and comparing them to the observed structure. Figure 1.2 (Geller, 1983) shows the latitudinal temperature structure up to 90 km during solstice conditions which results if it is assumed that local solar heating is exactly balanced by local infrared cooling, and the mean zonal geostrophic winds which would result. Due to the inappropriate nature of the geostrophic approximation at equatorial latitudes, wind values are not given within ±20° of the equator.

Positive zonal winds are westerly, that is from the west to the east, and negative zonal winds are easterly, or, from the east to the west. Positive meridional winds (southerlies) blow toward the north, while negative meridional winds (northerlies) blow toward the south. As the

RADIATIVE EQUILIBRIUM TEMPERATURE (°K)

SUMMER   WINTER

° LATITUDE
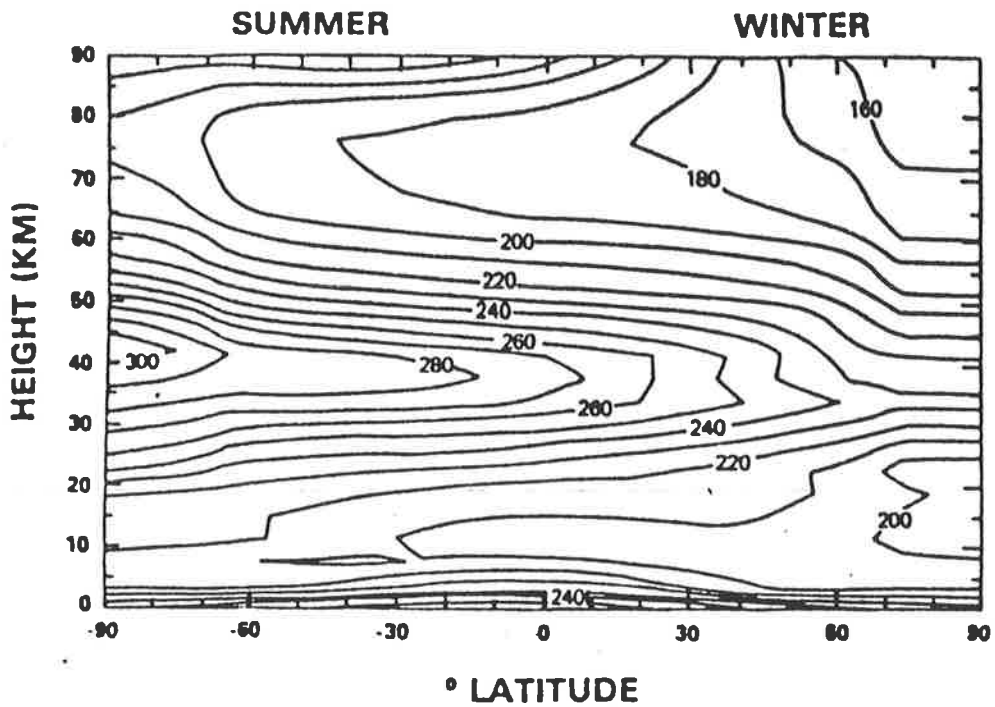
RADIATIVE EQUILIBRIUM ZONAL WIND (M/SEC)

SUMMER   WINTER

° LATITUDE
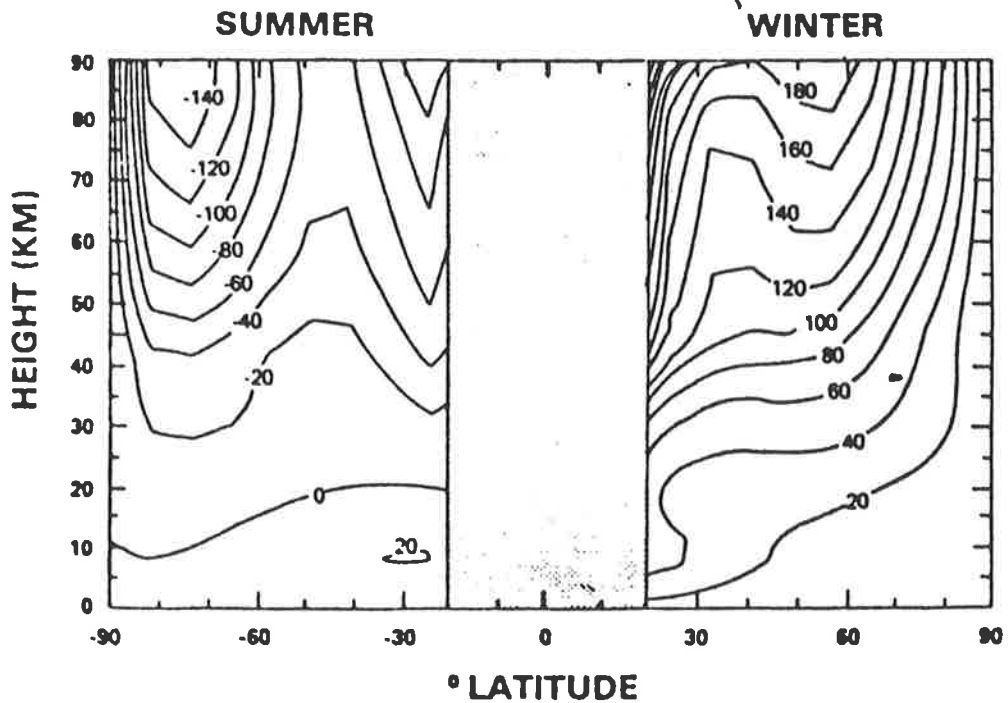
Figure 1.2.   Radiative Equilibrium Temperature and Radiative
Equilibrium Zonal Wind. (Geller, 1983).

thermal structure shown in figure 1.2 represents a state of radiative equilibrium, the resulting zonal flow is perfectly balanced, and there is no meridional or vertical motion.

Figure 1.3 (Barnett and Corney, 1985) shows the observed latitudinal temperature profile and the resulting mean zonal geostrophic winds (again, an inappropriate approximation at equatorial latitudes) for January, from ground level up to about 80 km. Above the 30 mb level, the temperature values were obtained from satellite data. The vertical coordinates of figure 1.3 are in log pressure units, but the bracketed quantities shown accompanying some of the pressure levels are values of geometric height obtained from a table of mean heights of constant pressure levels in the southern hemisphere - Koshelkov (1985).

Comparison of the temperature distributions shown in figures 1.2 and 1.3 shows that purely radiative considerations do not accurately model the observed temperature structure. Near 80 km for example, the winter mesosphere is observed to be warmer than the summer mesosphere. Comparison of the zonal mean geostrophic winds shows that the radiative model of figure 1.2 produces mesospheric winds which are too strong, and whose jets do not close as observed.

During solstice conditions, heating and cooling effects maximize near the stratopause, with net heating near the summer pole and net cooling near the winter pole. Above, a single thermally direct cell results, with rising motion in the summer hemisphere and sinking motion in the winter hemisphere. These vertical motions cause adiabatic cooling and heating in the summer and winter mesosphere respectively and are primarily responsible

MEAN ZONAL GEOSTROPHIC WIND (ms⁻¹)

OBSERVED LATITUDINAL TEMPERATURE PROFILE (°K)

Zonal mean temperature (K)   January
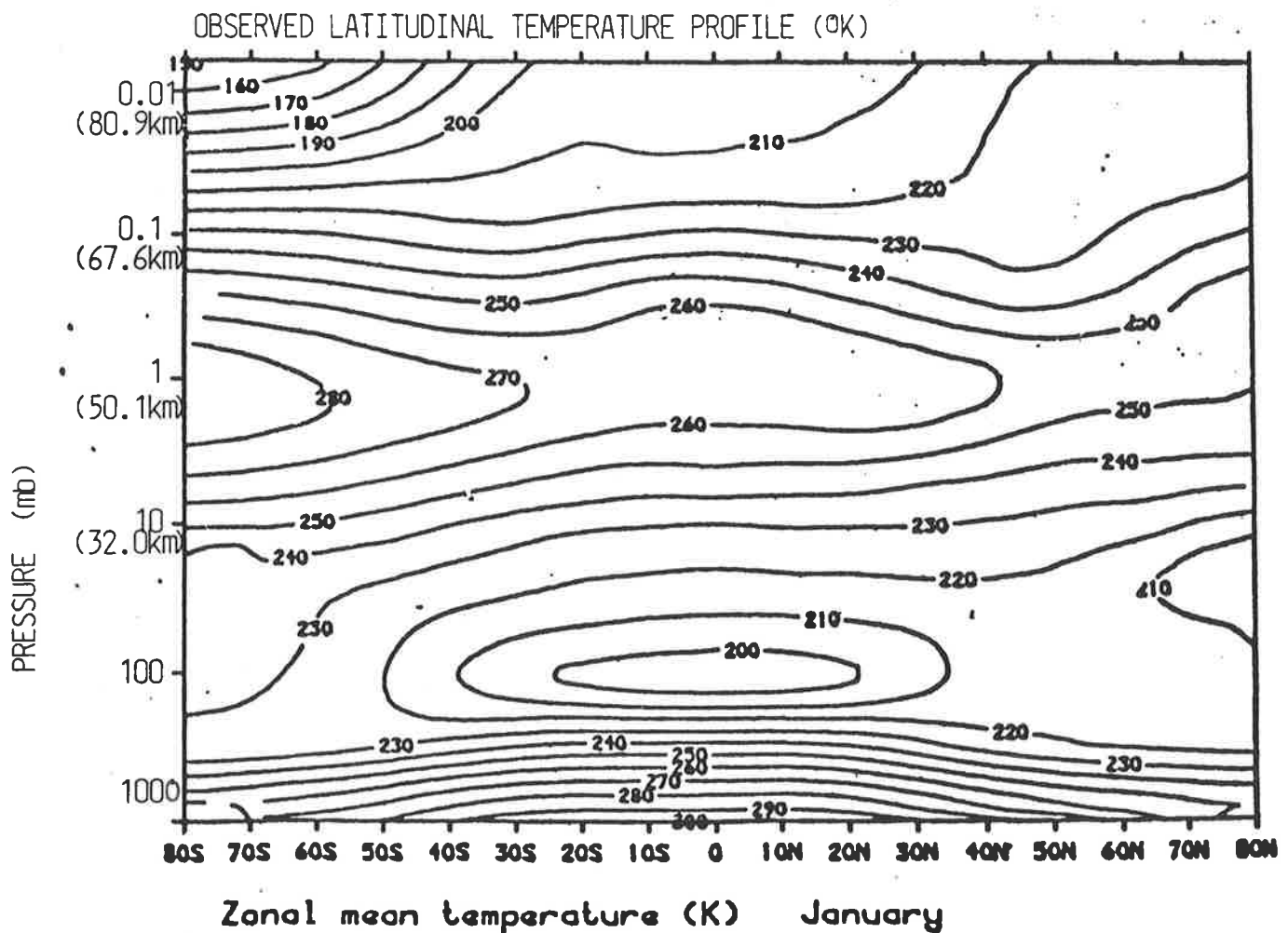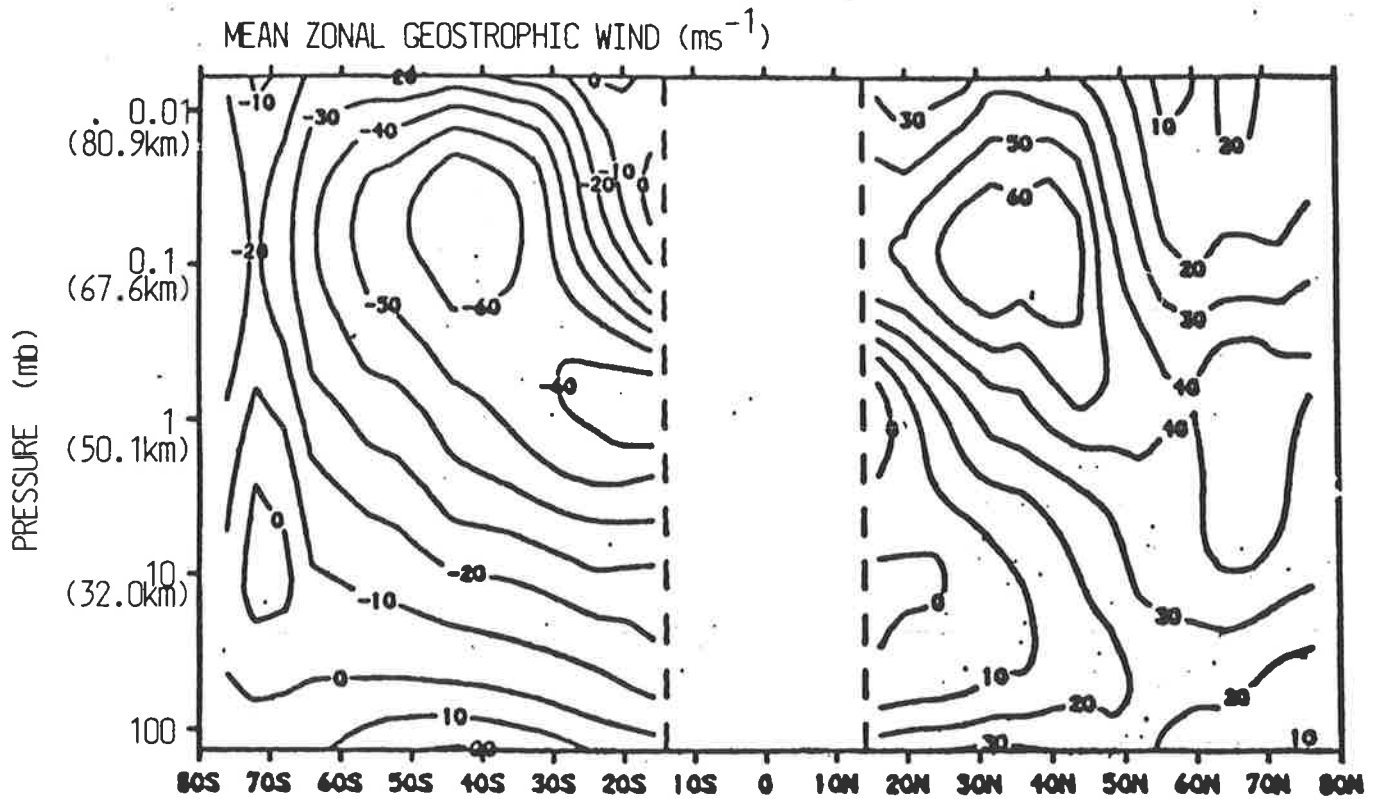
Figure 1.3   The Mean Zonal Geostrophic Wind and the Accompanying
              Observed Latitudinal Temperature Profile

(Barnett and Corney, 1985)

for the observed temperature structure. A compensating meridional flow is directed from the summer pole to the winter pole. The Coriolis force interacts with this meridional flow to produce an eastward acceleration in the winter hemisphere and a westward acceleration in the summer hemisphere. At the equinoxes, there is rising motion at the equator, poleward flow in both hemispheres, and subsidence near both poles.

Some of these features were successfully modelled by Murgatroyd and Singleton (1961), who calculated the meridional circulation required to transport heat between the radiative sinks and sources in the stratosphere and mesosphere. This model had no provision for the balance of angular momentum, and the zonal components induced from the interaction between the calculated meridional flow and Coriolis effects were in the wrong sense when compared to the observed behaviour.

Leovy (1964) studied the momentum budget of the mesosphere theoretically, and found that substantial mechanical dissipation was required to prevent the Coriolis force of the radiatively driven mean meridional circulation from generating excessively strong zonal flows. Leovy produced a model in which eddy momentum fluxes and the heat derived from them were represented by constant Rayleigh friction and Newtonian cooling coefficients. His results showed qualitative agreement with observed solstice conditions. Improvements to the radiative heating formulation and the use of height dependent Rayleigh friction terms lead to models which produce more realistic wind fields (Schoeberl and Strobel, 1978; Holton and Wehrbein, 1980), but the use of such coefficients can only reduce the mean wind to zero and are unable to simulate the observed mean zonal wind reversals in the lower thermosphere.

The height dependent Rayleigh friction coefficient was used by Holton and Wehrbein in order to simulate the strong mechanical dissipation thought to exist near the mesopause due to breaking tides (Lindzen, 1967) and gravity waves (Hodges, 1969). In a study of the role of wavebreaking in the mesosphere, Lindzen (1981) found that Rayleigh friction was not a suitable parameterization for the effects of wave breaking on the mean flow.

Lindzen (1981) examined the results of rocket observations, which suggested that gravity waves with vertical wavelengths of less than about 15 km might attain sufficient amplitudes in the mesosphere to produce layers with superadiabatic lapse rates. Convective overturning of these layers would generate turbulence, and by limiting the growth of wave amplitude (often called saturation), would also cause a divergence of the vertical momentum flux, leading to a net zonal drag force. The suggestions for parameterization of zonal drag and eddy diffusion effects proposed by Lindzen (1981) were tested in model calculations by Holton (1982), and produced realistic mean zonal winds in the mesosphere and zonal wind reversals above the mesopause.

Since the work of Lindzen (1981), a number of studies (Holton (1982), Matsuno (1982), Weinstock (1982 a,b), Fritts (1984)) have addressed the problem of gravity wave saturation and its effect on the mean momentum budget, but the theoretical predictions are difficult to quantify, as observational studies of the spectral distribution of gravity waves are scarce.

- 11 -

A spectrum of gravity waves propagating vertically upwards will have some of its members removed by critical level interactions, when their phase speeds are equal to the background flow speed. It can be expected that the phase speeds of most gravity waves will be very small in the region of generation, and as most gravity wave activity originates in the troposphere, the range of phase speeds will be roughly confined to the range of tropospheric wind speeds.

The seasonal variation of wind structure observed in the atmosphere is such that at mid-latitudes during winter, only those gravity waves with zonal phase speeds less than about 10 ms^{-1} can be allowed into the mesosphere, while in summer the zonal phase speed of a gravity wave must exceed about 20 ms^{-1} or more before it can propagate into the mesosphere. Gravity wave activity in the mesosphere is therefore expected to maximize in winter, and has been observed to do so (Lindzen, 1981; Balsley et al., 1983). In addition, due to the lower phase speeds associated with gravity waves propagating into the mesosphere during winter, it can be expected that wavebreaking effects should be evident at lower heights than they would be in summer. The seasonal variation in the minimum height of radio reflections observed by Balsley et al. (1980), from 50 km in winter to 70 km in summer, provides indirect evidence that such processes are in operation.

1.2.1 The Southern Hemisphere.

In a recent work, Manson et al. (1985) have discussed the prevailing circulation of the mesosphere and lower thermosphere from observations made with various radar systems during the last decade.

Although the distribution of these radars is not global, the results have demonstrated that there are seasonal, latitudinal, longitudinal and hemispheric differences. In addition, significant variation between these results and the widely-used models CIRA 72 and Groves (1969) have been noted. For the purposes of this thesis, the most pertinent examples of the prevailing circulation are those from Manson et al. (1985) for Townsville and Adelaide, and are shown in figure 1.4.

The main features of the zonal profiles are the strong eastward flow at most altitudes during winter months, and the descent of a westward flowing regime, beginning in winter near 100 km, dominating the summer wind field below about 85 km, and peaking in mid-summer near 70 km.

Zonal winds observed at Adelaide tend to be larger overall, and in winter, more variable than those at Townsville. Latitudinal differences are seen in the strength and position of the eastward winter jet, which for Adelaide, is stronger and lower than that at Townsville. Also the timing of the descent of the westward belt varies at each location. This can be seen by the observation of the zero value contour line on the zonal plots of figure 1.4. At Townsville, this contour line is close to 95 km at the beginning of August and near 75 km at the end of that month. At Adelaide, the same range is covered by the zero contour line from the beginning of September to the end of October. A similar effect can be seen at 80 km and below for the summer/autumn transition. Although the spring transition occurs later at Adelaide, the return to eastward flow above 84 km in spring/summer occurs very close to the same period at Townsville. At Townsville, westward winds are observed between 76 and 94 km during March.
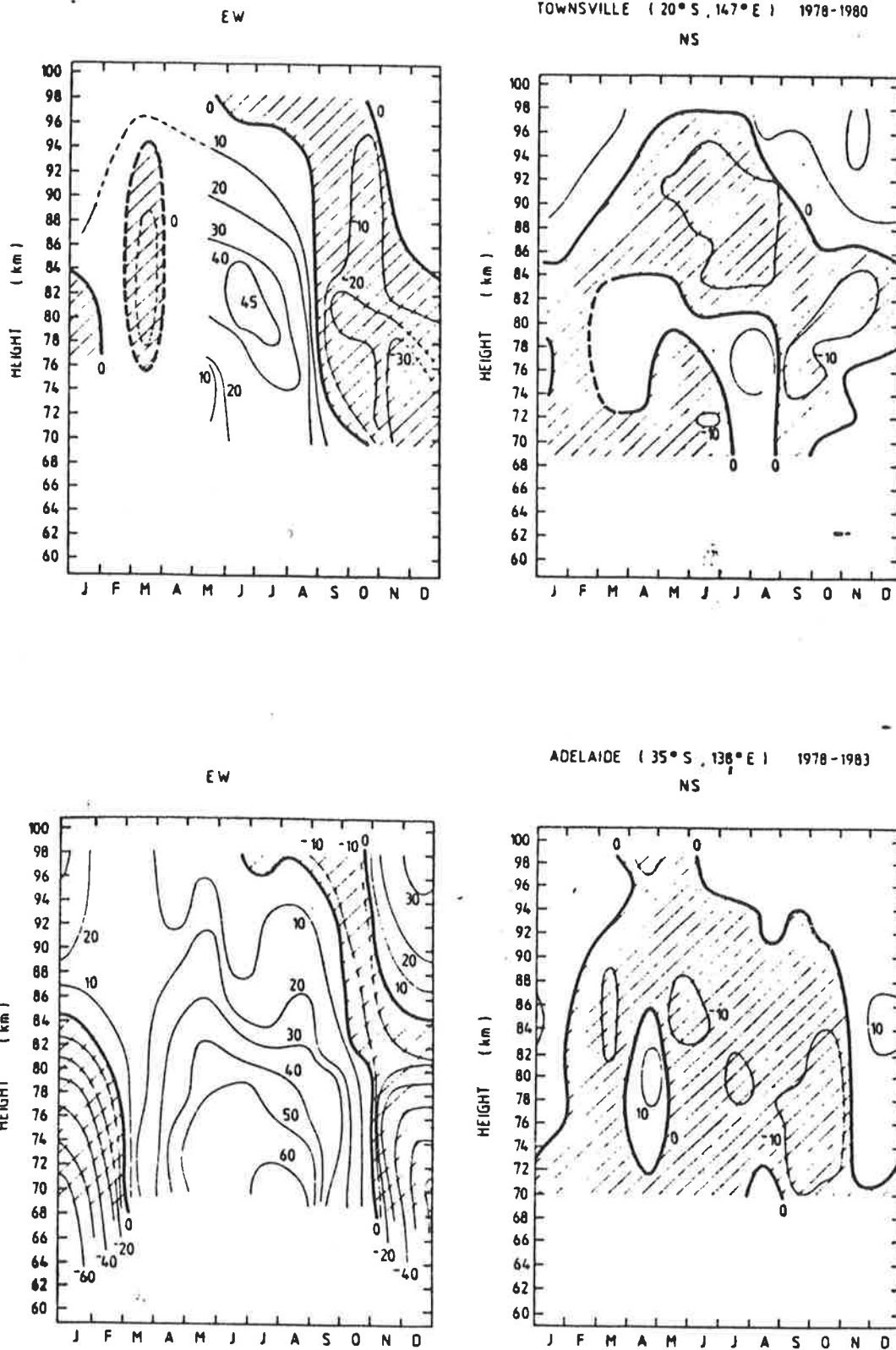
Figure 1.4   Annual Variation of Prevailing Zonal (EW) and
Meridional (NS) Winds at Townsville and Adelaide

(Manson et al., 1985)

From the meridional profiles of figure 1.4, it can be seen that, unlike the zonal winds, there is little difference in the magnitudes of meridional winds at each latitude; values rarely exceed $10ms^{-1}$.

Above 85 km at Townsville, poleward flow is observed at increasing altitudes from 85 km to 98 km during the autumn months. For most of winter, the altitude of the transition between poleward and equatorward flow remains steady near 98 km. From late winter to the middle of spring, the descent of the height of poleward flow closely reflects the ascent observed in autumn.

Below 85 km, equatorward flow is observed at Townsville from March until the end of April between 72 and 84 km. During May and June, equatorward flow is confined to a narrow region centred near 80 km. From mid-July to the end of August, equatorward flow is observed below 80 km. Equatorward flow is also evident below 70 km at the beginning of October and rising in altitude with time to peak near 80 km in mid-summer.

The meridional results for Adelaide show some features similar to those at Townsville, but the changes are more rapid and extensive. A region of equatorward flow occurs during April in the region 72 to 86 km, and there is equatorward flow below 72 km in August similar to the behaviour at Townsville. Apart from these excursions, poleward flow dominates this mid-latitude region below 90 km for all seasons of the year except summer. Above 90 km, poleward flow occurs during April and May up to 100 km.

Equatorward flow descends from 100 km at the beginning of winter to 90 km in the middle of spring, then a rapid transition occurs in which equatorward flow is observed at all levels above about 70 km. A swift reversion to poleward flow at most altitudes occurs near the end of summer.

A complete description of the prevailing winds in the Australian sector of the southern hemisphere cannot be accomplished without results from higher latitudes. Vincent (1984b) has produced a southern latitudinal cross-section of the prevailing wind systems in the 60 to 100 km altitude range for January (summer), shown here in figure 1.5. Results used to produce these profiles are from Townsville and Adelaide in Australia, Christchurch in New Zealand, and Mawson and Scott Base in Antarctica. The data from Mawson are discussed in more detail in this thesis.

The main features of figure 1.5, are the strong westward flowing jet near 40°S at an altitude close to 70 km, and the apparent upward tilt of the jet with increasing latitude. The meridional winds of figure 1.5 show systematic variation with latitude, with maximum values of about 15 ms^{-1} near 80 km at mid-latitudes, with most of the flow being equatorward, away from the summer pole. There is a weak poleward flow evident in figure 1.5 below 80 km. At these lower heights, observations are generally restricted to less than 12 hours per day, and may contain some unresolved diurnal tidal component which would have significant effects on the small values of observed meridional winds.

Recently, Koshelkov (1983, 1984, 1985) has published studies which are directed towards the provision of improved models of atmospheric parameters, including mean zonal winds, in the 25 to 80 km height range of
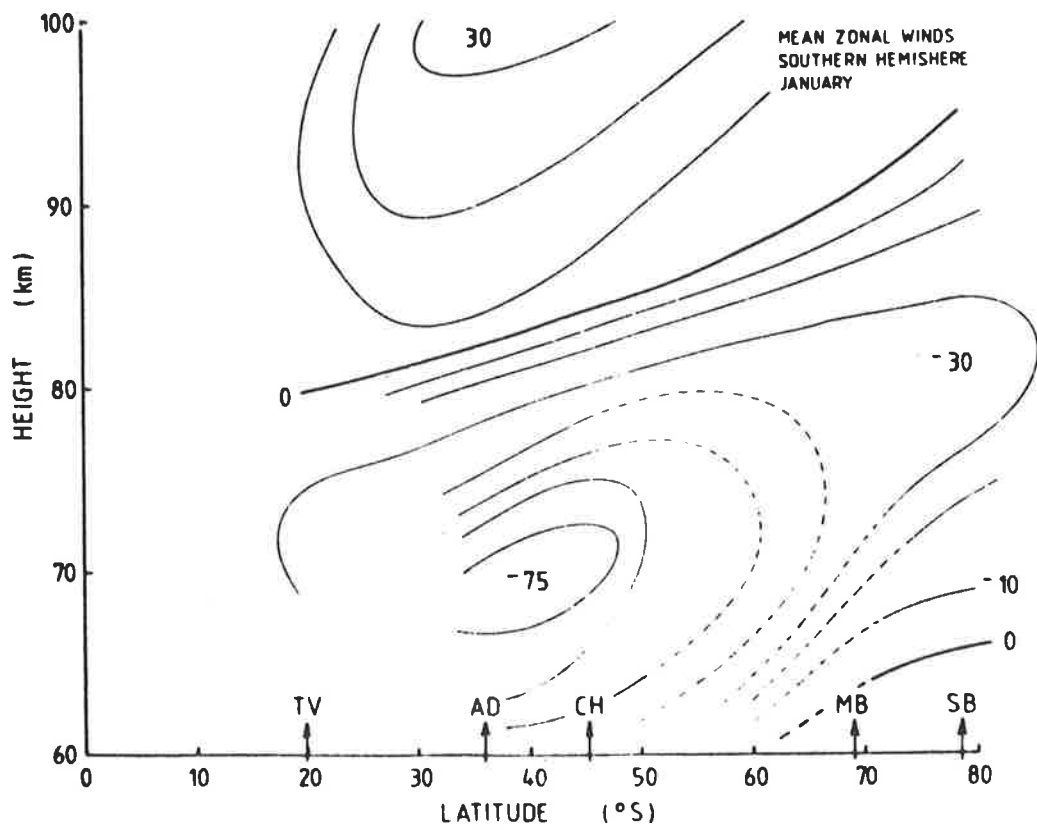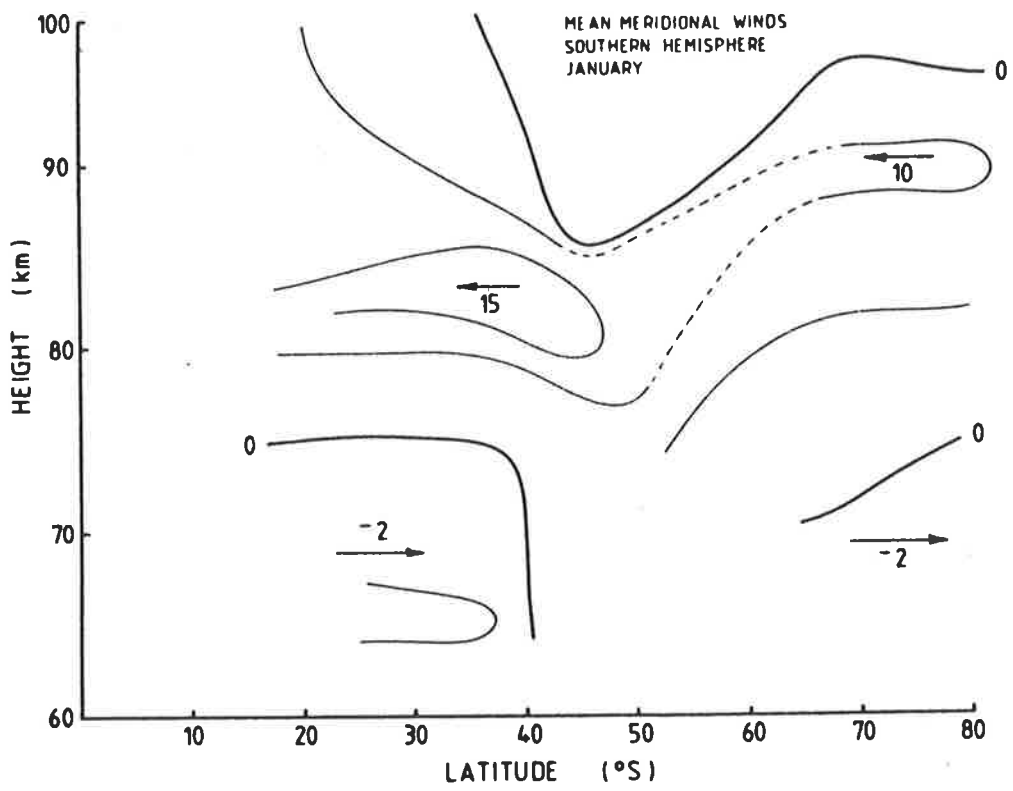
Figure 1.5   Southern Latitudinal Cross Section of the Prevailing Winds for January (Summer)

(Vincent, 1984b)

the southern hemisphere. The mean zonal winds of Koshelkov's model for January show agreement with regard to the location of the summer jet at mid-latitudes, but the wind profiles are approximately 5 km lower than those of figure 1.5. This difference could be attributed to the fact that Koshelkov's model has been constructed from relatively small amounts of data above 60 km.

Qualitatively, the main features of the prevailing zonal and meridional circulations and their variation with latitude are quite similar in both hemispheres. In both mid-latitude regions, the timing and rapidity of equinoctial changes are generally observed to be consistent from one year to the next at any particular site.

The most significant difference between the prevailing circulations of both hemispheres is the stronger flow observed at all latitudes in the southern hemisphere (e.g. Hirota et al., 1983), particularly in winter (Koshelkov, 1985) and above 90 km (Vincent, 1985).

1.3 Atmospheric Tides.

Atmospheric tides are driven by solar heating or by gravitational forces due to the sun or moon. The heating is due to insolation absorption by ozone and water vapour below 70 km, and by UV and EUV absorption in the lower thermosphere. The solar gravitational component is small compared to its thermal counterpart and very difficult to distinguish. Although lunar semidiurnal variations in the thermosphere may be as large as 20% of the solar component (Forbes, 1982b), the contribution of gravitationally induced tides to the total tidal budget in the mesosphere and lower thermosphere will not be considered in this study. A detailed account of

the generation and characteristics of gravitational tides is given by Chapman and Lindzen (1970). Non-migrating tides, which may be excited by topographical features or longitudinal variations in ozone or water vapour distributions, may also contribute significantly to the observed tidal budget. A discussion of thermally excited non-migrating tides has been presented by Kato et al. (1982).

1.3.1 Classical Tidal Theory.

In 'classical' tidal theory (Chapman and Lindzen, 1970; Groves, 1982a) it is assumed that tidal oscillations can be regarded as linearized perturbations on a static, inviscid atmosphere. Under these conditions, the governing equation is separable, and gives rise to vertical and latitudinal structure equations. The latitudinal structure is governed by Laplace's tidal equation; its associated eigensolutions, or modes, are the Hough functions. The vertical structure of each mode is defined by the corresponding eigenvalues, or equivalent depths. Negative equivalent depths correspond to evanescent modes which are attenuated outside their region of excitation. Diurnal modes may be symmetric or anti symmetric. Symmetric and antisymmetric modes are expected for the semidiurnal oscillations, but in classical theory, equivalent depths of all semidiurnal modes are positive, thus excluding evanescence.

S and L are used to represent tides resulting from solar and lunar effects respectively. A wave family may be represented by S_λ^s, where s is the longitudinal wave number, an integer representing the number of nodes around a circle of latitude, and $1/\lambda$ is the period of oscillation in terms of the mean solar day. Individual wave modes may be specified in the

form $S_{\lambda,n}^s$, where n denotes the particular wave mode, or the particular member of a wave family. In general, the larger the value of n, the more complex the latitudinal structure of the individual mode will be. If n is positive, the individual mode is propagating, if n is negative, the mode is evanescent. In this thesis, tides will be specified in the form (s,n), so that symmetric diurnal modes are (1,1), (1,3),..., and (1,-2), (1,-4),..., and antisymmetric modes are (1,2), (1,4),..., and (1,-1), (1,-3),... Symmetric semidiurnal modes are (2,2), (2,4),..., and antisymmetric semidiurnal modes are (2,3), (2,5),...

Hough functions and velocity expansion functions for some important diurnal and semidiurnal modes, from Forbes (1982 a, b), are shown in figures 1.6 and 1.7 to illustrate the variation in tidal behaviour with latitude predicted by classical theory. Rotation with time of the total tidal wind vector results from phase differences between zonal and meridional components. In the northern hemisphere, to which figures 1.6 and 1.7 apply, the meridional component generally leads the zonal component, so that the total tidal wind vector rotates in a clockwise direction when viewed from above. For the southern hemisphere, a reversal of sign of the meridional component causes the tidal wind vector to rotate in an anticlockwise direction. From figure 1.6, the characteristics of the predicted diurnal tide at a particular latitude are evident. At latitudes less than about 30°, the diurnal tide contains a large propagating (1,1) component. At mid-latitudes, the diurnal tide is a mixture of propagating and evanescent modes. At high latitudes, the diurnal tide contains a large evanescent contribution. In figure 1.7, the latitudinal variation of the semidiurnal tide is indicated. At all latitudes a mixture of symmetric and
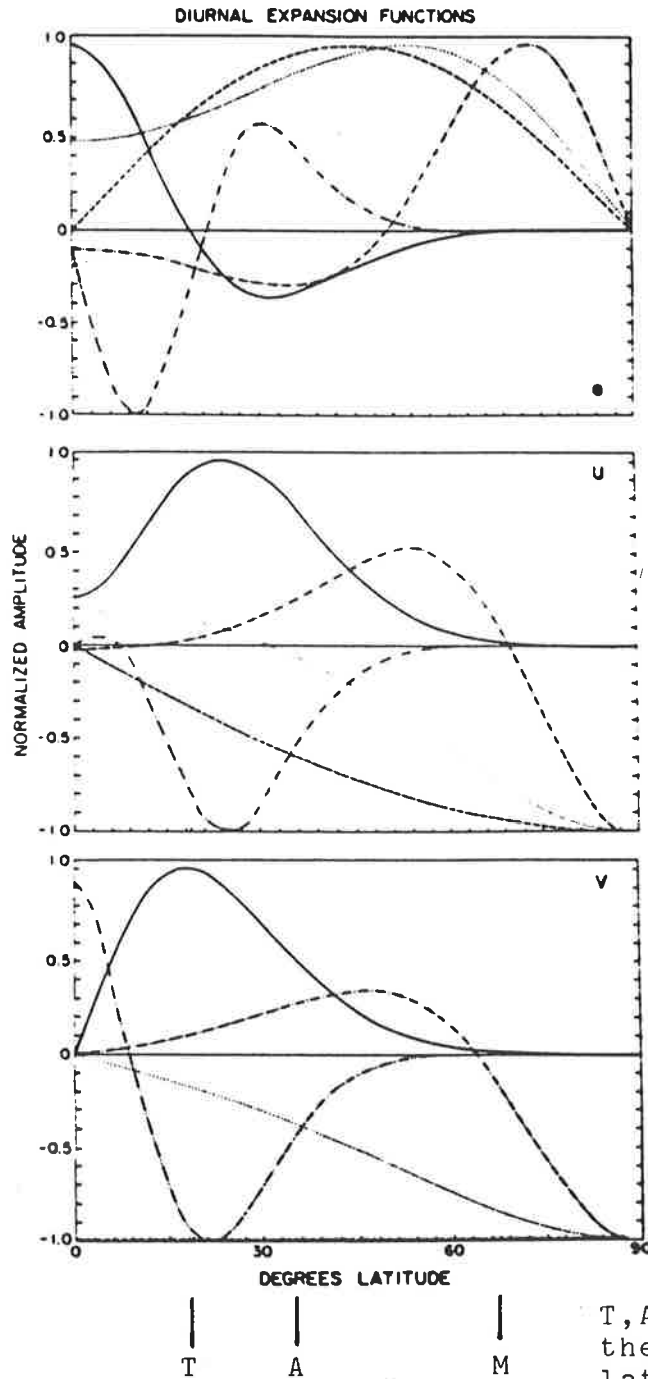
DIURNAL EXPANSION FUNCTIONS

T,A and M indicate
the approximate (southern)
latitudes of Townsville,
Adelaide and Mawson
respectively.

Figure 1.6   (Top) Hough functions for diurnal modes normalized to a
maximum value of unity. Keys and normalization factors
for each Hough mode are as follows: (1,1) (solid line,
0.606); (1,-1) (dashed line, 1.034); (1,-2) (dotted line,
1.054); (1,-4) (dashed-dotted line, 0.513); (1,2) (dashed-
double dotted line, 0.641). (Bottom) Northerly velocity
expansion functions for diurnal modes normalized to a maxi-
mum value of unity. Normalization factors are 0.026, 0.126,
0.100, 0.024, 0.015, respectively. (Center) Westerly
velocity expansion functions for diurnal modes normalized to
a maximum value of unity. Normalization factors are 0.038,
0.130, 0.100, 0.024, 0.018, respectively.

(Forbes, 1982a).
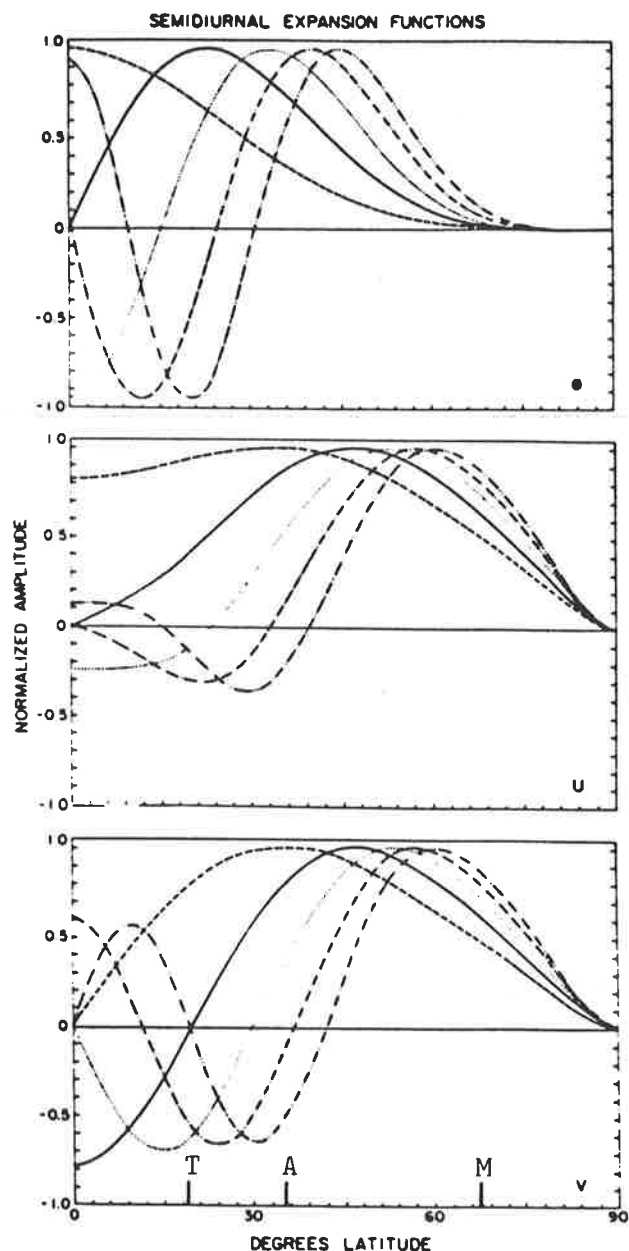
SEMIDIURNAL EXPANSION FUNCTIONS

T,A and M indicate the
approximate (southern)
latitudes of Townsville
Adelaide and Mawson
respectively.

Figure 1.7   (Top) Hough functions for solar semidurnal modes normalized to
a maximum value of unity. Keys and normalization factors for
each Hough mode are as follows: (2,2) (dashed line, 0.855);
(2,3) (solid line, 0.917); (2,4) (dotted line, 0.926); (2,5)
(dot-dashed line, 0.935); (2,6) (dashed-double dotted line,
0.935). (Bottom) Northerly velocity expansion functions for
solar semidurnal modes normalized to a maximum value of unity.
Normalization factors are, respectivley, 0.326, 0.171, 0.110,
0.078, 0.060. (Center) Westerly velocity expansion functions
for solar semidiurnal modes normalized to a maximum value of
unity. Normalization factors are, respectively 0.355, 0.182,
0.115, 0.081, and 0.062. Owing to the small difference between
the solar and lunar semidiurnal periods, these structures also
represent good approximations to the lunar semidiurnal expansion
functions.

(Forbes, 1982b).

asymmetric modes is apparent, with the amplitude of the semidiurnal tide maximizing at mid- to high latitudes.

Chapman and Lindzen (1970) neglected seasonal and latitudinal variations in the heating rates due to ozone and water vapour. Differences in the vertical heating structures with season, latitude, and tidal period were revealed by Hong and Lindzen (1976), Forbes and Garrett (1978), Walterscheid et al. (1980) and Bernard (1981a). Figure 1.8 provides a good example of the recent improvements made in the development of more realistic thermal excitation models.

Shown in figure 1.8 are height profiles of the Hough components of heating due to ozone and water vapour for the (2,2) mode from Groves (1983). Included for comparison in the figure are the heating profiles used by Chapman and Lindzen. The ozone heating profile for October has been omitted from figure 1.8, as it is very similar to that for April (Groves, 1983). It can be seen that Groves' results are smaller at most levels than the heating profiles used by Chapman and Lindzen. Groves has produced diurnal and semidiurnal heating profiles for various symmetric and antisymmetric modes which result from the absorption of solar radiation by ozone (Groves, 1982b) and water vapour (Groves, 1982c). These heating profiles include variations due to latitude and season. The maximum in heating due to water vapour for any particular mode occurs near or below 10 km, decreasing in amplitude and height of maximum with increasing latitude. In Groves' calculations for heating due to water vapour, the effects of clouds and longitudinal dependences are included. For ozone heating, Groves notes that observational data is limited above 55 km and at
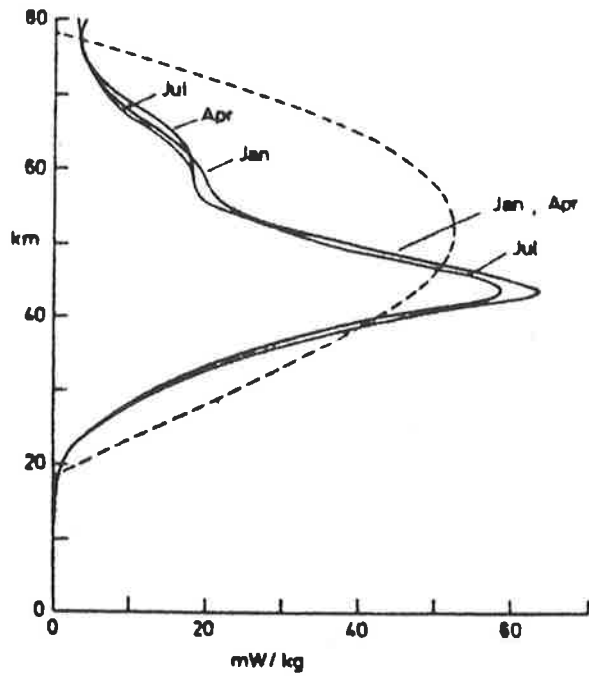
OZONE ABSORPTION

Key —— from Groves (1982b); ―――― from Chapman and
Lindzen (1970).
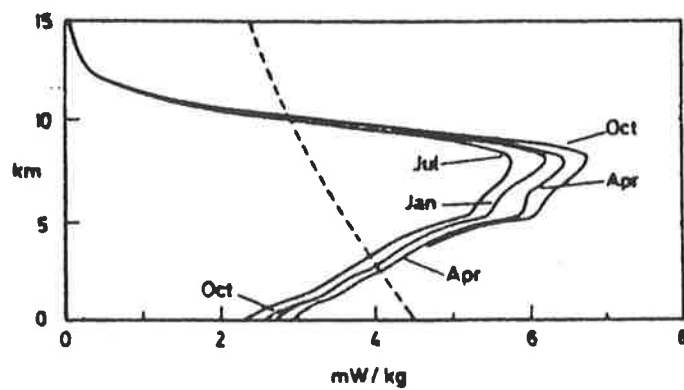
WATER VAPOUR ABSORPTION

Key —— from Groves (1982a); ―――― from Siebert (1961).

Figure 1.8   Heating rate profiles for the (2,2) mode due to ozone
and water vapour absorption (Groves, 1983).

high latitudes, and while considerable asymmetry in the total ozone content between hemispheres has been observed (e.g. Teitelbaum and Cot, 1979), there are still insufficient results with regard to the vertical distribution of ozone to perform a comparative analysis.

1.3.2 Non-classical Tidal Modelling.

For many purposes, classical tidal theory provides an adequate description of tidal behaviour. In particular, the magnitude of the solar diurnal and semidiurnal surface pressure variations and many features of the diurnal tide in the mesosphere are accounted for reasonably well by classical theory. At levels above about 70 km however, the effects of a variety of physical processes which are not considered in classical theory, such as: background winds, meridional temperature gradients, viscosity, thermal conductivity and ionization, must be incorporated into theoretical studies. The inclusion of these effects into classical tidal theory normally renders the relevant equations inseparable, demanding a numerical or non-classical approach for their solutions. A comprehensive review of non-classical models has been presented by Forbes and Garrett (1979). More recent developments in the theoretical modelling of atmospheric tides have been reviewed by Forbes (1984).

One of the first methods used to model the effects of vertical temperature structure and molecular dissipation, involved the use of an equivalent gravity wave (Lindzen, 1970; Richmond, 1975), which was chosen so that its vertical structure matched that of the tidal mode under investigation. It was argued by Lindzen that at the equator, the vertical structure of an equivalent gravity wave on a non-rotating plane

approximated that of the tidal mode in a viscous atmosphere. Forbes and Hagan (1979) later developed a rotating-plane analogue of Lindzen's model. This latter formalism was used by Forbes (1982a) to compute the (1,1) tidal fields of his extensive model of the solar diurnal tide.

As is the case for gravity waves in general, tidal modes with the shortest vertical wavelengths and lowest frequencies are attenuated by dissipative processes at the lowest altitudes. The most effective dissipative forces in the mesosphere and lower thermosphere are not the most effective at higher levels. In addition, both regions contain certain sources of tidal energy, caused by the insolation absorption of water vapour and ozone in the lower, and by the absorption of EV and EUV in the upper. For these reasons, theoretical tidal studies have normally dealt with each region separately. Between about 80 and 120 km, tidal structure is sensitive to many atmospheric features that most studies can only approximate in a general manner. The most comprehensive theoretical models currently available are those of Forbes, which cover the altitude range 0 to 400 km for both diurnal (Forbes, 1982a) and semidiurnal (Forbes, 1982b) tides.

Below 100 km, diurnal modes are excited almost exclusively in situ, as they are either trapped near the level of excitation, or they propagate with such short vertical wavelengths that they are severely attenuated near 100 km. Forbes (1982a) notes that the greatest inconsistencies between observations and theory occur in the 80 to 100 km region for the diurnal tide. For the purposes of this thesis, it is important to consider what processes might be responsible for such variation.

At low latitudes, the generation of turbulence due to the breakdown of the (1,1) mode (Lindzen and Blake, 1971; Lindzen and Forbes, 1983) is likely to cause variability. At mid-latitudes, the magnitudes of the propagating and trapped in situ tides are comparable in the 80 to 100 km region. Forbes (1982a) has pointed out that these modes can add vectorially to produce a variety of amplitude structures if there are small changes of phase between individual modes.

It is generally assumed that diurnal modes are relatively unaffected by background winds in the mesosphere and lower thermosphere due to their relatively high phase speeds when compared to typical values of zonal wind. Forbes (1982a) has suggested that at mid- to high latitudes, the presence of background winds may lead to changes in the vertical wavelength and phase of the (1,1) mode; a process he calls mode distortion. Vial and Teitelbaum (1984) have proposed that a similar process, resulting from the effects of turbulent diffusion on the (1,1) mode, may account for the annual variation in vertical wavelength of the diurnal tide observed at mid-latitudes. In addition, Vial and Teitelbaum suggest that at high latitudes, turbulent diffusion causes the vertical wavelength of the (1,1) mode to increase to such an extent, that experimental data which have been interpreted as being due to evanescent modes, may in fact be due to the 'distorted' (1,1) mode.

For semidiurnal tides, a major portion of direct thermal forcing goes into the (2,2) mode. Exponential growth of this mode is interrupted between 50 and 70 km not only because the background thermal structure tends to make the mode evanescent, but also because in the presence of

background winds and meridional temperature gradients, higher order modes are generated from the (2,2) mode by mode coupling (Lindzen and Hong, 1974; Walterscheid and Venkateswaren, 1979; Walterscheid et al., 1980). At the 100 km level, Forbes (1982b) estimates that the largest contributor to the semidiurnal tide is the (2,4) mode, with some contributions from the (2,5) and (2,2) modes. Forbes (1984) emphasises the difficulties in theoretical modelling of the semidiurnal tide in the 80 to 100 km region, where slight relative phase shifts between the several modes which will normally be present, can lead to considerable changes in phase of the total semidiurnal tide from day to day and with respect to latitude and height.

1.3.3 Observed Variability of Tides.

Recent observational studies (Bernard, 1981a; Ahmed and Roper, 1983; Manson et al. 1983; Manson and Meek, 1984a) have revealed that at mid-latitudes, both the semidiurnal and diurnal tides exhibit strong seasonal variations which may be amenable to theoretical modelling. At the 90 km level, the semidiurnal tide has the largest (>100 km) vertical wavelength in summer and the smallest (<50 km) vertical wavelength in winter, with relatively swift transitions from one regime to the other observed in most years during the equinoxes. Although the diurnal tide at the same level is much less regular, the shortest vertical wavelengths are observed during winter (Manson and Meek, 1984a). Manson and Meek (1984a) suggest that better agreement between observation and theory would result if the influence of asymmetric modes were to be larger in the theoretical models. Marked asymmetry between tidal oscillations at the geographically conjugate sites of Kyoto (36°N) and Adelaide (36°S) has been noted by Aso and Vincent (1982).

In experimental studies, it is conventional to treat observed oscillations with periods of 24 and 12 hours as tidal winds, and to use the slope of the phase variation with height over an observed height interval to estimate vertical wavelengths. In this manner, it is often difficult to unambiguously identify dominant tidal modes, as this and similar studies are generally restricted to a relatively narrow height range, and it is necessary to extrapolate outside that range to estimate vertical wavelengths. The best agreement with theory is generally found when the observational results are averaged over a month or more, so that much of the normally observed day-to-day variability is excluded. As major changes to tidal structures observed during equinoxes are known to occur on a regular basis over shorter periods than a month, processes which cause shorter-term variability than those already discussed, are likely to be important features of future theoretical tidal studies.

The time scales over which the changes in tidal structure occur during equinoxes are not reflected in the slower variation of background wind and temperature (Forbes, 1984). This leads Forbes to conclude that seasonal tidal characteristics are more strongly associated with variations in thermal forcing than in mean winds and meridional temperature gradients, and that mode coupling may be less important as a source of day-to-day variability than previously supposed. The coupling between variations in background atmospheric structure and the semidiurnal tide has been discussed by Bernard (1981b), who suggested that non-migrating modes as large as 50% of the primary tidal amplitudes may result from the interaction, and could also be responsible for observed longitudinal phase differences. Walterscheid (1981) has proposed a mechanism in which the

imposed semidiurnal oscillation may modulate the momentum deposition of gravity waves and thereby introduce a secondary oscillation close to the semidiurnal frequency (a pseudotide). Experimental results have yet to confirm Walterscheid's predictions.

The variability of the semidiurnal tide was examined by Bernard (1981b), who concluded that it could be described as a combination of three effects: variation of the relative amplitude or phase of the main tide over periods longer than 5 days, shorter time scale variation due to local effects, and longitudinal variations due to non-solar migrating modes. Bernard estimated the time necessary for a tidal mode to establish stationarity around the earth by equating it to the travel time of an equivalent gravity wave. In this way Bernard argued that if the stationarity hypothesis held for main tidal modes on time scales of a week or more, it could not be maintained for higher order modes and shorter time scales, as the time taken for an equivalent gravity wave to travel around the earth increases as the vertical wavelength decreases. In this scheme, stationarity for diurnal modes could not be established under 10 days and this could explain the strong short-term variability of the diurnal tide.

Local effects such as latent heat release associated with daily variations in tropical rainfall (Lindzen, 1978), and at high latitudes, geomagnetic effects during active solar periods, are also likely to cause variability, but until more comprehensive observations on the short-term variation in water vapour and ozone distributions are forthcoming, it is not possible to be more precise about which processes are the most important contributors to the short-term variability of tidal structure.

1.4 Contents of the Thesis.

In the preceding discussion, it was pointed out that the region in which the largest discrepancies between theory and observation exist, is the region between 80 and 100 km. The PRW method is particularly suitable for wind observations in this height range, as the partially reflecting irregularities upon which this method depends are most prevalent in that range.

In the second chapter, the details of the construction of the spaced antenna system at Mawson, and a description of its operation will be given. In chapter 3, partially reflecting irregularities, and the methods used to estimate their horizontal velocities are briefly discussed, then the performance of the system in the Antarctic is compared to the performance of similar systems at other sites. Chapter 3 concludes with discussions of the echo distribution observed at Mawson, the need for incoherent averaging to extend the relatively sparse results, and the prevailing winds observed over the whole observation period.

Results for the whole acquisition period are presented first in chapter 4 and are followed by a week by week discussion of the prevailing winds and tidal structures in order to demonstrate the underlying transitions in each system over the period of observation. This same approach has been adopted for the results obtained at Townsville and Adelaide which follow.

Conclusions and future recommendations are presented in Chapter 5.

2 EQUIPMENT.

The PRW system used in this work was designed specifically for operation at a remote low-latitude site. It was installed at Townsville in 1976. Space limitations and logistics meant that transmitting and receiving antennas had to be simple, easy to transport, and easy to maintain. The electronics which controlled the transmission and reception of signals were located in a caravan. Four dipoles were used for transmission and three pairs of crossed dipoles were used for reception. A sketch of the configuration used at Townsville is given in figure 2.1.

Beginning in July of 1980, the author spent approximately 2 months at Townsville in order to obtain low-latitude results, and to familiarize himself with the construction and operation of the system. At the end of this period, the system was dismantled by the author and transported to Adelaide, where it was overhauled and checked. Finally it was dismantled again, packed and dispatched to Melbourne, from where it was shipped to Antarctica.

2.1 Aerial Array Sites in the Antarctic.

The configuration used in Townsville could not be used at Mawson for various reasons. The Townsville site was flat and relatively spacious, and all anchorage points consisted of steel hoops embedded in concrete and fixed in earth. In the Antarctic space was very limited, the surface was extremely rugged and all anchorage points had to be secured in rock. Necessary modifications made to the equipment contributed to an overall decrease in the signal to noise ratio of the Mawson configuration. The difficulties encountered at Mawson and the methods used to overcome them in

N

Receiver Dipole ⟶

Transmitter Dipole

Feeder Line

$\lambda/2$

165 m

$\lambda/2$

Caravan containing
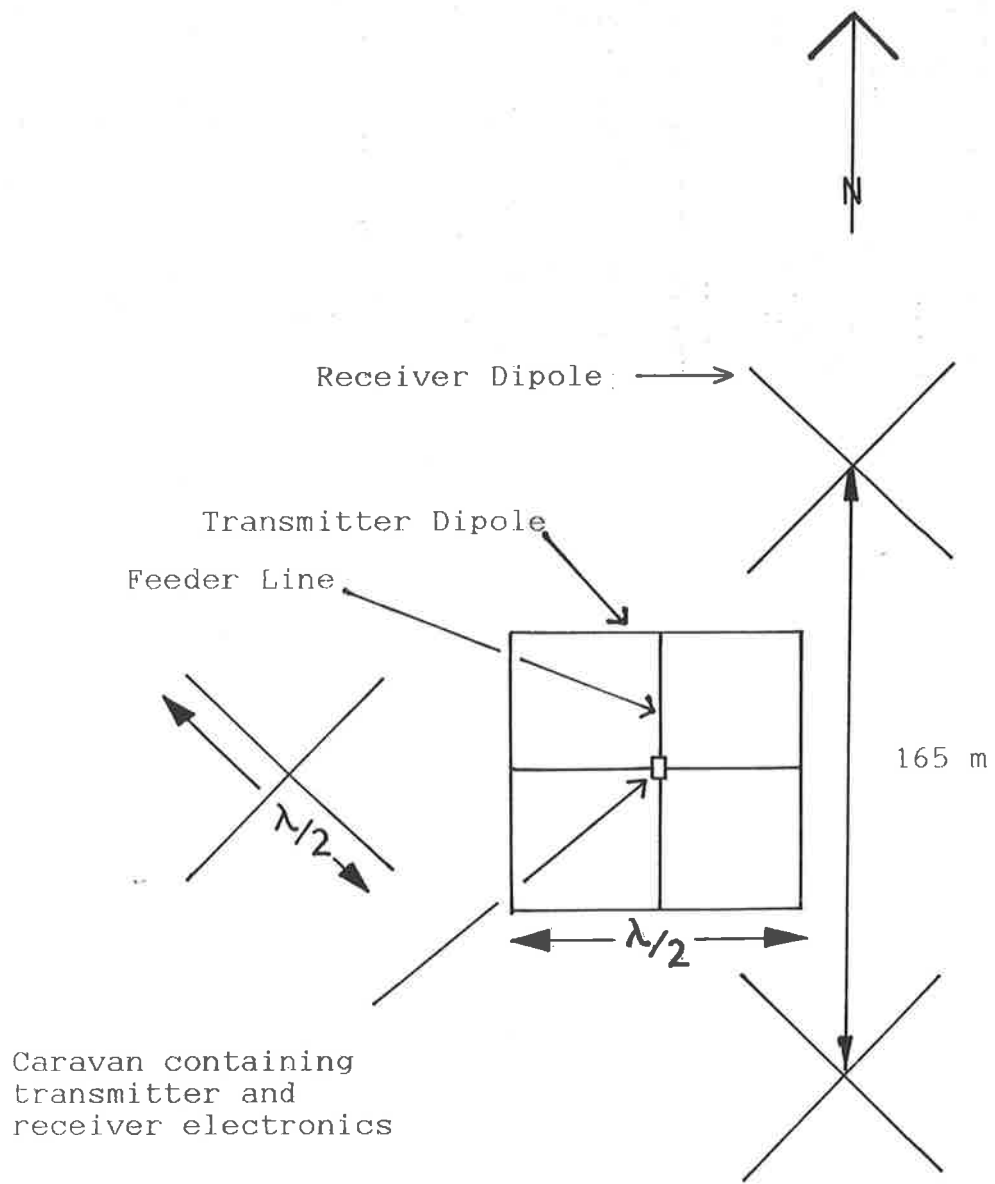transmitter and
receiver electronics

Figure 2.1   Townsville configuration of PRW antennae.

order to produce an experimental system suitable and sufficiently robust for Antarctic conditions will now be discussed. Figure 2.2 shows a sketch of Mawson base during 1981/1982 on which is shown the approximate positions of the transmitting and receiving arrays. Due to the limited usable area available for this experiment and to prevent interference with normal base communications, the transmitting and receiving arrays had to be erected at different sites. Figure 2.3 is an aerial photograph of the Mawson base, taken early in 1982, in which the transmitting and receiving sites are visible.

2.1.1 Transmitting Array Site.

When the sites allocated to the PRW experiment were examined, it was found that the transmitting dipole supporting tower in the south-east corner of the proposed site was in a melt lake. For the major part of the year (from March to December) this lake was frozen. Also the towers on the eastern side of the proposed transmitting array site were so close to the sea, that they could not be adequately guyed.

An alternate site was sought, but several factors compounded the situation. It was not possible to shift the arrays too far from their designated positions because there was not enough material on hand to physically link all the parts together. The transmitting site, in particular, had to be as close to horizontal as possible to allow the transmitted beam to be directed vertically upwards. The transmitting array was finally sited 10 m from the allocated site along a line 12° east of south (geographic). Figure 2.4 is an aerial photograph of the transmitting array site taken early in 1982 after completion of the PRW system.

SKETCH OF MAWSON BASE (67°36'S 62°53'E)

N
(GEOGRAPHICAL)

WEST ARM

EAST ARM

HORSESHOE HARBOUR

TRANSMITTER BUILDING ———— X

Tx ARRAY

MELT LAKE

EDGE OF ICE

3

Rx ARRAY

AERONOMY ———— O
BUILDING

1

2

EDGE OF ICE

0   100   200 METRES
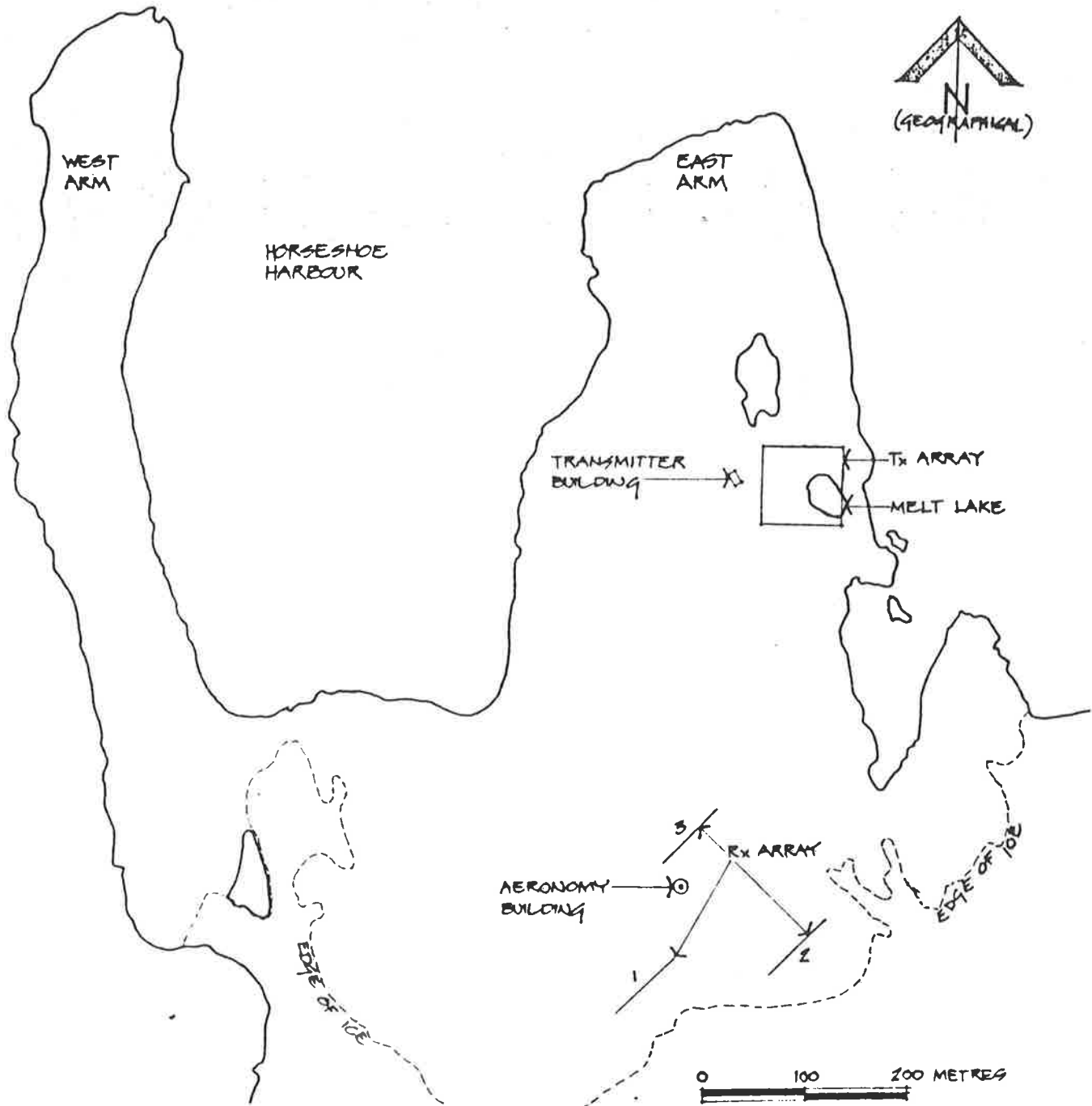
Figure 2.2   A sketch of Mawson base during 1981/1982
             on which is shown the approximate positions
             of the aerial arrays used in the spaced
             antenna drifts experiment.

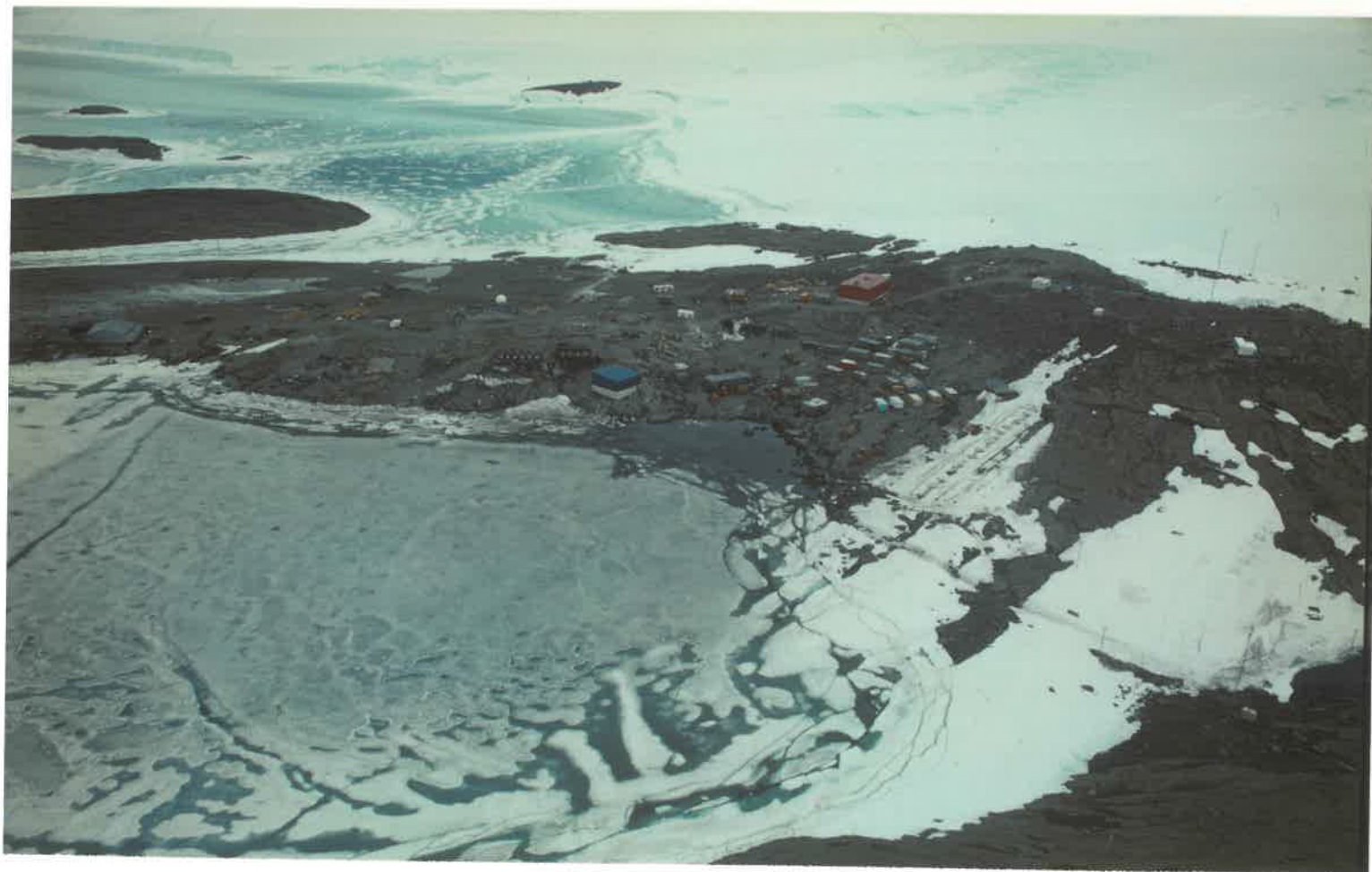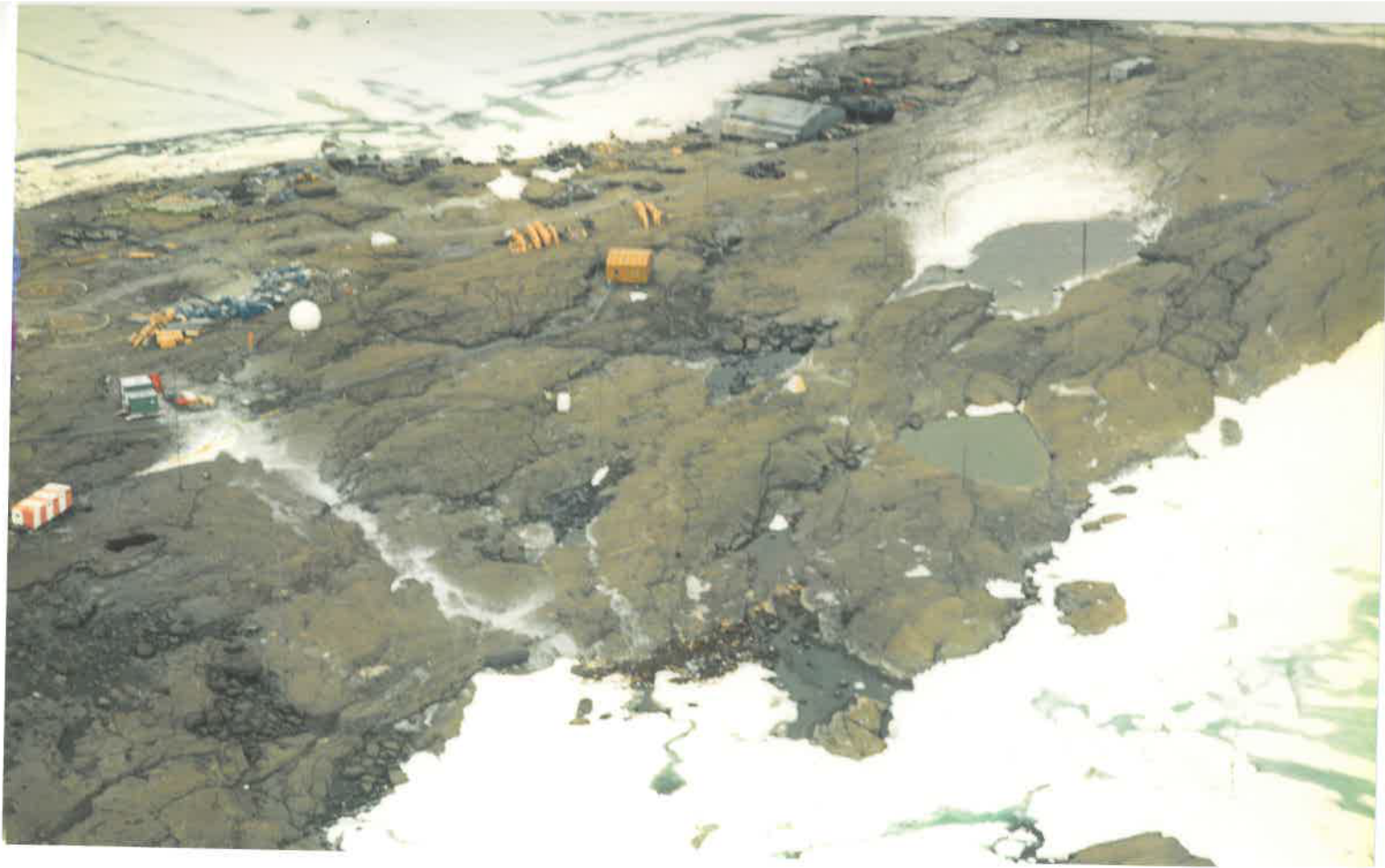Figure 2.3 Aerial photograph of Mawson base taken in early 1982

Figure 2.4 Aerial photograph of the transmitting array site taken
in early 1982, after the completion of the PRW system.

The transmitting towers were normally erected at a height of 30 m. After inspection of similar towers in the Antarctic and the experience of a blizzard it was clear that if the towers were erected at their full height using the standard rigging, it would be fortunate indeed if they remained upright for very long. There was insufficient material to re-rig the whole array.

The transmitting towers were telescopic in that their top two sections slid down into the bottom section. The transmitter dipoles were attached to 3 m sections of tower which were bolted on top. A collapsed tower with the dipole support stood approximately 13 m high. It was at this height that the towers were erected. Figure 2.5 is a photograph taken after completion of the system, and shows a view looking from south of the transmitting array approximately towards geographic north. The dipole shown is the westernmost one, that is, the one closest to the base transmitter hut.

The effect of lowering the height of the transmitting dipoles was to broaden the transmitted beam. This and the use of only single receiving dipoles at each receiver site contributed to an overall reduction in the signal to noise ratio of the Mawson installation.

2.1.2 Receiving Array Site.

The receiving array site was very cluttered. Under normal circumstances each receiving array element consisted of crossed half-wave dipoles. The receiving site was used to store construction material and had access roads running through it. One receiver site (designated 1 in figure 2.2) was very close to a large antenna used for base radio

Figure 2.5   The westernmost transmitting dipole, looking
            approximately towards geographic north.

reception. Consequently it was not possible to erect crossed receiver dipoles with the same orientation at these sites and single half-wave dipoles had to suffice. A view, looking roughly westward, of receiver 1 is shown in figure 2.6. The receiver 1 centre pole is the slender pole to the left on the photograph.

2.2 Construction in the Antarctic.

The Australian bases are at present undergoing a large construction program to upgrade facilities. This program will take many years. Most outside construction takes place in the summer. For this reason, the normal complement at Mawson (about 30 people) was more than doubled during the summer. As supply ships came in, they had to be unloaded. This had to be done as quickly as possible, in case of bad weather, so everybody helped.

Materials and supplies are brought to Mawson only during the summer months. If any particular items are required after the latter part of summer, they must be manufactured at the base. All of the fittings for the PRW arrays were made by the author. Their manufacture and installation took several months.

As materials were limited, most fittings for the PRW experiment were manufactured from scrap. Accurate dimensions for most fittings were not important and have not been included in the text. Scavenging for material at times took on the proportions of a treasure hunt. Without real continuity of personnel or organization from year to year it was never known where one might find what one was looking for. Frequent deposits of drifting ice added to the confusion, and an innocent mound of drift would

Figure 2.6 A view of receiver site 1. The slender pole visible
on the left of the photograph is the supporting pole
at the centre of receiver dipole 1. The rigging to
the right of the photograph is part of the receiving
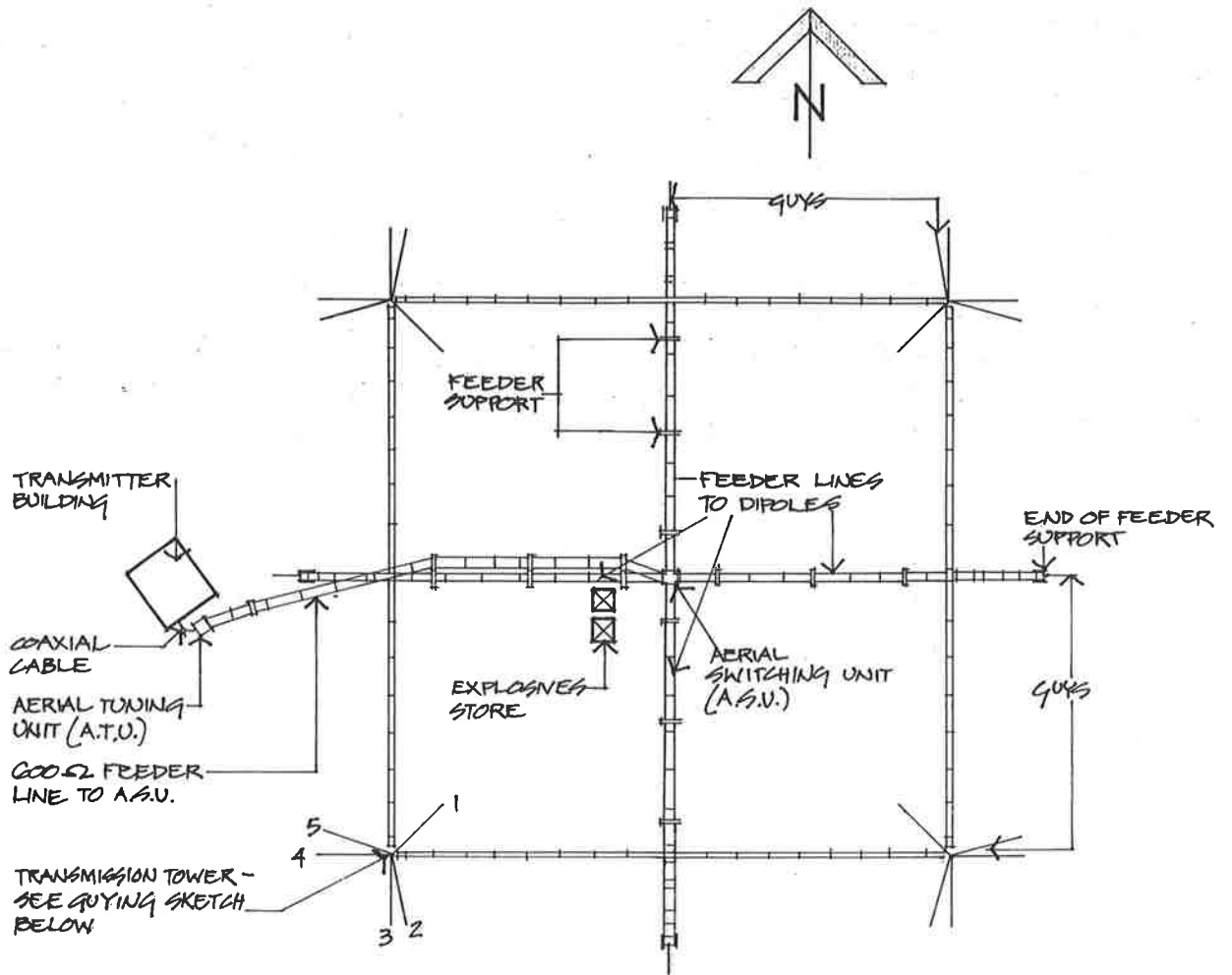array for normal base communications.

occasionally turn out to be a cache of useful material. Nevertheless, by choosing the simplest materials to start with, for example steel rod, plate and pipe, sufficient quantities of each were found to eventually complete the job.

Problems with the PRW sites, lack of fittings, construction work involving heavy machinery and blasting, frenetic activity during unloading and storing of supplies, overcrowding of the base facilities and unfamiliarity with the base's potential and normal operation made it impossible to begin work immediately on the construction of the PRW arrays.

It was decided to break down the work involved into 4 main tasks. These were: erection of the transmitter dipole supporting towers, erection of the receiver array, installation of the transmitter dipoles and the associated open wire feeder network and finally overcoming the problem of supplying the transmitter's power to the centre of the transmitting array.

2.2.1 Erection of Transmitting Towers.

Once the site for the transmitting towers had been surveyed and marked out, rock anchors were installed in the appropriate positions (see figure 2.7). A rock anchor was installed in the following manner. A 25 mm diameter hole approximately 30 cm deep was drilled using a hand held two-stroke motor powered rock drill. A steel wedge was put into a slot in the bottom of the rock anchor and the combination placed in the previously drilled hole. It was made fast by pounding the top of the rock anchor with a sledge hammer, then molten sulphur was used to seal the hole and secure the device.

GUYS

FEEDER
SUPPORT

FEEDER LINES
TO DIPOLES

END OF FEEDER
SUPPORT

TRANSMITTER
BUILDING

COAXIAL
CABLE

AERIAL TUNING
UNIT (A.T.U.)

600Ω FEEDER
LINE TO A.S.U.

EXPLOSIVES
STORE

AERIAL
SWITCHING UNIT
(A.S.U.)

GUYS

TRANSMISSION TOWER –
SEE GUYING SKETCH
BELOW.

5
4
3 2
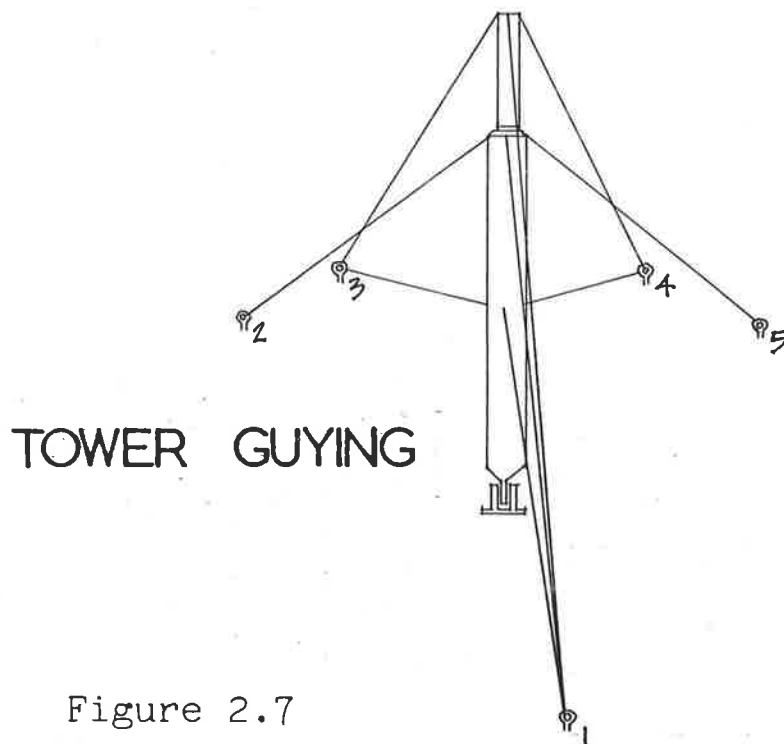1

TRANSMITTING ARRAY – PLAN 1:1000

TOWER GUYING

Figure 2.7

The rock drill was difficult to keep running for more than a few minutes in temperatures below -15 ^{0}C. It was not possible to get a vehicle near most of the drilling positions and the rock drill had to be manhandled. It was an awkward and heavy tool to work with.

Molten sulphur was prepared by heating powdered sulphur in an iron crucible with a butane gas flame. This had to be done out of the wind in order to prevent too much heat from being lost. At times it was difficult to find a spot sheltered enough to melt the sulphur and yet close enough to prevent the sulphur from solidifying before it was used. Often the sulphur had to be ignited to keep it hot enough and care had to be taken to prevent the unpleasant consequences of contact with sulphur dioxide fumes.

Once the rock anchors were all in place, a method of securing the base plates of the transmitting towers had to be found. 60 cm lengths of mild steel reinforcing rod were turned down in a lathe then threaded. Four of these rods were used for each base plate. They were fixed in the rock by drilling out suitable holes and using molten sulphur to hold them fast.

2.2.2 Erection of Receiving Array.

It had been intended to support the bottom of the poles used in the receiver array by drilling holes (~ 50 mm diameter) in the rock and placing the poles in them. This was not possible. A large compressed air driven rock drill was to have been used, but in late April, it was too cold for this equipment to work satisfactorily. Attempts were made to drill these holes with the same drill used for the rock anchors, but, without success.

Suitable large diameter lengths of pipe welded to steel plates were used to secure the bottoms of the centre poles. These were held fast by rock bolts, and allowed the poles to be put up and pulled down very easily. The holes for the rock bolts were drilled out with an electric hammer drill which worked well even at temperatures of $-30\,^{\circ}C$.

A source of power was required at the receiving site. Portable generators were tried, two different generators were reconditioned for the purpose, but both were inadequate. Extension cords (up to 200m in total length at times) were used.

A sketch of the receiving array is shown in figure 2.8. The centre poles for each receiver dipole were erected first, then positions for the end poles for each dipole were chosen. End poles were made by welding 4 chain links to 3m lengths of scaffold tube (3 links for guys, 1 link to attach the dipole).

2.2.3 Open Wire Feeder Network.

In the Antarctic, particularly at Mawson, extremely strong winds prevail. On most days at Mawson wind gusts of 50 km/hr or more are recorded. The maximum wind speed recorded at Mawson during 1981 was in excess of 180 km/hr. The wind direction was virtually constant from the south-east. Temperatures ranged between $+5\,^{\circ}C$ and $-35\,^{\circ}C$. These conditions necessitated the use of a more robust open wire feeder network than that used in Australia. Also because the transmitting towers were not erected at their full height, the configuration of the open wire feeder network had to change.
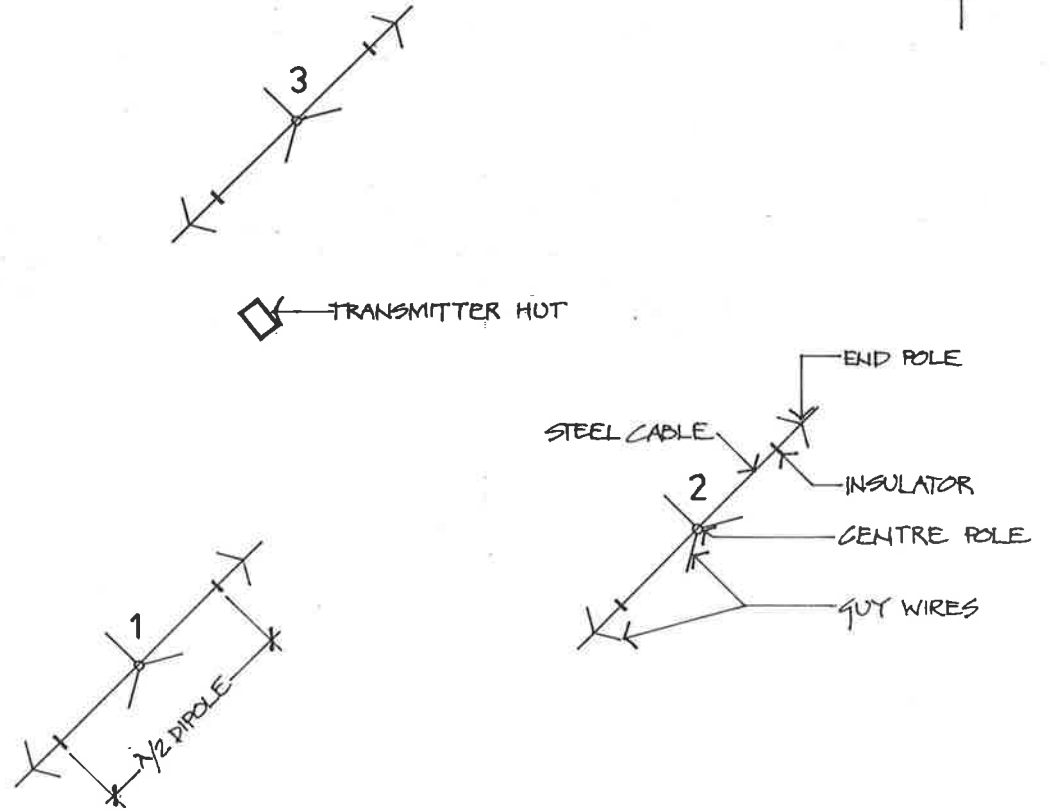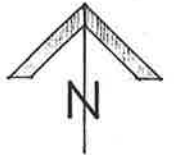
RECEIVING ARRAY – PLAN 1:2000

Figure 2.8

All four feeder lines from the centre of the array to the transmitter dipoles were 75m long. In Australia, with the supporting towers at their full height, the feeders would be attached at the centre of the dipoles and the centre of the array, essentially hanging, with a couple of cross arm supports on each feeder to prevent contact with the ground. Damage to the feeder lines by winds at Townsville had not been a major problem.

In order to reduce wind damage in the Antarctic, the horizontal sections of the feeder array had to be tensioned. Also fittings had to be devised which would allow the feeder lines to run outside the extremities of the transmitting array, then up and in towards the dipoles. Figure 2.9 is a view of the transmitter site looking in a south-east direction. In the bottom left hand corner, is a frame which held the Aerial Switching Unit (A.S.U.); to the right of this, two feeder supports, one with insulators, are visible, and on the right-hand side of the photograph, the tower in the south-east corner of the transmitting array can be seen.

The insulated terminals on the top of the A.S.U. were not strong enough to be held under tension. A supporting arrangement (figure 2.10), attached to the A.S.U. frame, was made by the author. This allowed the east-west and north-south feeder lines to be tensioned right across each axis of the array.

Although the feeder lines were tensioned in the horizontal, this same tension could not be allowed on those parts of the feeder lines which ran up to the dipoles. The folded dipoles were made from hard drawn cadmium-copper wire which was larger in diameter than the soft copper wire

Figure 2.9   The transmitter site during construction.   A view
             looking from near the centre of the transmitting
             array towards the south-eastern supporting tower.

Figure 2.10   Frame devised to hold the Aerial Switching Unit (ASU)
and to allow the tensioning of the horizontal parts
of the open wire feeder network.
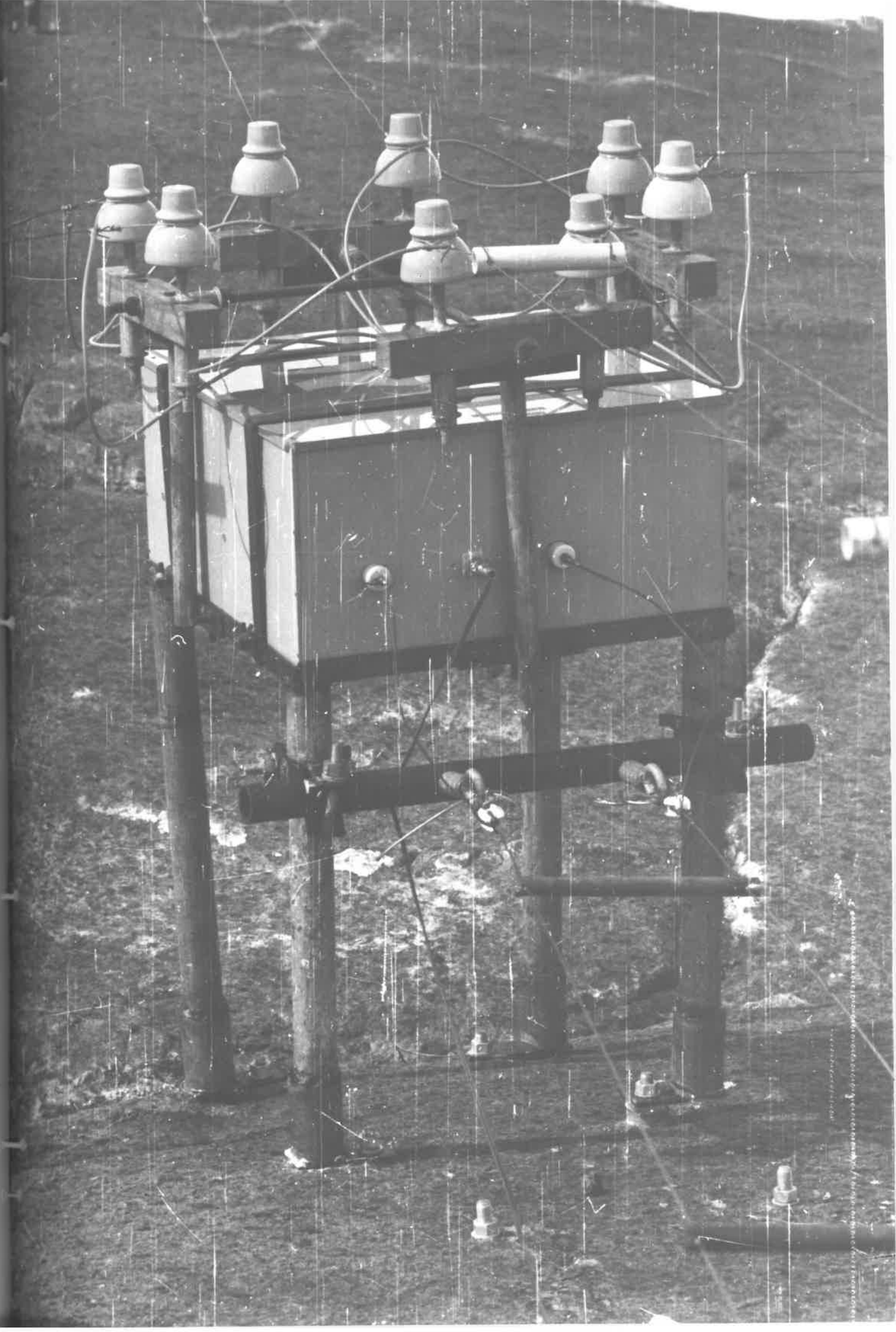
used in the feeder lines. The dipoles could be tensioned to some degree, but over a horizontal distance of 75m they would still move a metre or two in the middle during strong winds. Tensioning the upright section of feeder to the same extent as the horizontal caused excessive breakage, particularly at the joins of feeders to dipoles, during gusty conditions.

The optimum solution, though not entirely satisfactory, was to fix the feeder lines to supports with insulated staples. This allowed the horizontal sections to be under tension, and the untensioned upright sections to move freely with the dipoles.

2.2.4 Power to the Centre of the Transmitting Array.

The Aerial Tuning Unit (A.T.U.) and the A.S.U. were the last two stages in the transmitting system before power was fed to the transmitting dipoles. In Australia these two units were simply mounted in the transmitter rack which was placed in the centre of the array. In Antarctica facilities were not available to set up the transmitter rack in the centre of the array. The transmitter was housed in the base transmitter hut approximately 70m from the centre of the array (see figure 2.7). The A.T.U. was encased in a sturdy plastic box and held in a steel frame which was bolted to the rock just outside the transmitter building. The A.S.U., from which power was fed to the transmitting array, was mounted in the centre of the array.

Originally it had been proposed to tune the output from the A.T.U. to 600Ω, feed the power along a 600Ω feeder line, then use a 4-wire $\lambda/4$ transformer attached to the A.S.U. to match the impedance of the array (~~approx. 75Ω~~). Such a device would have been almost 38m in length. This

device could have been built, but to guarantee accuracy of spacing over such a distance and to have made it impervious to outside conditions would have required considerable effort. An alternative was sought.

The A.T.U. was moved to the centre of the array and connected directly to the A.S.U. Power was fed to the A.T.U. from the transmitter rack by a length of 75Ω coaxial cable. This proved to be unsatisfactory as the cable was so brittle outside that any movement, either manually or by the wind, caused the outer casing and insulation to shatter.

The Ionospheric Prediction Service of Australia operates an Ionosonde at Mawson. Their method of matching impedances from feeders to arrays is to use impedance matching transformers. These consist of insulated wire wound on a ferrite core. A spare ferrite core was found and an impedance matching transformer was made to suit the PRW transmitting system. This unit was small enough to be mounted inside the box containing the A.S.U.

With the A.T.U. outside the transmitter hut, connected to the transmitter by a short length of coaxial cable, power was fed along a 600Ω open wire feeder to the A.S.U., where the impedance was transformed then fed to the array. In a direct line between the A.T.U. and the A.S.U., there were the two containers used for storing explosives (see figure 2.7). It was not possible to move these explosives at the time, so the 600Ω feeder line was routed around them.

2.2.5 Finishing Touches to the System.

The final step in making the PRW system work was to put in cables from the Aeronomy Laboratory to the Transmitter hut which would carry the signals required for the transmitter's operation. These cables were over 400 metres in length and for about half that distance were placed in a cable tray which serviced the transmitter building.

In addition to the cables connecting the transmitter rack to the receiver rack there were 3 lengths $(^3/_2\lambda)$ of coaxial cable from the receivers to the receiver rack. These coaxial cables had to cross access roads at some stage. The only sure way of protecting these cables from damage by heavy machinery was to encase the cables in steel at the appropriate places then, if possible, bury them, or cover them in a mound of concrete.

Care had to be taken when laying out cables. If winds were allowed to bear on coaxial cables running across exposed rock, the outer insulation and outer conductor of such cables could be abraded away in less than 24 hours. By using natural fissures in the rock and burying the cables in drifted snow where possible, this abrasion was reduced to a minimum.

2.3 Comments.

Work on the construction of these arrays began in February 1981 and was completed in October 1981. Even in February the conditions for working outside were not good, but the worst weather was in the Winter months (June, July, August). Difficulties in producing fittings and solutions to problems which occurred during the construction, combined with

vagaries of weather, made it impossible to have a concerted effort by several people, so the task became a one man job. Help was freely given and generally available, but in the Antarctic everyone has a job and permanent help cannot be sought. When a tower or pole needed to be put up, there were always willing hands.

Figure 2.11 shows a view looking approximately north-east, of the transmitting array once it was completed. PRW towers had their top sections painted red, and three are included in the photograph. Also visible are some of the white spacers on the closest dipoles. The circular structure in the right foreground is a meteorological radome, the truncated pyramid shaped structure behind the closest PRW tower is a detonator store.

Once the whole system was running, it was a full-time job to keep it all together and working. Twice, during blizzards, a transmitting tower came down. The centre poles of the receiving dipoles came down several times during similar conditions. The transmitter feeder network suffered the greatest amount of damage, but fortunately, was not difficult to fix and rarely kept the system from operating for very long. Heavy machinery caused inadvertent damage on occasion, and for a time the husky pups found coaxial cable irresistible.

As with many experiments, electronic problems developed once the system began operating. These kept the system out of operation for approximately 5 weeks shortly after the first results had been obtained. The most perplexing problem occurred in the square pulse modulator board in the transmitter rack. With approximately 30kw of radio frequency power being transmitted for most of the day from the building in which the PRW

Figure 2.11 A view of the completed transmitting array looking
approximately towards geographic north-east.

transmitter was housed it was very difficult to ascertain what was really happening in the faulty circuit. The base transmissions ceased at about local midnight and began again at 5am local time. During these intervals the problem could be studied properly and was eventually solved.

On 14th February 1982, a blizzard destroyed the entire transmitter feeder network and all the dipoles. One of the transmitter towers was knocked down and there was minor damage to the receiving array. Most of the copper wire was recovered and the dipoles and feeders were rebuilt.

We were due to leave the base at the beginning of March 1982. It was important to this project to try and have the system running during the Winter of 1982. Members of the 1982 wintering party were willing to run the equipment during this time, so an effort was made to have the system running when we left. Fortunately the system was repaired and running on 28th February 1982, the day before the author left.

2.4 System Operation.

The system operates at a frequency of 1.94MHz, with a peak power of up to 15kw. By introducing an appropriate phase change of $^{\pi}/_{2}$ radians between orthogonal pairs of transmitting dipoles, ordinary (O) or extraordinary (E) modes of circularly polarized radiation may be transmitted. Under normal operating conditions, O mode is used during the day and E mode at night.

The whole system was microprocessor controlled and receiver gains were automatically adjusted for changes in echo strengths. The majority of

results were obtained in the height range 60 to 100 km. Gaussian shaped pulses 30µs wide were transmitted at a pulse repetition frequency of 20Hz, generally for 4 minutes in every 20. The whole system was phase coherent, and each receiver yielded in-phase and quadrature components, so that complex echo amplitudes were obtained. The two signals from each receiver were sampled at 2 km intervals over a selected 40 km height range, then digitized with an 8-bit analogue-to-digital converter. The digitized signals from each receiver channel and 2 km height interval were integrated over 8 successive pulses to give an effective sample rate of 2.5Hz. The integrated signals were recorded on magnetic tape in 2 minute blocks for subsequent analysis at Adelaide.

Figure 2.12 is a photograph of the PRW receiving rack in operation in the Aeronomy Laboratory at Mawson.

2.4.1 Transmission.

A sketch of the transmitter is shown in figure 2.13 and a block diagram showing the major functions appears in figure 2.14. Signals were generated in a master oscillator housed in the receiver chassis. In Townsville, two control signals were sent from the from the receiver to the transmitter; one was the pulse repitition frequency of 20Hz, and the other was a 1.94MHz signal, used to control the transmitted output. At Mawson, the distance between the transmitter and receiver systems was approximately 400 metres. Problems of signal leakage and subsequent pick - up by the receiving antennae were minimized by using a 9.7MHz signal instead of the usual 1.94MHz. On arrival at the transmitter, the 9.7MHz signal was divided by 5 to give 1.94MHz, before being used in the pulse modulator.

Figure 2.12 A photograph of the receiving rack in operation
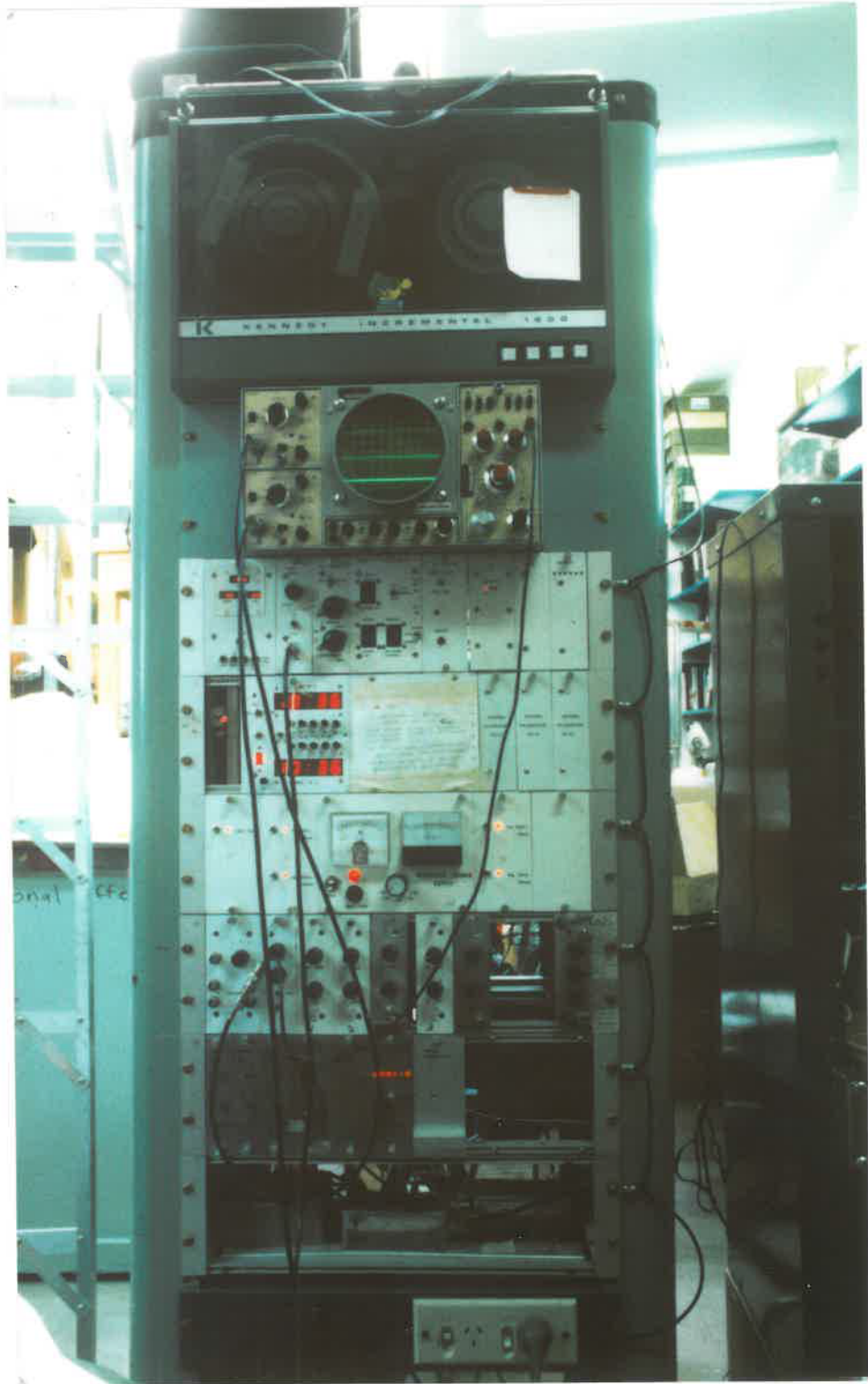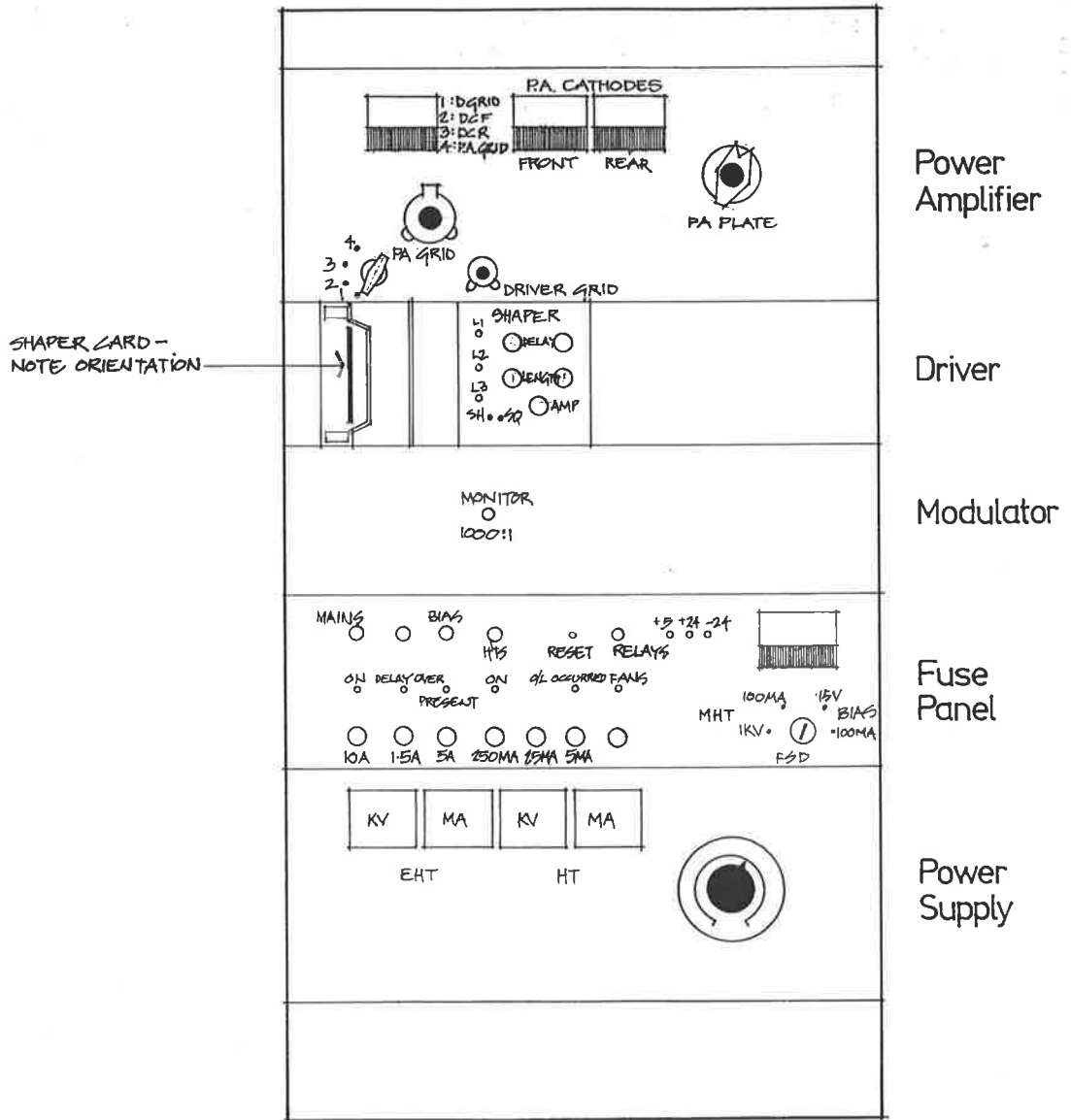
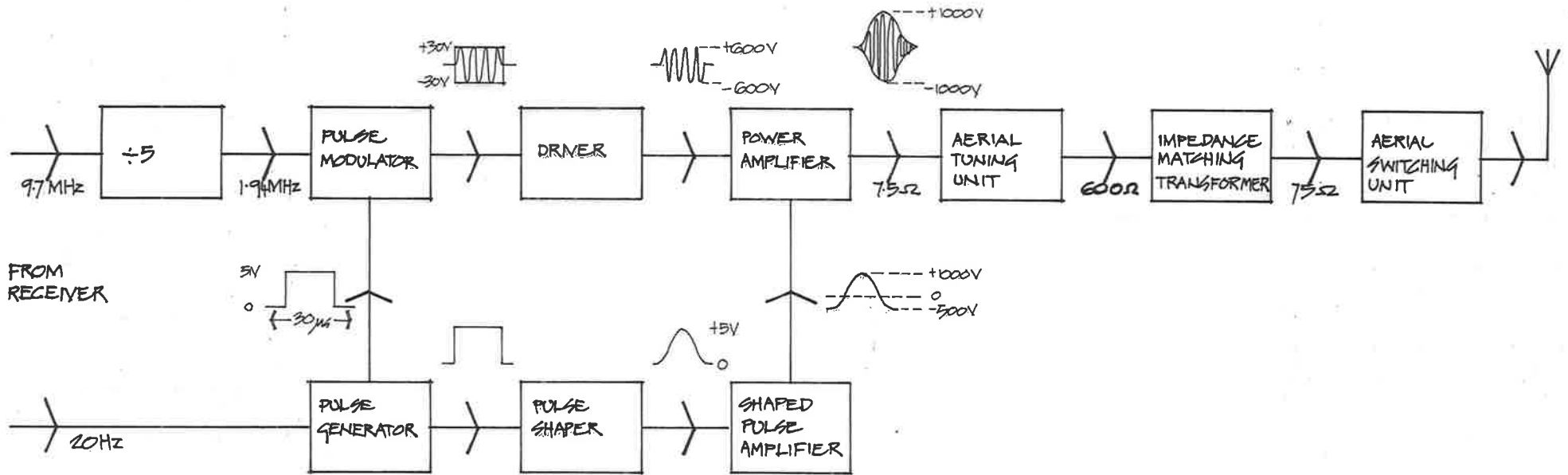Figure 2.13   TRANSMITTER RACK

Figure 2.14 TRANSMITTER BLOCK DIAGRAM

The appropriate modifications to the electronics were undertaken by the author during the course of setting up the equipment.

A 20Hz square pulse, 30µs wide, derived from the 20Hz signal sent from the receiver, was used to modulate the 1.94MHz signal. The output from the pulse modulator was a 1.94MHz signal 30µs wide with an amplitude between -30V and +30V. This signal was amplified in preparation for the final modulating stage.

An identical 20Hz square pulse signal was used to produce a gaussian shaped pulse with a peak voltage of 5V. This shaped pulse was then used to produce a similar shaped pulse which varied between -500V and 1000V.

The amplified 1.94MHz square pulse signal was modulated by the amplified shaped pulse to produce the final gaussian shaped 1.94MHz transmission signal.

The last two stages before power was fed to the transmitting dipoles were the A.T.U. and the A.S.U. The A.T.U. was used to match the impedances of the transmitter and the transmitting array and the A.S.U. provided the means to change the polarization of the transmitted wave. In Townsville these units were colocated, but not so at Mawson.

2.4.2 Reception.

Returned signals were received by 3 half-wave dipoles aligned parallel to one another, supported by steel poles arranged at the vertices of an equilateral triangle (see figure 2.2). An impedance matching transformer (tuning box) was located at the centre of each dipole to allow

the matching of impedances between the dipoles (~30Ω) and the coaxial cables (nominally 50Ω) carrying the received signals to the recording system. The recording equipment was designed to yield complex amplitude information by detecting the in phase and quadrature components of these returned signals.

The received signal may be expressed in the complex form E(t) where

$$E(t) = E_{ip}(t) + iE_q(t). \tag{1}$$

$E_{ip}(t)$ is the in phase component and $E_q(t)$ is the quadrature component.

The actual signal E(t) can be obtained from its complex form by first multiplying (1) by exp(-iωt) to give

$$E(t)\exp(-i\omega t) = E_{ip}(t)(\cos\omega t + i\sin\omega t) + iE_q(t)(\cos\omega t + i\sin\omega t)$$

The real part of this expression is E(t), where

$$E(t) = E(t)\exp(-i\omega t) = E_{ip}(t)\cos\omega t - E_q(t)\sin\omega t$$

The receivers used to observe the fading pattern of received signals have a gain of about 100 dβ and a bandwidth of 25kHz. Figure 2.15 shows a block diagram of the electronics of a receiver module used to obtain in phase and quadrature components of the received signal.

Incoming signals with an angular frequency ω_r are amplified, then mixed with a local oscillator frequency of angular frequency ω_{lo}. The resulting output is filtered to preserve only the $(\omega_{lo} - \omega_r)$ component, the

$f_{LO} = 2.425 \text{ MHz}$

$f_T = 1.94 \text{ MHz}$

$f_{LO} - f_T = 485 \text{ kHz}$

$\cos \omega_{R} t$

MIXER

FILTER

$\cos(\omega_{LO} - \omega_{R}) t$

MIXER

FILTER

$\cos(\omega_R - \omega_T) t$
IN PHASE

MIXER

FILTER

$\sin(\omega_R - \omega_T) t$
QUADRATURE

$\cos \omega_{LO}$

1.94 MHz
CRYSTAL
OSCILLATOR

$\div 97$

20 kHz

FREQUENCY
SYNTHESIZER

$\cos(\omega_{LO} - \omega_T) t$

$-\pi/2$

$\sin(\omega_{LO} - \omega_T) t$
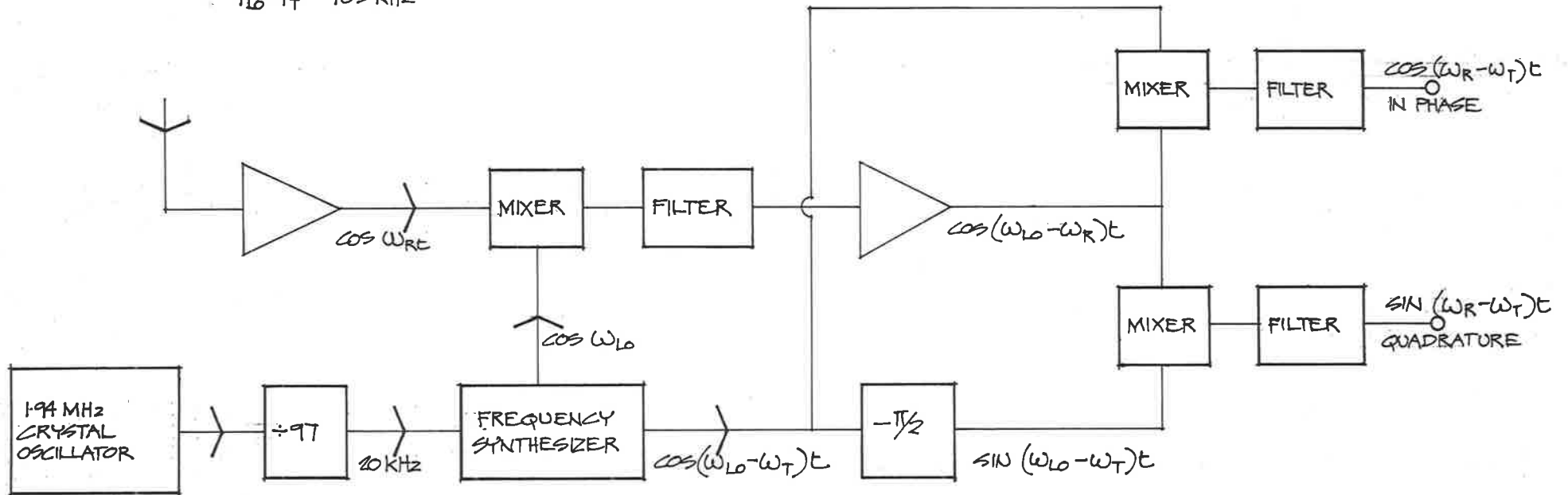
SIGNAL RECORDING BLOCK DIAGRAM
Showing the steps in recording the "IN PHASE" and
"QUADRATURE" components of a received signal $E(t) = \cos \omega_R t$

Figure 2.15

intermediate frequency. This signal is then amplified and mixed with a reference signal of angular frequency $(\omega_{lo}-\omega_t)$. The output produced from this mixing consists of 2 frequencies, $[(\omega_{lo}-\omega_t)+(\omega_{lo}-\omega_r)]$ and $[(\omega_{lo}-\omega_t)-(\omega_{lo}-\omega_r)]$.

The final stage of the amplifier is a low pass filter with a bandwidth of approximately 50kHz. The frequency $(\omega_r-\omega_t)$ is very low compared to the other frequencies produced, since ω_r is essentially a slightly modified form of ω_t. The final stage effectively removes all frequencies except $(\omega_r-\omega_t)$.

If the received signal is of the form $E(t) = E_0\cos(\omega t+\phi)$, where $\phi = (\omega_r-\omega_t)t$, then the in phase output will be $E_{ip} = E_0\cos\phi$ and the quadrature output $E_q = E_0\sin\phi$. The amplitude and phase of the received signal at any time t may be calculated from the expressions:
$E_0=[E_{ip}^2(t)+E_q^2(t)]^{\frac{1}{2}}$ and $\phi=\tan^{-1}E_q(t)/E_{ip}(t)$.

2.5 <u>Data acquisition and Recording.</u>

Figure 2.16 shows a block diagram of the data logging system used in the PRW experiment. For every transmitted pulse, 20 digitized complex values of the returned signal were obtained from each of the 3 receivers. These 3 groups of 20 values correspond to the signals returned from evenly spaced (2 km) intervals within the designated height range. These data were stored temporarily in the buffer memories. The digitizer control then passed these values to the accumulating microprocessor, where the results from 8 consecutive pulses were coherently averaged. The coherently averaged information was stored in the dual memory and held there until 19.5 sec after the start of a 20 sec acquiring period. At this 19.5 sec
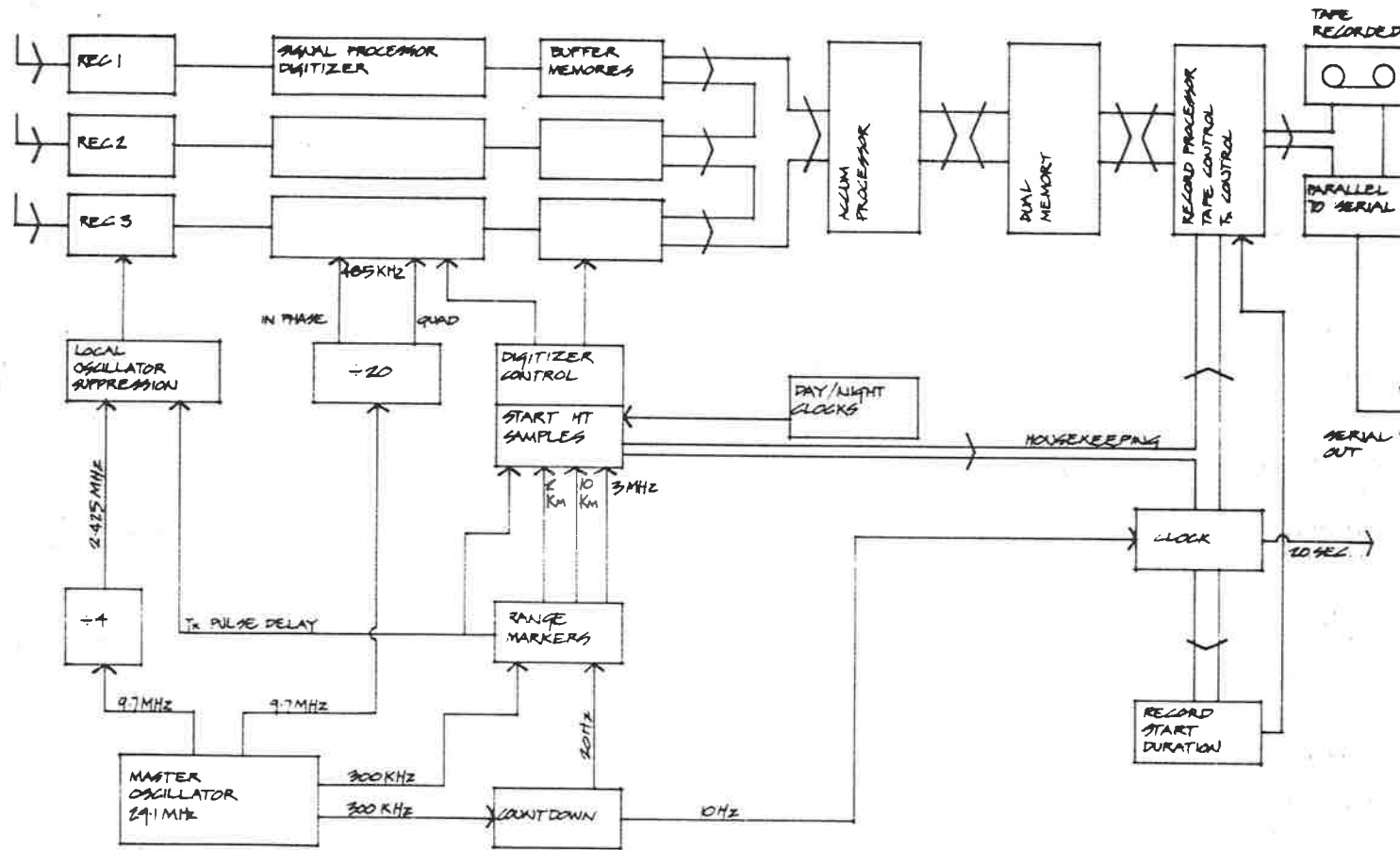
Figure 2.16   DATA LOGGER BLOCK DIAGRAM

mark, the information from the dual memory was passed to the recording microprocessor, from where the results were taken and written onto magnetic tape.

Data were written onto magnetic tape in 120 sec blocks. By coherently averaging 8 consecutive pulses (0.4 sec), 300 complex values of the returned signal were obtained for each height from each receiver for every 120 sec period. A typical data block contained first a time word and the number of height intervals (in this instance 20) being recorded. This housekeeping record was followed by the in-phase then quadrature information for receivers 1,2 and 3, for the lowest height level examined, then the same information for the subsequent height levels.

3 DATA ANALYSIS.

The PRW method for estimating mesospheric wind velocities was developed from the spaced antenna method for measuring winds in the ionosphere using total reflections (Mitra, 1949) in conjunction with studies made of partial reflections from the lower ionosphere (Gardner and Pawsey, 1953; Gregory, 1956, 1961). The first estimates of mesospheric wind velocities using this method were reported by Fraser (1965, 1968).

The so-called full correlation analysis was developed to include random changes in the irregularities as they moved (Briggs et al, 1950) and elongation of the diffraction pattern in a preferred direction (Phillips and Spencer, 1955). The method of analysis used in this thesis follows the work of Briggs (1984) and allows the use of any number of receiving aerials in arbitrary positions.

In the spaced antenna method, radiowaves are transmitted vertically and are reflected back by naturally occurring irregularities in refractive index in the 60 to 100 km range. Although variations in refractive index occur mostly in the vertical direction, horizontal variations modulate the incident radiation so that the reflected radiation may be treated as an angular spectrum of plane waves. Interference between these angular spectrum components forms a Fresnel diffraction pattern on the ground. The velocity of travel of this pattern across the ground, is twice the velocity of travel of irregularities at the height of reflection. (Felgate, 1970; Briggs, 1980).

Reflected radiowaves exhibit fluctuations in amplitude and phase which result from random internal motions and systematic drift of reflecting ionized irregularities. This radiowave fading (Gardner and Pawsey, 1953; Ratcliffe and Weekes, 1960) provides a means of identifying features within the diffraction pattern. If at least three spaced receiving antennae are used to record time histories of radiowave fading, the results can be used to estimate the horizontal velocity of the diffraction pattern and hence the horizontal velocity of the reflecting region.

Current spaced antenna systems at Adelaide are constructed so that the radiation transmitted is circularly polarized, either O-mode or E-mode. O-mode radiation is usually used during the daytime, for although the E-mode is more strongly reflected, it is also more strongly absorbed . At night, the observation of partially reflecting irregularities is usually restricted to altitudes in excess of 80 km (Vincent and Stubbs, 1977; Vincent and Ball, 1981), with the E-mode yielding the better results.

Observation has shown that in the region between 60 and 100 km, the movement of partially reflecting irregularities is indistinguishable from that of the neutral atmosphere (Vincent et al., 1977; Briggs, 1977). Wind measurements made using partial reflection techniques have recently been reviewed by Fraser (1984b).

In addition to the estimation of wind velocity, electron concentration in the D-region can also be estimated by the study of partial reflections; Gardner and Pawsey (1953) were the first to do so. By recording the partial reflections from alternate O-mode and E-mode pulses,

the electron density may be determined from the amplitude ratio of the two components in conjunction with an assumed collision frequency profile. In a similar manner, if the phases of the reflected O- and E-mode waves are measured as functions of height, electron density can be calculated from the phase differences between them. Partial reflection methods are suitable for electron density estimation in the altitude range 60 to 90 km under ideal conditions, but are subject to error due to off-vertical reflections. The determination of electron densities using partial reflection techniques and the limitations of the various methods are discussed by Manson and Meek (1984b).

Vertical drift velocities can also be estimated from partial reflection experiments if complex data are recorded. A vertical wind will produce a Doppler shifted spectrum of the signal received on the ground. Changes in the Fourier transform of the spectrum will be confined to phase changes. The vertical velocity can therefore be calculated from the slope of the phase of the autocorrelation function at zero lag. A narrow transmitted beam is essential for this purpose as contributions from scatterers moving horizontally at off-zenith angles will also affect the phase of the autocorrelation function. Details of this method are discussed by Murphy (1984).

In the following discussion, an account of the characteristics and the formation of partially reflecting irregularities will be presented. This is followed by an account of analytical methods used to estimate the apparent and 'true' velocities. In full correlation analysis, various diffraction pattern parameters are calculated in order to produce the

'true' velocities. Diffraction pattern parameters calculated from data obtained in the Antarctic are then compared and contrasted to the same parameters calculated from data obtained at Adelaide (mid-latitude) and Townsville (low latitude), in order to demonstrate the variation with latitude of the diffraction patterns formed by partially reflecting irregularities. The distribution of echoes observed and the average daily prevailing winds over the period of observation in the Antarctic are then presented. Incoherent averaging of the Mawson data was performed, in an attempt to extend the number of hourly wind estimates, and this is discussed next. Finally, average zonal and meridional wind profiles for the whole acquisition at Mawson, as obtained from the incoherently averaged results, are discussed.

3.1 Partial Reflections.

Partial reflections observed in the atmosphere may be up to 100dB weaker than the total reflections observed from the E and F layers (Belrose, 1970). Partial reflection of an electromagnetic wave occurs when the incident wave encounters a boundary between two regions of different refractive index whose thickness is less than one wavelength of the probing radiation (Gregory and Manson, 1969a; Briggs and Vincent; 1973). The characteristics of partial reflections observed therefore depend on the choice of probing frequency.

The relatively abrupt change in refractive index causing partial reflections is due to the presence of naturally occurring irregularities in the atmosphere. Irregularities in refractive index occur throughout the atmosphere due to fluctuations in the neutral air density, but in the

mesosphere, changes in refractive index are accentuated by the presence of free electrons (Briggs, 1980). A change in the electron concentration of a few percent between the irregularity and its surroundings within a distance of the order of the incident radio wavelength is sufficient to cause a partial reflection (Gregory and Manson, 1969a,b).

3.1.1 Characteristics.

For radio wave lengths of about 150m, at mid-latitudes, the angular distribution of reflected power from partially reflecting regions is found to differ significantly for altitudes below 80 km compared to those above (Hocking, 1979). Below 80 km, most reflected power is confined to off zenith angles less than $10°$, while above, the angular spread of returned power is consistently greater (Vincent and Belrose, 1978). Similar results have been obtained by Fukao et al. (1980), using a 50MHz VHF radar at Jicamarca, a low-latitude site. Some results from a high-latitude site (Thrane and Grandal, 1981; Thrane et al., 1981) imply however that scatter is isotropic in the region 65 to 95 km. These observations provide evidence that there is a wide variety in the spatial scales, and changes in the shape, of the partially reflecting irregularities with altitude and latitude.

Irregularities with the largest horizontal dimensions (1 km or more) occur at the lower altitudes, while at 95 km the horizontal scales of irregularities may be as small as the wavelength of the probing radiation (150m). The angular spread in returned power is related to the ratio between the horizontal and vertical dimensions of the irregularity (Vincent and Belrose, 1978). The larger this ratio, the narrower is the angular

spread. It is therefore inferred that irregularities below 80 km are therefore highly anisotropic, but less so above.

Studies of the angular spectra of partially reflected waves (Lindner, 1975a,b) show that in the region below 85 km, returned signals may exhibit some degree of phase coherence, but above, the spectra are characteristically random. Also, the vertical thickness of the partially reflecting regions is greater at higher altitudes (Gregory and Vincent, 1970) and therefore more likely to contain a greater number of independent reflected components.

Another indication of the change with height in the structure of partially reflecting irregularities may be gained by an examination of the fading of returned signals. Measurements of amplitude fading speeds, determined from mean intervals between amplitude maxima (Lindner, 1975b) show that the fading speed decreases with altitude. This is consistent with previous observations, in that longer period fading is identified with more coherent reflections than the shorter period fading expected for a more randomly phased model.

3.1.2 Formation.

Kent and Wright (1968) have reviewed the movements of ionospheric irregularities and the mechanisms most likely to produce them. Their conclusions were that irregularities produced in the D and lower E regions are due to, turbulence, meteor ionization, particle precipitation at high latitudes, and gravity wave action.

Gregory et al (1982) have shown that particle precipitation during magnetic storms and auroral events produces an increase in ionization at lower altitudes and a corresponding increase in the number of observable partial reflections.

Rottger (1980) has discussed the reflection and scattering of VHF radar signals from atmospheric refractivity structures and has concluded that reflection from refractivity laminae corrugated by turbulence appears to be an appropriate model for many observations.

Hodges (1967) has shown that temperature fluctuations associated with gravity waves are often of sufficient amplitude to produce convective instabilities in thin layers that propagate with the waves.

Fritts (1978) has examined the non-linear interaction between gravity waves and critical layers and concludes that this interaction can explain some of the thin turbulent layers observed in the atmosphere. The critical level-gravity wave interaction (Fritts, 1979) and regions of unstable velocity shear (Fritts, 1984) both provide further sources of radiating gravity waves.

Calculations made by Lindzen (1981) show that turbulence is likely to result from the breakdown of unstable tides and gravity waves, with the largest contributions coming from the main propagating diurnal mode at tropical latitudes, and gravity waves at higher latitudes. Convectively stable internal waves may also generate turbulence by a cascade process where shorter wavelength unstable waves are generated from the original stable wave (Lindzen and Forbes, 1983).

Turbulence, acting in a gradient in electron concentration, accounts for many of the observed features of partial reflections. Turbulence tends to mix thoroughly the medium in which it acts so that the density becomes uniform throughout. If a horizontal layer of intense turbulence is present in a region containing a gradient in electron density, there will be sharp steps in that gradient at the top and bottom of the turbulent layer. These sharp steps will give rise to partial reflections. This model was proposed by Bolgiano (1968).

Bolgiano points out that the thickness of the boundary between the turbulent layer and the surrounding medium occurs in a distance comparable to the Kolmogŏrov inner scale of turbulence, whereas the undulating structure of the surface reflects principally the scale of the energy bearing ~~containing the~~ eddies. These two scales are normally widely separated in high intensity turbulence, so that a discontinuity structure in which irregular, wave-like variations in surface altitude have a wavelength very much larger than the thickness of the transition region may be anticipated. This model seems appropriate for partially reflecting irregularities below 80 km.

One feature of partial reflections which has been reported by many authors (e.g. Gregory, 1961; Schlegel et al., 1978; Fukao et al., 1980; Vincent and Ball, 1981; Hocking and Vincent, 1982a, b), is the tendency for radiowave scattering to occur at 'preferred' heights. In simultaneous experiments which measured the fine structure of the electron density and the strength of partial reflections at a mid-latitude site, Hocking and Vincent (1982a) concluded that near 80 km, partial reflections

were related to a small ledge of decreasing electron density; at about 85 km, scatter was probably due to a combination of horizontally stratified steps in electron density or electron density gradient and turbulence, and that in the region 92 to 94 km, echoes appeared to be related to an irregular region of electron density fluctuation.

In summary, it may be said that the characteristics of partial reflections observed throughout the 60 to 100 km altitude range vary broadly from specular-like reflections with long fading times from structures of large horizontal extent near 60 km to more diffuse reflections with shorter fading times above 80 km. It seems probable that this variation is related more to the stability of the background atmosphere rather than specific irregularity producing mechanisms. For example, the changes in lapse rate which occur near the mesopause (at 90 km in figure 1.1) are probably responsible for the larger number of partial reflections generally observed at that level. Hocking (1981) has discussed the production of partially reflecting irregularities in detail, and has pointed out that turbulence generated in a region of high stability (below 80 km) is likely to form thin turbulent sheets of relatively long duration, whereas turbulence generated by the same processes acting in a region of low stability (above 80 km) will produce reflecting structures which are much more quickly dispersed.

The most likely processes responsible for the type of irregularities observed in the spaced antenna method are dissipative atmospheric wave processes; some evidence for correlation between scattered VHF power and gravity wave activity has been presented by Harper and

Woodman (1977), and Miller et al. (1978). These processes include; filtering of short vertical wavelength waves at low altitudes (Hines and Reddy, 1967), critical level interactions, generation of waves in situ and wavebreaking.

Hocking (1981) has proposed that the wind jet observed just above 70 km at Adelaide may be related to scatterers at this height, because, for upward propagating gravity waves, an interaction with this jet would be the first encounter with wind speeds greater than 50 ms^{-1}, so critical level effects are possible. Teitelbaum and Sidi (1976) and Sidi and Teitelbaum (1978) have suggested that the non-linear interaction between gravity waves and tides can produce large wind shears at heights above 90 km, which in turn can lead to the production of turbulence. Also, between 85 and 90 km, large phase changes in tides (Elford and Craig, 1980) sometimes occur which could lead to the production of turbulence. Either or both of these latter processes could be of significance with regard to the preference of echoes to occur close to 90 km.

In the averaged results to be presented for the Antarctic (figure 3.12) a broad westward jet is observed between 70 and 90 km and maximum meridional winds of less than 10 ms^{-1} occur near 90 km, close to the height where the maximum numbers of acceptable echoes occur (see figures 3.7 and 3.11). The preference of echoes to occur near 70 km at Adelaide is not evident in the Antarctic results. Also due to particle precipitation associated with auroral activity at high latitudes, increased electron concentrations are likely to produce a corresponding increase in observed echoes (Gregory et al., 1982) at lower altitudes, although under the same

conditions, there is likely to be a decrease in the echo rate at higher altitudes due to increased absorption.
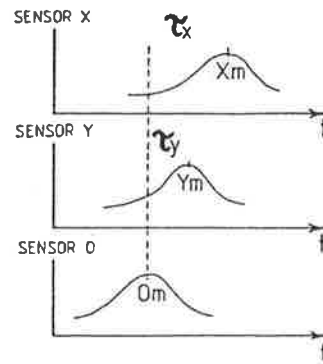
3.2 Velocity Estimation.

For simplicity the following discussion assumes that sensors form the vertices of a right angled triangle. The diffraction pattern is conveniently represented by contours of the intensity of the radiation forming the pattern. Figure 3.1(a) represents the intensity contours of an idealized diffraction pattern moving in the direction indicated at a constant speed V. If the pattern moves without change of shape, the outputs from the sensors will look like those sketched in figure 3.1(b).

The line joining X_m, O_m and Y_m, the line of maximum, may approximated as a straight line if the pattern size is large compared to the spacing of the sensors. It will also tend to be perpendicular to the direction of motion on average, exactly so if the contours are circular. This line of maximum enables a common feature to be identified in the records from each sensor. Figure 3.1(a) has been simplified to figure 3.1(c) for the purpose of velocity estimation.

From figure 3.1(c) the time differences t_x and t_y can be calculated, they are, $t_x = \xi_0 \cos\theta / V$, and $t_y = \eta_0 \sin\theta / V$. The velocities at which the line of maximum travels to X and Y from O are V_x and V_y where, $V_x = \xi_0 / t_x = V / \cos\theta$, and $V_y = \eta_0 / t_y = V / \sin\theta$. V_x and V_y are not components of V. To obtain V, the geometrical construction shown in figure 3.1(d) is used. Calculated in this fashion, V is known as the 'apparent' velocity.
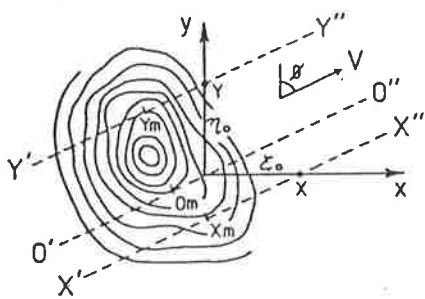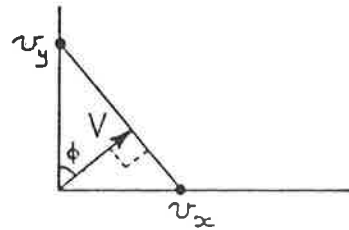
(a) Idealized diffraction pattern.

(b) Output from sensors at O, X, Y.
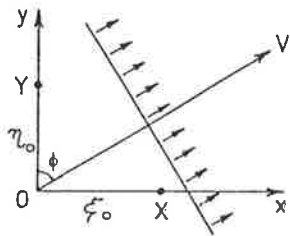
(c) Line of maximum.

(d) Calculation of apparent velocity.

Figure 3.1

3.2.1 'True' Velocity

A more realistic pattern which moves and evolves in time is represented by figure 3.2(a). The magnitude of the apparent velocity estimated by the time shift method is too large if the pattern is subject to random change, and the calculated direction of motion may be in error if the pattern is systematically elongated in a particular direction.

The complex correlation function, $\rho(\xi,\eta,\tau)$ can be expressed as

$$\rho(\xi,\eta,\tau) = \frac{<E(x,y,t).E^*(x+\xi),(y+\eta),(t+\tau)> - <E(x,y,t)>^2}{<E(x,y,t).E^*(x,y,t)> - <E(x,y,t)>^2}$$

Where ξ and η are spatial shifts in the x and y directions and τ is a temporal shift in the t direction. E is the complex amplitude of the reflected signal. The brackets (<>) indicate an average and the asterisk denotes a complex conjugate.

In full correlation analysis, a quadratic function is used to describe correlation functions near correlation maxima if the signal is continuous and a smoothly varying function of x, y, and t. The contours of constant correlation are assumed to be ellipsoidal in (ξ,η,τ) space as shown in figure 3.2(b). $\rho(\xi,\eta,\tau)$ is of the form:
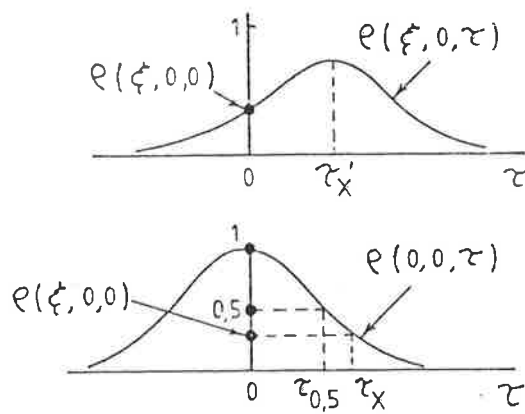
$$\rho(\xi,\eta,\tau) = \rho(A\xi^2+B\eta^2+C\tau^2+2F\xi\tau+2G\eta\tau+2H\xi\eta) \qquad 3.1$$

To obtain the velocity of a pattern, two independent components are needed, so a minimum of three sensors is required. Experimental observations are used to determine the functional form of ρ and the values of the coefficients A, B, C, F, G and H.
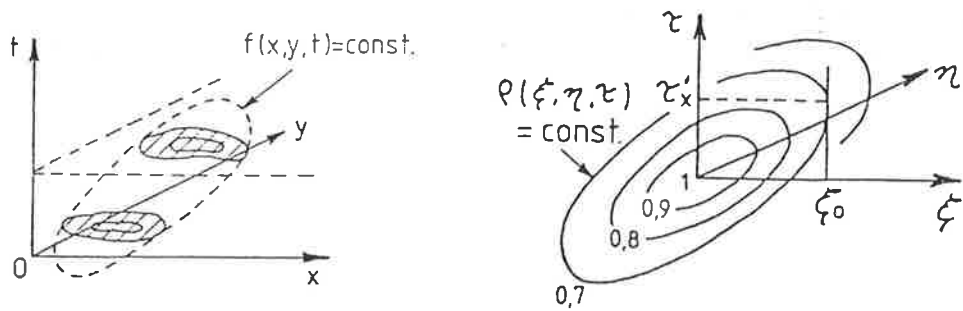
(a) Moving evolving
    diffraction pattern.

(b) Contours of
    constant correlation.

(c) Correlation functions.

Figure 3.2

Consider a cross correlation function for the pair of sensors on the x axis: a maximum in the correlation function would be expected for a specific time shift, say τ_x in figure 3.1(b). This function can be obtained from equation 3.1 by the substitutions $\xi = \xi_0$, $\eta = 0$, so that,

$$\rho(\xi_0, 0, \tau) = \rho(A\xi^2 + C\tau^2 + 2F\xi_0\tau).$$

The maximum is found by setting $\partial\rho/\partial\tau = 0$, which gives

$$\tau'_x = -\frac{F}{C}\xi_0.$$

Similarly, for sensors in the y direction separated by η_0, the time lag for maximum correlation (τ'_y) is given by

$$\tau'_y = -\frac{G}{C}\eta_0.$$

The mean auto correlation function is used to proceed further. Ideally, the auto correlation functions for each sensor should be identical, but in practice statistical errors produce differences. The mean auto correlation function of the sensors is equated to the theoretical auto correlation function, $\rho(0, 0, \tau)$, obtained from equation 3.1.

From figure 3.2(c), the correlation coefficient between the sensors, $\rho(\xi_0, 0, 0)$ can be measured, as can the time shift (τx) at which the auto correlation function has the same value. Mathematically, τx satisfies the equation

$$\rho(\xi_0, 0, 0) = \rho(0, 0, \tau x).$$

Using equation 3.1 this may be expressed as

$$\rho(A\xi^2) = \rho(C\tau^2), \text{ so that,}$$

$$A/C = \tau^2 x / \xi_0^2.$$

In the same manner the sensors on the y axis can be used to find τy and so yield

$$B/_C = \tau^2 y /_{\eta_0{}^2}.$$

For zero time shift, the cross correlation between the pair of sensors situated at $(\xi_0, 0)$ and $(0, \eta_0)$ is

$$\rho(\xi_0, \eta_0, 0) = \rho(A\xi_0{}^2 + B\eta_0{}^2 + 2H\xi_0\eta_0).$$

The auto correlation function takes the same value for a time shift τxy given by

$$\rho(A\xi_0{}^2 + B\eta_0{}^2 + 2H\xi_0\eta_0) = \rho(C\tau^2 xy).$$

Which gives

$$H/_C = \tau^2 xy /_{2\xi_0\eta_0} - A\xi_0 /_{2C\eta_0} - B\eta_0 /_{2C\xi_0}.$$

The velocity of the pattern can now be calculated. To do so it is convenient to consider an observer moving with the pattern. Under these conditions, the pattern appears to only change randomly. If the coordinates (x', y', t') are used for the moving observer, the pattern is represented by $E(x', y', t')$ and the correlation function is

$$\rho(\xi', \eta', \tau) = \rho(A\xi'^2 + B\eta'^2 + K\tau^2 + 2H\xi'\eta') \qquad\qquad 3.2$$

The coordinates of a stationary observer who records the same pattern $E(x, y, t)$ are related to those of the moving observer by the equations

$$x = x' + Vt\sin\phi = x' + V_x t$$

and

$$y = y' + Vt\cos\phi = y' + V_y t.$$

Where $V_x = V\sin\phi$ and $V_y = V\cos\phi$ are components of motion of the pattern. Also, $\xi = \xi' + V_x\tau$ and $\eta = \eta' + V_y\tau$. Substitution into equation 3.2 yields

$$\rho(\xi,\eta,\tau) = \rho(A(\xi-V_x\tau)^2 + B(\eta-V_y\tau)^2 + 2H(\xi-V_x\tau)(\eta-V_y\tau)) \qquad 3.3$$

Equating coefficients of $\xi\tau$ and $\eta\tau$ in equations 3.1 and 3.3, the equations

$$AV_x + HV_y = -F \qquad\qquad 3.4$$

and

$$BV_y + HV_x = -G \qquad\qquad 3.5$$

are obtained.

If equations 3.4 and 3.5 are divided through by C, a pair of simultaneous equations for V_x and V_y are obtained in which the coefficients $A/_C$, $H/_C$, $F/_C$, $B/_C$, $G/_C$ are known. Thus V_x and V_y can be found.

V_x and V_y are true components of the velocity V. The magnitude and direction of V are given by $|V|^2 = V_x^2 + V_y^2$ and $\tan\phi = V_x/_{V_y}$.

The velocity V determined in this way is known as the "true" drift velocity, as distinguished from the apparent drift velocity derived from mean time shifts, and has been corrected for pattern anisometry and

random change. Both the "apparent" velocity and the "true" velocity refer to the velocity at which the diffraction pattern, formed by the reflection from ionospheric irregularities, passes over the ground. In order to find the "apparent" and "true " drift velocities of the irregularities at the height of reflection , the velocities calculated for the diffraction pattern must be divided by a factor of 2.

The "true" drift velocity, interpreted as a measure of wind velocity, may still be in error as the corrections used in its derivation involve assumptions which may be invalid in practice. If possible, comparisons with more direct methods of determining wind velocity are advisable. The limitations of full correlation analysis, sources of error and rejection criteria for data are discussed by Briggs (1984).

3.3 Diffraction Pattern Parameters.

While the type of equipment described in the previous section has been used at various sites throughout Australia, it had not been used to study the Antarctic mesosphere prior to 1981. As the same equipment had been used prior to 1981 in Townsville, it is of interest to compare the characteristics of fading pattern at both sites as a comparative guide to the performance of the equipment in the Antarctic. Of more significance, is a comparison of these characteristics between Townsville, Adelaide and Mawson, which will provide insight into the southern latitudinal variation of several important parameters measured by the PRW method. Townsville and Adelaide results presented by Ball (1983) will be used for comparison in this discussion.

3.3.1 Pattern Scale and Pattern Elongation.

In addition to the determination of drift velocities, full correlation analysis also allows various physical characteristics of the diffraction pattern formed by the reflection of transmitted radio waves from ionized irregularities to be estimated. From full correlation analysis, it has been shown that the contours of constant correlation of observed diffraction patterns, suitable for drift velocity estimations, are concentric ellipses, which can be represented by equation 3.1. The spatial correlation function derived from this expression is given by

$$\rho(\xi,\eta,0) = \rho(A\xi^2 + B\eta^2 + 2H\xi\eta) \qquad\qquad 3.6$$

The 'characteristic' ellipse is defined as that particular ellipse for which $\rho=0.5$, so that equation 3.1 can be written as

$$\rho(A\xi^2 + B\eta^2 + 2H\xi\eta) = 0.5. \qquad\qquad 3.7$$

The fading time, $\tau_{0.5}$, is defined as the time lag for which the auto-correlation function for a stationary observer falls to 0.5 and is given by

$$\rho(0,0,\tau_{0.5}) = \rho(C\tau^2_{0.5}) \qquad\qquad 3.8$$

Combining 7 and 8 gives the general equation for the 'characteristic' ellipse:

$$A\xi^2 + B\eta^2 + 2H\xi\eta = C\tau^2_{0.5}. \qquad\qquad 3.9$$

If a and b are taken to be the semi-minor and semi-major axes respectively, then

$$a^2 = 2C\tau^2_{0.5}/[(A+B)+(4H^2+(A-B)^2)^{\frac{1}{2}}]$$

and

$$b^2 = 2C\tau^2_{0.5}/[(A+B)-(4H^2+(A-B)^2)^{\frac{1}{2}}].$$

The pattern scale is defined as $\sqrt{ab}$, and the pattern elongation, or axial ratio, is $r = {}^b/_a$. The pattern orientation is the angle between true north and the major axis of the 'characteristic' ellipse measured in a clockwise direction.

3.3.2 $T_{0.5}$ and V_0.

Other parameters of interest, associated with the random changes of a diffraction pattern, are the 'characteristic' fading time, $T_{0.5}$, and the RMS random velocity, V_0. For an observer moving with the pattern, the only changes observed are those due to random fading. The auto-correlation function associated with a moving observer is given by equation 3.2.

The 'characteristic' fading time is defined as the width of this function when $\rho = 0.5$, i.e.

$$\rho(0,0,T_{0.5}) = \rho(KT^2_{0.5}) \qquad\qquad 3.10$$

Comparing equations 3.8 and 3.10, the relationship $T_{0.5} = \tau_{0.5}({}^C/_K)^{\frac{1}{2}}$ is obtained. The coefficient ${}^C/_K$ can be obtained by equating terms of τ^2 in equations 3.1 and 3.3.

V_0 is calculated from the relationship

$$V_0 = \frac{\lambda(\ln 2)^{\frac{1}{2}}}{4\pi T_{0.5}} \quad \text{(Booker et al., 1950).}$$

3.3.3 Latitudinal Variation.

Figures 3.3(a), 3.3(b) and 3.3(c) show the variation in pattern scale ($\sqrt{ab}$), pattern elongation (r) and characteristic fading time ($T_{0.5}$) with altitude for Townsville, Adelaide and Mawson. This is figure 4.12(a) from Ball (1983) with Mawson values included. The Townsville and Adelaide results were obtained during January of 1980 (southern hemisphere summer) and the Mawson results were for the same season in 1981/1982. The values of pattern scale for Mawson have been divided by a factor of $\sqrt{2}$; this has been done to allow direct comparison with Ball's results which included both complex and amplitude only data, but were scaled for amplitude only data.

Ball (1983) has pointed out that comparisons between Townsville and Adelaide results must be done cautiously as the widths of the receiving beams at these sites were different (the Townsville receiving beam was broader). The ground diffraction pattern parameters depend on the range of angles over which the scatterers contribute to the received signal. The larger the range of angles over which signals are received, the smaller will be the scale of diffraction patterns observed on the ground, with subsequent effects on the various parameters. In the ideal situation where V_0 is isotropic, $T_{0.5}$ will not be affected by the receiving beam width. The widths of receiving beams at Townsville and Mawson were very similar.

Before discussing the results shown in figure 3.3, it must be stressed that because of the smaller data rate associated with the Antarctic results below 80 km, it is possible that they may be biased, and not entirely representative of typical atmospheric behaviour. Figure 3.3(a)
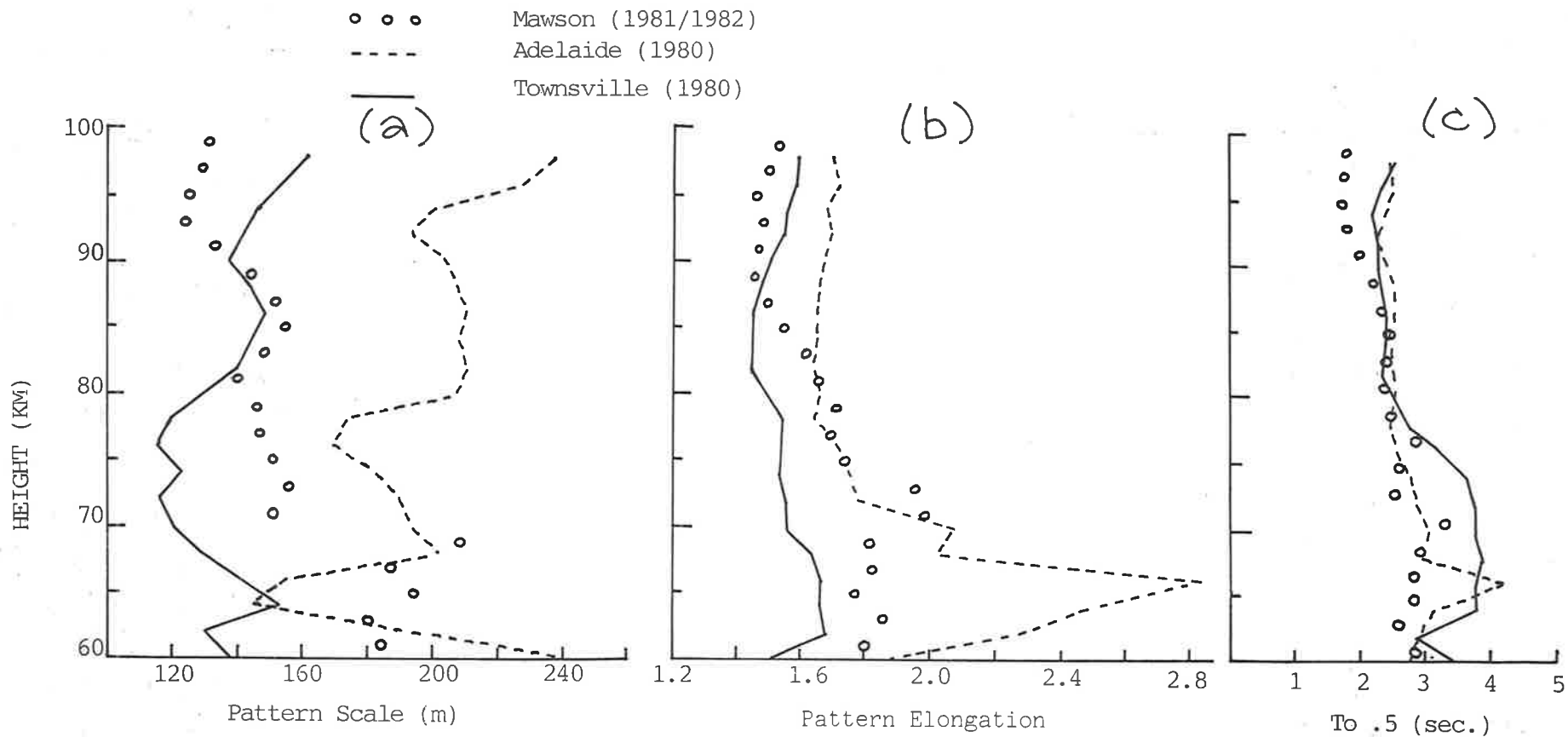
Figure 3.3   Height variation in the ground diffraction parameters at Adelaide and Townsville for January 1980 (Ball, 1981) and Mawson for summer 1981/82.

shows the variation with altitude of pattern scale for Townsville, Adelaide and Mawson. Below 70 km, the figure shows that pattern scales at Mawson tend to be large and of the same order as those observed at Adelaide. Between 70 and 80 km pattern scales at Mawson decrease, until near 80 km, the scales are of the same order as those observed at Townsville. Above 90 km, pattern scales at Mawson are smaller than those observed at other latitudes.

An important feature of figure 3.3(a) is that pattern scales at Mawson appear to decrease from about 200m near 65 km to about 120m at 92 km. Between 70 and 90km, the pattern scales are very close to the spacing of the receiving dipoles. This is fortunate, as Rossiter (1970) (using amplitude only data) concluded that the most accurate and reliable measurements of drift velocity are obtained when the triangle size is comparable to the scale of the diffraction pattern. This is in contrast to the other results which show a decrease in pattern scale between about 65 and 75 km, then an overall increase above. There are local maxima near 85 km and local minima near 90 km at all latitudes.

Figure 3.3(b) shows the distribution of pattern elongation with altitude for the three sites. Below about 75 km, pattern elongations at Mawson are intermediate between those at the other sites, with values of about 1.8 up to 70 km and a possible maximum near 72 km. Between 80 and 90 km the pattern elongation at Mawson decreases, in contrast to the other results, from 1.7 to about 1.4. Above 90 km, pattern elongations at Mawson are smaller than those observed at the other sites.

At Townsville and Adelaide, pattern elongations maintain an almost constant difference of about 0.3 above 72 km. At Mawson this trend was absent.

From figure 3.3(c), it can be seen that below 80 km the values of $T_{0.5}$ observed at Mawson are more similar to those observed at Adelaide than those observed at Townsville. Above about 85 km, the values of $T_{0.5}$ observed at Mawson are smaller than those observed at the other sites. Manson and Meek, (1980) have reported fading times of 1.5-3.0 s at Saskatoon (52°), in good accord with the results presented here for Mawson.

3.3.4 Orientation.

In figure 3.4, the area under each histogram has been scaled to a value of one. The height of each column is therefore a measure of the proportion of the of diffraction patterns that have a particular orientation. This figure has been adapted from figure 4.12(f) of Ball (1983), who presented the results for Adelaide and Townsville. Except for one difference, the results from Mawson were prepared in the same manner as those of Ball for ease of comparison. The difference between the results of Ball and those presented for Mawson is that Ball calculated the orientation of the irregularities with respect to magnetic north, whereas the orientations calculated for Mawson are with respect to geographic north. This has little effect at Adelaide or Townsville, but is significant at Mawson. For the Mawson data, values of pattern orientation were initially sorted into twelve groups 15° wide for each 2 km height band. Four lots of results from three adjacent height bands (76-78-80, 82-84-86, 88-90-92, 94-96-98) were then used to produce the histograms shown in figure 3.4.
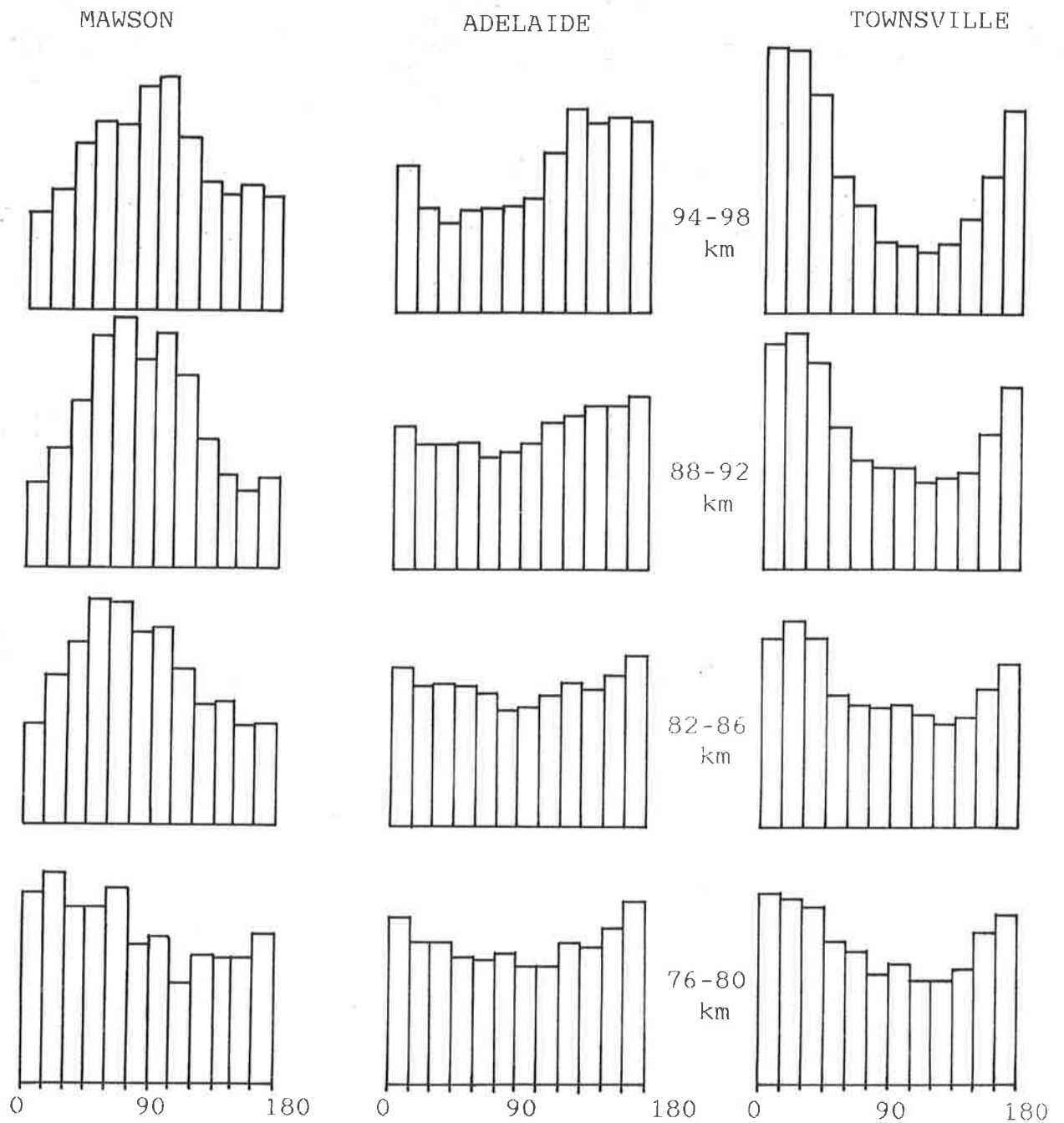
Figure 3.4   Orientation of the ground diffraction pattern
with respect to magnetic north for Townsville
and Adelaide (Ball, 1983) and with respect to
geographic north for Mawson.

The variation in pattern orientation with latitude as shown in figure 3.4 is striking. The results show that on the whole, above 80 km, the patterns observed at Mawson tend to be elongated in the east-west direction. A similar effect has been noted by Maehlum (1962) for the drift pattern irregularities of sporadic-E measured by the spaced receiver experiment at Tromso (69.99°N,18.94°E). Patterns observed at Adelaide are oriented between the extremes exhibited at low and high latitudes, with a more Townsville-like orientation at the highest levels.

3.3.5 Diurnal Variation.

Figures 3.5(a)-(d) show the diurnal variation of RMS velocity, V_0, pattern scale, pattern elongation and 'characteristic' fading time, $T_{0.5}$, for three height bands between 80 and 92 km. All relevant data taken at Mawson were used in the construction of these figures and each height band represents the average of results from adjacent 2 km layers (80-82, 84-86, 90-92).

The most significant departures from orderly behaviour occur at the highest level (90-92 km), for the values of RMS velocity (figure 3.5(a)), pattern scale (figure 3.5(b)) and $T_{0.5}$ (figure 3.5(d)). Figure 3.5(a) shows large fluctuations in RMS velocity at this level, from a value of approximately 3.5 ms^{-1} at 0700 hrs to about 8.5ms^{-1} at 1000 hrs local time, decreasing to a mean value of about 6ms^{-1} by 1400 hrs local time. The pattern scale at this level decreases from about 240 m at 0700 hrs to about 160 m at 1400 hrs and then increases to about 200 m by 2200 hrs. A maximum in $T_{0.5}$ at the 90-92 km level of 2.9 sec at 0700 hrs is followed by a minimum of 1.3 sec at 1000 hrs. From 1000hrs until 2300 hrs, the value of $T_{0.5}$ increases from 1.3 sec to a value near 2.0 sec.
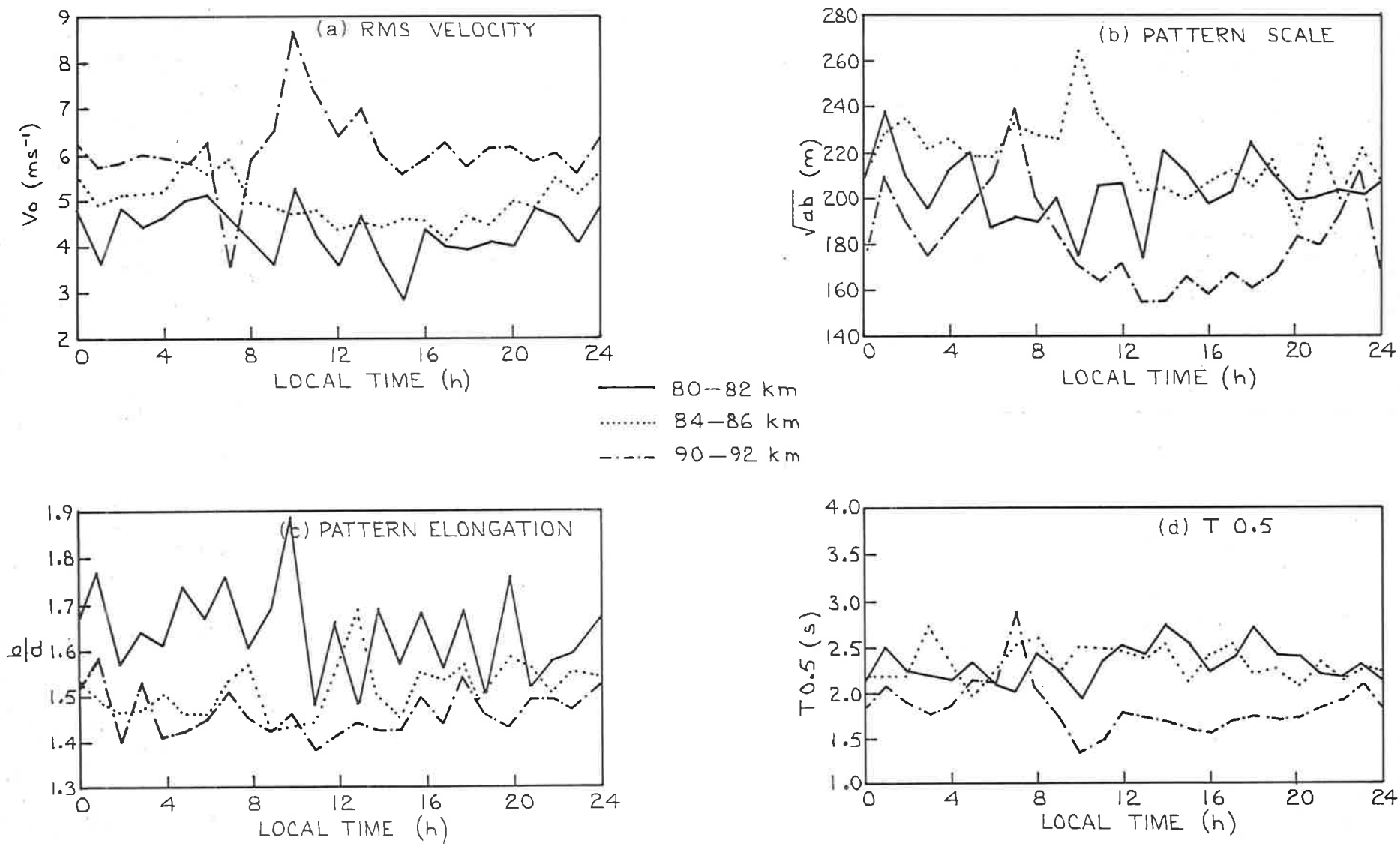
Figure 3.5   Diurnal variation of observed diffraction pattern parameters.

It is of interest to view these results bearing in mind the time Mawson spends inside the auroral oval. This time increases with geomagnetic activity, but for minimum activity, it is between 2200 hrs and 0200 hrs local time (Kilfoyle and Jacka, 1968). The diurnal behaviour of the diffraction pattern parameters at the 90-92 km level may then be interpreted as arising from three periods of differing influence: a relatively ordered period when the partially reflecting irregularities are dominated by effects in the auroral zone, which last until a few hours after the passage of the auroral zone, a disordered period between about 0700 hrs and 1200 hrs, when there is no dominant control, and finally a period from about 1200 hrs to 2200 hrs, when the irregularities are under the control of more normal atmospheric processes.

3.4 Data.

The performance of the system at Mawson was poorer than that at Townsville due to a slightly broader beam (the transmitting towers were fixed at a lower height) and the use of single receiving dipoles at each receiving site, rather than the crossed pairs of dipoles used at Townsville. The first results were obtained on 29/Oct/81, more than 8 months after landing at Mawson, although this was not confirmed until some months later, when a thorough analysis could be undertaken in Adelaide. Facilities were not available in the Antarctic to replay or analyse the recorded data.

Initially, the system ran from 29/Oct/81 until 4/Nov/81, at which time some inadequacies in the equipment installed outside and electronic problems became manifest. Problems with the outside equipment were minor,

but electronic problems kept the system out of commission until 13/Dec/81. From that time until 3/Feb/82 data were recorded daily. During the period from 13/Dec/81 until 3/Feb/82, damage to the equipment from the elements and heavy machinery was common. Constant attention at all times, in sometimes atrocious weather conditions, was necessary to keep the system running. Figure 3.6 shows the height range observed during the period of observation at Mawson.

3.4.1 Height Distribution of Usable Echoes.

Figure 3.7 shows the number of echoes accepted for drift estimation in each 2 km height band for each hour expressed as a percentage of the total number of accepted echoes in each 2 km height band from 60 to 100 km This echo distribution is similar to that presented by Fraser (1984a) for Scott base. At mid- and low latitude sites, a secondary maximum in echo distribution is often observed below 80 km (Ball, 1983; Vincent, 1984b). No such maximum has been reported for Antarctic observations to date. Ecklund and Balsley, (1981) have found that mesospheric echoes show a marked seasonal variability, in which echoes observed with a 50Mhz MST radar occur in the height range 80 to 100 km in summer and between 55 and 80 km at other times. Figure 3.8 shows the percentage of usable echoes obtained during each hour of the day for each 2 km height band from 60 to 100 km in altitude for all the data gathered during the 1981/1982 Antarctic summer. One feature of figure 3.8 is the orderly pattern of the profiles above 80 km compared to those below. Data for all heights below 80 km represents less than 20% of the total and is much more likely to suffer from statistical variations. In addition, the region below 80 km produces most results during geomagnetically active

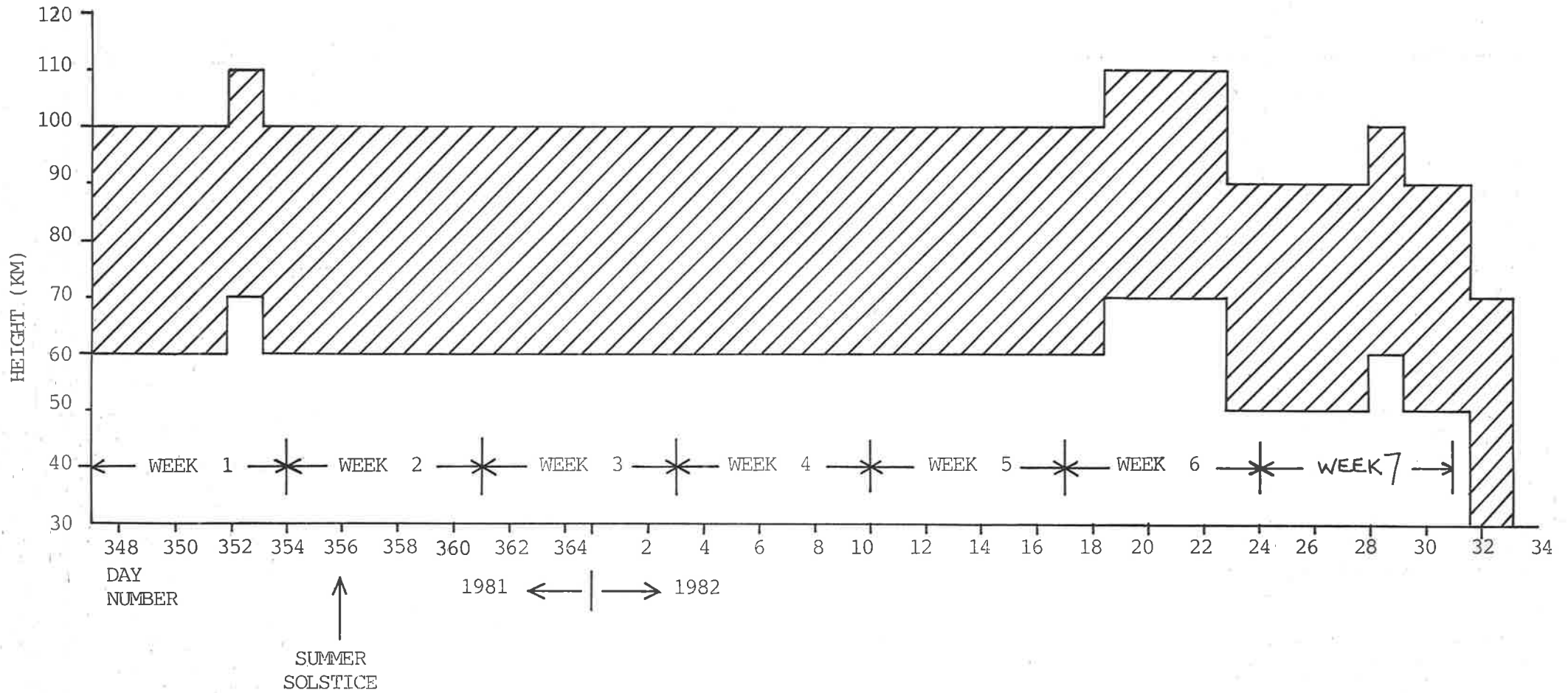Figure 3.6.   Height range covered during the period of observation at Mawson.
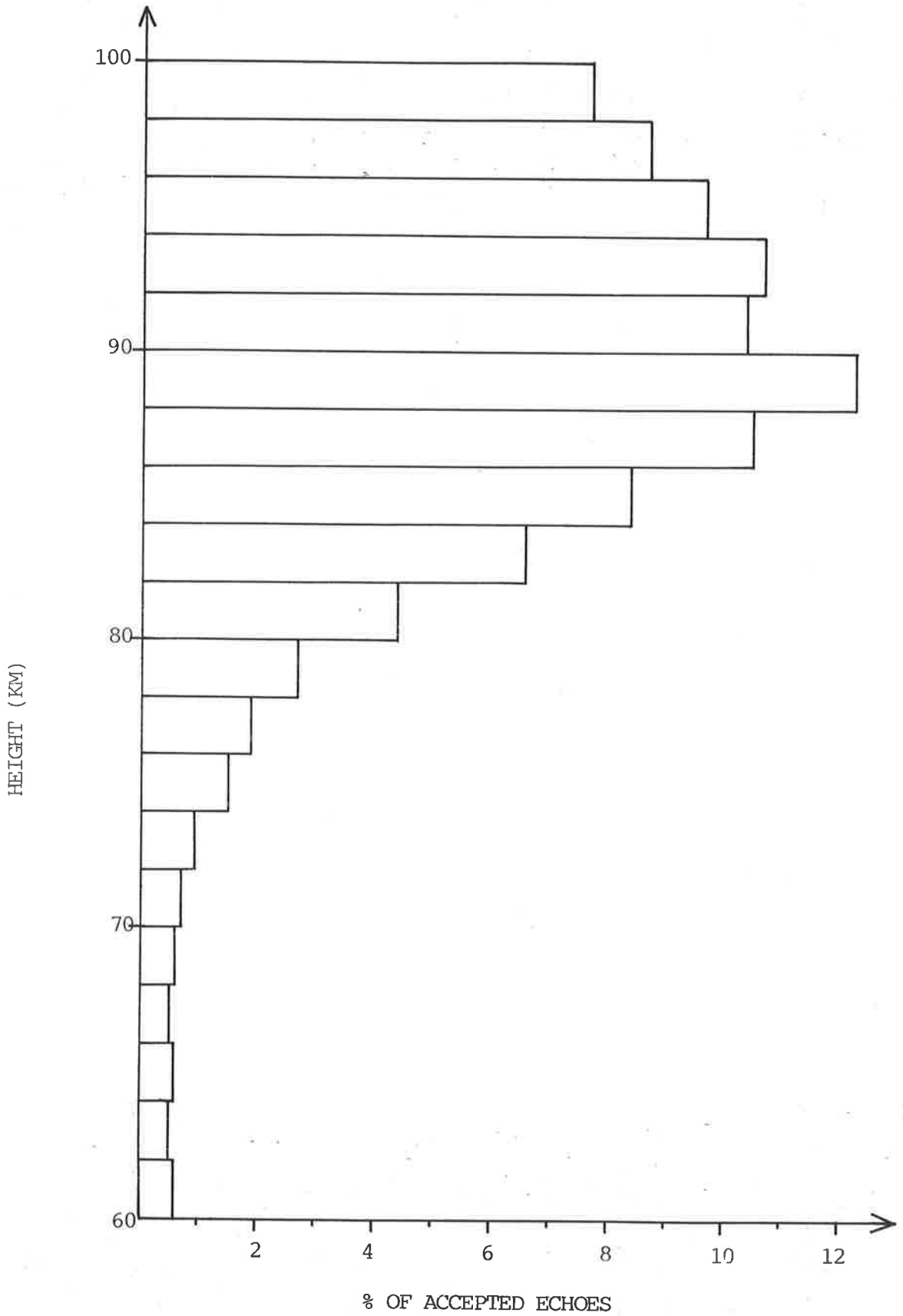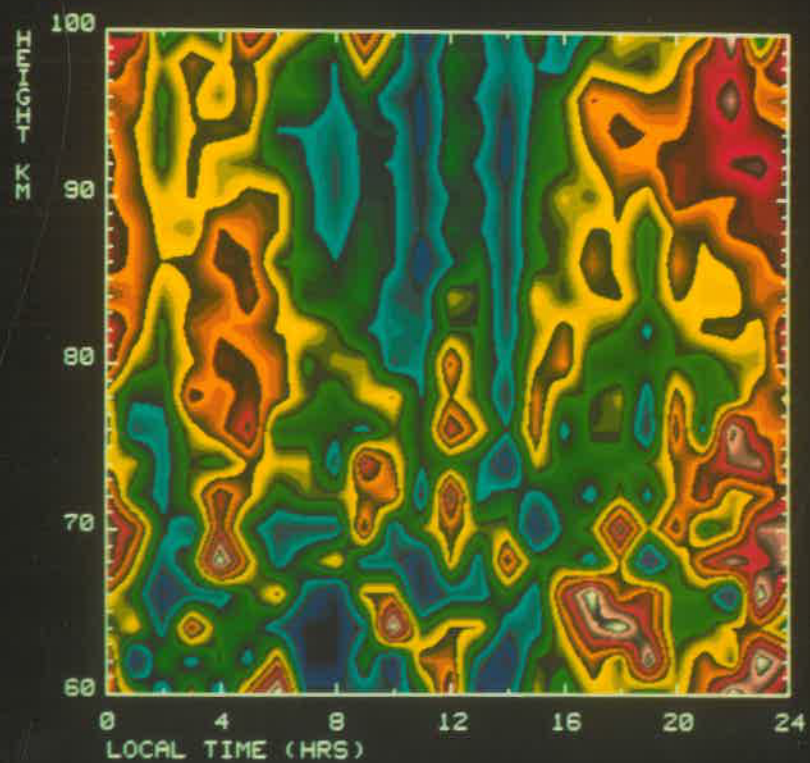
Figure 3.7.   Accepted echo distribution from Full Correlation Analysis (FCA).

Figure 3.8 The percentage of usable echoes obtained during each hour of the day for each 2 km height band from 60 to 100 km in altitude for all data gathered during the 1981/82 Antarctic summer.

ECHO DISTRIBUTION   13/12/85

conditions when the ionization source is much more variable than that produced by solar electromagnetic radiation.

3.4.2 Daily Variation of Echo Distribution.

One feature of figure 3.8 is of particular interest, and that is the distribution of echoes during the time that Mawson spends inside the auroral oval. For minimum geomagnetic activity, the auroral oval is generally directly overhead at Mawson between 2200 hrs and 0200 hrs local time (Kilfoyle and Jacka, 1968). From figure 3.8 it can be seen that there is a maximum in the relative number of accepted echoes during this time. There are also definite minima approximately 3 hours either side of local noon at all heights above about 70 km. Gregory et al. (1982) have noted an increase in the ionization at low heights during the night at Saskatoon, which is on the edge of the Northern auroral oval.

3.4.3 Prevailing Winds (Hourly Averages).

Figures 3.9 and 3.10 have been produced by averaging all available data in each 2 km height band from 70 km to 100 km for each hour of the day. The resulting 'snapshots' are therefore void of any short-term variability, and are indicative of the daily variation in the underlying prevailing wind systems during the observation period.

Figure 3.9 shows that the zonal flow is mainly eastward between 70 and 75 km throughout the day. There is a strong westward component for most of the day between approximately 78 and 90 km, maximizing near 78 km at 0400 hrs LT (Local Time), although there is a weakening of this flow between 1800 and 2000 hrs LT, close to the time Mawson enters the auroral oval. Above 90 km, there are two periods of westward winds centred near

Figure 3.9   Mean daily variation of hourly averaged zonal
             prevailing winds in the altitude range 70 to 100 km
             during the period of observation.
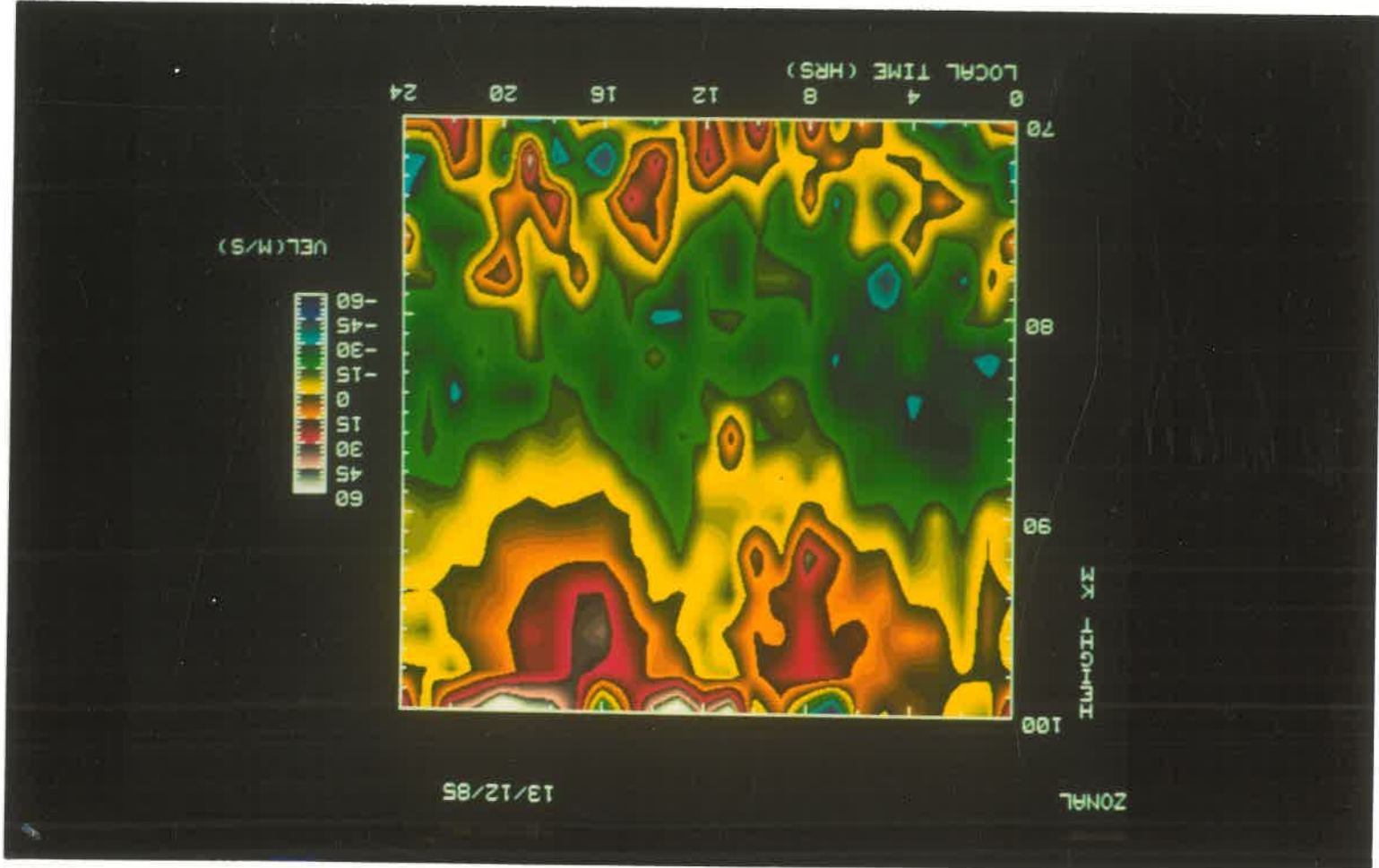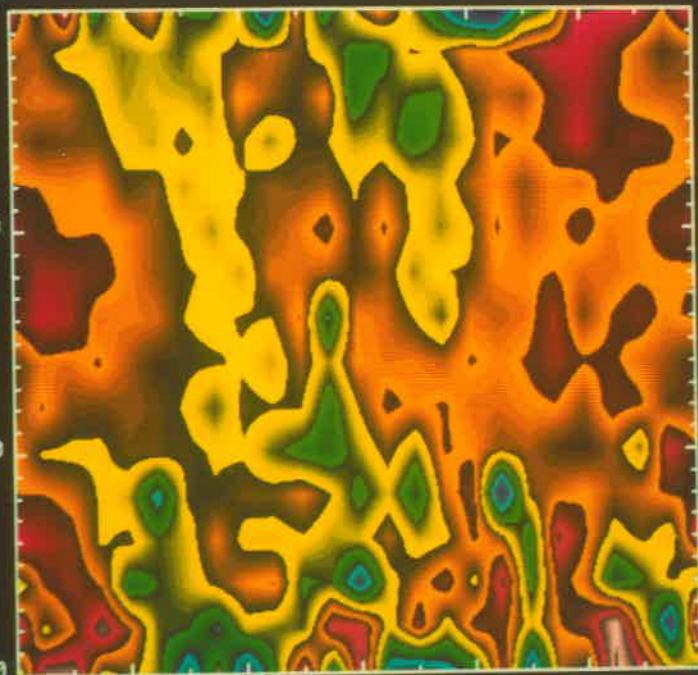
Figure 3.10 Mean daily variation of hourly averaged meridional
            prevailing winds in the altitude range 70 to 100 km
            during the period of observation.

MERIDIONAL   13/12/85

1200 and 2400 hrs LT. Eastward winds maximize at 0800 hrs LT near 92 km and at 1800 hrs LT near 95 km.

The meridional winds shown in figure 3.10 are highly variable below 80 km with moderate northward components near 72 km at 0300 and 2100 hrs LT. Maxima in southward (poleward) winds occur at 0500 hrs LT and 1700 hrs LT near 78 km. Above 80 km, northward winds are strongest between about 1600 and 0400 hrs LT and southward winds are evident between 0600 and 0800 hrs LT. There are local maxima in southward winds between 80 and 86 km at 1100 hrs LT and near 95 km between 1200 and 1500 hrs LT.

The results presented here indicate that the entry into the auroral oval is accompanied by enhanced westward and northward (equatorward) winds, in agreement with other findings. Balsley et al. (1982) reported an enhanced westward flow during a period of increased electrojet activity at Poker Flat, just outside the auroral oval. Hook, (1970) reported enhanced equatorward flow on the night side of the auroral oval, during periods of auroral activity.

3.5 Incoherent Averaging.

The comparatively low data yield at Mawson warranted some attempt to extend it. The raw data were re-analysed and values of auto and cross - correlation functions, used in the full correlation analysis were averaged over one hour of data before further processing. The incoherent averaging of correlation functions in this manner is the spaced antenna equivalent of the incoherent averaging of power spectra used in Doppler wind studies made with MST radars operating at VHF frequencies (Rottger, 1984). Hourly averages are suitable for a study of prevailing winds and tides, as changes

in these systems due to fluctuations with time scales less than one hour will tend to be averaged out over any reasonable period of interest.

The "true" drift velocity calculated using full correlation analysis uses the mean autocorrelation functions of the sensors, and the cross correlation functions between pairs of sensors. In this study 3 sensors were used. In the normal analysis, the mean autocorrelation function ρ_a may be expressed as $\rho_a = \frac{1}{3}(\rho_{a_1} + \rho_{a_2} + \rho_{a_3})$ where ρ_{a_1} is the autocorrelation function of receiver 1 etc.

The cross-correlation functions between sensors 1-2, 1-3 and 2-3 are denoted as ρ_{12}, ρ_{13} and ρ_{23}.

In the incoherent averaging process, the auto- and cross-correlation functions from 1 hour of data (6 lots of records) were averaged before further processing. The auto-correlation functions of each sensor were accumulated before producing the final incoherently averaged mean auto-correlation function (ρ_{ai}). Thus,

$$\rho_{ai} = \frac{\Sigma \rho a_1(j) + \Sigma \rho a_2(j) + \Sigma \rho a_3(j)}{18}$$

The cross-correlation functions were averaged in a similar fashion to yield the incoherently averaged cross-correlation functions ρ_{12i}, ρ_{13i} and ρ_{23i}. Where

$$\rho_{12i} = \frac{\Sigma \rho_{12}(j)}{6},$$

$$\rho_{13i} = \frac{\Sigma \rho_{13}(j)}{6},$$

$$\rho_{23i} = \frac{\Sigma \rho_{23}(j)}{6}.$$

The functions ρ_{ai}, ρ_{12i}, ρ_{13i} and ρ_{23i} were used in the subsequent analysis.

It was hoped that echoes rejected for predetermined quality criteria could be useful if averaged in this way. From nearly 7 weeks of continuous observation (figure 3.6), a total in excess of 10,000 wind estimates were obtained from the initial analysis which, for 6 two minute records every hour, is equivalent to about 1700 hourly averages. Of course, these results are not distributed uniformly, as within any hour there are not necessarily 6 wind estimates at a particular level. Hourly averages of wind estimates from the normal analysis are highly variable and often show large uncertainties. In addition, tidal analyses require evenly spaced recordings throughout the day, as large gaps can significantly reduce the effectiveness of harmonic analysis (Crary and Forbes, 1983). Incoherent averaging, which does utilize all the data gathered during any particular hour, helped to cover some of the gaps in the hourly records, and yielded nearly 3500 hourly averages. Except where indicated, incoherently averaged hourly means have been used in the following analyses.

The incoherent averaging procedure also produced a small improvement in the height distribution of usable echoes. This can be seen by comparing figures 3.7 and 3.11, where the echo rate in each 2 km height range from 60 to 100 km in altitude is shown as a percentage of the total number of accepted echoes for both analyses. Incoherent averaging has had little effect on the broad maximum in accepted echoes near 90 km, but below about 74 km, the effective yield of usable echoes has been nearly doubled.
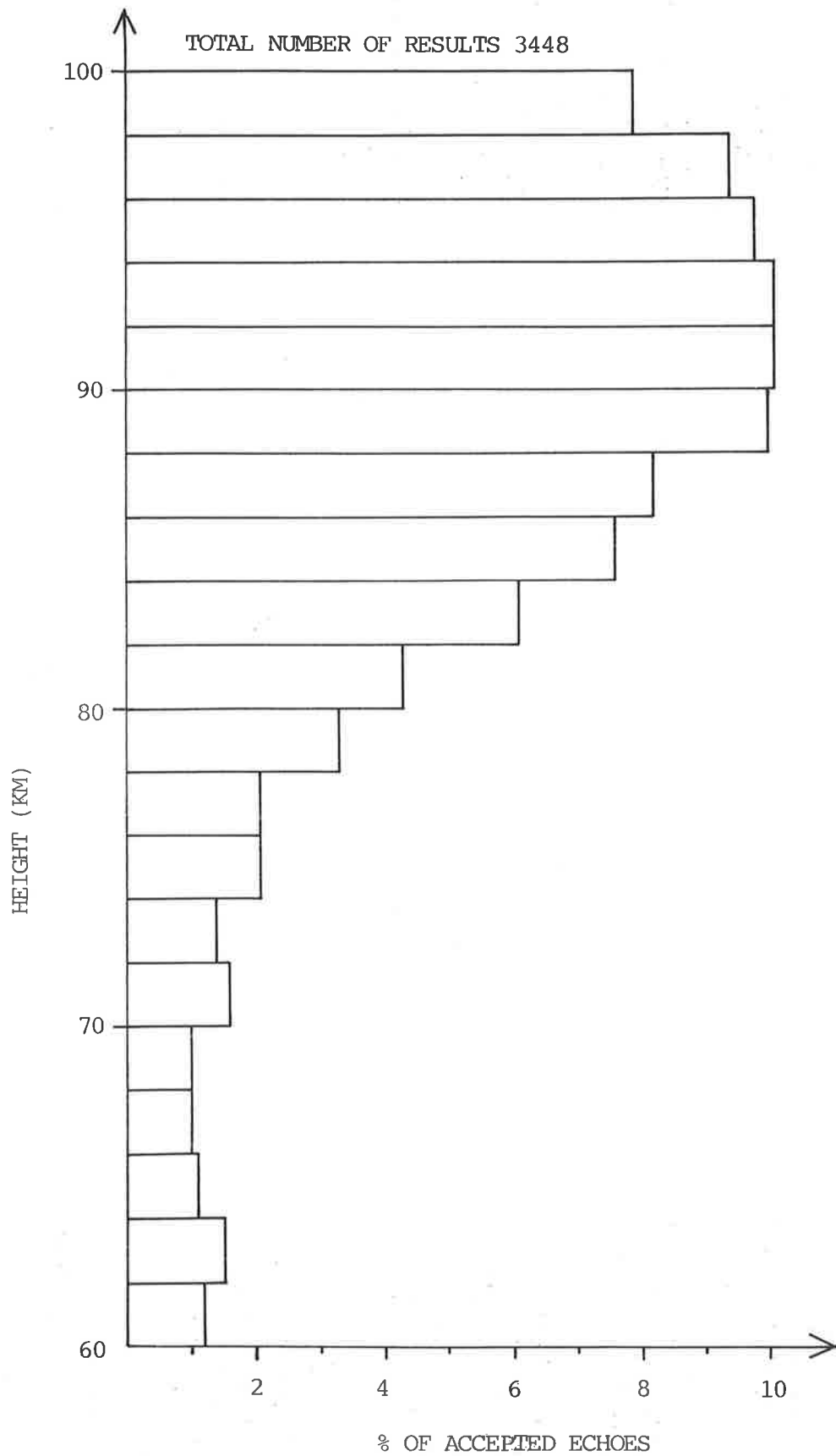
Figure 3.11. Accepted echo distribution from incoherently averaged results.

3.5.1 Incoherent Average of All Results.

Figure 3.12 (from MacLeod and Vincent, 1985) shows the mean zonal and meridional wind profiles observed at Mawson during the total period of observation. Standard errors range from about 10 ms^{-1} near 60 km to 2ms^{-1} at 100 km. Observations made during summer at Poker Flat (Carter and Balsley, 1982) and Scott Base (Fraser, 1984a) are shown for comparison. Appropriate profiles from the zonal models of CIRA (1972) and the meridional wind model of Groves (1969) are also shown.

All observations show the zonal flow to be westward at most heights, although the Mawson results are significantly smaller. The same effect is seen in the Mawson meridional profile (Poker Flat data must be reversed for comparison to allow for the change in hemisphere). Differences between these profiles may result from interhemispheric and interannual variability, but the average results shown here for Mawson are composed of data obtained over a period of approximately two months, in which systematic changes with time are evident, and likely to account for the smaller total averages.

The annual variations in prevailing zonal and meridional winds at Poker Flat have been presented recently by Manson et al. (1985) and are shown here in figure 3.13. The most suitable month for comparison with the results presented in figure 3.12 is July (northern hemisphere summer). By comparing these figures, it can be seen that the more recent results from Poker Flat are closer in magnitude to those from Mawson than the Poker Flat results plotted in figure 3.12. Also, the height of transition from westward to eastward winds (the height of zero crossing) is lower than the other results presented for Poker Flat.
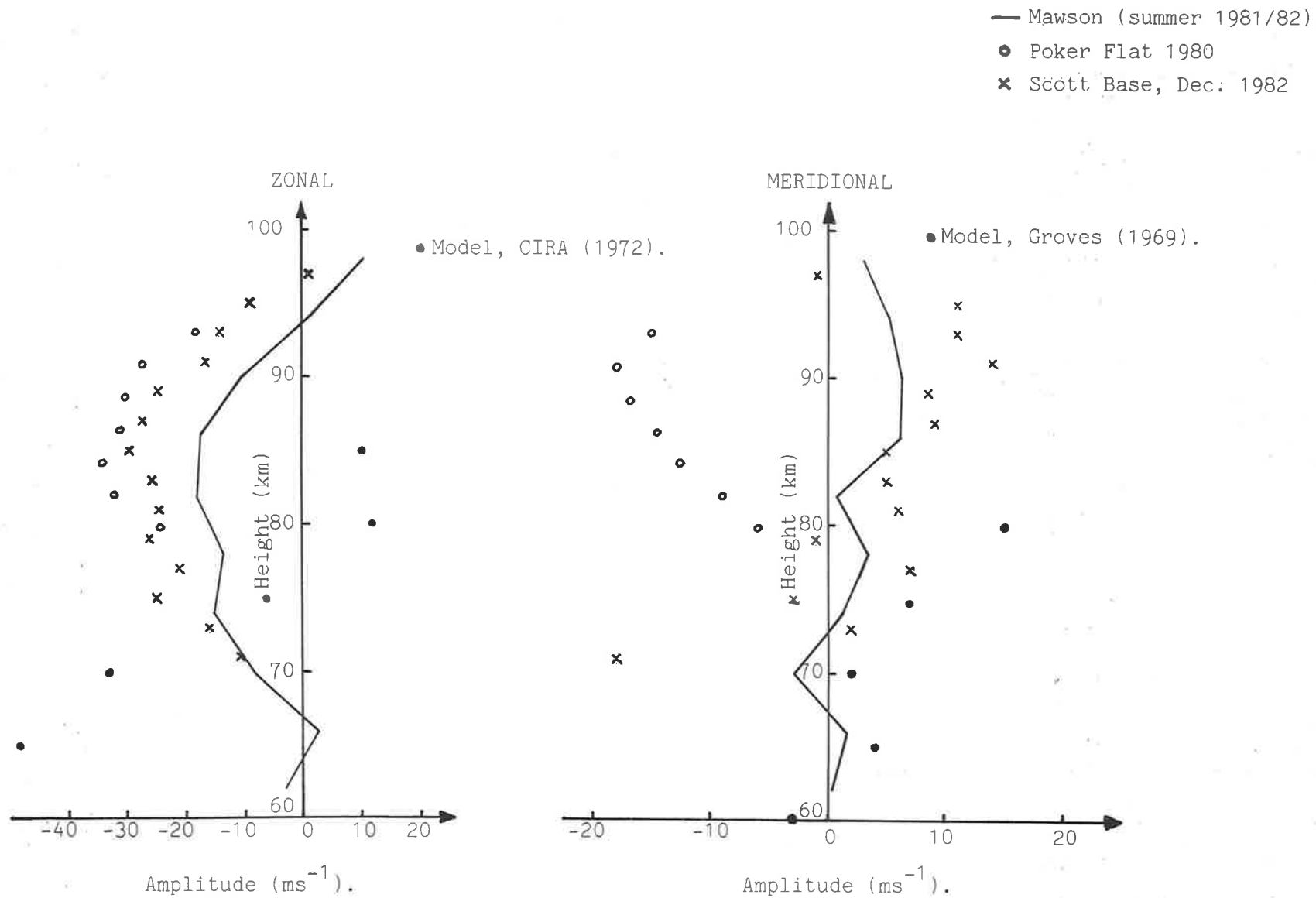
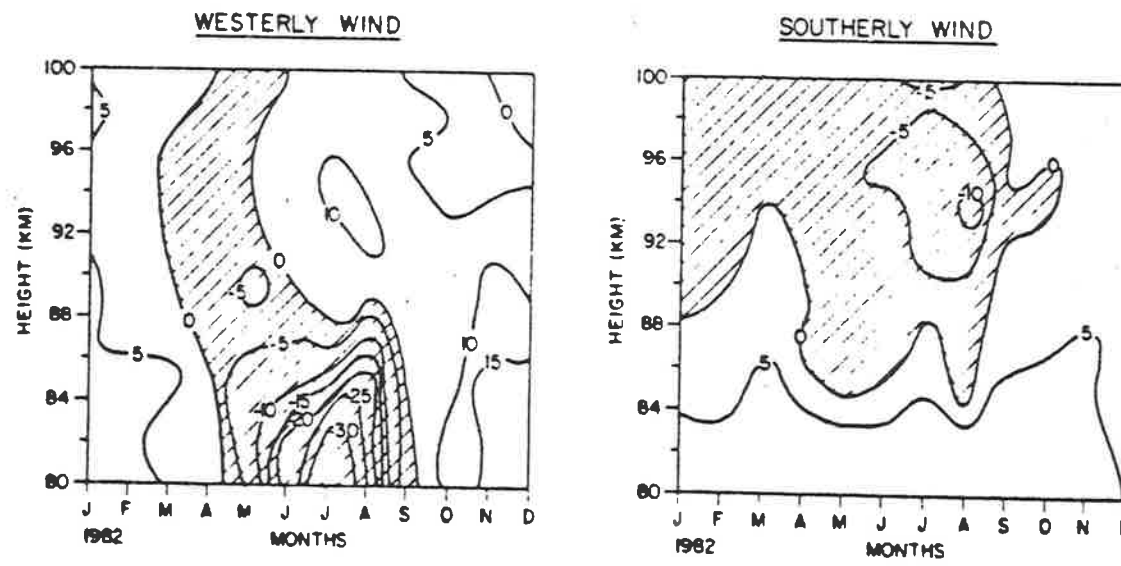Figure 3.12   Mean prevailing winds as a function of altitude at Mawson, summer 1981/1982.

Figure 3.13. Annual variation in prevailing zonal and meridional winds at Poker Flat (Manson et al., 1985).

4 <u>RESULTS</u>.

Once the records from Antarctica had been analysed, it was apparent that tidal analyses could not be applied reliably to all the results on a day to day basis. This was often due to inadequate and non-uniform data rates, particularly at the lower altitudes, although equipment damage caused data losses at all heights. Closer examination showed that by grouping 7 days of data into one 'equivalent' day, the hourly distribution of results over each 'equivalent' day for altitudes between 80 and 100 km was much more suitable for harmonic analysis. This was true for any group of 7 consecutive days within the observation period.

Similar observations at other sites in the southern hemisphere, for example at Townsville (Craig et al., 1980) and Adelaide (Vincent and Ball, 1981), have shown evidence of day to day variability in the prevailing winds suggesting the presence of longer period oscillations. In addition to the likely presence of longer period oscillations at the latitude of Mawson, day to day variability is also likely due to geomagnetic activity. By averaging the results of several days observations (in this case 7), a more accurate determination of the prevailing winds and major tidal components should result. The observation period at Mawson was such that 7 'equivalent' days resulted. The data obtained during the periods designated as week1, week2 etc. in figure 3.6 were used in each of the respective 'equivalent' days.
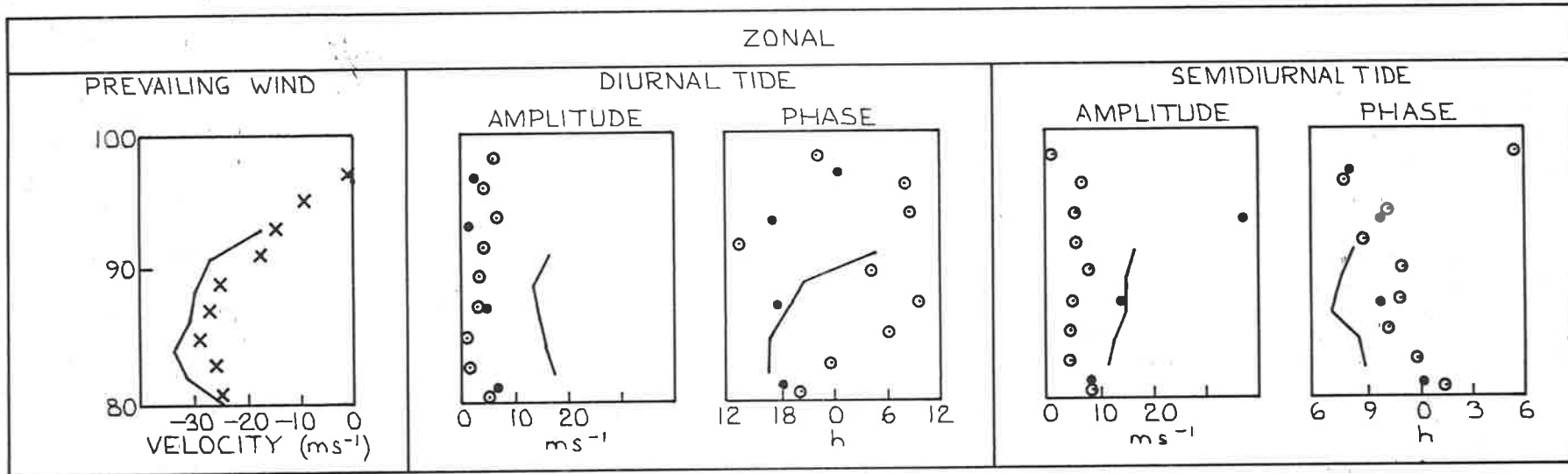
The results obtained in the Antarctic will be discussed in the following order, prevailing winds, diurnal tides and semi-diurnal tides. The results for the average prevailing winds over the whole observation

period were discussed at the end of the last chapter, but the changes in the prevailing winds during this period will be presented in this chapter from the analysis of the 7 equivalent days. The sections concerning the diurnal and semi-diurnal tides contain discussions referring to the average results for the whole observation period, followed by a week to week description of the tidal systems for the same period. A spectral analysis of the hourly averaged Mawson data at the 92-94 km level concludes the discussion of the Antarctic results.

As has been stated earlier, the equipment used to obtain results at Mawson had been installed previously at Townsville (20°S, 147°E). The author ran the equipment for five weeks during July and August (26/July/80 to 29/Aug/80) of 1980 (southern hemisphere Winter months), prior to its transport to Antarctica. The results from that period at Townsville and concurrent results taken by the Radiophysics group of the University of Adelaide at Buckland Park (35°S,138°E) will be discussed at the end of this chapter.

4.1 Antarctic Results.

Figure 4.1 is included for comparison with the results presented in figures 4.10, 4.14 and 4.19. Included in figure 4.1 are experimental results from Poker Flat (prevailing winds and tides) and Scott Base (prevailing winds). Theoretical results from Forbes' (1982a, b) tidal models are also included, the numerical values for which have been taken from the tabulations of Forbes and Gillette (1982).
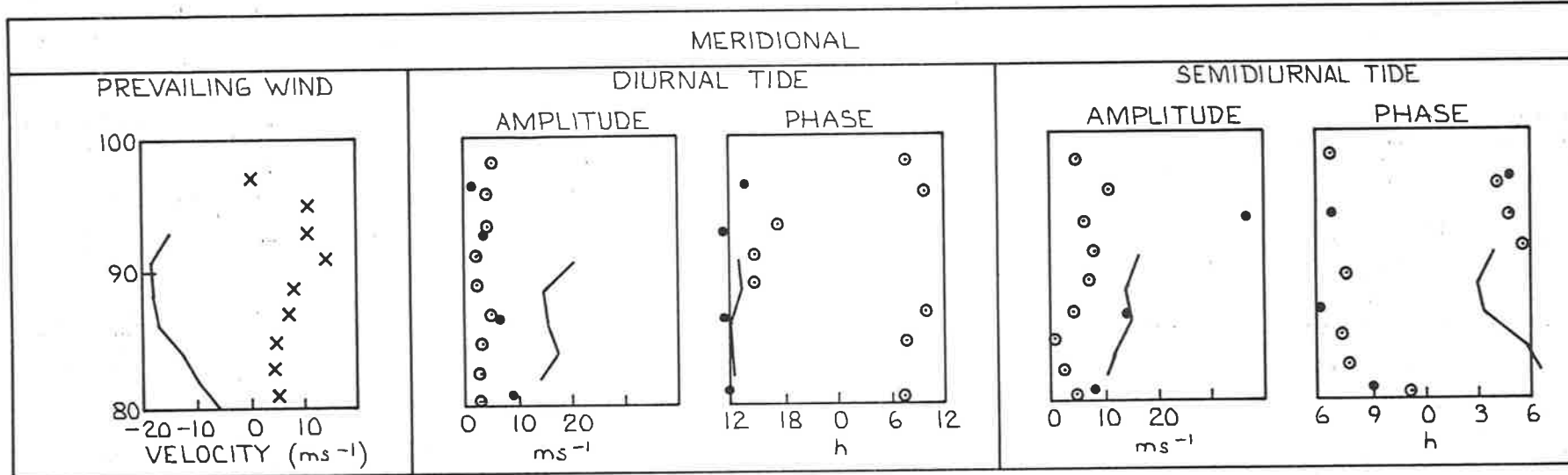
Figure 4.1.   Comparative Results.

4.1.1 Prevailing Winds.

Figure 4.2 shows the zonal and meridional wind profiles covering the 80 to 100 km altitude range in steps of 2 km for the 7 'equivalent' days. The values which were used to produce these profiles are the zero order terms of the harmonic analysis performed on each 'equivalent' day. The values used to produce the 'equivalent' day were obtained from incoherently averaged hourly means.

The zonal flow is westward at most heights, although over the period of observation, the systematic descent of an eastward flow is evident. This is in accord with current observations in the southern hemisphere at Christchurch, New Zealand (44°S) (Smith, 1983) and Adelaide (Vincent, 1984b), which show that the height of zero crossing to be below 90 km during the same period of the 1979/1980 southern hemisphere summer. The westward jet appears to occur higher in altitude at higher southern latitudes. These results are at variance with current models (CIRA, 1972; Koshelkov, 1984), which place the peak of the westward jet below 75 km.

Overall, the magnitude of the zonal flow agrees better with results taken at Scott Base (78°s) (Fraser, 1984a) than those from Poker Flat (65°N), (Carter and Balsley, 1982). The southern hemisphere values tend to be smaller than those of the northern hemisphere. Averaging zonal wind values over an extended period of time may produce apparently small values if the underlying prevailing systems are undergoing systematic large scale changes. The smaller averaged values observed in the southern hemisphere may be a real difference between hemispheres, but there is insufficient evidence; interannual variability could also account for the difference.
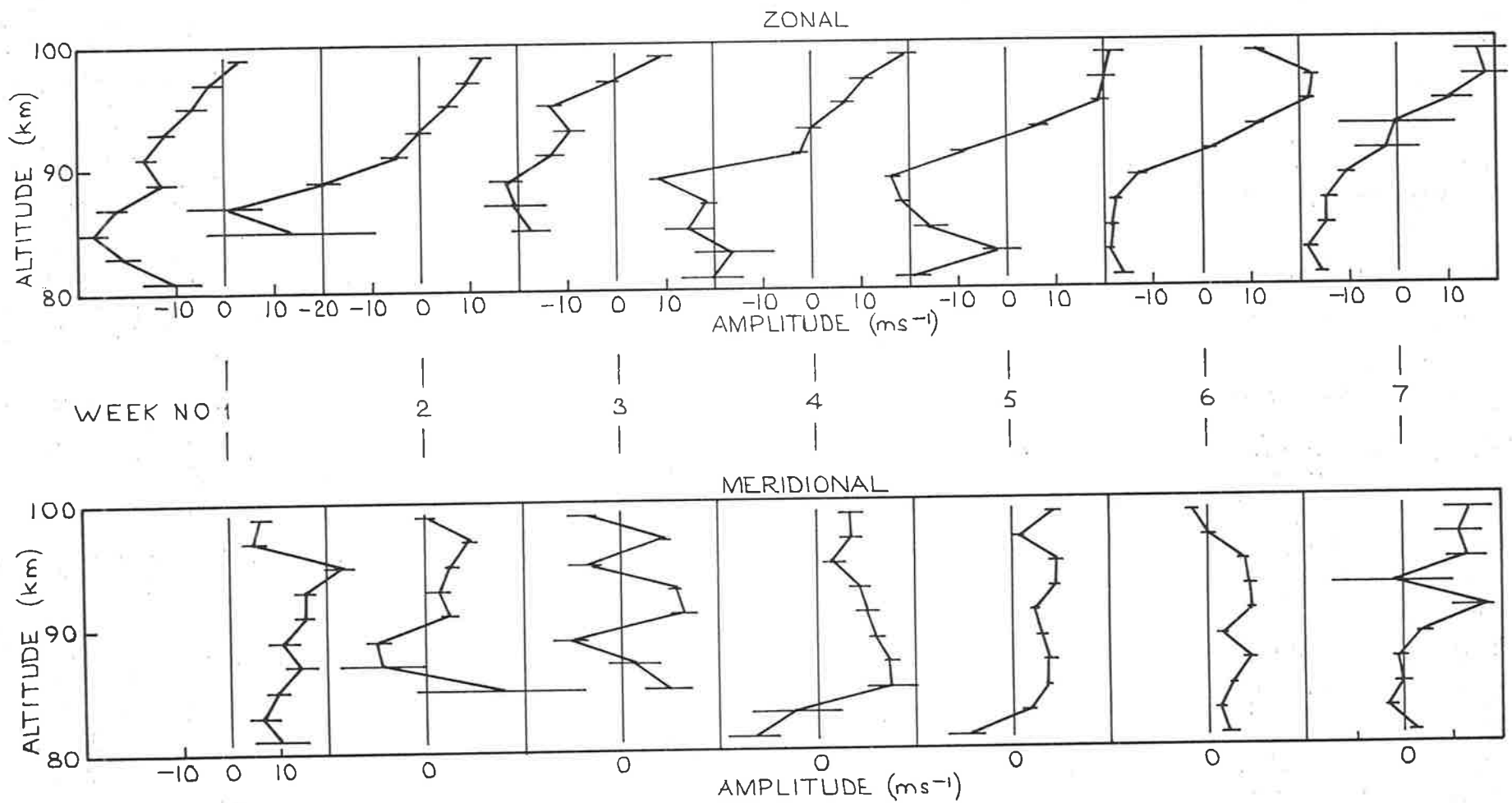
Figure 4.2.   Prevailing winds at Mawson: weekly averaged results.

The meridional profiles for the same period are shown in figure 4.2. The flow is towards the equator (northwards) at most heights, with maximum values between 10 and 20 ms^{-1}. The wind magnitudes observed at Scott base are again closer to the Mawson results than those from Poker Flat (figure 4.1). The flow from the pole is in agreement with the results of Nastrom et al, (1982), and larger than predicted by earlier numerical models, e.g. Holton and Wehrbein (1980), although later models which use gravity wave drag better simulate the observed meridional flow (Holton, 1982; Matsuno, 1982).

The major deviations from the orderly behaviour during the observation period occurred in the second and third weeks. There had been damage to the transmitting array between these two periods, which is evident in the lack of sufficient reliable data below about 84 km. The strongest westward flow, of approximately 40 ms^{-1} occurred during the second week near 87 km. It is probably fortuitous, but the southern hemisphere summer solstice occurred during the second week. It is tempting to attribute the strong westward flow to this event, but this seems most unlikely.

Figure 4.3 has been included to provide information on the geomagnetic conditions at Mawson during the period of observation. It can be seen that the third, sixth and seventh weeks were more geomagnetically active than the others. Sudden commencements (shown in figure 4.3) also occurred at these times. Due to high radiowave absorption above 90 km towards the end of the sixth week, the receiver had been set to a lower height range. Suitable echoes above 90 km were not observed until after
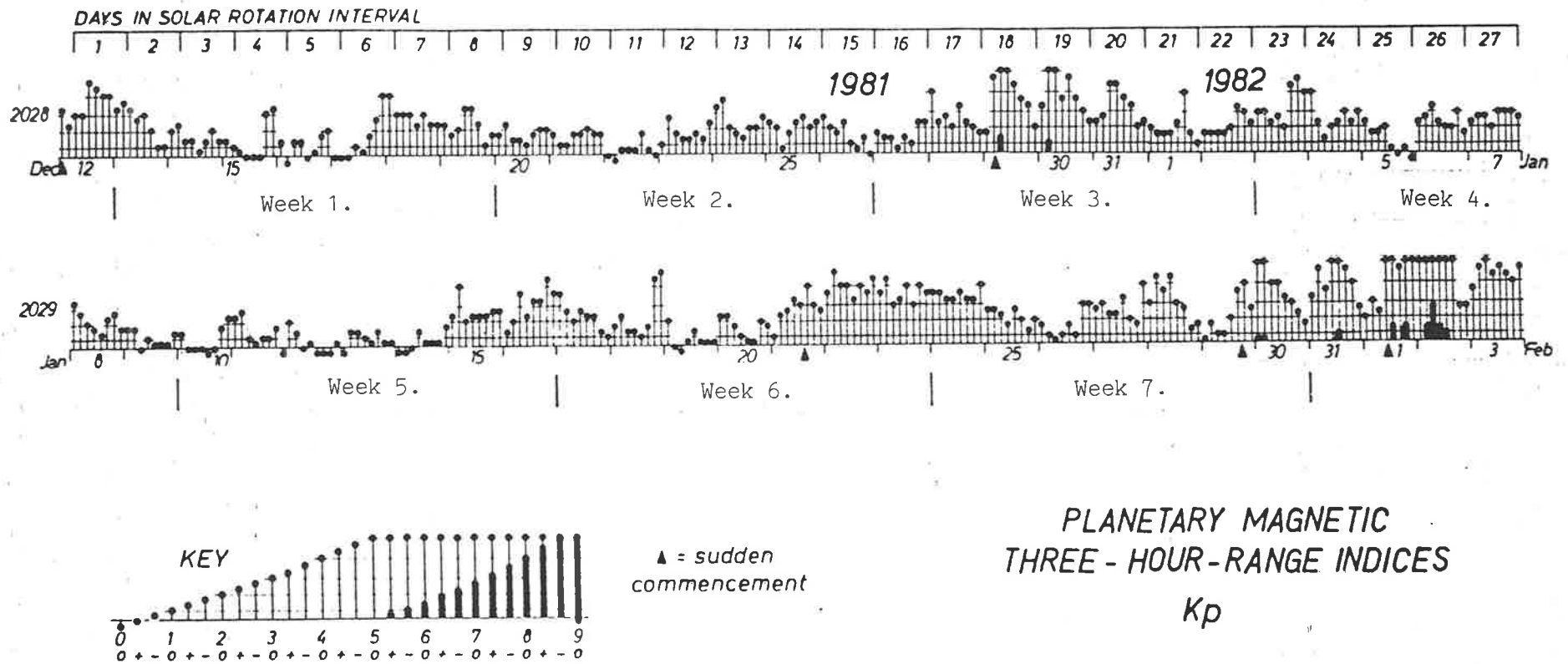
Figure 4.3.

the fourth day of the seventh week, and then only for about 36 hours. The lack of results is reflected in the relatively large errors for winds measured at heights above 90 km in the seventh week.

While the major fluctuations in the wind fields appear to be associated with periods of geomagnetic activity, there were some differences in the geomagnetic conditions of weeks 3, 6 and 7. In week 3, a sudden commencement was followed by sharp increases and decays in K_p index for the next few days. In week 6 a sudden commencement preceded a period of 3 days of relatively uniformly disturbed conditions, of which two were included in the results for week 6 and the other included in the results for week 7. In week 7, a sudden commencement occurred on the sixth day, so any effects above 90 km due to this event would not have been recorded.

In the profiles of weeks 2 and 3, the regions of maximum zonal shear correspond to a poleward meridional flow. In week 7 the region of maximum zonal shear lies between 91 and 93 km, while the corresponding meridional profile shows a possible poleward flow at 93 km. These observations are at variance to those of Vincent (1984b), who notes that for the systematic variation with latitude and altitude, maximum meridional winds occur in regions of maximum zonal shear. The quality of the data in weeks 2, 3 and 7 is somewhat poorer than that of the other weeks. It is therefore possible that there may be some unresolved tidal contribution which produced these effects. Another possibility is that planetary wave activity is responsible. Planetary wave activity at these levels of the atmosphere during summer has been discussed in the introductory chapter

(see page 5). During week 4, the region of maximum zonal shear occurs near 90 km, and corresponds to a broad maximum in the meridional profile, in agreement with Vincent's observations. It is of interest to note that for the geomagnetically active weeks, regions of maximum zonal shear are associated with a reduction (more poleward) in the mean meridional flow.

Changes in the dynamical behaviour in the 80 to 100 km altitude range during this period of observation are perhaps better represented by figure 4.4. In this figure, the weekly averaged results used in figure 4.2 have been averaged over 4 km height bands and plotted as shown.

The zonal profiles clearly show a progression towards more eastward winds in the late summer, particularly at the higher levels where the rate of change is greatest. The meridional profiles show an overall weakening of the equatorward (northward) flow, with the largest effects occurring during the second and third weeks.

Figure 4.5 provides further insight into the systematic changes with time of these wind systems. Data for the height ranges 82 to 88 km and 92 to 98 km have been averaged together, harmonically analysed and a 4-day running mean performed on the resulting data sets to produce these results. A small increase in the zonal component at the higher level is evident. For the meridional component, a poleward trend is apparent at the lower level, while there is evidence of an increase in the equatorward flow at the higher level.

The most significant effects appear to be associated with the sudden commencement during the third week. For the zonal components, this
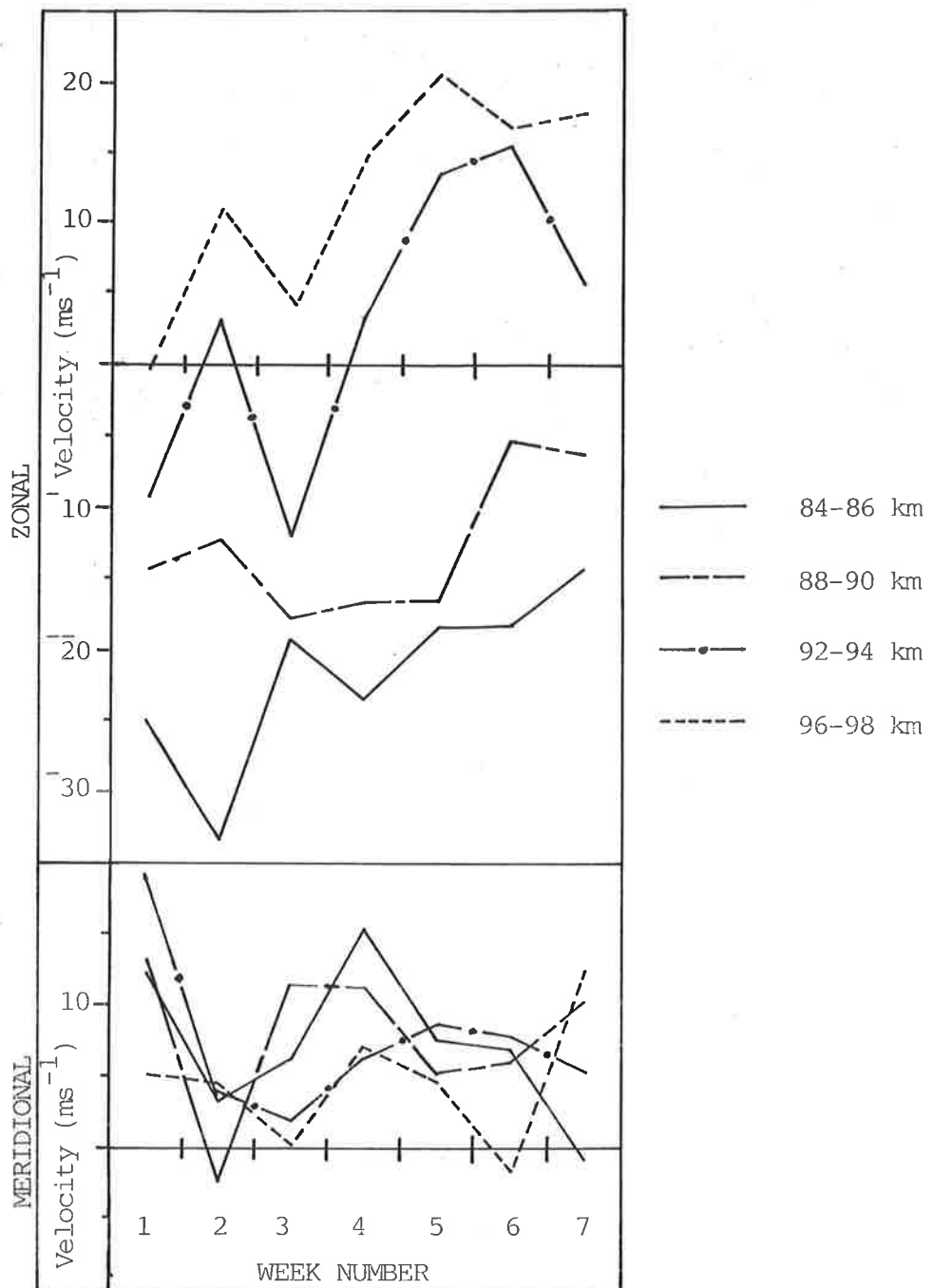
Figure 4.4. The variation in weekly averaged prevailing winds for the altitude ranges shown over the period of observation at Mawson.
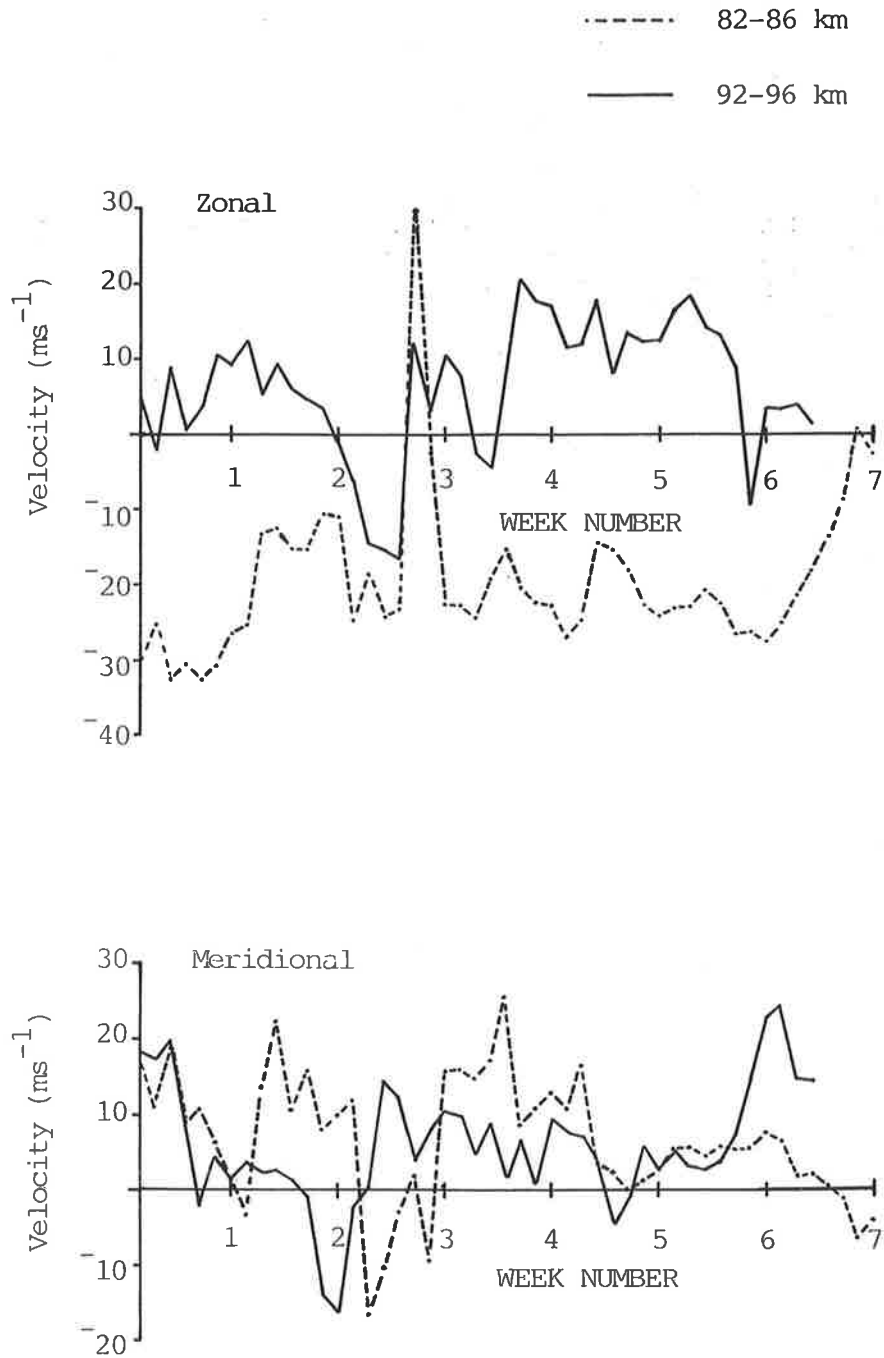
Figure 4.5.   4-day running means for the altitude ranges shown over the period of observation at Mawson.

event is accompanied by a strong deceleration of the flow at the higher levels, with little effect at the lower levels, but between two and three days later, there is a large recovery, particularly at the lower level. For meridional components during the same period, the upper level is subject to an increase in the equatorward flow, while the lower levels show an increase in poleward flow.

Balsley et al. (1982) and Johnson and Luhman (1985) have examined data obtained at Poker Flat for evidence of geomagnetic effects on mesospheric winds. Both groups noted changes in spectral power of diurnal and semi-diurnal tidal components during geomagnetically active periods. Balsley et al. (1982) reported an observed correlation between short-term fluctuations in the zonal wind field at Poker Flat and the intensity variations in the auroral electrojet. This correlation was observed during weakly disturbed conditions, and was evident throughout the range 83 to 90 km. They observed no such behaviour for the meridional winds. Their results refer to data taken during the 1979 northern hemisphere summer, and during their period of observation, they noted that increases in local auroral electrojet were accompanied by increases in the prevailing zonal wind. The results presented in figure 4.5 show a deceleration to the zonal flow occurring close to the time of a sudden commencement (eg. weeks 3 and 6), but then an enhancement of the flow in the geomagnetically unsettled period after, in accord with the results of Balsley et al. (1982).

Johnson and Luhman (1985) presented the results of spectral analyses of auroral zone neutral winds at a height of 86 km, measured using the MST radar at Poker Flat and obtained during northern hemisphere summer

periods of approximately the same duration as the Antarctic results presented here, for the years 1980, 1981 and 1982. They found that for spectral components with periods less than about 8 hours, there was no discernable difference between geomagnetically active and quiet periods.

For longer period components, they proposed that the response of the atmosphere at the 86 km level depended on whether there were, on the average, well established diurnal and semidiurnal fluctuations or not. For well established tidal fields, their results indicated that an increase in geomagnetic activity corresponded to a decrease in the power of low frequency components, and vice versa. In particular, their results indicated that in June and July of 1981, increases in geomagnetic activity corresponded to increases in the spectral power of the low frequency components, whereas the reverse was true for 1980 and 1982.

Although there is a time lag of 6 months between the 1981 results of Johnson and Luhman and those presented here, the results presented in figure 4.5 for the 82-86 km level during week 3 are in accord with those from Poker Flat. For the 92-96 km level shown in figure 4.5, the results are more ambiguous. During week 3, an increase in the zonal component of $\sim$25 ms^{-1} is accompanied by a decrease in the meridional component of a few ms^{-1} close to the time of the sudden commencement. In week 6 however, at the time of the sudden commencement, the zonal component decreases by $\sim$10 ms^{-1}, while there is a similar increase in the meridional component.

Whilst the departures from the orderly seasonal behaviour appear to be associated with geomagnetically active periods, the exact mechanism is not clear. Increased particle precipitation, causing an increase in ion

drag, could no doubt contribute to an overall deceleration. The change in the distribution of tidal modes associated with such events may account for a general variability. The timing of these events with respect to the summer solstice may be of significance, but more information, obtained during geomagnetically active periods, is needed to clarify the present observations.

4.1.2 Diurnal Tide.

The hourly means which were derived from the incoherently averaged correlation functions for the whole observation period were averaged and placed into respective hourly bins. The resulting 24 hour data set was then harmonically analysed. Figure 4.6 (from MacLeod and Vincent, 1985) shows the diurnal amplitudes and phases obtained, which are representative of the mean state of the diurnal tidal system during the period of observation. Velocity errors range from 2-3 ms^{-1} at the lower levels to 1-2 ms^{-1} at the upper levels, corresponding errors in phase are ±1-2 hr and ±0.5-1 hr. Plotted for convenience on these diagrams are the model results and observations given in figure 4.1.

The Poker Flat summertime amplitudes were obtained by averaging the amplitudes of the harmonic analyses of individual days data (Carter and Balsley, 1982), whereas the Mawson amplitudes were averaged vectorially. This probably accounts for the comparatively large amplitudes of the Poker Flat summertime results. The wintertime Poker Flat results, which were taken at the same time as the Mawson results, were obtained using meteor echoes, and were provided by Avery (1983). The wintertime Poker Flat results were averaged vectorially and show very small amplitudes, which
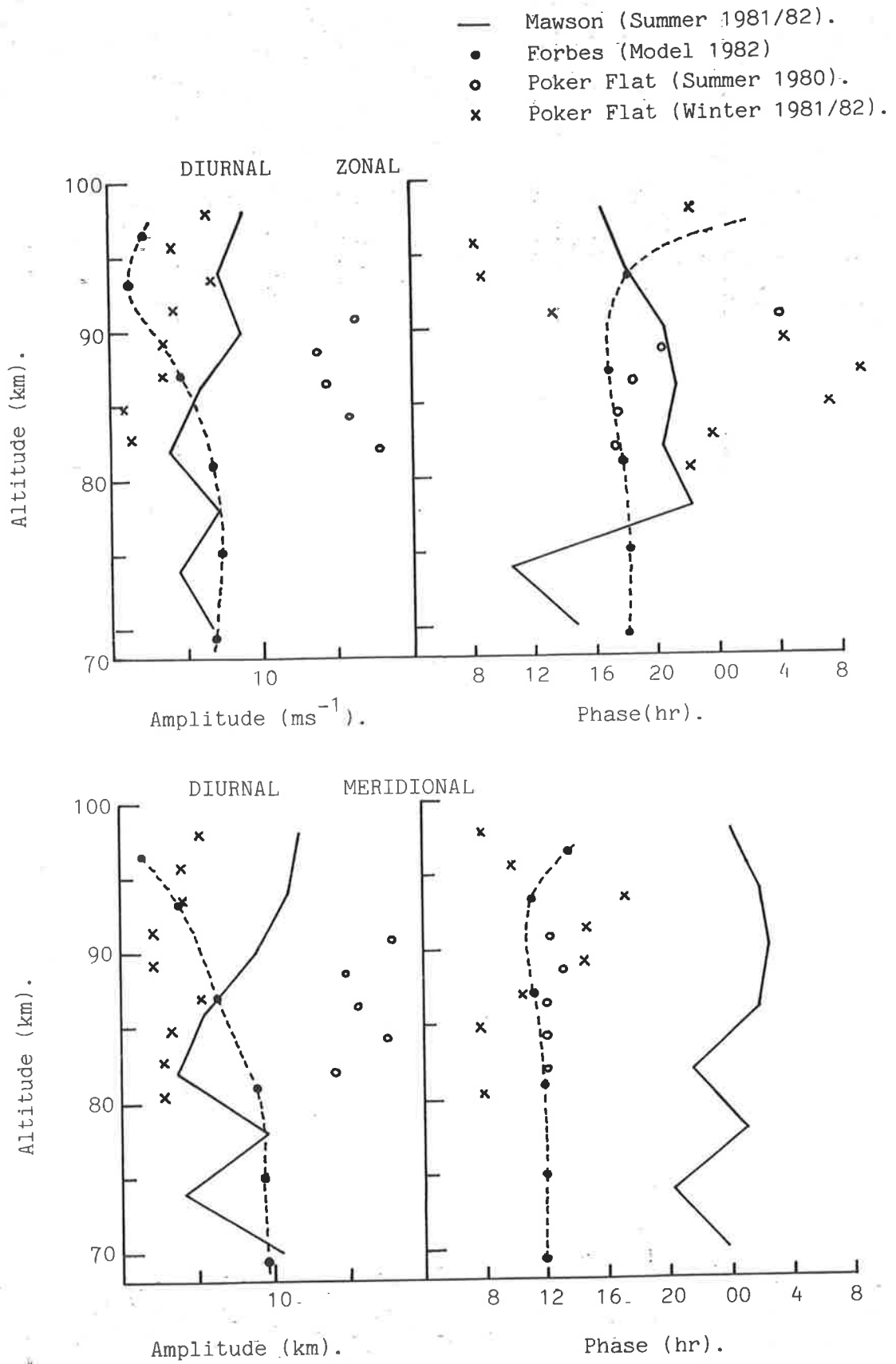
Figure 4.6. Mean diurnal tide at Mawson (MacLeod and Vincent, 1985).

would contribute to the erratic phase behaviour with height. Notwithstanding this, the wintertime Poker Flat phase results broadly agree with those from Mawson.

Lysenko et al (1979), referring to a mean altitude of 94 km at Molodezhnaya, report mean phases for the zonal and meridional diurnal tides of about 19 hrs and 1 hr respectively. Figure 4.6 shows good agreement with the Molodezhnaya phase results. The amplitudes at Molodezhnaya are significantly larger than those observed at Mawson, but it is not clear how the Molodezhnaya data were averaged.

The Mawson diurnal amplitudes are in general agreement with Forbes' tidal model below 85 km, but there are discrepancies at higher altitudes. Observed amplitudes tend to grow with height, and Poker Flat results also show evidence of this behaviour, while the model results decay rapidly with height. Rapid decay in amplitude with increasing height is the expected behaviour for evanescent modes generated at lower heights. The growth with height in the amplitudes of the diurnal tidal components observed in both hemispheres, provides some evidence for an unresolved in situ tidal source.

There is good agreement in phase for the Mawson and Poker Flat summertime results. For the Poker Flat wintertime results, taking into account the small amplitudes, there is resonable agreement, particularly for the meridional components. Taking into account the errors, the results indicate that the zonal oscillations are approximately in phase in the north and south hemispheres and the meridional oscillations are in antiphase. This indicates the presence of symmetric tidal modes. The

almost constant phase structure, above about 85 km, has generally been taken to indicate that it is evanescent modes which dominate. This has been the expected result for high latitudes. As was discussed in section 1.3.2 of the introductory chapter, Vial and Teitelbaum (1984) have questioned the validity of this assumption. In their work, they studied the effects of turbulent diffusion on the latitudinal structure of the first diurnal propagating mode, and concluded that turbulent dissipation extended the Hough functions of the (1,1) mode to higher latitudes, and that this mode was responsible for many diurnal tidal effects which had been ascribed to evanescent modes.

Some evidence for a small propagating diurnal tidal component is given in figure 4.7, in which the amplitudes and phases of the observed diurnal components are compared with the theoretical calculations of Forbes and Gillette (1982). The results from Mawson show that above 90 km the rotation of the tidal vector is in the correct sense, and the phase difference between the zonal and meridional components is close to 90° which is expected for propagating and evanescent modes. In addition, there is evidence for a small amplitude growth in the Mawson results from the lowest to highest level in both meridional and zonal components. The results of Forbes (1982a) show none of these effects.

The amplitudes and phases of the weekly averaged diurnal tidal oscillation are shown in figure 4.8. The mean amplitude of the zonal diurnal tide increases over the 7 week period from about 10 ms^{-1} to 20 ms^{-1}. The results from Poker Flat (fig. 4.1) are of a similar order. The mean amplitude of the meridional diurnal tide is more variable, but
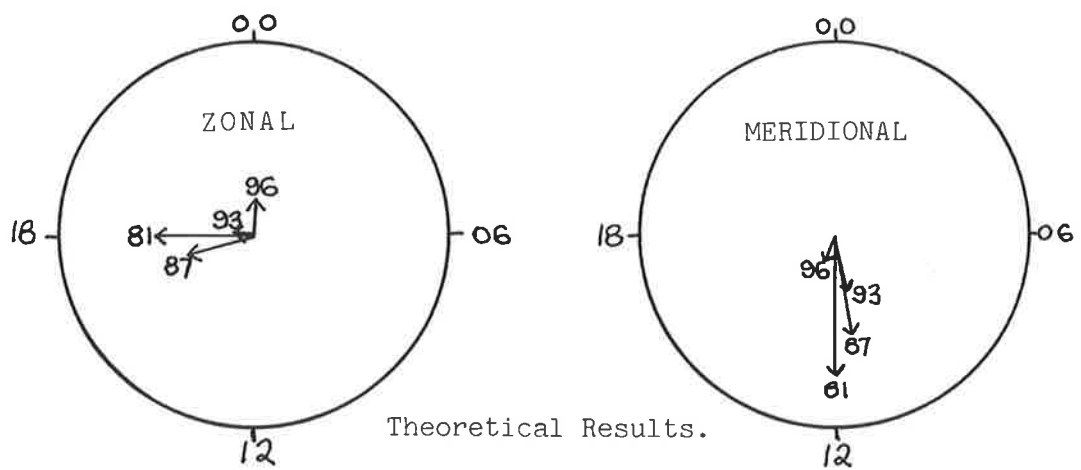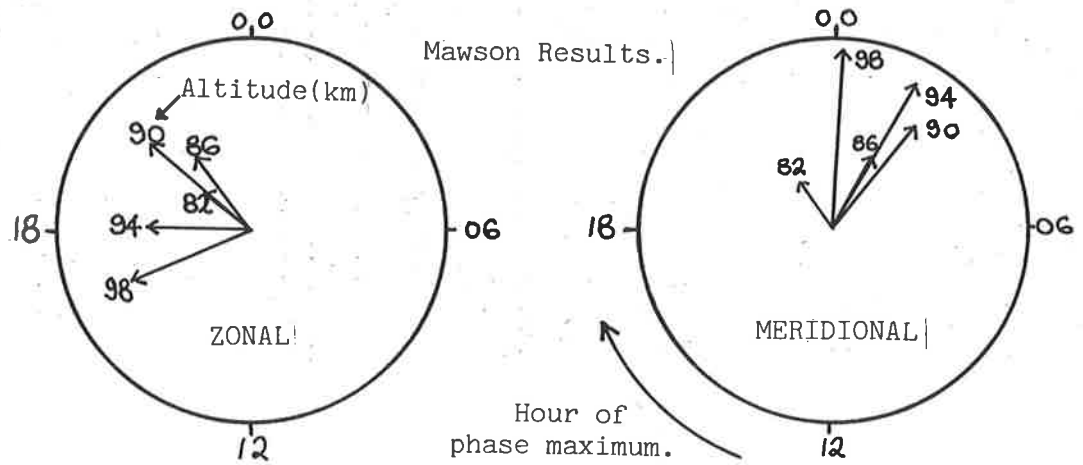
Figure 4.7. Comparison of the Diurnal Tidal Vectors Observed at Mawson
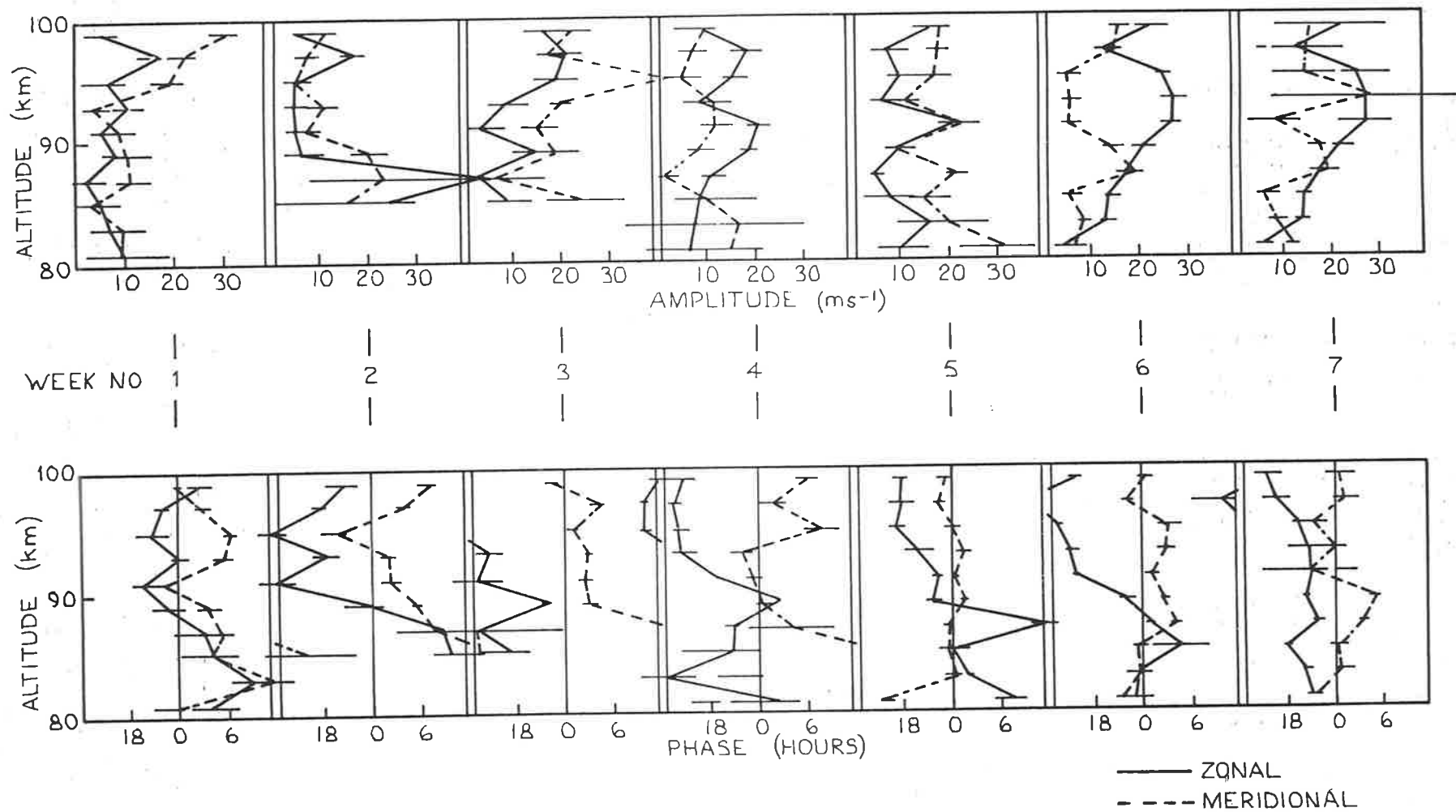with those Calculated Theoretically.

Figure 4.8. Diurnal tide at Mawson: weekly averaged results.

generally lies somewhere between 10 and 20 ms^{-1}. Again these results are similar to those from Poker Flat. The magnitudes of zonal and meridional components of the diurnal tide are larger than those predicted by Forbes (see figure 4.1).

For altitudes below 90 km, the magnitudes of the zonal diurnal components for weeks 4, 5, 6 and 7 increase from about 10 ms^{-1} or less at 80 km to approximately 20 ms^{-1} at 90 km. In week 1, the amplitudes from 80 to 90 km are small, not exceeding 10 ms^{-1}. Week 2, which, like week 3, has no suitable results below 84 km, shows a large peak in the diurnal component at 86 km followed by a sharp decrease in amplitude at 88 km. For week 3, the zonal component at 86 km is very small, increasing to a little more than 10 ms^{-1} at 88 km and decreasing again at 90 km.

Except for week 2, the zonal diurnal components above 90 km tend to be larger than those below. Weeks 1, 2, 3 and 4 show a local maximum at 96 km of approximately 20 ms^{-1}, while the latter 3 weeks show a local minimum at the same height.

The magnitudes of the meridional diurnal components are more variable. Weeks 1, 3 and 7 show some tendency for overall amplitude growth with increasing altitude, but the other weeks show more random distributions. There is a maximum in the meridional component of about 20 ms^{-1} associated with the zonal maximum at 86 km during week 2. The largest meridional component is approximately 40 ms^{-1} and occurs in the geomagnetically active third week.

It is of interest to examine some features of figure 4.8 in view of the findings of Johnson and Luhman (1985), that is, under conditions when no well developed diurnal and semidiurnal tidal fields were present on the average, increased geomagnetic activity correlated positively with an increase in spectral power at low frequencies. In figure 4.8, for the geomagnetically active weeks 3, 6 and 7, relatively broad maxima in zonal velocities are apparent above 90 km. For the meridional profiles, week 3 shows the largest meridional velocities at 95 km, week 6 shows the smallest velocities around the same height, while the results for week 7 are inconclusive due to large errors.

The results presented here show considerable week to week variability. Large changes in amplitude and phase, below about 90 km, for example near 87 km during the second week, are most likely due to interference effects between diurnal modes. Nevertheless, weeks 3, 4, 6, and 7, show a very similar zonal phase structure between 88 and 96 km, which has the characteristics of a propagating tide (i.e. time of maximum phase decreases with altitude), the wavelength of which would be approximately 25 km, close to the wavelength of the (1,1) propagating diurnal mode as predicted by classical tidal theory.

Figures 4.9 and 4.10 show the results of the harmonic analyses of a series of 4-day running means performed on two averaged altitude bands, 82, 84, 86 km and 92, 94, 96 km respectively, for the period corresponding approximately to weeks 4, 5, 6 and 7. At the lower levels (figure 4.9), there are no discernable trends. As mentioned previously, amplitudes tend to be of similar magnitudes with considerable variability, and there are no
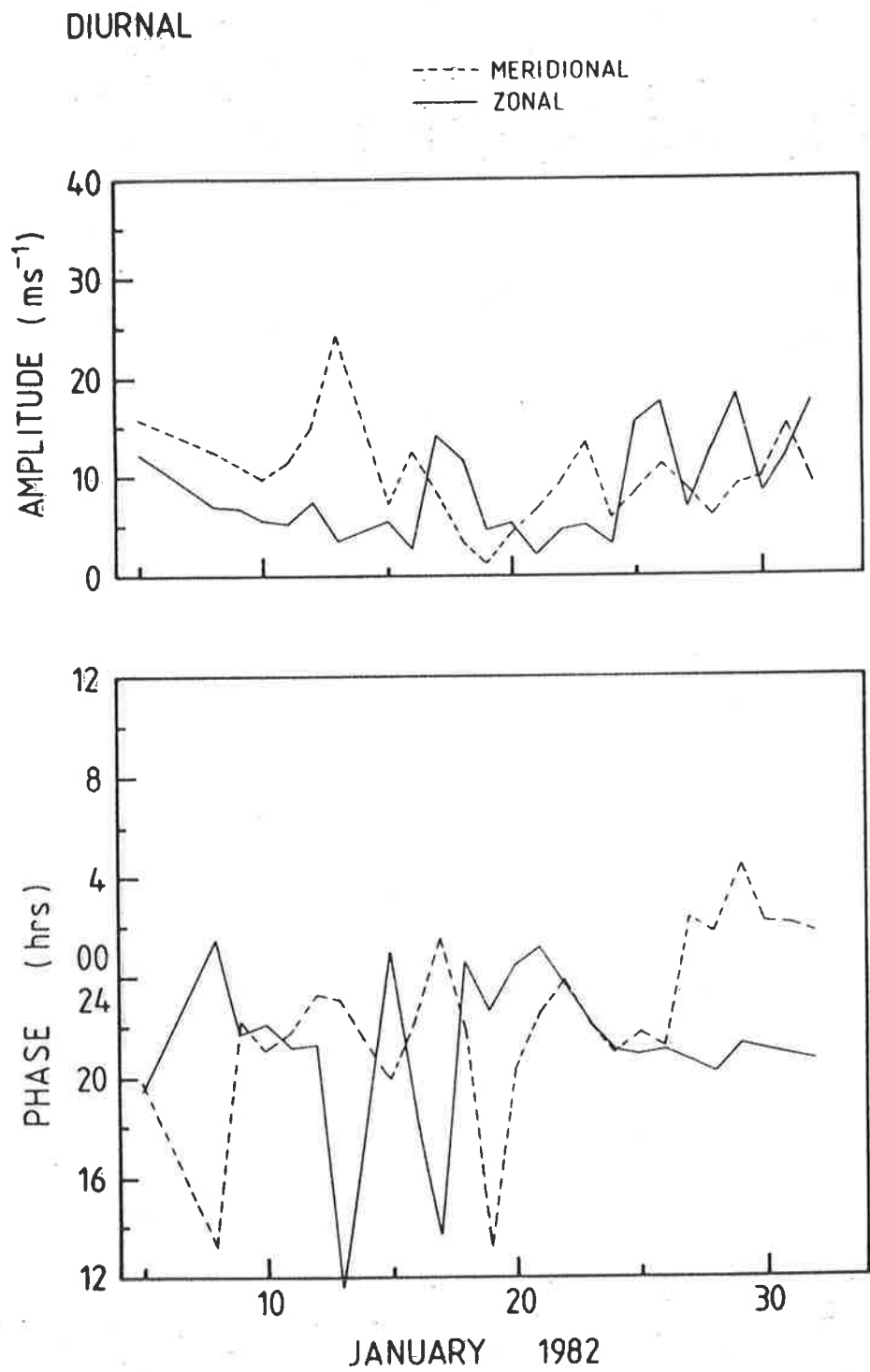
Figure 4.9. Diurnal tide at Mawson: 4-day running means for the altitude range 82-88km.
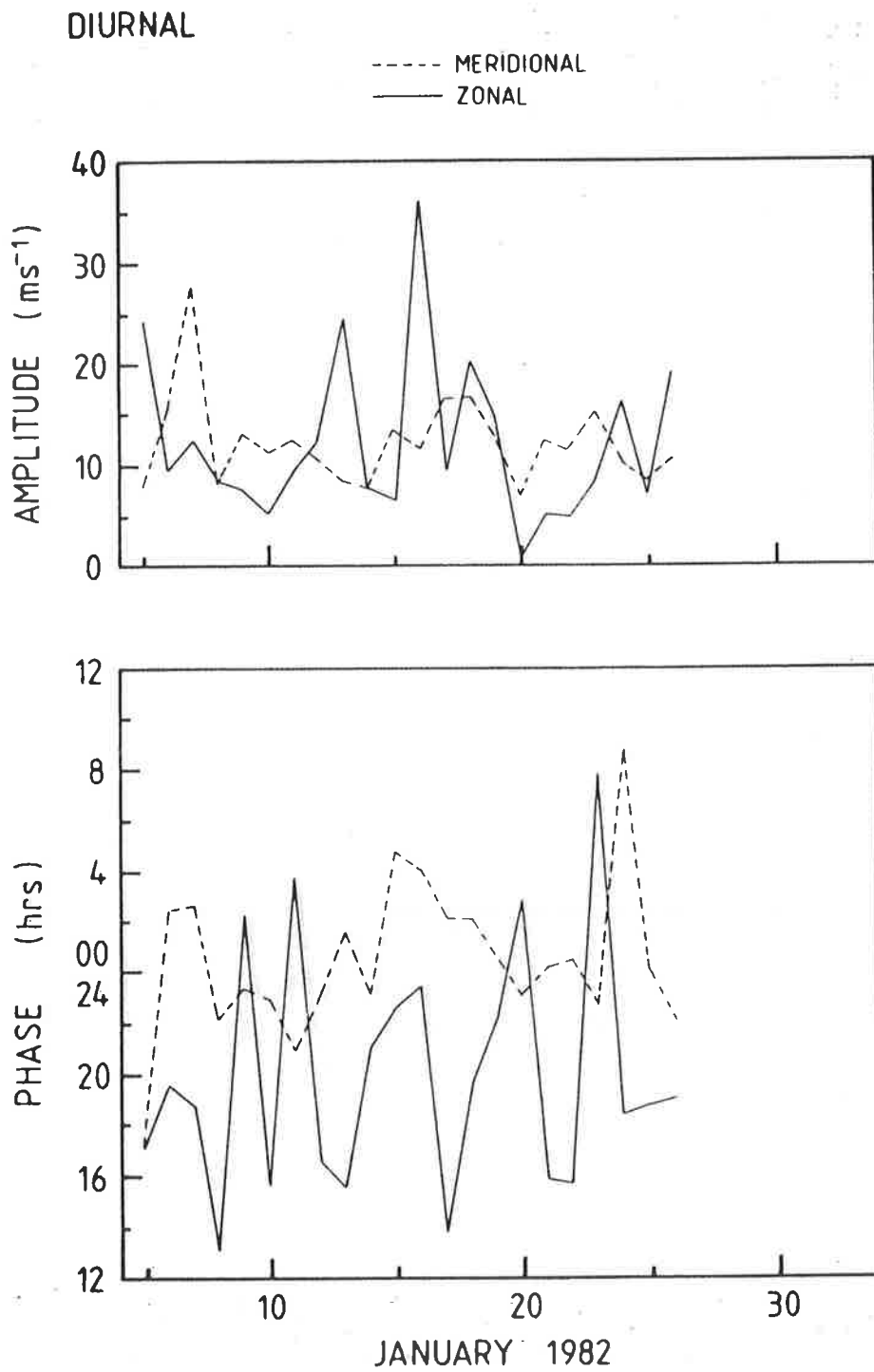
Figure 4.10. Diurnal tide at Mawson: 4-day running means for the altitude range 92-98km.

obvious trends in phase. At the higher levels (figure 4.10), the overall amplitudes of meridional and zonal components are similar, and slightly larger than those of the lower level. The phase results at the higher level show that overall, the zonal phase tends to lead the meridional by about 6 hours, and both appear to be subject to a similar phase retardation.

4.1.3 Semidiurnal Tide.

Figure 4.11 (from MacLeod and Vincent, 1985) is constructed from all available data, in the same manner as figure 4.6, and is intended to show the average semidiurnal tide system over the observation period. The uncertainties in the amplitudes and phases are similar to those for the diurnal tide shown in figure 4.6, although the uncertainty in the phases of both components is several hours at heights near 85 km. Again the experimental observations from Poker Flat and the results of Forbes' tidal model have been included on the figure as indicated.

The experimental results from Poker Flat taken during the same period (figure 4.1 - northern hemisphere winter 1981/1982) show the best agreement with those presented for Mawson. Amplitudes overall are similar for the Mawson and both sets of Poker Flat results. Near 95 km, the zonal components are approximately in phase, while the meridional components are in approximate antiphase. This suggests the dominance of symmetric modes.

Above about 90 km, the model results shown in figure 4.11 are larger than those observed mainly because it is assumed in the model that there is constructive interference between modes. The phase results are in closer agreement with the model, particularly above 90 km, where the zonal
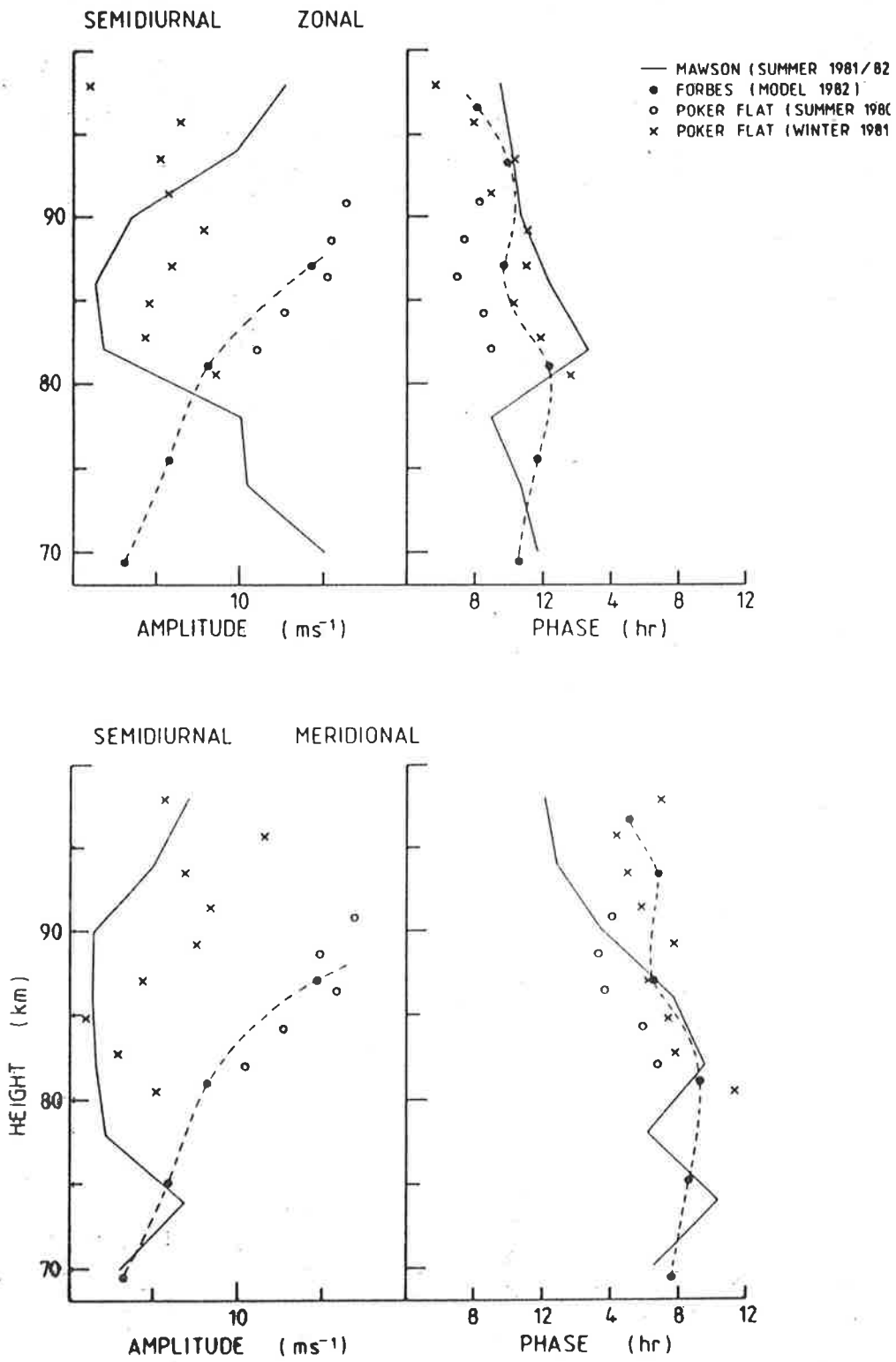
Figure 4.11. Mean semidiurnal tide at Mawson (MacLeod and Vincent, 1985).

components generally lead the meridional components by a few hours. This is expected in the southern hemisphere.

Figure 4.12 compares Forbes' results with the average tidal vectors for the whole observation period at Mawson in 4 km steps. While there is occasional agreement in the phase between these results, the discrepancies in amplitudes are obvious, in that the model results are much greater than those observed. In addition, with increasing altitude, the Mawson observations show a clear increase in amplitude and a smooth progression in the earlier time of maximum phase. Again, these are characteristics of propagating tides which are expected for the semidiurnal tidal field at high latitudes.

Height profiles of the semidiurnal amplitudes and phases for the 7 weeks of observation are given in figure 4.13. The uncertainties in these values, as shown, are similar to those of the diurnal tide over the same period. The zonal semidiurnal components in general show an overall increase in amplitude with inceasing altitude, although there are local maxima at 82 km in week 5 and at 90 and 94 km in week 6, which contradict this general observation. The meridional amplitude components tend to be smaller than their zonal counterparts, with slightly less large scale variation. There is little evidence of growth in amplitude with height for the meridional components.

While the semidiurnal meridional phase results presented in figure 4.13 show a general decrease in time of maximum phase with increasing altitude, there are significant variations from week to week, particularly in the altitude range 85 to 95 km. The difference in phase

Mawson Results.

Altitude(km)

ZONAL

MERIDIONAL

Hour of
phase maximum.

Theoretical Results.

(from the tabulations of Forbes and Gillette, 1982)

$(38ms^{-1})$ 93

ZONAL

$(56ms^{-1})$

MERIDIONAL

93
$(37ms^{-1})$
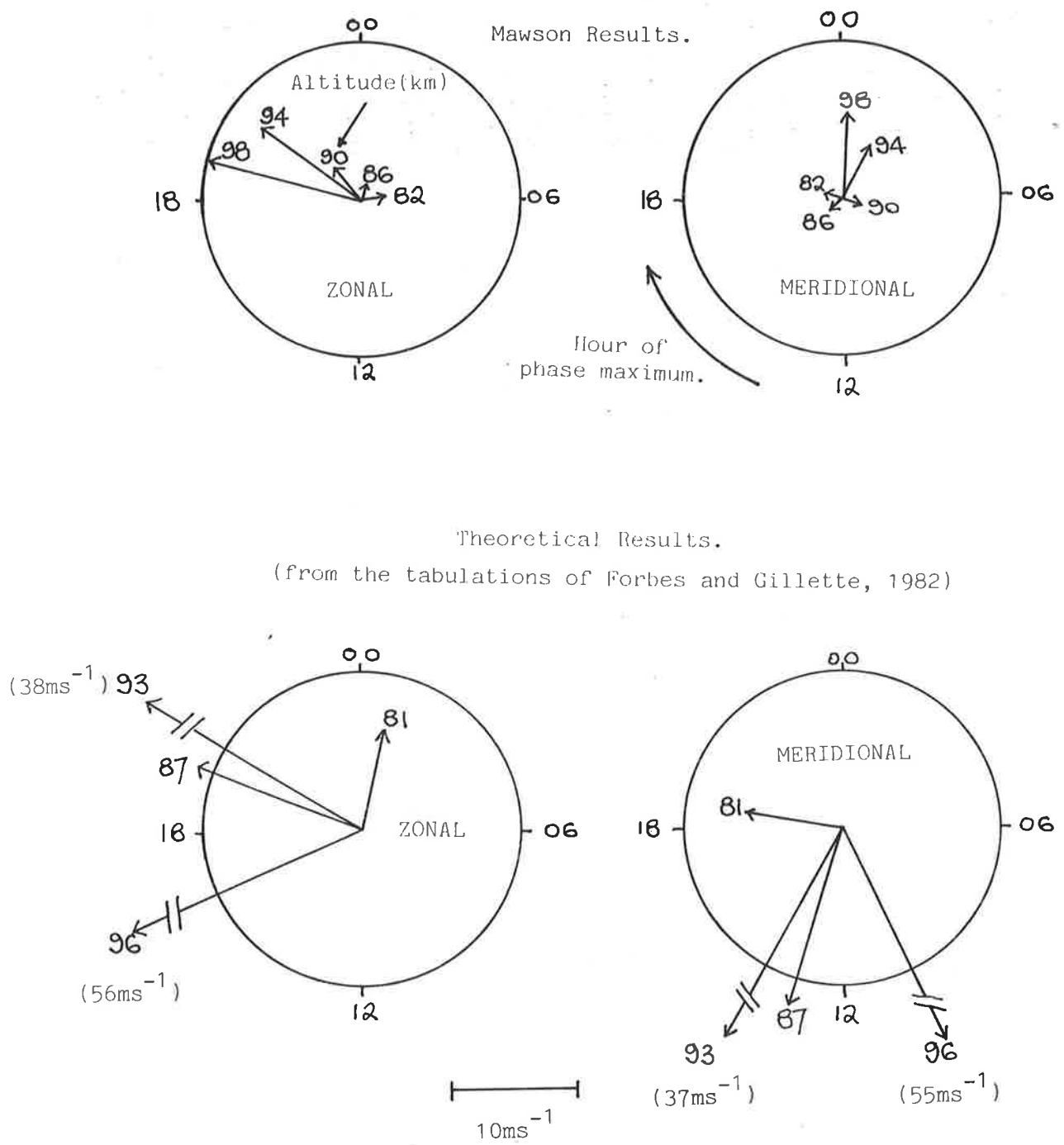
96
$(55ms^{-1})$

10ms^{-1}

Figure 4.12. Comparison of the Semidiurnal Tidal Vectors Observed at Mawson
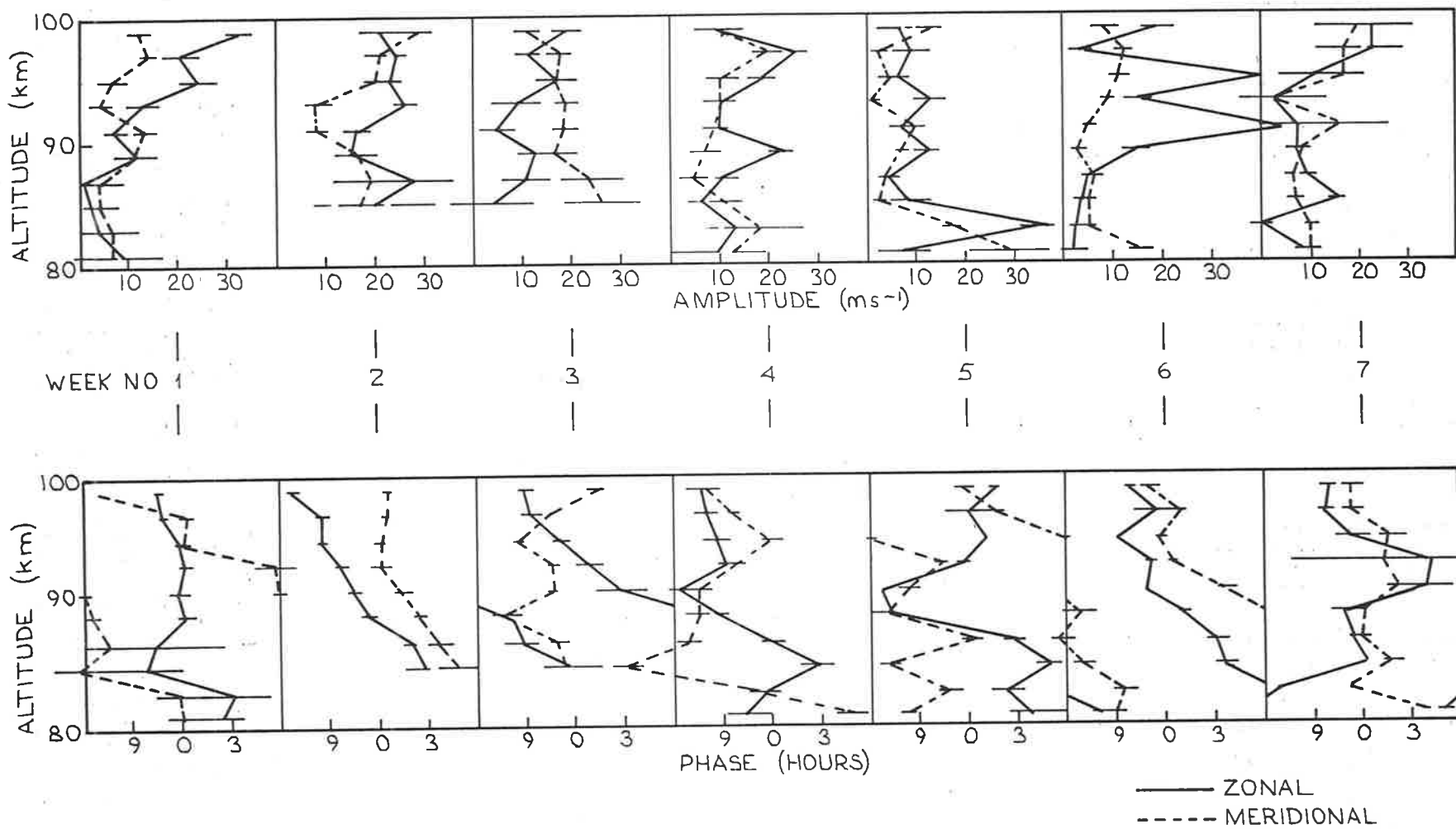with those Calculated Theoretically.

Figure 4.13.   Semidiurnal tide at Mawson: weekly averaged results.

between the zonal and meridional components in this altitude range is also variable from week to week. Near 90 km for example, week 1 and week 6 show a phase difference of approximately 6 hours between components, weeks 2 and 3 show a phase difference of about 3 hours, and during weeks 4, 5 and 7, the phase difference is consistently less than 3 hours. It is of interest to note that for week 2 the phase structure is very steady, with the zonal and meridional components in approximate phase quadrature over most of the observed range, indicative of a propagating tide. The vertical wavelength of this structure is approximately 30 km, which corresponds closely to the (2,6) mode.

Such variability is predicted by theoretical models (Forbes, 1982b) due to the presence of various tidal modes in the 80 to 100 km region. Tidal variability has been discussed in more detail in the introduction, where it was emphasised that slight shifts in the relative phases among various modes can lead to considerable changes in phase of the total semidiurnal variation from day to day with respect to latitude and height. The variability of the semidiurnal tidal components generated from week to week as demonstrated in figure 4.13, particularly below about 90 km, is no doubt responsible for the very small amplitudes in this range shown in figure 4.11, through the destructive interference of the various modes generated from week to week when averaged over the length of the observation period.

Figures 4.14 and 4.15 show the semidiurnal results of the harmonic analysis of a 4-day running mean performed on the data set used to produce figures 4.9 and 4.10. At the lower level (figure 4.14), except for
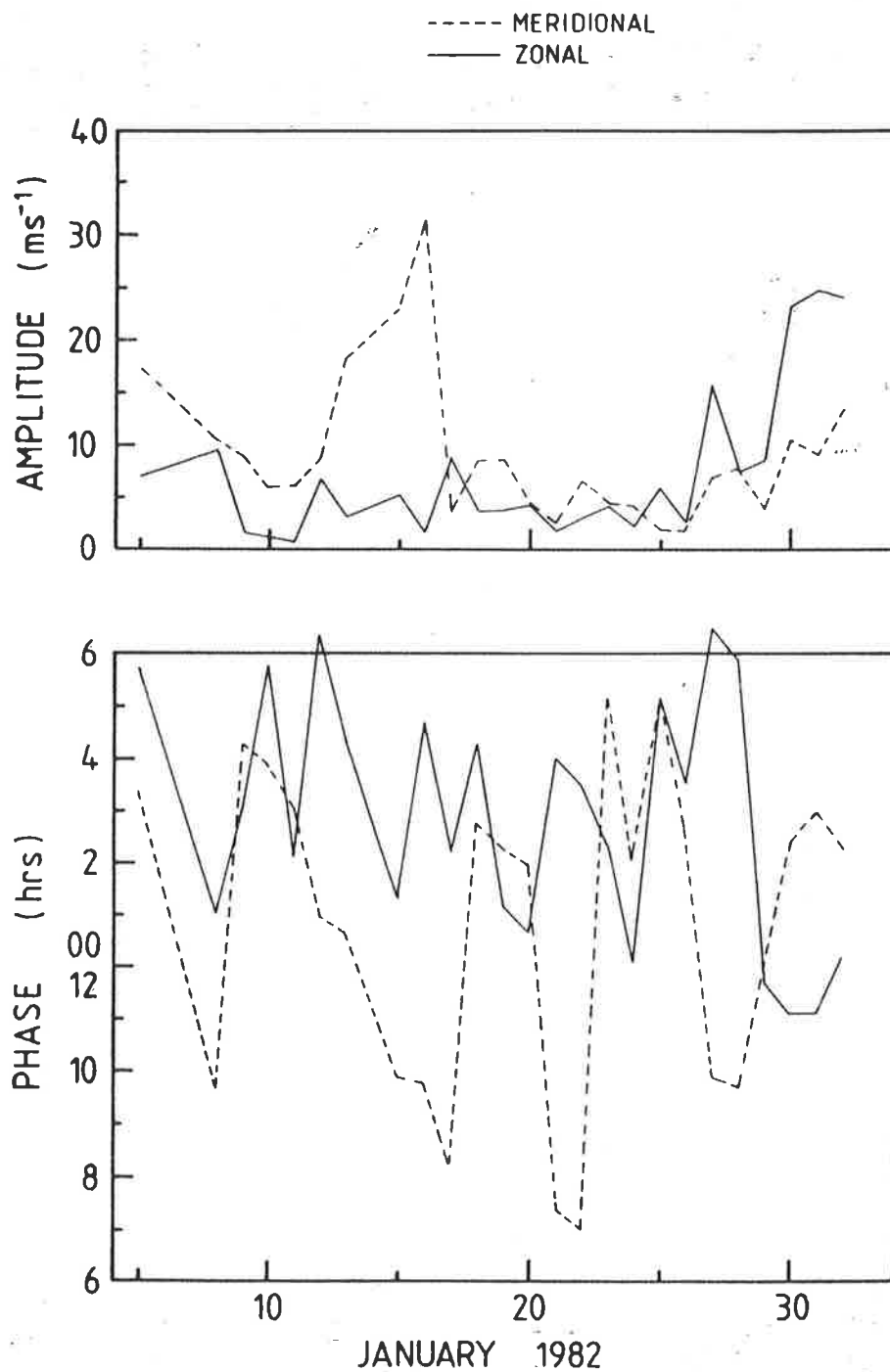
Figure 4.14   Semidiurnal tide at Mawson: 4-day running means
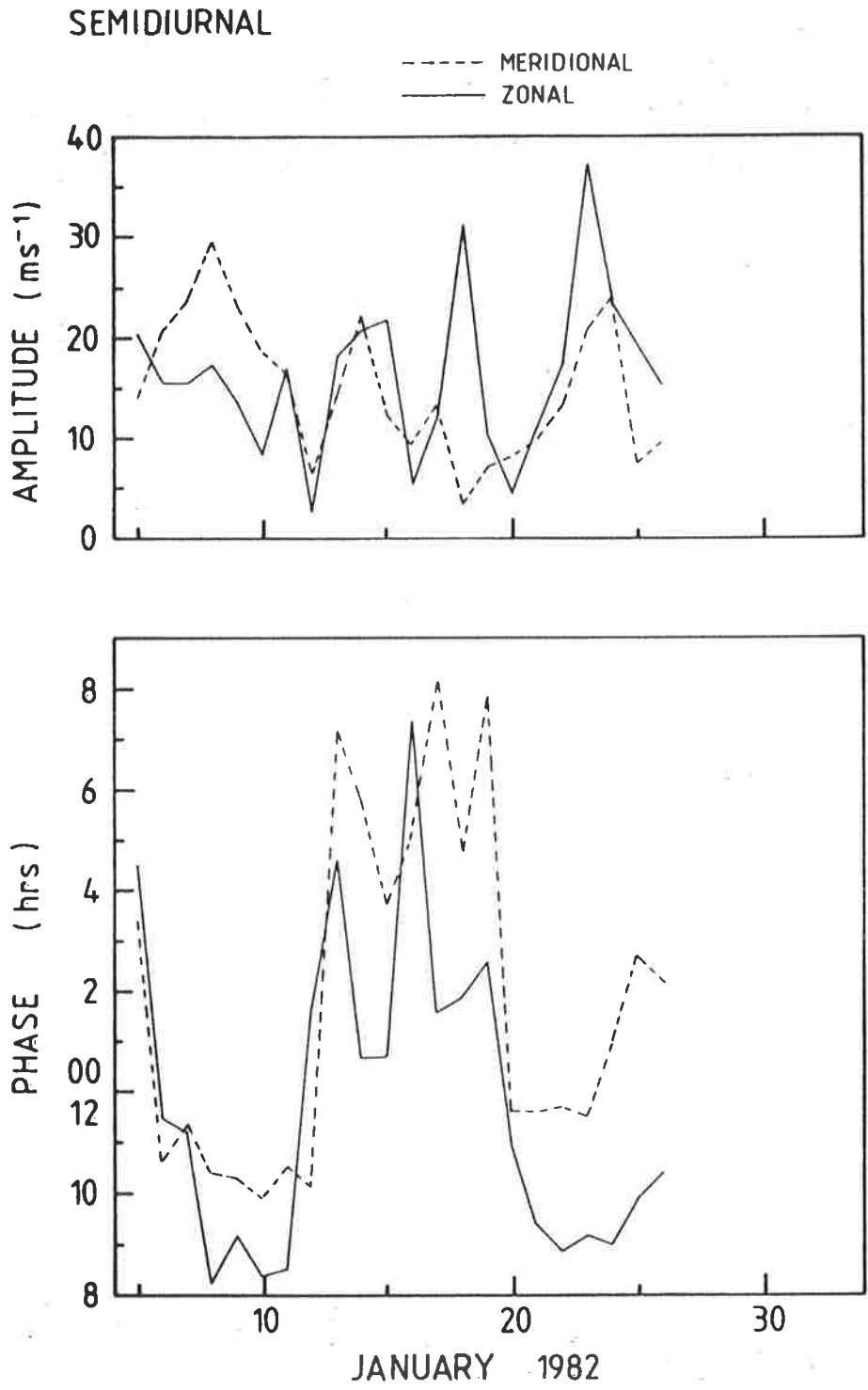for the altitude range 82-88km.

Figure 4.15. Semidiurnal tide at Mawson: 4-day running means for the altitude range 92-98km.

a large meridional excursion centred near January 15, and a zonal increase near January 30, the amplitudes are small, less than 10 ms^{-1}, with the meridional components being slightly larger overall up to January 24. The phase results show large shifts over the period of a few days for both components, with the zonal component generally leading the meridional by about 4 hours.

For the higher level (figure 4.15), the zonal and meridional components are of similar magnitude, with the zonal component tending to incease over the period shown, while the meridional shows a slight decreasing trend. The phase results indicate that the relationship between components remains approximately constant , with the meridional component leading the zonal by 2 to 3 hours throughout the period shown, but that the whole semidiurnal system undergoes a large shift of about 6 hours every few days.

4.1.4 Spectral Analysis.

A spectral analysis of the data obtained at Mawson is the best way to gain insight into the nature of the dominant atmospheric oscillations. The nature of the experiment at Mawson, and the constraints of its use there, meant that it was not possible to spectrally analyse the data and obtain information on short-period oscillations, such as high frequency gravity waves. The best suited data to spectral analysis in this case were the hourly averaged wind values discussed in much of this thesis, which constrains any analysis to periods greater than 2 hours. On examination, it was found that the best compromise for the purposes of spectral analysis was to use the hourly averaged results of the 92 and 94 km height bands.

The data set used in the spectral analysis shown in figure 4.16 begins at the start of week 1, and, at the 92 - 94 km level, contains the most continuous data available. Even so, slightly less than 50% of the following 1024 hours contained no measured wind values. This must be stressed before any further discussion of the spectral analysis.

The gaps in the data were filled by interpolating between measured values. The resulting data sets were then transformed to have zero means, and any linear trends were removed by a least squares fit to the data and subsequent transformation. A cosine taper was then applied to the 10% of data at either end of each data set, to reduce sideband leakage, before applying a Fast Fourier Transform (FFT). Finally, the spectral powers were calculated and frequency averaged over 4 bins. Assuming that the random error associated with the data has a chi-squared distribution (Bendat and Piersol, 1971), then there are 8 degrees of freedom associated with each spectral estimate. The actual error is likely to be larger due to the paucity of the data.

The general shape of the curves shown in figure 4.16 is very similar to those presented by other authors for other sites, e.g. Vincent and Ball, 1981; Bell, 1983; Vincent, 1984a; Vincent, 1985 (which primarily deal with results from Adelaide and Townsville) and Johnson and Luhman, 1985 (for Poker Flat). For comparison, the results of Johnson and Luhman, 1985; are included (figure 4.17) because they were obtained at a high latitude site, and they represent the spectral analysis of data sets of similar length to that obtained at Mawson.
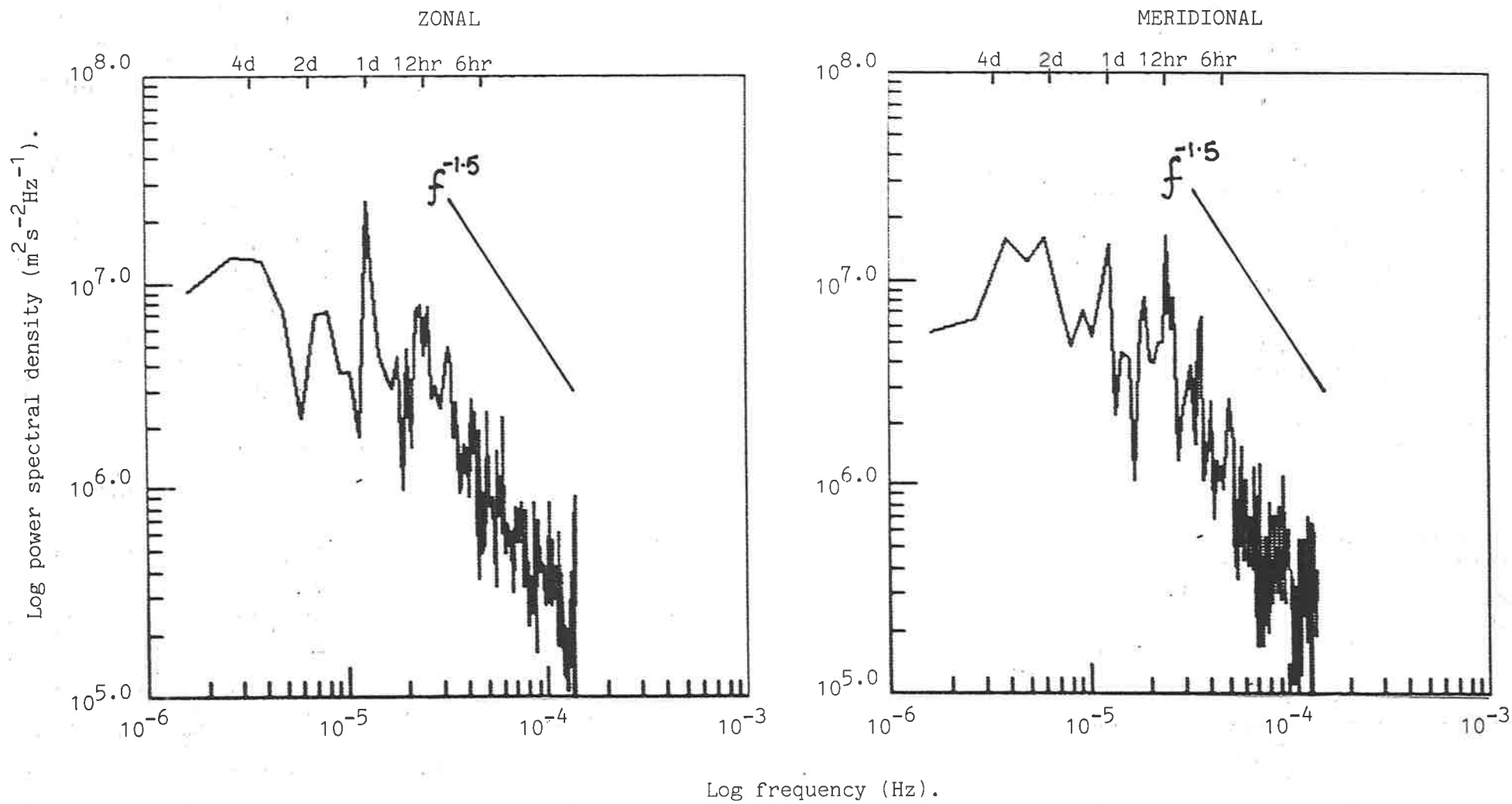
Figure 4.16. Zonal and meridional spectra of the 92-96km altitude range at Mawson (1981/1982 Summer).
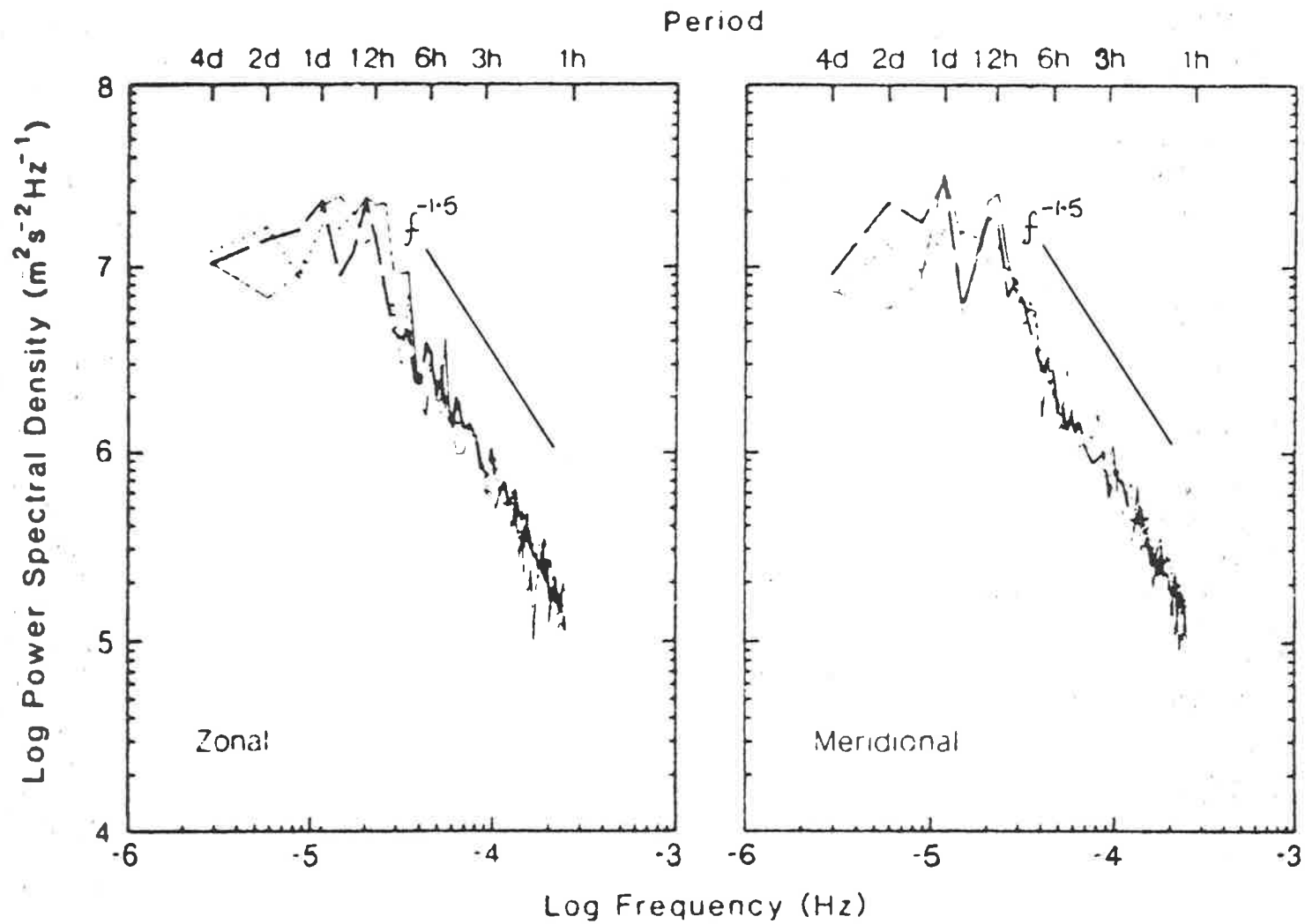
Figure 4.17. Zonal and meridional power spectra for 1980-1982 from Poker Flat superimposed. Solid, dotted and dashed lines correspond to 1980, 1981 and 1982 respectively.

(Johnson and Luhman, 1985).

Analysed in this way, the data shown has a cut-off period of 2 hours. In his discussion of spectral densities observed at Adelaide and Townsville, Vincent (1984a) notes that these spectra are best represented by two segments, a constant power segment at long periods and a power law segment of the form $S(f) \propto f^{-k}$ at shorter periods, with the break between these segments occurring close to the inertial period at the two sites. The inertial period in hours is $\tau_i = {}^{12}/_{\sin\phi}$, where ϕ is the latitude. At Mawson τ_i is 12.9 hours. A break at this period is expected theoretically as internal gravity waves cannot exist at intrinsic periods greater this. Background winds may Doppler shift some wave energy to longer periods relative to a ground based observer and cause apparent variation in the period at which the break between the constant power and power law segments occurs. The constant power law segment of the data shown in figure 4.16 begins close to the inertial period, as do the results shown in figure 4.17. The slope of the spectra of figure 4.16 at periods less than about 12 hours is approximately 1.5, close to the value found by other workers (e.g. Vincent, 1984a).

A measure of the root mean square gravity wave amplitude at Mawson can be obtained by integrating under the spectra of figure 4.16 between the appropriate frequency limits. The best fit (excluding contributions from any prominent tidal peaks) to the power law segment of data obtained at Townsville, Adelaide and Poker Flat has been estimated by Vincent (1984a) as:

$$S(f) = 0.66f^{-1.5} m^2 s^{-2} Hz^{-1} \quad \text{(Townsville)},$$

$$S(f) = 0.96f^{-1.5} m^2 s^{-2} Hz^{-1} \quad \text{(Adelaide)},$$

$$S(f) = 0.33f^{-5/3} m^2 s^{-2} Hz^{-1} \quad \text{(Poker Flat)}.$$

Using these expressions, the root mean square gravity wave amplitudes of waves with periods between 2 and 12 hours have been calculated for each site. These values are shown below, along with the estimated root mean square gravity wave amplitude at Mawson for the same range of periods. Included in the table are the inertial periods at each site.

	V_{rms} (ms^{-1}).	τ_i (hours).
Townsville	12.7	36.9
Adelaide	15.4	20.9
Poker Flat	20.6	13.2
Mawson	15.0	12.9

Vincent (1984a) discussed the mean square gravity wave amplitudes at Townsville, Adelaide and Poker Flat, and noted little difference between the amplitudes at each site, but stressed that spectral estimates for periods less than 2 hours are less reliable than those for longer periods. With the additional observations from Mawson, it does appear that the southern hemisphere results in the 2 to 12 hour period range are smaller and more similar to each other than the equivalent result at Poker Flat.

From figure 4.16, it can be seen that there is evidence of a large contribution to the dynamic wind field from waves with periods greater than 2 days in both zonal and meridional profiles. There are also significant peaks at the diurnal and semidiurnal periods. In the zonal profile there also appears to be some contribution at 16 and 8 hours. Evidence of a 16 hour component has also been presented by Carter and Balsley, (1982) for the Arctic summer mesosphere.

4.2 Townsville and Adelaide Results.

The profiles shown in figures 4.18, 4.20, 4.23, 4.26, 4.28 and 4.31 were obtained by sorting all available data for each site into respective 24 hourly bins, then performing harmonic analyses on the resulting data sets. In this manner the average prevailing, diurnal and semidiurnal results were obtained.

Also as with the Mawson results, each week of data from Townsville and Adelaide has been treated as an 'equivalent' day and analysed harmonically. These results are presented in figures 4.19, 4.22, 4.25, 4.27, 4.20 and 4.33. For figures 4.18 and 4.26, typical standard errors for the means are about 2 ms^{-1}, and for figures 4.19 and 4.27 about 4 ms^{-1}. The uncertainty in the amplitudes of figures 4.20, 4.23, 4.28 and 4.31 is about ±2 ms^{-1}: the corresponding errors in phase are ±1 hr. Errors for the weekly averaged results presented in figures 4.22, 4.25, 4.30 and 4.33 are estimated to be ±5 ms^{-1} in amplitude and ±2 hr in phase. For levels where tidal amplitudes are very small however, the corresponding uncertainties in phase may be much larger.

4.2.1 Townsville Prevailing Winds.

Figure 4.18 shows the average zonal and meridional wind profiles between 80 and 100 km observed at Townsville during the period 26/July/80 to 29/Aug/80. These data were used by Manson et al. (1985) in the production of the prevailing wind profiles shown in figure 1.4 for Townsville.

The zonal component profile shows a steady decrease in the vertical gradient of the zonal component from approximately 2.5 ms^{-1}km^{-1} at 80 km to about 1 ms^{-1}km^{-1} near 95 km. The height of zero crossing is close to 92 km.
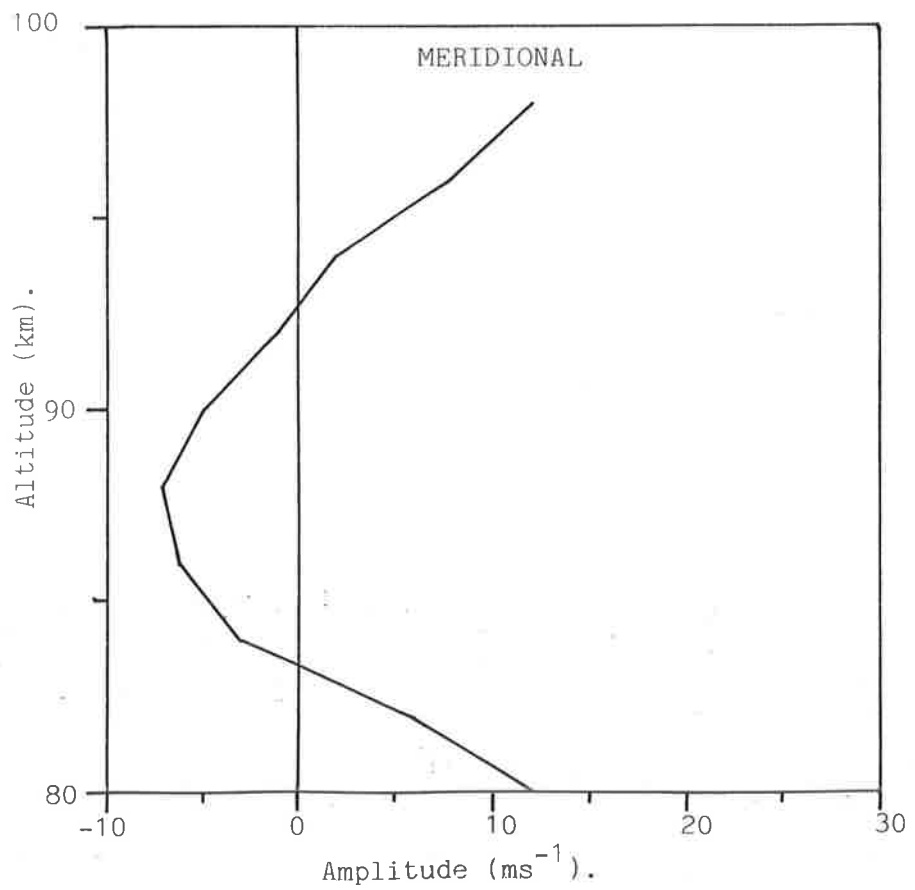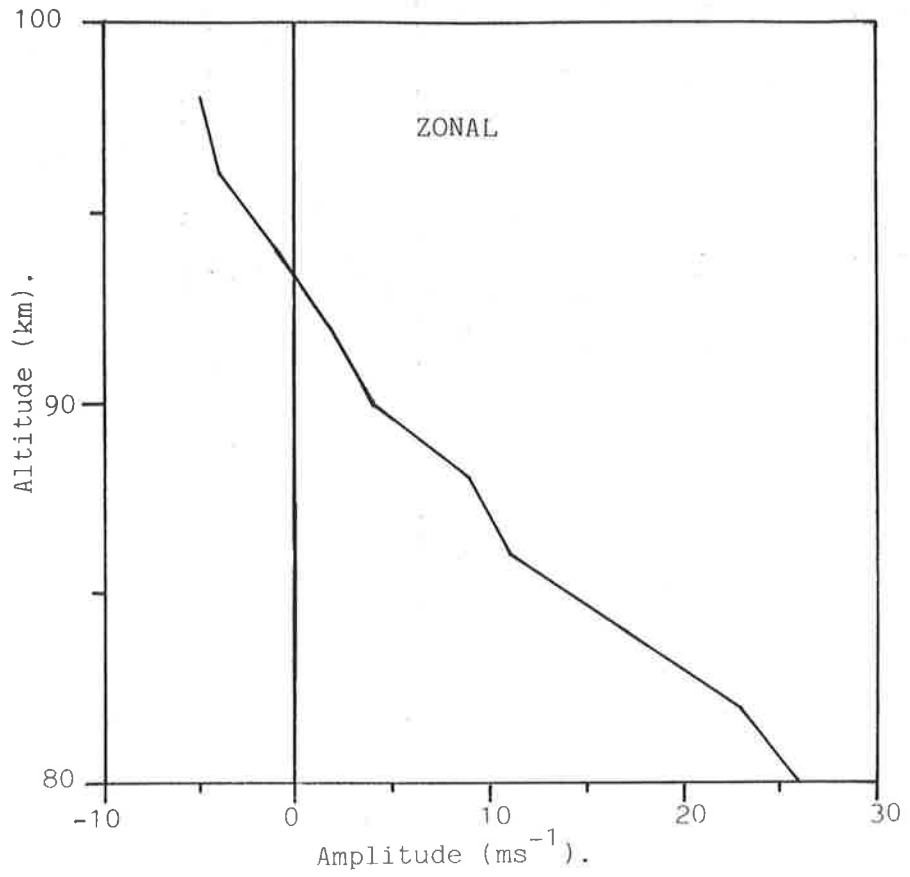
Figure 4.18. Mean prevailing winds at Townsville.

The meridional profiles show a decrease of about 3 $ms^{-1}km^{-1}$ between 80 and 85 km, changing from equatorward (northward) winds to poleward (southward) winds near 84 km. A poleward maximum of 7 ms^{-1} is seen at 88 km, and from 90 to 98 km, the meridional values increase by about 2 ms^{-1} with the flow changing from poleward to equatorward flow near 92 km.

The weekly averaged results for the zonal and meridional prevailing winds are shown in figure 4.19. Overall, the zonal profiles show a decrease in amplitude from >20 ms^{-1} at 80 km to values generally less than -10 ms^{-1} at 98 km. Major deviations from the mean zonal profile shown in figure 4.18 occur in the first and second weeks below 90 km. In the second week, no westward winds are observed, although above 84 km, the flow is weak, with amplitudes of only a few ms^{-1}.

In the meridional profiles of figure 4.19, weeks one, two and three show profiles whose overall structure is very similar to the meridional profile of figure 4.18, with the magnitudes in week three at 80 and 98 km being approximately 10 ms^{-1} and 20 ms^{-1} respectively, greater than those in week one. Week two also shows a similar structure to weeks one and three, except that the southward jet appears to occur at a slightly lower altitude (86 km) than it does in the other weeks. Week four shows a relatively large region between 84 and 94 km in which the mean meridional wind is close to zero with an apparent weak southward flow at 88 km. The meridional profile shown in week five is similar to the average profile for the whole observation period except for a local maximum in northward flow at 90 km. It is of interest to note the gradual increase in the strength of the meridional jet which occurs in the range 86 to 90 km, from a value of -15ms^{-1} in week one to an average value near zero in week 5.
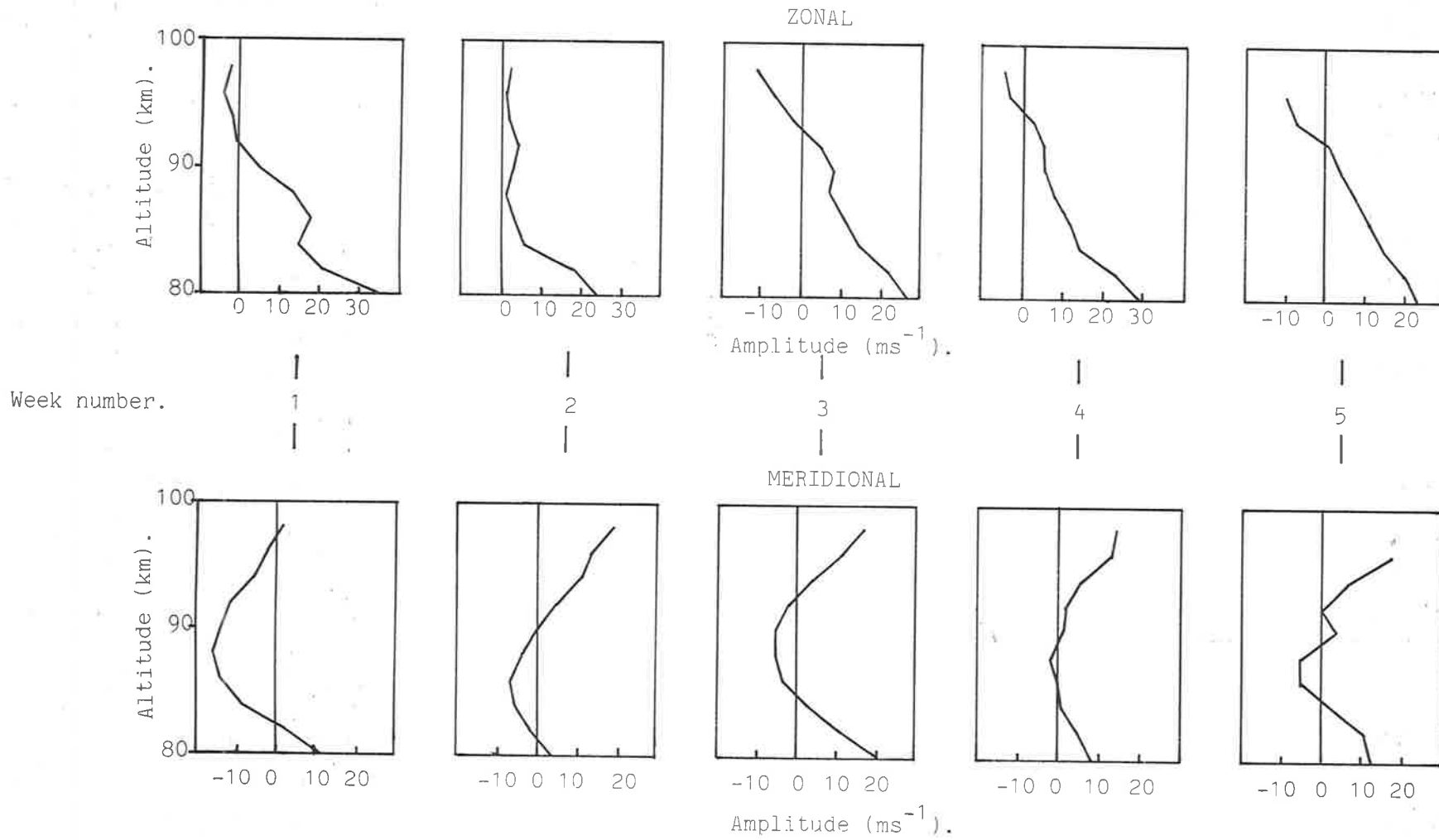
Figure 4.19. Prevailing winds at Townsville: weekly averaged results.

4.2.2 Townsville Diurnal Tide.

The average diurnal tidal results for the observation period at Townsville are shown in figure 4.20. Both profiles show smooth and similar transitions in amplitude and phase throughout the range 80 to 100 km.

Meridional amplitudes are more than double the corresponding zonal amplitudes at all levels. A zonal maximum of 25 ms^{-1} can be seen near 90 km and, at the same level, a meridional maximum of 53 ms^{-1}. At 80 and 98 km the amplitudes of both profiles are about half the corresponding maximum values.

The phase variation with height is very stable and similar for both components, each showing a decrease in the time of maximum phase with increasing altitude, indicative of a propagating tide. The implied vertical wave length of the diurnal tide is close to 40 km.

Results have been presented by Vincent and Ball (1981) for Townsville during June (southern hemisphere winter) and November (southern hemisphere spring) 1978. These results are shown in figure 4.21. The profiles of figure 4.21 show that both zonal and meridional components increase significantly from June to November 1978. The November 1978 results are closer to those presented in figure 4.20 than are those for June 1978. Also, the meridional amplitude maxima shown in figure 4.21 occur at 95 km in June 1978 and at 86 km in November 1978. The zonal profiles of Figure 4.21, show no maximum in June, but in November there is a maximum at 86 km. The profiles of figure 4.20, show both zonal and meridional amplitude maxima near 90 km, well placed for smooth transitions in the peak of the diurnal flows from June to November. The timing of the
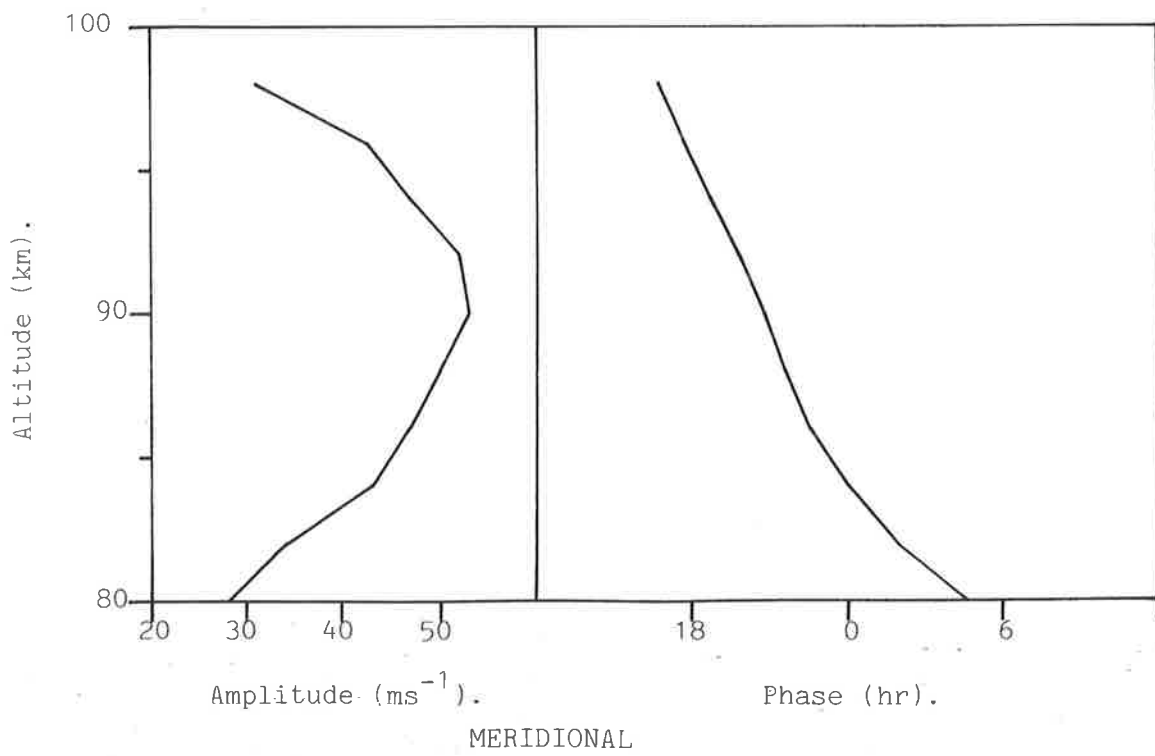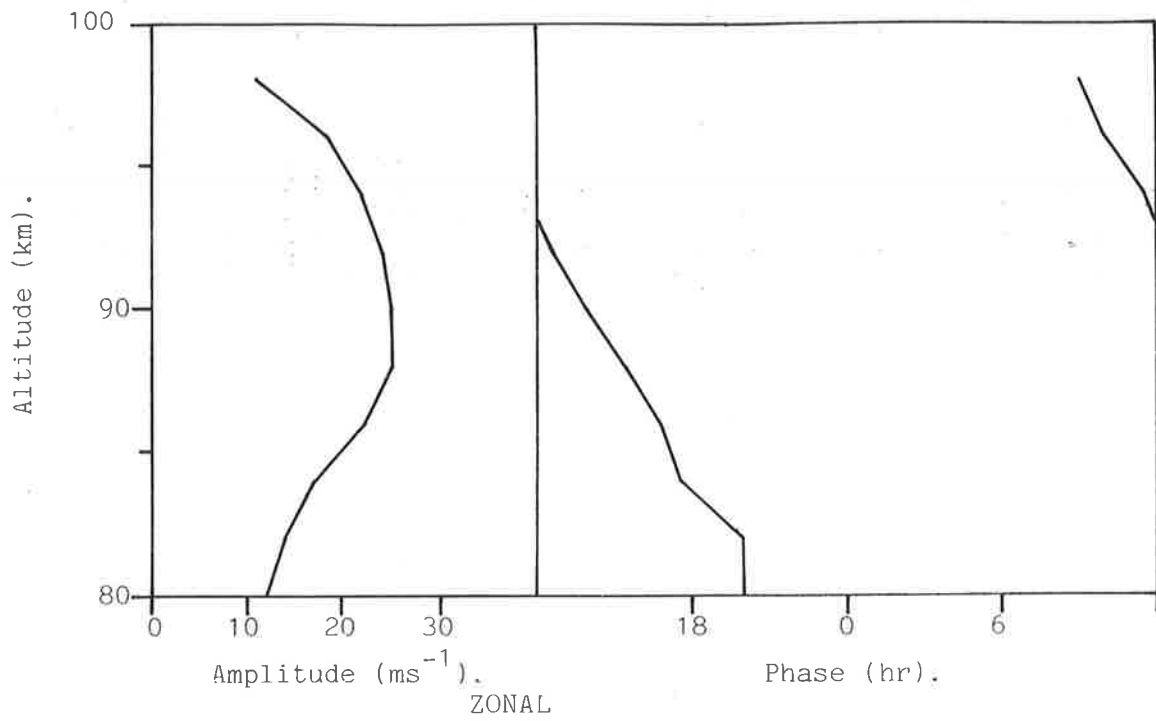
Figure 4.20. Mean diurnal tide at Townsville (July/August 1980).

ZONAL
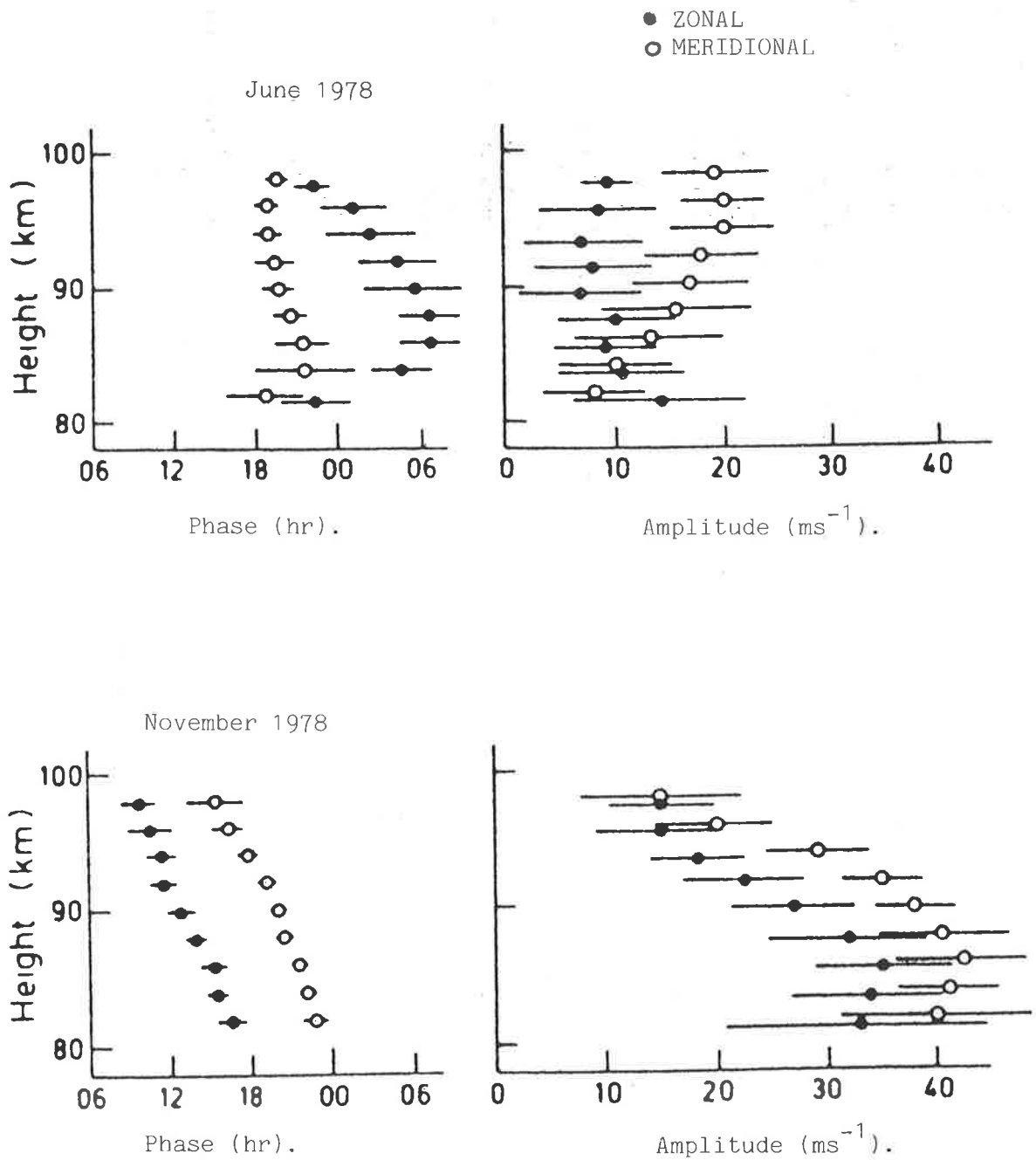MERIDIONAL

June 1978

November 1978

Figure 4.21. Townsville diurnal tide (Vincent and Ball, 1981).

July/August 1980 results is important as can be seen from figure 1.4, in which rapid equinoctial changes, especially in the zonal component, are apparent near the end of August.

Examination of the phase results of figures 4.20 and 4.21 show that the July/August 1980 observations are more spring-like than winter-like. The implied vertical wavelength of the diurnal tide in June 1978 was ~75 km, and in November 1978 was ~50 km, closer to the value of 40 km estimated for the July/August 1980 diurnal tide.

The weekly averaged results for the diurnal tides observed at Townsville are presented in figure 4.22. Over the period of observation, the zonal diurnal amplitude at 80 km increases from close to zero during week one to about 30 ms^{-1} in week five. Also, the height of maximum diurnal amplitude varies from 94 km in week one to 88 km in week five.

The meridional profiles of figure 4.22 show some week to week variability in the overall shape of the profile, but maximum values are all ~50 ms^{-1} and all occur between 88 and 92 km.

The diurnal zonal phase results show a similar structure with height for all profiles above 84 km, above which level, the time of maximum phase at all levels increases by about 4.5 hr over the observation period. This is in accord with the results of Vincent and Ball (figure 4.21). Most variability is seen in the zonal phase results below 84 km.

The diurnal meridional phase results show very similar structures and times of phase maxima over the whole observation period. Above 90 km however, weeks one, two and three show a tendency towards either a longer
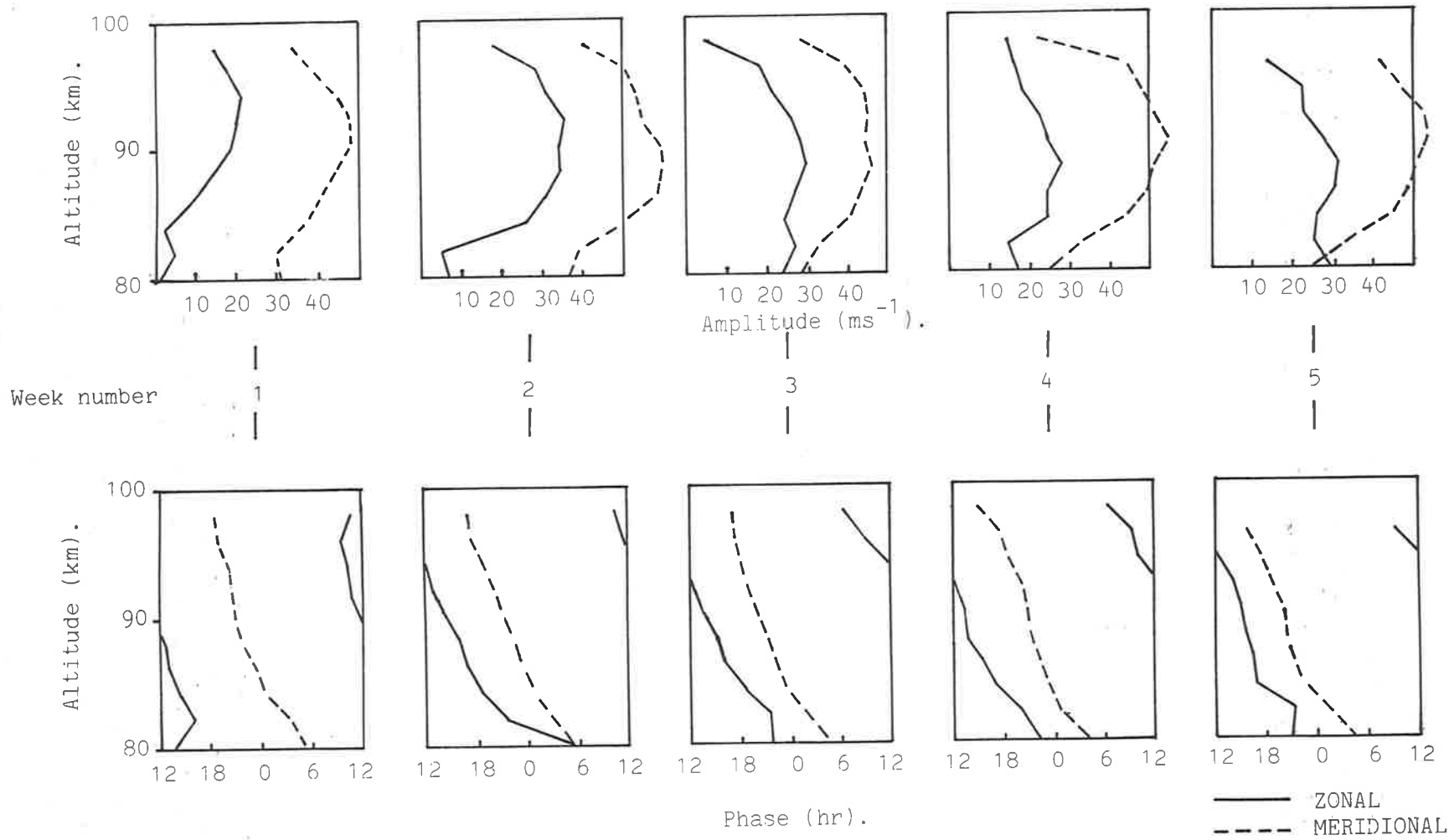
Figure 4.22.   Diurnal tide at Townsville: weekly averaged results.

vertical wavelength or an evanescent diurnal tide, whereas in weeks four and five, the upper levels indicate shorter vertical wavelength modes. This tendency is also reflected to some extent in the zonal phase results of figure 4.22.

Also over the period of observation, above about 84 km, the phase difference between the zonal and meridional components varies from approximately 10.5 hr in week one to 4.5 hr in week 5.

4.2.3 Townsville Semidiurnal Tide.

The average semidiurnal results for the July/August observation period at Townsville are given in figure 4.23. Although the zonal and meridional semidiurnal amplitudes are small, there are increases of a few ms^{-1} from 80 to about 90 km in both profiles, with a reduction in amplitude and less orderly behaviour above 90 km.

For the zonal phase structure below 92 km and at all heights for the meridional phase profile there is good evidence of a propagating semidiurnal tide with a wavelength of approximately 100 km. In the zonal profile, at 92 km, the phase structure breaks down. The zonal semidiurnal amplitudes above this level are small and erratic.

The Townsville semidiurnal tidal results of Vincent and Ball are shown in figure 4.24. Overall, the July/August results are more similar to the June 1978 results than to those of November 1978. This can be seen in the amplitudes of the semidiurnal tide, where for the June 1978 profiles, there are no results greater than 10 ms^{-1}, and local maxima near 88 km. The November 1978 results show a steady increase in amplitude with increasing height.
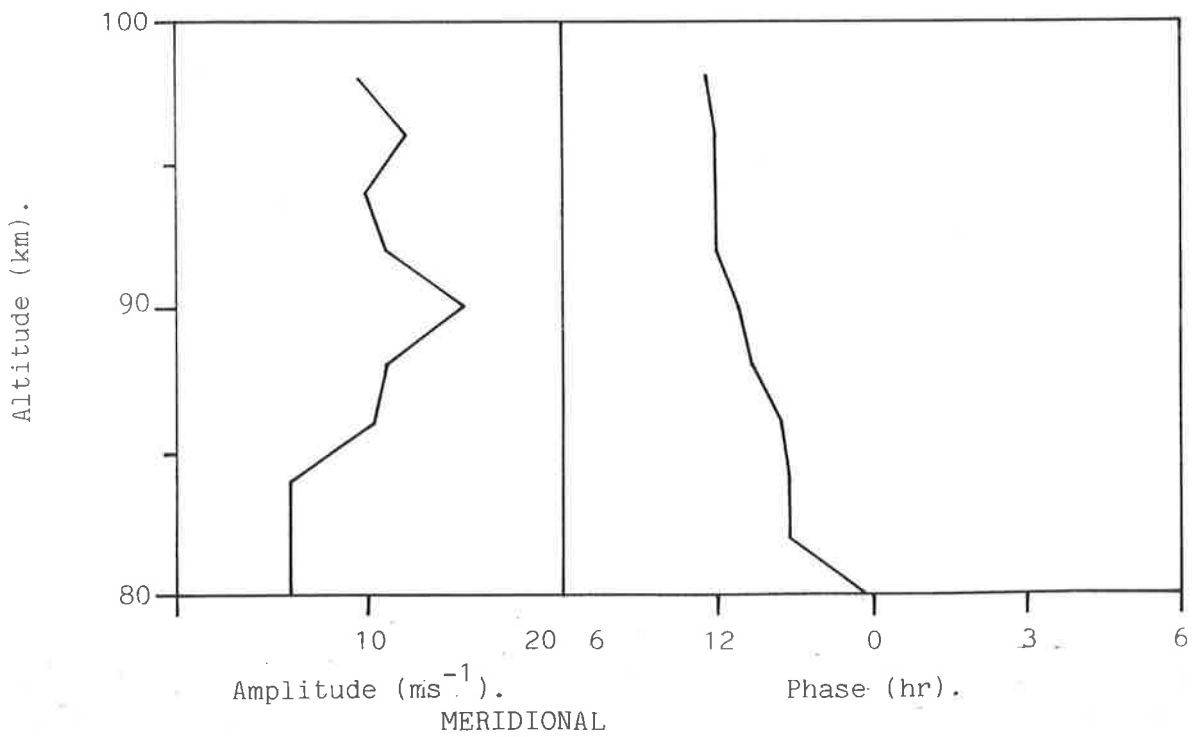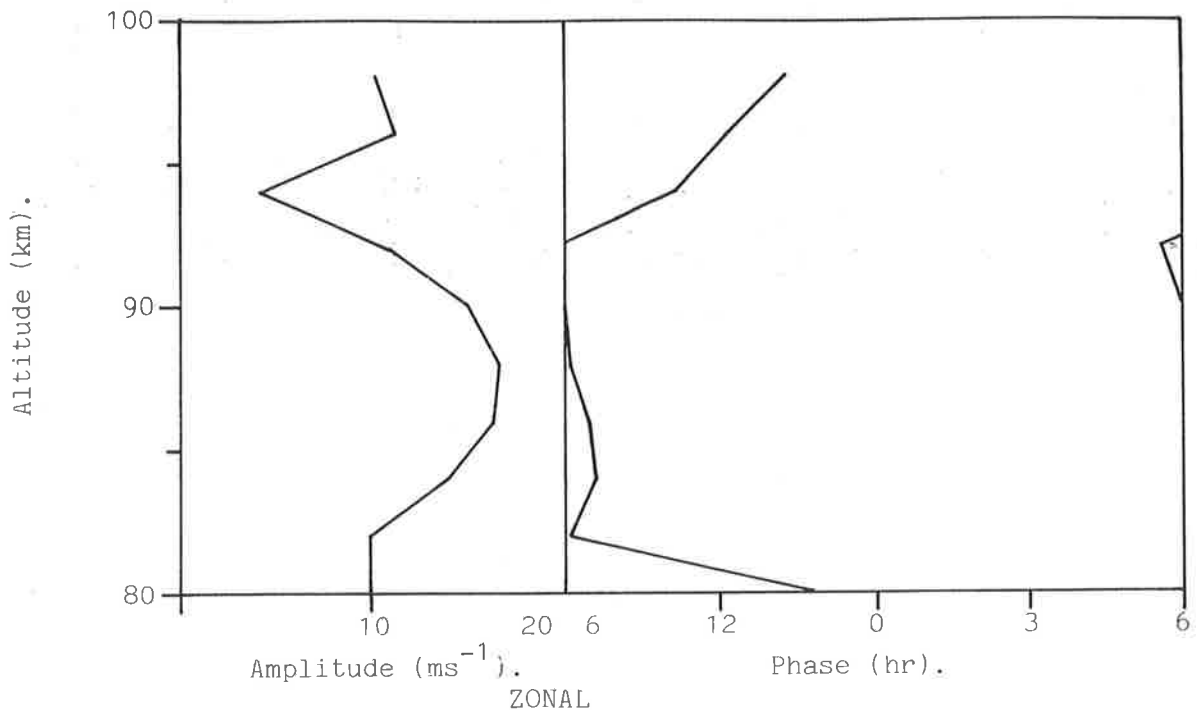
Figure 4.23. Mean semidiurnal tide at Townsville (July/August 1980).
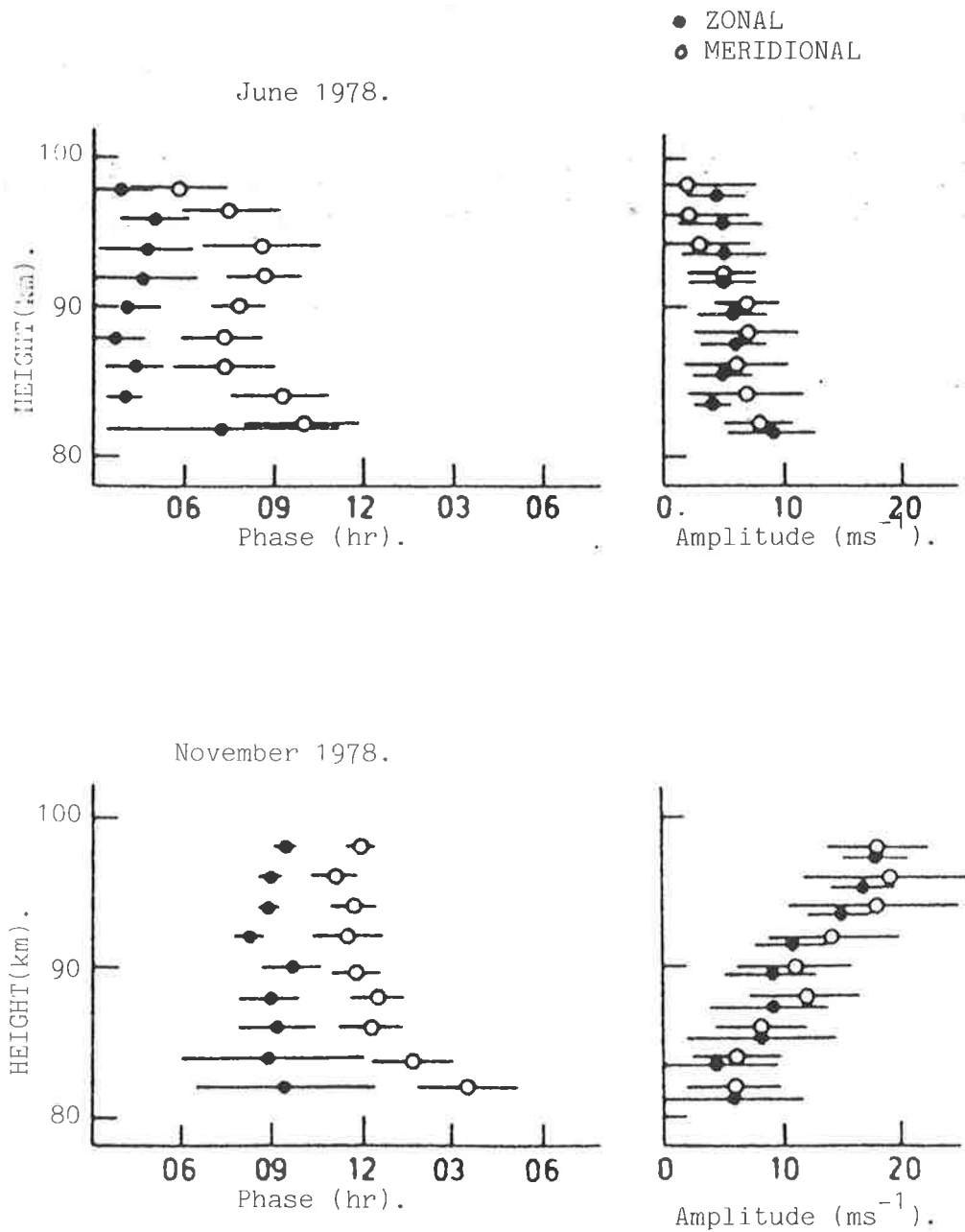
Figure 4.24.   Townsville semidiurnal tide (Vincent and Ball, 1981).

The phase results of June 1978 are overall, more similar to the July/August 1980 results than are the November 1978 results, although the latter zonal results above 92 km are very much like those of July/August 1980. This may be of significance when the dramatic equinoctial changes seen in figure 1.4 are taken into account.

The weekly averaged semidiurnal tidal results for Townsville are given in figure 4.25 and show considerable week to week variability. The amplitudes are fairly weak, with zonal components, apart from week three, rarely exceeding 10 ms^{-1}. In general the meridional amplitudes are larger than the zonal.

Except for those heights at which the semidiurnal zonal amplitudes are small (week 1, 82 and 94 km; week 3, 94 km; week 5, 92 and 94 km), the semidiurnal phase results indicate a long vertical wavelength (~100 km from figure 4.23) or an evanescent semidiurnal tide. Again as with the weekly averaged diurnal results, the meridional phase structure tends to remain more consistent over the observation period with mean values close to 9 hr. The zonal component generally leads the meridional component. At the 88 to 90 km level, this phase difference is close to 3 hours in weeks one and two and six hours in weeks three, four and five.

4.2.4 Adelaide Prevailing Winds.

The averaged prevailing winds observed in the period 26/July/80 to 29/Aug/80 are shown in figure 4.26. The zonal flow, eastward at all altitudes, is characterised by a smooth decrease in amplitude from 36 ms^{-1} at 80 km to about 7 ms^{-1} at 98 km, a decrease of about 1.6 ms^{-1}km^{-1}. The meridional flow is very weak below 92 km, with amplitudes of 2 ms^{-1} or
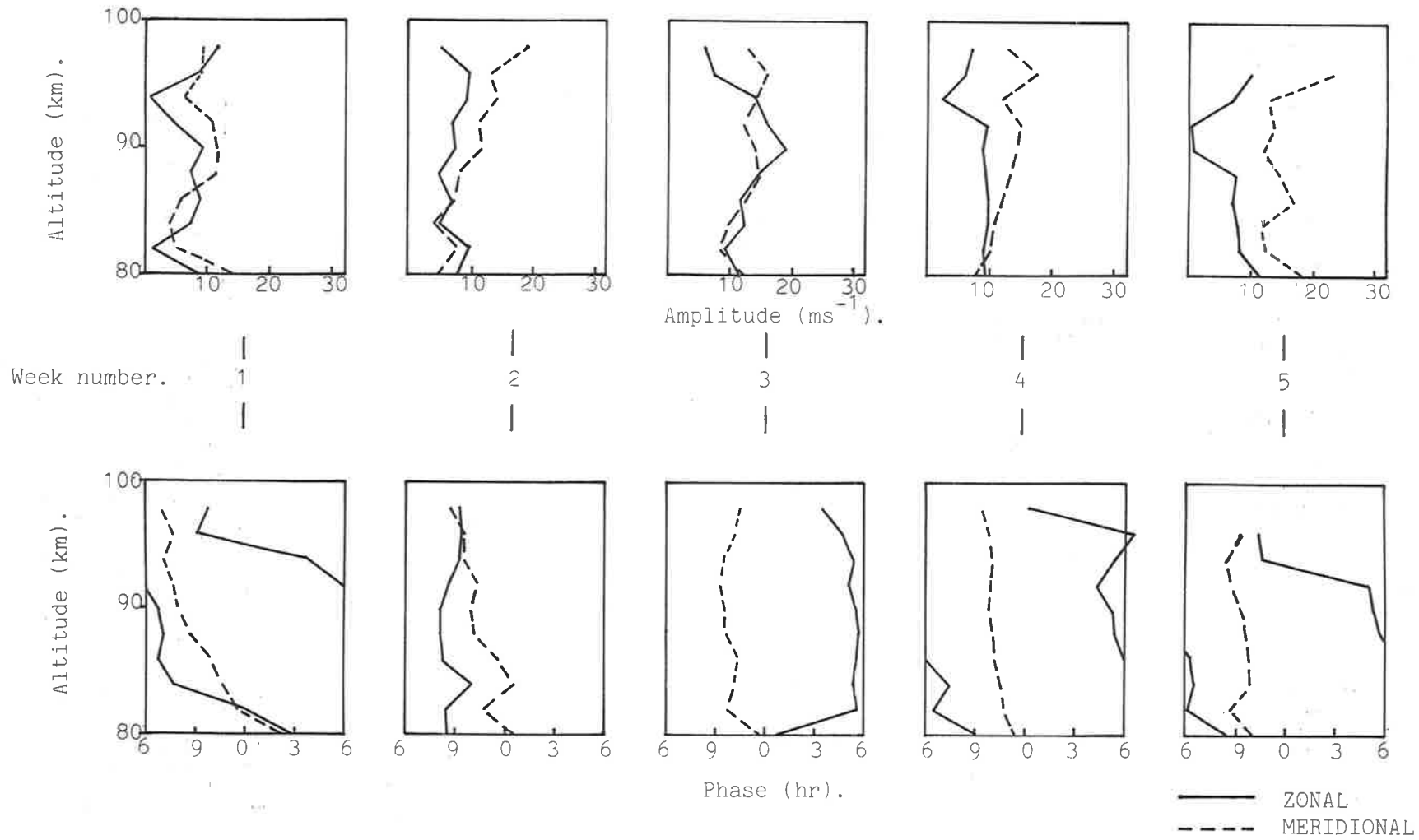
Figure 4.25. Semidiurnal tide at Townsville: weekly averaged results.
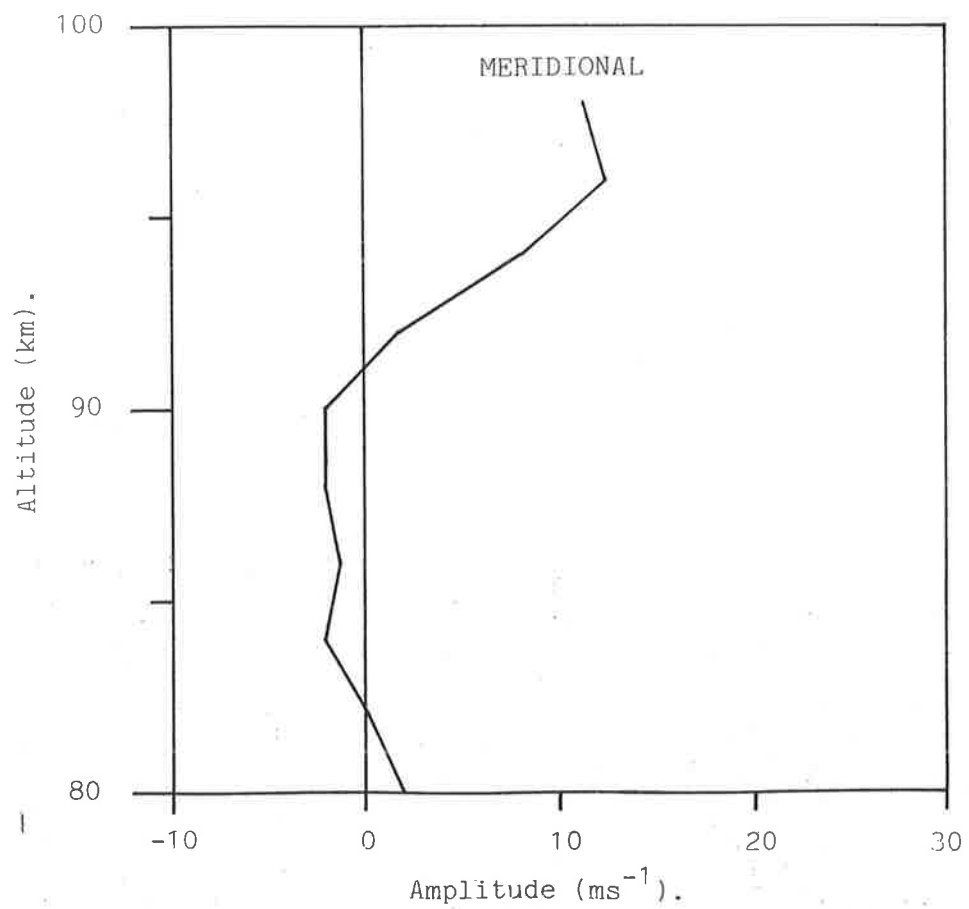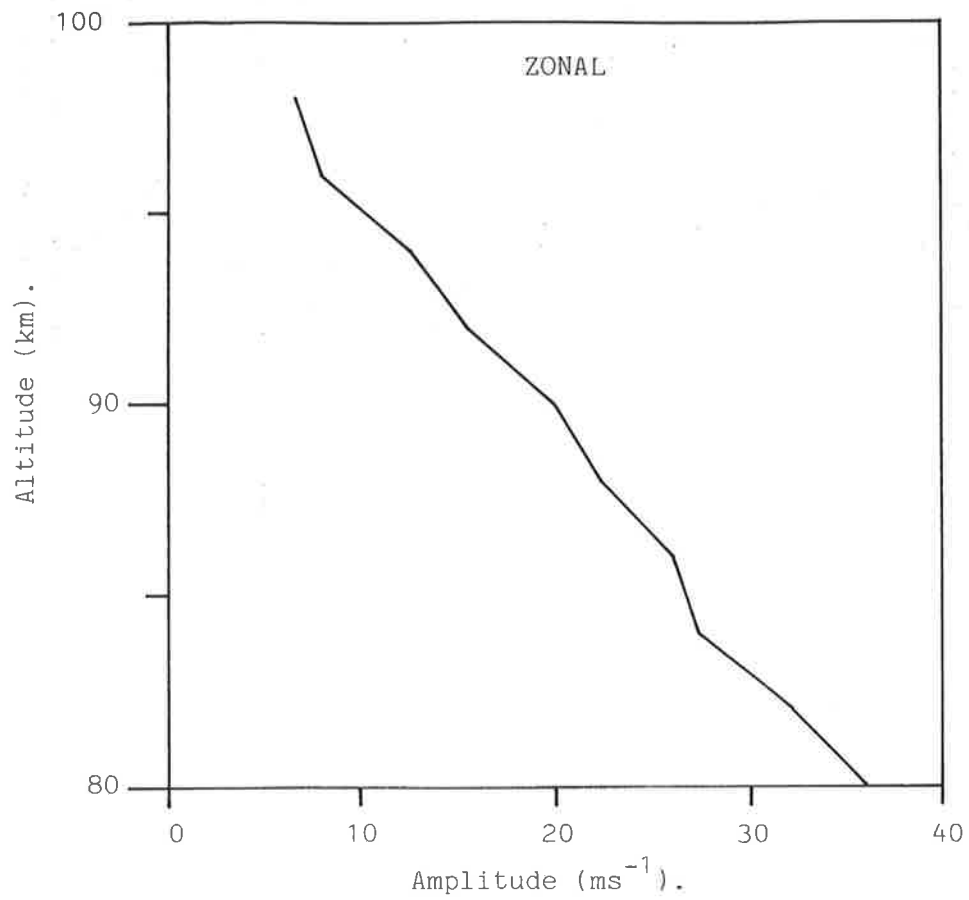
Figure 4.26. Mean prevailing winds at Adelaide.

less. Between 84 and 90 km there is evidence of a weak southward jet.
Above 90 km the meridional profile increases from -2 ms^{-1} to a maximum of
12.5 ms^{-1} at 96 km. These results were included in figure 1.4 presented by
Manson et al. (1985) as part of the total dataset (~5 years of data in
all) from which the figure was constructed.

In the weekly averaged zonal profiles of figure 4.27, the major
changes in the profiles from week one to week five is a steepening of the
mean profiles for each week from about 2ms^{-1}km^{-1} in week one to 1.5
ms^{-1}km^{-1} in week five. the largest departures from the mean state occur in
the region 84 to 94 km.

All meridional profiles of figure 4.27 except that of week five
show a general increase of slightly more than 20 ms^{-1} from the lowest to
the highest levels. The profile of week five shows a similar but weaker
(<10ms^{-1}) amplitude growth with height. The strongest southward flow
occurs in week one below 96 km. Again, the largest departures the mean
state occur in the 84 to 94 km region.

4.2.5 Adelaide Diurnal Tide.

The average diurnal tide observed at Adelaide in July/August 1980
is presented in figure 4.28. Both the zonal and meridional amplitude
components are large (~30 ms^{-1}) up to 90 km, and show minima near 95 km
(10 ms^{-1} for the zonal and ~20 ms^{-1} for the meridional), with slight growth
above.

The phase results show very stable structures, with the zonal
component leading the meridional by 6 hr, indicating a propagating diurnal
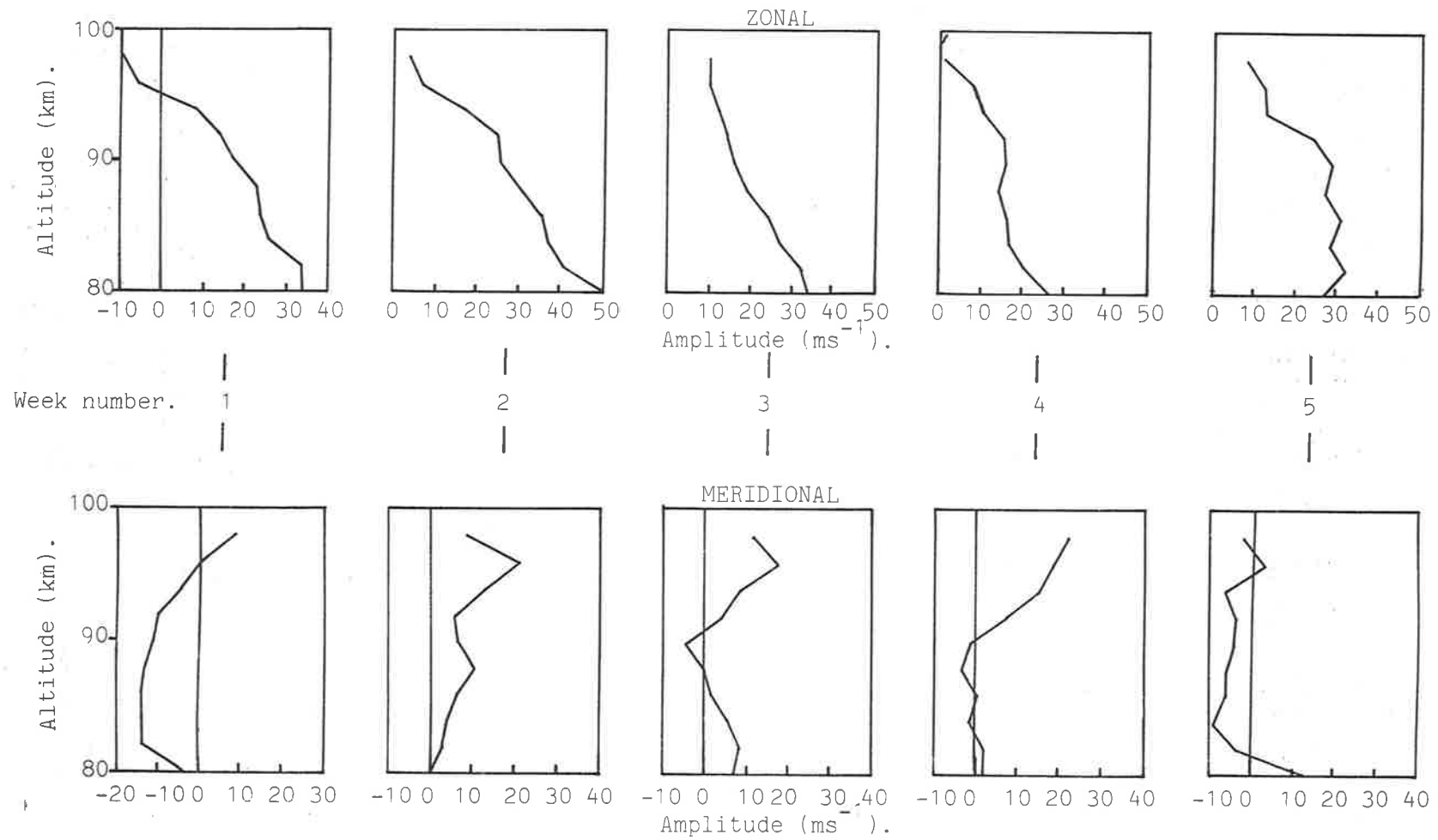
4.27. Prevailing winds at Adelaide: weekly averaged results.
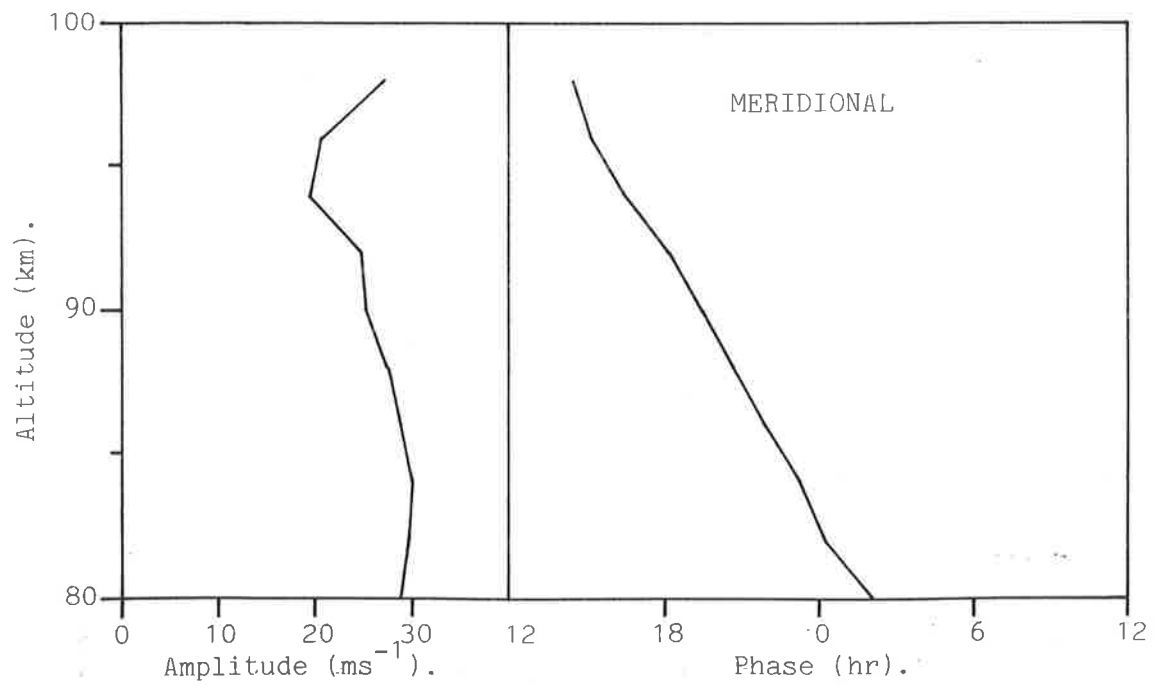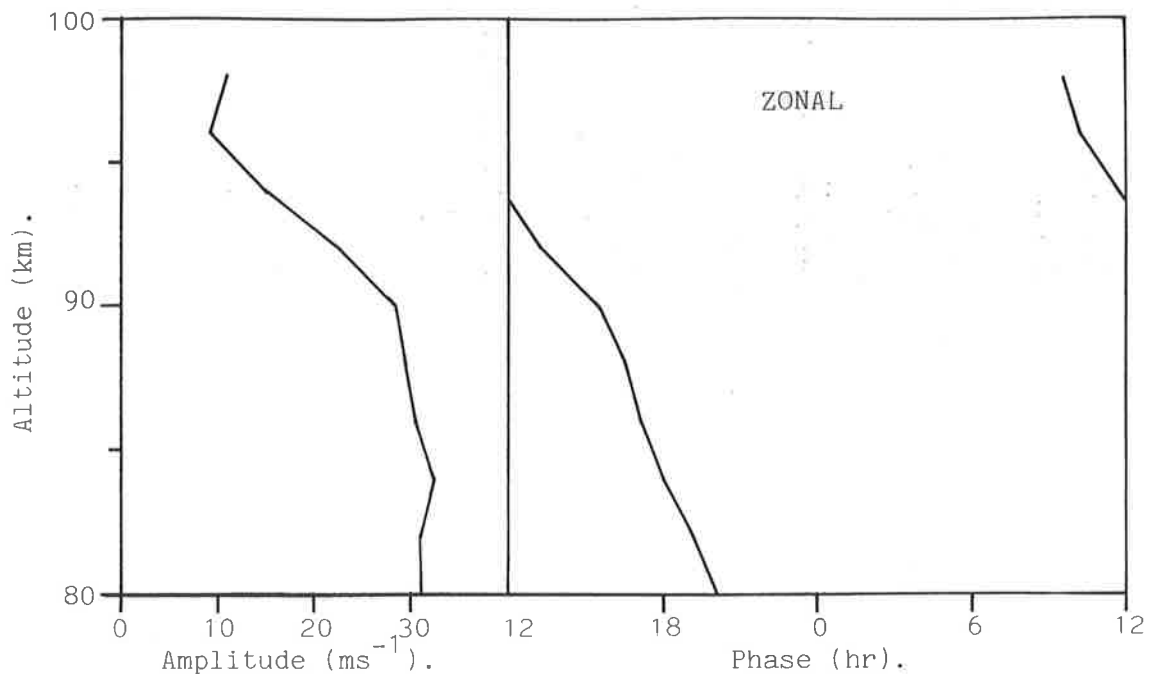
Figure 4.28. Mean diurnal tide at Adelaide (July/August 1980).

tide with an implied vertical wavelength close to 40 km. The phase results shown here are remarkably similar to those presented in figure 4.20 for the same period at Townsville.

Comparison of figure 4.28 with the June and November 1978 results of Vincent and Ball, (1981), given in figure 4.29, show that the phase structure of the July/August results is more similar to the June 1978 results than to those of November 1978. The zonal and meridional diurnal amplitudes shown for July/August 1980 show little similarity with either of those presented by Vincent and Ball. There is one important common feature in all amplitude profiles and that is the persistence with which minima occur close to 95 km.

The weekly averaged results for the diurnal tide at Adelaide are shown in figure 4.30. There is an increase in amplitude at the 80 to 90 km levels from week one to week 5, especially in the meridional component, from less than 10 ms^{-1} to ~30ms^{-1}. Above 90 km, the amplitudes over the period of observation are much more variable, although there is an increase in the meridional component from 20 ms^{-1} to 45 ms^{-1} from week 1 to week 5.

The phase results show very stable profiles varying only slightly above 90 km throughout the observation period. The comments made previously when discussing the average diurnal phase results apply here also, especially below 90 km. The most important features of the phase results of figure 4.30 are that the phase decreases with increasing altitude, the zonal and meridional components are in phase quadrature and that the implied vertical wavelength throughout the five weeks of observation is close to 40 km.

Figure 4.29. Adelaide diurnal tide (Vincent and Ball, 1981).
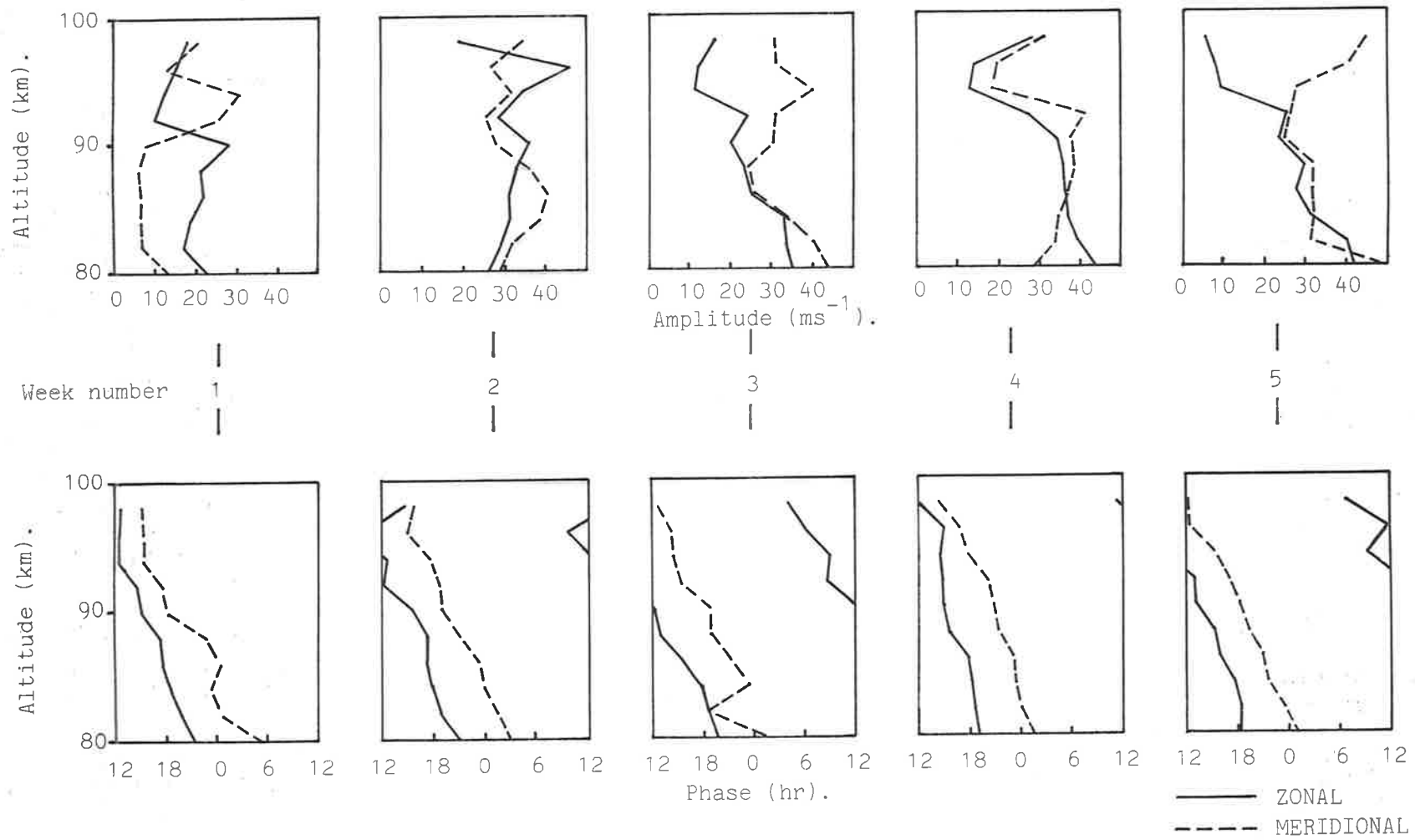
Figure 4.30. Diurnal tide at Adelaide: weekly averaged results.

4.2.6 Adelaide Semidiurnal Tide.

The average semidiurnal tide observed at Adelaide during July/August 1980 is shown in figure 4.31. Both amplitude components are relatively weak, and show some variability. The zonal amplitude increases from 2 ms^{-1} at 82 km to ~9 ms^{-1} at 98 km. The meridional amplitude results are much more variable.

The zonal phase structure at all levels, and the meridional phase below ~92 km, show evidence of a relatively short wavelength (~25 km) propagating mode.

The results of Vincent and Ball (1981) presented in figure 4.32 show little similarity with those of figure 4.31. Amplitude results shown in figure 4.32 for June and November 1978 are of the same order as those of figure 4.31, but there are no apparent common features. The phase results for June 1978 are indicative of a much longer vertical wavelength mode than that observed in July/August 1980, while the phase results for November 1978 are erratic.

The weekly averaged semidiurnal tidal results for the five weeks of observation are shown in Figure 4.33. They show considerable week to week variability.

In general, zonal and meridional amplitude components are of similar magnitude, and show a slight increases with altitude from about 5 ms^{-1} at 80 km to >10 ms^{-1} at 90 km. Above 90 km the results are much more variable.

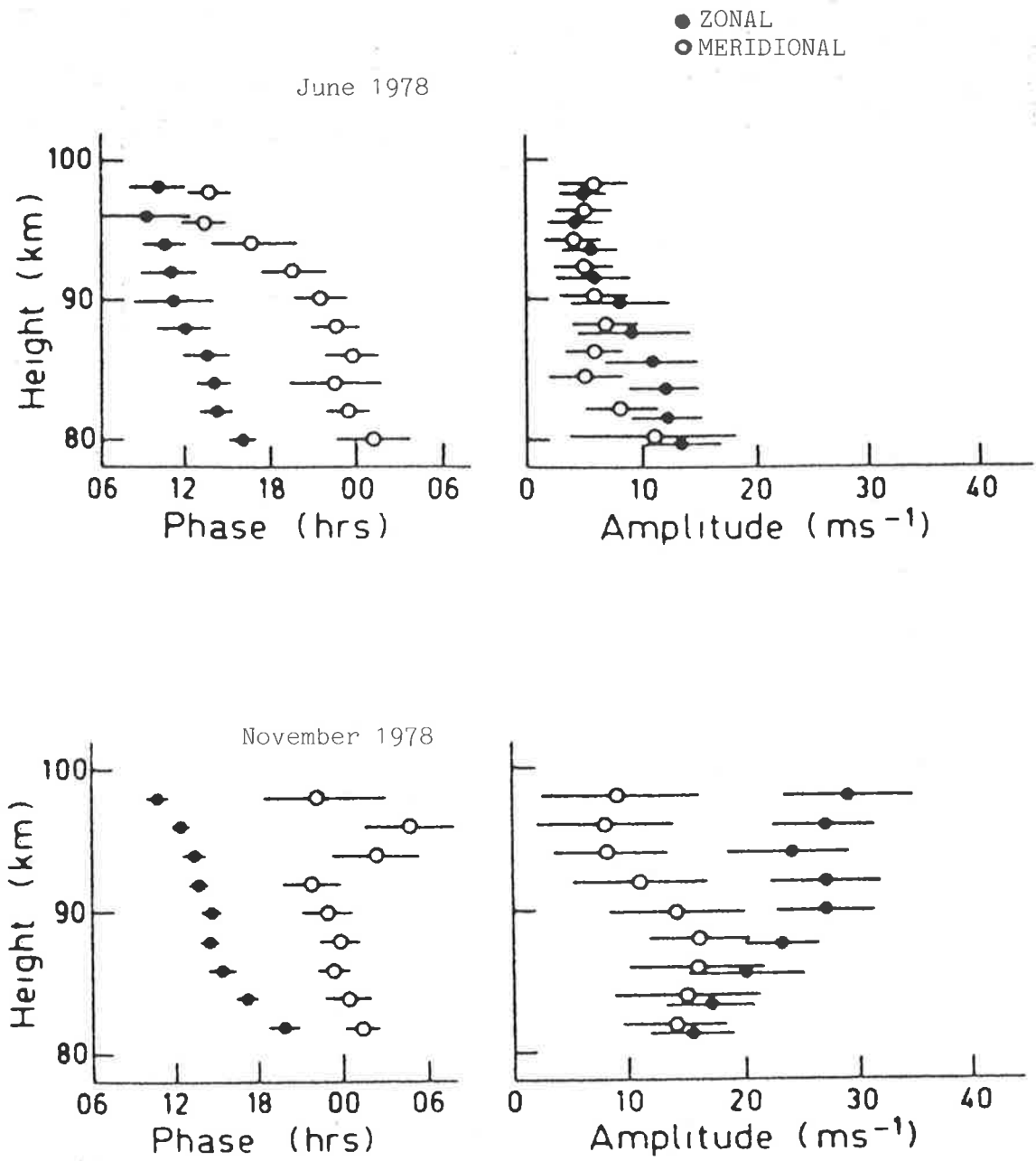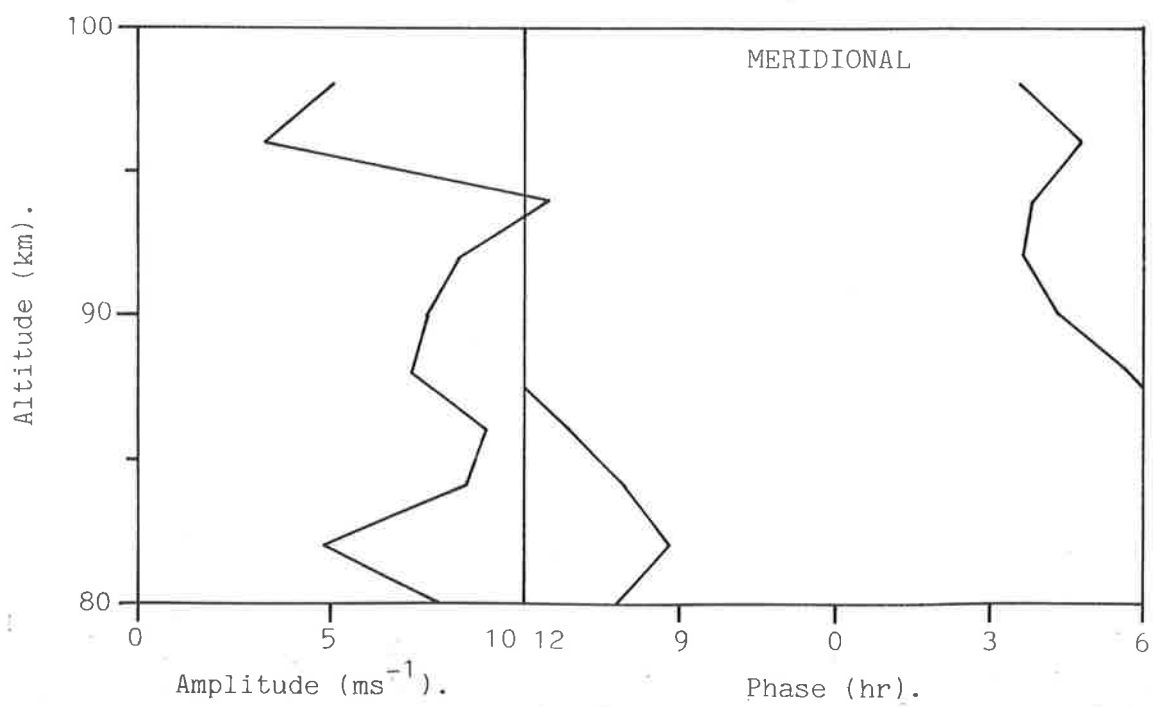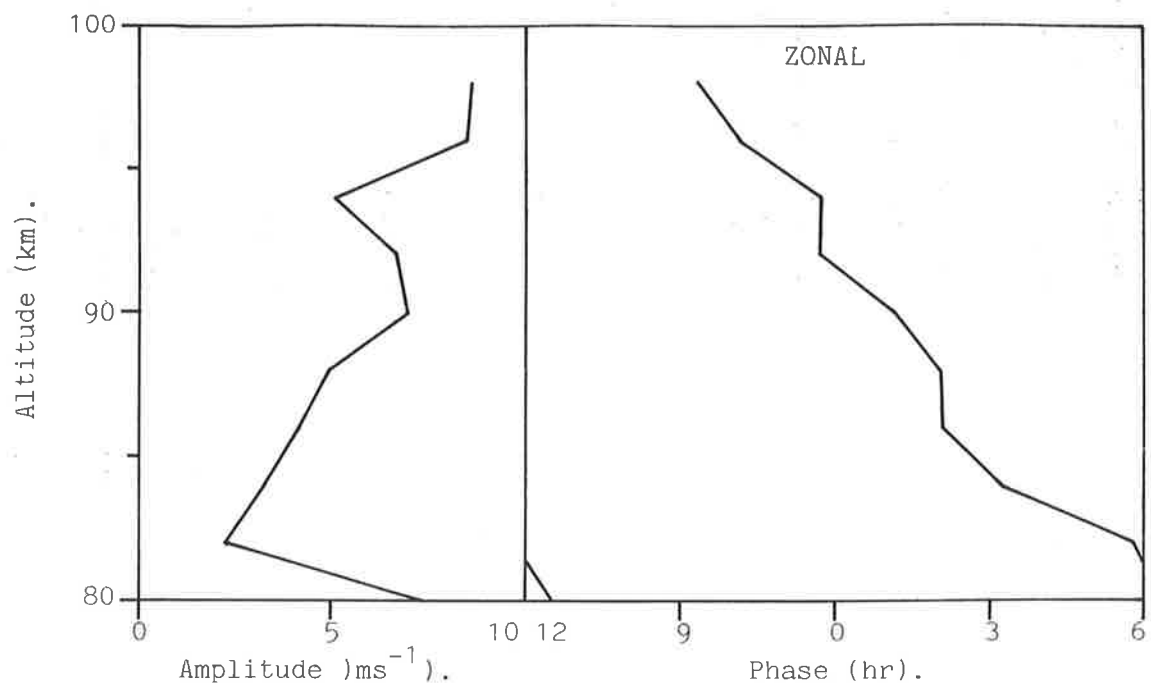Figure 4.31. Mean semidiurnal tide at Adelaide (July/August 1980).
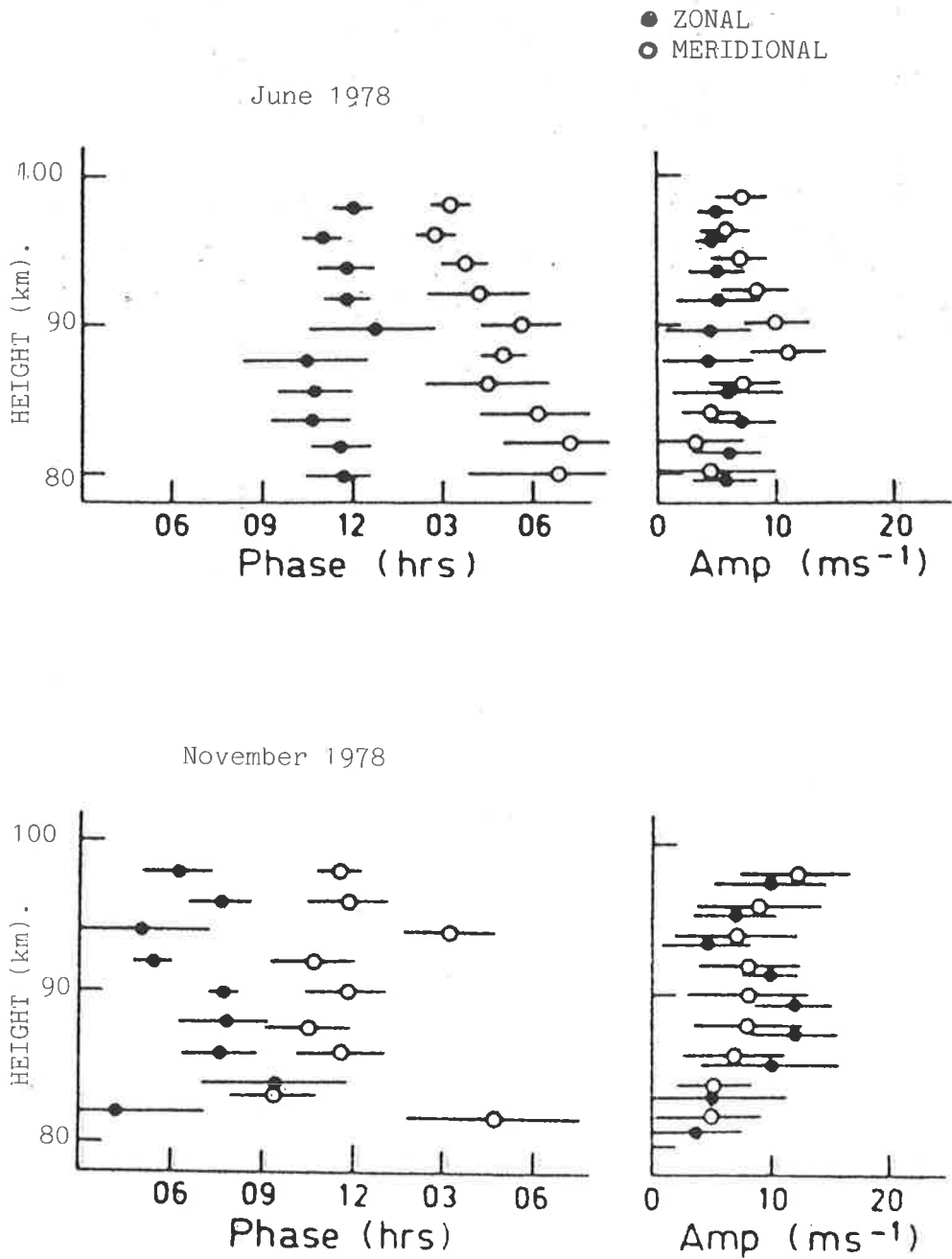
Figure 4.32.   Adelaide semidiurnal tide (Vincent and Ball, 1981).
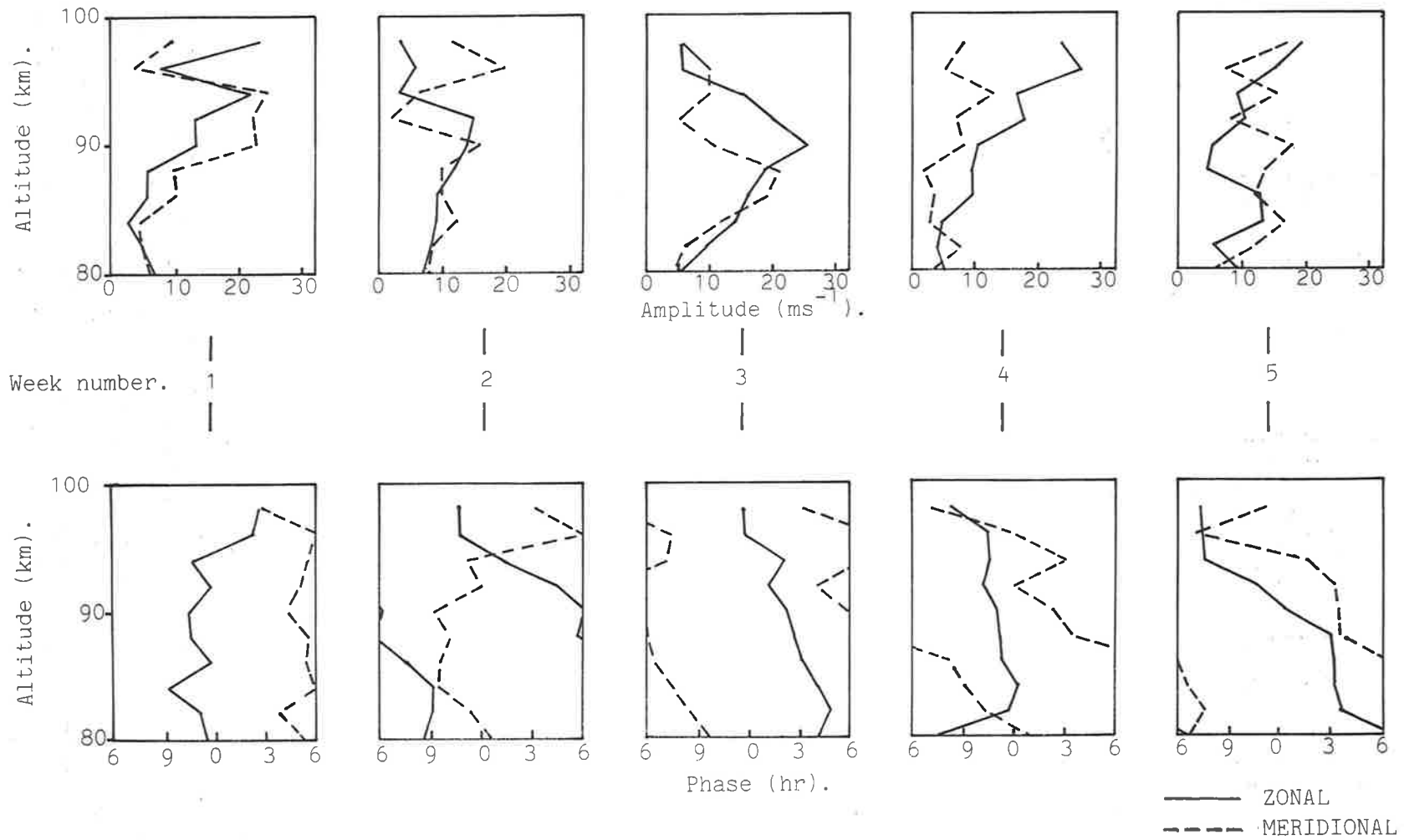
Figure 4.33.   Semidiurnal tide at Adelaide: weekly averaged results.

The semidiurnal phase results given in figure 4.33 show shifts in phase of a few hours for both components at all levels from week to week. These results suggest the interaction of various semidiurnal modes during the period of observation.

4.2.7 Comparison of Prevailing Winds at Adelaide and Townsville.

The average results for the prevailing winds over the whole observation period at Townsville and Adelaide (figures 4.18 and 4.26) agree very closely with the results presented by Manson et al. (1985) shown in figure 1.4. Large changes in the prevailing zonal flow at all heights are indicated by the Manson et al. figures near the end of August for Townsville and near the end of September for Adelaide. Examination of the weekly averages presented in figures 4.19 and 4.27 do not give any indication of large systematic changes to the prevailing systems, which, for the zonal winds would be expected to occur earlier at Townsville than at Adelaide. It is of interest to note that the Townsville meridional results given in figure 4.19 show less variability than any other profiles in figures 4.19 and 4.27, and may indicate that this period is characteristic of the meridional wind system at Townsville.

4.2.8 Comparison of Diurnal Tides at Townsville and Adelaide.

Of all the results presented for Townsville and Adelaide, the average diurnal tidal results given in 4.20 and 4.28 and the weekly averaged results given in 4.22 and 4.30 are the most striking. The very similar phase structure of both zonal and meridional components at both latitudes are indicative of a common tidal mode. The implied vertical wavelength of this mode is approximately 40 km. Fellous et al. (1975) have

shown that the vertical wavelength of the diurnal tide in the northern hemisphere is 27 km in winter and 50 km in spring. The value of 40 km for July/August in the southern hemisphere is therefore in good agreement.

Examination of the velocity expansion functions for diurnal modes given in figure 1.6 shows that for the (1,1) propagating mode, the ratio of the zonal amplitude components at Townsville and Adelaide is 1.22, and the ratio of the corresponding meridional components is 1.94. Taking the zonal and meridional amplitude components at 90 km in figures 4.20 and 4.28, the measured ratios are 0.89 and 2.07. The close correspondence of the theoretically predicted and experimentally derived ratios suggest that the diurnal mode which dominated at Townsville and Adelaide was the (1,1) propagating mode. The difference in the 'classical' (1,1) vertical wavelength of 25 km and the measured value of 40 km, and the discrepancies between theoretical and measured velocity ratios could be accounted for by the effects of turbulent diffusion on the diurnal thermal tide as proposed by Vial and Teitelbaum, (1984).

4.2.9 Comparison of Semidiurnal Tides at Townsville and Adelaide.

In the average semidiurnal tidal results of figures 4.23 and 4.31, it can be seen that the mean semidiurnal tide at Townsville is dominated by a long vertical wavelength (~100 km) mode, possibly the (2,2) or (2,3) mode. Adelaide is dominated by a short vertical wavelength (~39 km) mode, possibly the (2,5) or (2,6) mode. At Townsville, the smooth progression of zonal phase breaks down above 92 km, while at the same level at Adelaide, it is the meridional profile which breaks from the orderly progression.

Shorter vertical wavelength modes can be excited through mode coupling (Lindzen and Hong, 1974; Forbes and Garrett, 1978) due to mean zonal winds and meridional temperature gradients. The amplitude of the mean zonal winds at Adelaide (figure 4.26) are ~10ms^{-1} greater at all levels than those of Townsville. This may be of significance in the production of higher order modes at Adelaide.

The weekly averaged semidiurnal profiles of figures 4.25 and 4.33, although variable, show quite similar changes from one week's average to the next. This is true for both amplitude and phase results. In week three for example, both Adelaide and Townsville results show a zonal amplitude maximum at 90 km, while the zonal phase leads the meridional by about 4 hr at heights below 90 km. This suggests that there may be similar semidiurnal effects in operation at both sites.

5 CONCLUSIONS and RECOMMENDATIONS.

The purpose of the experimental work presented in this thesis was to provide quantitative information in order to examine the large-scale dynamical behaviour of the Antarctic mesosphere and lower thermosphere using PRW equipment operating at MF (1.94 Mhz). Many details of the true conditions under which the experiment was to be conducted could not be ascertained until the author actually arrived in the Antarctic. The resulting modifications to the system and the protracted installation period have been discussed in chapter 2 and each affected the ultimate nature of the experiment in different ways. Obviously, the long installation period meant that a discussion on seasonal variations could not be undertaken. If the equipment could have been installed in Antarctica in the same configuration as that used in Townsville, there would have been a significant improvement in signal-to-noise ratio. This would probably have resulted in the improvement of temporal resolution in both tidal and spectral analyses. The use of incoherent averaging offset the effects of the reduced signal-to-noise ratio to some extent by providing improvements in both the effective number and the distribution of hourly mean wind estimates.

The working conditions in the Antarctic were such that a great deal of improvisation was required at times, and it was so remote that it was not possible to know whether or not the experiment had worked at all until a few weeks before the author returned from the Antarctic. It was a daunting situation for an experimentalist.

Evidence that the system performed in a manner consistent with other similar experiments has been offered in figure 3.3, in which the diffraction pattern parameters observed at Mawson were compared and contrasted with those from Adelaide and Townsville. The only significant departure of the Mawson results occurs above 90 km, where the values of pattern scale, pattern elongation and $T_{0.5}$ are consistently smaller than those of the other sites. The smaller values of these parameters observed at Mawson may be interpreted as a relatively greater degree of variability at these levels in the Antarctic.

Figure 3.4 demonstrates that there is a variation in the direction of elongation of diffraction patterns with latitude, particularly at the higher (~100 km) altitudes. Diffraction patterns at Townsville tend to be elongated in the NS direction, whereas those at Mawson tend to be elongated EW. Further investigation of this effect is recommended, as it may lead to a better understanding of the nature of partially reflecting irregularities.

The mean prevailing zonal and meridional winds observed during the 1981/1982 summer at Mawson were shown in figure 3.12 and agree reasonably well with theoretical results, with observations made at similar northern latitudes, and with observations made at Scott Base during the following summer. The prevailing westward winds show a peak near 80 km, which is approximately 10 km higher than the location of the summer jet observed at Adelaide. Equatorward winds at Mawson show a similar increase in the altitude of maximum flow. The increase in the altitude of maximum zonal flow with increasing southern latitude during summer is possibly due

to changes in the spectral distribution of vertically propagating gravity waves or the level at which wavebreaking occurs, or both. The prevailing winds observed at Townsville (figure 4.18) and Adelaide (figure 4.27) show good agreement with results presented by Manson et al. (1985) shown in figure 1.4.

Figure 4.2 showed the prevailing winds observed at Mawson on a week-to-week basis. The zonal profiles tended to be the more orderly, and as can be seen clearly in figure 4.4, over the period of observation, the prevailing zonal wind system was being accelerated towards the east at all levels, with the most rapid effects occuring at the highest altitudes. The meridional winds were generally directed towards the equator at all levels, although poleward flow was occasionally observed, often in association with geomagnetically active periods. Also during geomagnetically active periods, it was noted that both zonal and meridional profiles tend to be less orderly than at other times. By comparison, the prevailing winds at Townsville and Adelaide are more orderly, showing smooth progression from week to week at all altitudes.

The tidal results for Townsville, Adelaide and Mawson confirm other observations and are in accord with the theoretical predictions of Forbes (1982a, b) shown in figures 1.6 and 1.7. These results show that at Townsville, there is a strong propagating diurnal tide and a relatively weak variable semidiurnal tide. At Adelaide a propagating diurnal tide was observed, and the semidiurnal tide showed a similar week to week variability to that observed at Townsville, with slightly larger amplitudes overall. The tidal analyses of the Mawson data have revealed that both the

diurnal and semidiurnal tidal systems are relatively weak and show considerable short-term variability and mixed mode structure.

Comparison of the diurnal tidal structure at Townsville and Adelaide enabled the identification of the (1,1) propagating mode. Examination of the semidiurnal tidal structure at both sites showed that at Townsville a long vertical wavelength (~100 km) mode, possibly the (2,2) or (2,3) mode, was evident, while at Adelaide a much shorter vertical wavelength (~30 km) mode was predominant, possibly the (2,5) or (2,6) mode. The observation of higher-order semidiurnal modes at the higher latitude site of Adelaide is predicted theoretically (Forbes, 1982b) as shown in figure 1.7.

Theory (Forbes, 1982a) predicts that a mixture of evanescent tidal modes will dominate at high latitudes (see figure 1.6). From the results presented in figure 4.8 for the week to week results from Mawson, this appears to be the case if each week is regarded separately, as the phase structure tends to vary little with altitude where amplitudes are moderate ($10ms^{-1}$ or more) and is generally erratic where amplitudes are less. When the results for the whole observation period are averaged, there is some evidence to suggest that for the diurnal tide above 90 km (figure 4.7) and for the semidiurnal tide between 80 and 100 km (figure 4.12), relatively small amplitude propagating modes may persist.

An estimation of the vertical wavelength of this diurnal tidal component can be made from figure 4.7 from the anticlockwise rotation of the tidal vector from 90 to 98 km. It is calculated to be between 60 km (from the zonal results) and 80 km (from the meridional results). The most likely mode is again the (1,1) propagating mode.

A similar calculation can be made for the semidiurnal results shown in figure 4.12. For the zonal component, the vertical wavelength is estimated to be about 40 km, while for the meridional component, a value of approximately 20 km results. At Atlanta, Ahmed and Roper (1983) have reported discrepancies of similar magnitudes for the zonal and meridional estimates of the vertical wavelength of the semidiurnal tide made from data gathered between August 1974 and February 1978. During winter at Atlanta, the vertical wavelength of the zonal component of the semidiurnal tide was estimated to be 120 km, while the meridional component was 63 km; in summer, from data below 94 km in altitude, these wavelength components were estimated to be 71 km and 150 km respectively.

The very small values of amplitude between 80 and 90 km for both zonal and meridional components at Mawson (figure 4.11) may lead to large inaccuracies in phase at these heights and are likely to affect the estimation of vertical wavelength. Nevertheless, the zonal estimate is probably the better result. On that basis it is proposed that the semidiurnal tidal mode evident in the long-term average results is the (2,5) mode.

The difficulties in modelling the effects of tides in the 80 to 100 km altitude region, which were discussed in chapter 1 of this thesis are demonstrated by figures 4.9 and 4.10 for the diurnal tide below and above 90 km respectively and figures 4.14 and 4.15 for the semidiurnal tide in the same altitude ranges. These figures show that large fluctuations in amplitude and phase were present in both tidal components during most of January 1982. Of these figures, the semidiurnal results show the greatest

variability. In particular figure 4.15, for the semidiurnal phase above 90 km, indicates that the zonal and meridional components of phase remain relatively steady for several days before jumping approximately 6 hours to other relatively steady values (MacLeod and Vincent, 1985). The joint presence of several higher order semidiurnal modes could be responsible for this behaviour.

For the diurnal tide above 90 km, there are relatively large fluctuations in amplitude and phase evident in figure 4.10, but the mean phase results show a similar linear trend in both zonal and meridional components, which amounts to an increase of about 4 hours during January 1982. The separation between the mean phase components remains approximately constant, with the zonal component leading the meriodional by about 6 hours.

The jumps observed for the semidiurnal phases above 90 km (figure 4.15), and the relatively slow increase in the phase of the diurnal components above 90 km (figure 4.10) are reminiscent of the stationarity hypothesis proposed by Bernard (1981b), and discussed in section 1.3.3. Bernard (1981b) calculated that the equivalent gravity waves of the (2,3), (2,4), (2,5) and (2,6) modes would require 4.2, 6.1, 8.0 and 10.1 days respectively to travel around the earth and so attain stationarity. These periods are close to the periods of relative stability shown in figure 4.15. Much slower travel times are predicted for the equivalent gravity waves of diurnal modes. Bernard (1981b) quotes figures of 11.9 days for the (1,1) mode and 27.3 days for the (1,3) mode. With such long periods of time required for diurnal modes to attain stationarity, it is unlikely that

the step-like discontinuites in phase observed in the semidiurnal results of figure 4.15, would be observed for the diurnal tide.

The results of the spectral analysis shown in figure 4.16 show good agreement with other results discussed. Johnson and Luhman (1985) have proposed that the response of the atmosphere at the 86 km level to geomagnetic activity depends on whether well established tidal fields are present on the average. If tidal fields are well established, Johnson and Luhman maintain that increased geomagnetic activity results in a reduction of power in low frequency components and vice versa. The average tidal fields observed at Mawson were not particularly well established, and the large spectral components near three to four days evident in figure 4.16 support the contention of Johnson and Luhman.

An examination of the root mean square gravity wave amplitudes of waves with periods between 2 and 12 hours at Townsville, Adelaide, Poker Flat and Mawson showed that the southern hemisphere results are smaller than the result from Poker Flat. There is insufficient evidence to suggest that the spectral energy contained in gravity waves of these periods varies significantly between the hemispheres, but further investigation is recommended.

After the author's experience in the Antarctic there were several obvious recommendations to be made in order to improve the performance of the PRW system at Mawson; most of these have already been implemented. These include more robust external supporting structures, crossed receiver dipoles at the receiving sites and the provision of a minicomputer to make real-time wind observations. This has resulted in a system which allows

more frequent observations to be made and should allow studies of gravity waves, in addition to the longer period phenomena discussed in this thesis. Further results from Mawson will be presented in due course.

The provision of a minicomputer not only improves the efficiency of the system to make wind estimates, but also dramatically reduces the amount of computer tape required to store the results. The output from the system now is magnetic tape containing wind estimates, rather than raw data from which wind estimates must be obtained. The number of tapes needed for the present configuration is conservatively estimated to be fifty times less than that needed for the system described in this thesis. This is an excellent feature; however there are good reasons to retain some examples of the raw data. Mawson is a unique site geographically and geomagnetically and there are several phenomena, including aurorae and Polar Cap Absorbtion (PCA) events, whose study could well benefit from a thorough examination of raw data gathered at the appropriate time with the PRW system. Also it is recommended that this equipment be used to estimate electron concentrations (see chapter 3 for details of the method), which would not only assist in the interpretation of local phenomena, but would also be invaluable for comparative purposes.

It has been mentioned several times in this thesis that space for aerial arrays is becoming relatively scarce at Mawson. This is mainly due to the fact that such semi-permanent structures have traditionally been mounted on the limited amount of exposed rock at Mawson. If suitable fittings could be devised, there should be no reason why aerial arrays could not be erected over the Antarctic plateau, which extends to the east,

west and south of Mawson base. The Antarctic plateau rises sharply over relatively short distances from Mawson so that within a few kilometres of the base, the ice thickness can be measured in hundreds of metres. As plateau ice is salt free, it is effectively dielectric and the possibility that transmitting aerials might be placed directly on the ice plateau and operated in a free space mode should not be overlooked. If the plateau could be used for siting aerials, it would mean that virtually unlimited space would be available and could provide a substantial increase in the sensitivity of the system if a large receiving array were constructed.

The author is confident that aerials placed on the ice plateau would work, and this raises another possibility for extending the work in the Antarctic. A traverse van, fitted with a transportable PRW transmitter and receiver could be used for obtaining mesospheric wind estimates and electron concentrations almost anywhere on the Antarctic continent. Traverse trains are commonly used by Australian expeditions in the Antarctic and are able to support themselves for several months at a time. A traverse van, suitably equipped, could be towed to any site, where transmitting and receiving arrays would be pegged out on the ice; a portable generator would then be used to power the system. In good weather this could be accomplished in a very short time. Such a system would allow studies of the polar cap region, the southern magnetospheric cusp region and any part of the southern auroral oval.

Information on longitudinal variations in the prevailing winds, tides and gravity wave spectra, particularly at high southern latitudes would be of particular value to the task of atmospheric modelling.

Australia has 3 bases on the Antarctic mainland all close to 70°S and each has well maintained and relatively powerful (~30 kw) transmitting facilities for base communications. If suitable aerial arrays could be provided, it should not be too great a task to modify the communications equipment so that it can be used for atmospheric sounding purposes. A receiving system similar to the one presently installed at Mawson would be needed at each site, this would provide the signals appropriate for PRW work and would be used to analyse the received signals. Transmission could then be integrated with the base communications; a cooperative undertaking like this is recommended.

APPENDIX

"Observations of winds in the Antartic summer mesosphere
using the spaced antenna technique"

By R.I. MacLeod and R.A. Vincent

Observations of winds in the Antarctic summer mesosphere using the spaced antenna technique

R. MacLeod

Mawson Institute for Antarctic Research, University of Adelaide, Adelaide, South Australia 5001, Australia

and

R. A. Vincent

Physics Department, University of Adelaide, Adelaide, South Australia 5001, Australia

Abstract—Observations of winds in the 60–100 km height range were made at Mawson (68°S, 63°E) during December 1981 and January 1982 with the MF spaced antenna technique. The prevailing winds are in accord with other recent observations made at high latitudes and show a peak in the zonal wind near 80 km with westward winds of 30 m s^{-1}. The meridional winds maximize near 90 km with an equatorward flow of 10 m s^{-1}. The diurnal tidal components are in reasonable agreement with recent model predictions, especially in phase. The amplitudes tend to be larger than the model values. The semidiurnal tide is not as stable as the diurnal tide and shows evidence for interference effects between different modes.

1. INTRODUCTION

Observations of mesospheric and lower thermospheric winds have been made at mid-latitudes for many years, but to date there have been relatively few measurements made at high latitudes. Measurements at high latitudes are important for a number of reasons. Amongst these are the need to investigate latitudinal and longitudinal changes in the prevailing circulation, as well as possible hemispheric differences. Information about tides at high latitudes is also important since theory suggests that the modal composition of the diurnal and semidiurnal tides will change with latitude. For example, at high latitudes the evanescent modes are expected to be dominant for the diurnal tide, so measurements at these latitudes will help to determine the contribution of these modes at mid-latitudes where there is a mixture of evanescent and propagating modes.

Some long sequences of wind observations using the meteor technique were reported for Heiss Island (81°N, 55°E) and Molodezhnaya (68°S, 45°E) by Lysenko *et al.* (1979). They analyzed the winds into prevailing and tidal components, but, because of the lack of height finding equipment, the results must be referred to a mean height of 94 km with no height variations being available. Elford and Murray (1960) also carried out meteor-wind measurements at Mawson Base (68°S, 63°E) during 1957–1958. However, their results were restricted by low meteor echo rates.

The MST radar facility at Poker Flat (65°N, 147°W) operating at VHF frequencies has been used to measure winds both by observing echoes from turbulent irregularities (Carter and Balsley, 1982) and from meteor trails (Avery *et al.*, 1983). Recently, Fraser (1984) summarized the first wind observations made with a partial reflection (PR) spaced antenna system located at Scott Base (78°S, 168°E). Fraser presented observations showing the prevailing zonal (EW) and meridional (NS) winds in the 70–100 km height range measured in December 1982 (summer).

Here we discuss preliminary observations of the prevailing and tidal winds measured using PR spaced antenna methods at Mawson Base. The measurements were carried out in December 1981 and January 1982. In Section 2 the equipment and data analysis methods are outlined. The prevailing circulation is discussed in Section 3, while in Section 4 the tidal oscillations are presented.

2. EQUIPMENT AND DATA ANALYSIS

The system used for the measurements was basically the same as that used in previous observations made at the low-latitude site of Townsville (Vincent and Ball, 1981). Pulsed transmissions were used at a frequency of 1.94 MHz with a pulse length of 30 μs and peak powers of 10–15 kW. The pulse repetition frequency was 20 Hz. The transmitting antenna consisted of 4 folded dipoles

arranged in a square and phased to transmit circularly polarized waves. Usually, the 0-mode of polarization was used.

The receiving antennas were half-wave dipoles suspended 10 m above ground. Three antennas were used, arranged in the form of an equilateral triangle with a basic spacing of 165 m (1.1 λ). The signals from each antenna were fed via coaxial cable back to a central receiving and control building, where they were connected to separate receivers. The whole system was phase-coherent, with the receiver outputs consisting of in phase and quadrature components, so that the complex echo amplitudes were recorded. The dual-channel signals were sampled at 2 km height intervals over a 40 km height range and digitized with an 8-bit A/D. The digitized signals at each height and for each receiver (6 channels in all) were averaged by a microprocessor over 8 successive pulses, so that the effective sampling rate was 2.5 Hz. The signals were then stored on magnetic tape for subsequent analysis in Adelaide.

It is noted that the averaging over 8 pulses of the complex signal corresponds to coherent integration, because the echoes did not change their amplitude or phase significantly in 0.4 s, while the noise was incoherent from one pulse to the next. This integration led to an 8-fold improvement in the power signal-to-noise ratio and partially compensated for the small antennas and low mean transmitter powers used.

The whole system was under microprocessor control, with receiver gains being automatically adjusted to compensate for the change in mean echo strengths with height and time. Data were collected over the height range 60–100 km in 2 min blocks, with six such blocks per hour.

The data were analyzed with the so-called full correlation analysis (FCA) method in which the temporal auto- and cross-correlation functions are used. Since the complex signals were available, the complex correlation functions were computed and used in the analysis. Details of the FCA and the rejection criteria used may be found in BRIGGS (1984).

As the prevailing and tidal winds were of primary interest, the individual 2 min wind values obtained at each height were averaged to give an hourly mean value. However, it was found that, with this method, many of the data were being rejected because of the frequent occurrence of inadequate signal-to-noise ratio. This was especially the case at the lowest heights. In order to improve the quality of the data a different technique was therefore developed. The 6 individual unnormalized cross-correlation functions calculated for a given height in a given hour were averaged and then normalized using the three mean square signal

strengths for that hour. The mean auto-correlation functions were calculated in the same manner. This incoherent averaging of the correlation functions is the spaced antenna analogue of the incoherent averaging of power spectra often used during Doppler wind studies made with MST radars. In the present case a $\sqrt{6}$ improvement in power signal-to-noise should have resulted. An improvement of this order was found and the amount of available data increased by a factor of about two.

In all 3448 hourly wind values over the height range 60–100 km were available for subsequent analysis. Figure 1 shows their distribution with height, indicating that most wind values were obtained at heights above 80 km. The distribution is very similar to that given by FRASER (1984) for Scott Base, which had a maximum at heights near 90 km. Similar to Fraser, we found that the times when observations were possible were spread quite evenly as a function of time throughout the day. This is in contrast to the diurnal variation found at mid-latitudes (VINCENT, 1984).

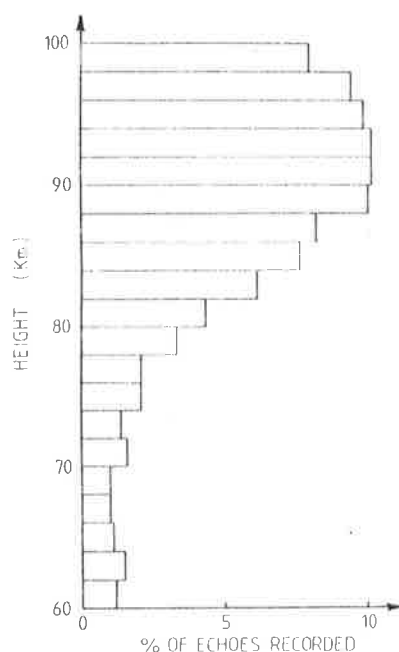TOTAL NUMBER OF RECORDS   3448   (60–100 Km)

Fig. 1. Distribution with height of echoes producing reliable wind observations for the period 13 December 1981 to 30 January 1982 at Mawson (68°S).

3. THE PREVAILING WINDS

Figures 2a and b show the mean zonal and meridional wind profiles observed at Mawson during the period mid-December 1981 to 31 January 1982. For clarity, error bars have been omitted, but typical standard errors for the means range from about 10 m s^{-1} at the lower heights to about 2 m s^{-1} at the upper levels. Observations made in summer periods at Poker Flat (CARTER and BALSLEY, 1982) and Scott Base (FRASER, 1984) are shown for comparison. Representative profiles from the zonal wind models of CIRA (1972) and the meridional wind model of GROVES (1969) are also given.

All three sets of observations show the zonal flow to be westward at most heights. The Mawson values are, however, somewhat smaller in magnitude than those observed at the other locations. The data profiles for the meridional wind components also show the same behaviour (after reversing Poker Flat to allow for the change in hemisphere). The differences in magnitude may reflect differences between hemispheres and also the effect of interannual variability, but it is probable

MERIDIONAL

Fig. 2b. As for Fig. 2a, except for the meridional component (northward positive).

ZONAL

Fig. 2a. Mean zonal wind (eastward positive) as a function of height at Mawson, summer 1981/1982 (solid line). The open circles and crosses refer to summer observations taken at Poker Flat (CARTER and BALSLEY, 1982) and Scott Base (FRASER, 1984), respectively.

that it is also caused by the timing of the present observations with respect to the summer solstice. The Mawson data were taken primarily in January and, as shown in Fig. 3, the prevailing winds were tending to change systematically with time. Particularly at 94 km, there was a clear trend in both the EW and NS components to become more eastward and southward (poleward) as January progressed.

One notable feature of Fig. 2 is that all three stations show wind profiles that are at variance with the models. The summer westward jet at 70° in the CIRA (1972) model peaks at heights below 70 km. In contrast, the observed jet maximizes near 80 km. A more recent model constructed specifically for the southern hemisphere by KOSHELKOV (1983) shows somewhat better agreement with the observations, but with the jet still peaking between 70 and 75 km at a latitude of 70°. The observations strongly suggest that the models need revision for high latitudes.

The meridional winds also show a maximum, with equatorward flow maximizing near 90 km with velocities of about $10\text{–}20 \text{ m s}^{-1}$. The Mawson observations are in general accord with previous observations of the meridional flow near the summer mesopause at high latitude sites. Latitudinal variations

ZONAL

MERIDIONAL
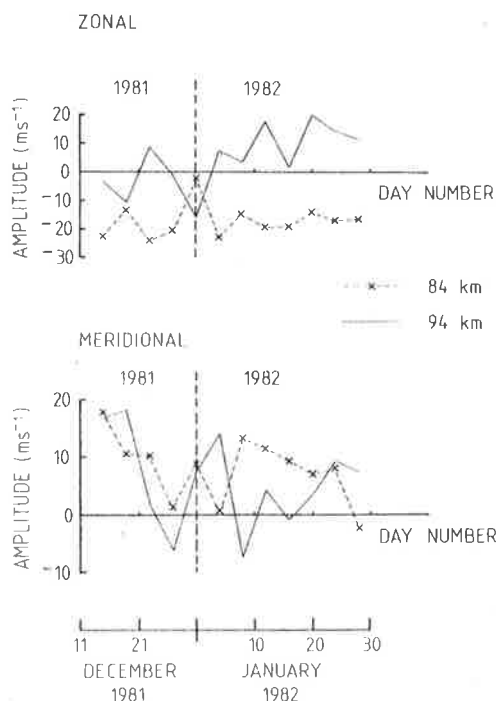
Fig. 3. Four day averages of the mean wind at 84 and 94 km altitude plotted as a function of time.

and the significance of the relatively high speeds have been discussed recently by NASTROM et al. (1982) and FRASER (1984).

4. THE TIDAL OSCILLATIONS

The data were harmonically analyzed in order to obtain the prevailing winds and the amplitude and phases of the diurnal and semidiurnal tidal oscillations. In order to study the 'steady' or mean state of the tides, all the data at a given height were accumulated in such a way as to produce a time series for one 'effective day'. In this way the effects of transient or short term effects were partially averaged out.

(a) The diurnal tide

Figures 4a and b show the diurnal amplitudes and phases for the zonal and meridional wind components, respectively. Again, error bars have been omitted for clarity, but typically the uncertainty in the amplitude range from ± 2-3 m s^{-1} at the lower heights to ± 1-2 m s^{-1} at the upper levels; the corresponding errors in phase are ± 1-2 h and ± 0.5-1 h. On the same diagrams are shown the mean amplitudes and phases

for Poker Flat for summer taken from CARTER and BALSLEY (1982) and for December 1981 and January 1982, i.e. winter. The latter data were obtained using meteor echoes and were provided by AVERY (1983). The dotted line indicates the expected response as taken from the recent theoretical model of FORBES (1982a). The actual values were taken from the tabulations given by FORBES and GILLETTE (1982) and refer to a latitude of 66° and the summer season. The corresponding model values for winter show very similar phases, but somewhat smaller amplitudes.

The main features of the results are the good agreement in phase for the Mawson and summer Poker Flat observations and the model predictions. Taking into account the errors, the observations indicate that EW oscillations are in phase and that the NS oscillations are in anti-phase for opposite hemispheres, which shows the predominance of symmetric modes. Furthermore, the almost constant phase structure with height shows that, as is expected at high latitudes, it is the evanescent modes which dominate.

The Poker Flat summertime amplitudes are appreciably larger than those observed at Mawson, but this is very probably due to the different ways the data were analyzed. The Poker Flat amplitudes were obtained by averaging the *amplitudes* produced by the harmonic analyses of individual days data (CARTER and BALSLEY, 1982), whereas the present analysis corresponds to a vectorial average which takes into account both amplitude and phase. For comparison purposes the Mawson data were re-analyzed on a daily basis and the amplitudes were averaged. Typical values for both diurnal components are about 10 m s^{-1} at 84 km and 13 m s^{-1} at 94 km. As expected, there values are somewhat larger than the vectorial average results shown in Fig. 4.

The Poker Flat winter data were averaged vectorially. The winter results show very small amplitudes, which partially accounts for the erratic phase behaviour with height. Nevertheless, the EW phases in particular show general agreement with the Mawson phases and those for Poker Flat in summer. Further evidence for the basic stability of the tidal phases for the summer season come from the meteor wind data obtained at Molodezhnaya. LYSENKO et al. (1979) report mean phases of about 19 h and 1 h for the EW and NS diurnal tides, respectively, for December and January. As noted, these observations refer to a mean height of 94 km. There is excellent agreement with the Mawson observations. However, the Molodezhnaya amplitudes are quite large in comparison, being about 15 m s^{-1} for the EW component and of the order of 20 m s^{-1} for the NS component. It is not clear whether this is due to averaging of amplitudes,
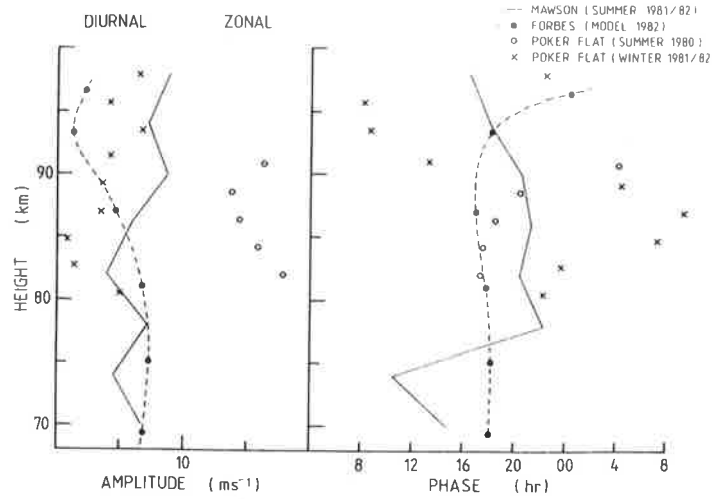
DIURNAL ZONAL

Fig. 4a. Amplitudes and phase of the mean zonal component of diurnal tide at Mawson (solid line) and Poker Flat. The model data are from FORBES (1982a). The phases are the time of maximum eastward wind.

Although the Mawson diurnal amplitudes are in general agreement with the values from the FORBES (1982a) model at heights below 85 km, it is apparent that there is a discrepancy at higher altitudes. The observed amplitudes tend to grow with height, whereas the theoretical amplitudes decay rapidly, which is the expected behaviour for evanescent modes generated at lower heights. It is noteworthy that the Poker Flat amplitudes also show some evidence for growth with height. It may well be that these observations indicate that there is an unresolved *in situ* tidal source.

(b) *The semidirunal tide*

Height profiles of the semidiurnal tidal amplitudes and phases are given in Figs. 5a and b. The uncertainties

DIURNAL MERIDIONAL
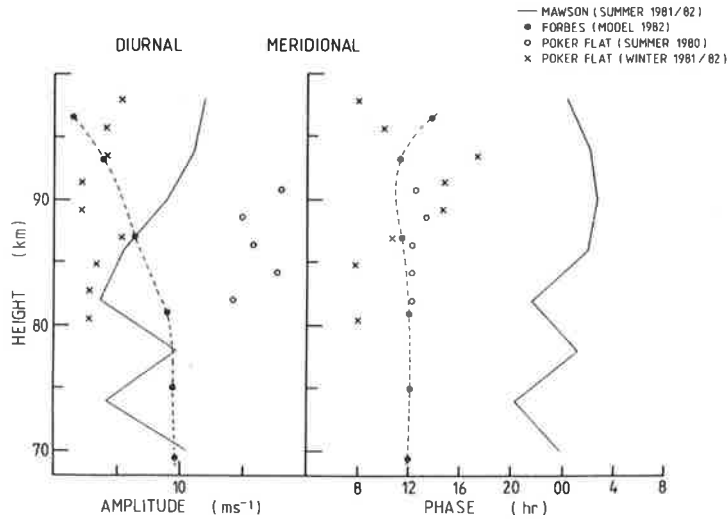
Fig. 4b. As for Fig. 4a, except for the meridional component. The phase refers to the time of maximum northward wind.

R. MacLeod and R. A. Vincent
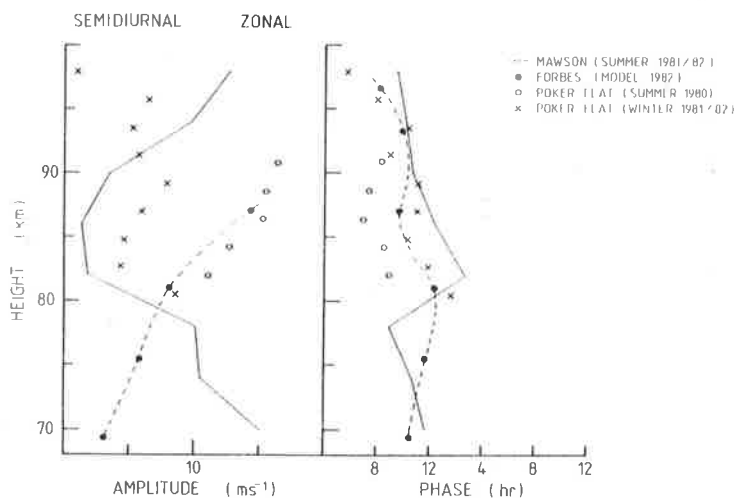
Fig. 5a. As for Fig. 4a, except for the mean zonal component of the semidiurnal tide. The model data are from
Forbes (1982b).

in the amplitudes and phases are similar to those for the diurnal tide, although there is a significant degree of uncertainty of several hours in the phases of both wind components at heights near 85 km, where the amplitudes at Mawson are small.

In general, the amplitudes and phases show more variability with height than was the case for the diurnal tide. In particular, the pronounced minima observed in the amplitudes at 85 km is probably caused by interference between different wave components. These could be due to upgoing and downgoing waves, but are most likely due to interference between the various semidiurnal modes, which are believed to exist with similar amplitudes in the 80–100 km region (Forbes, 1982b). The strong amplitude growth shown by the Forbes (1982b) model calculations in Fig. 5 is not only due to the wave growth with height associated with propagating modes, but also to constructive interference between modes. Other models (e.g. Aso et al., 1982) also show the effects of constructive interference. As Forbes (1984) notes, the joint presence of the (2, 2), (2, 3), (2, 4) and (2, 5) modes in the 80–100 km region can lead to difficulties in modelling. Small changes in the relative phase differences between components can lead to large changes in the resultant phase of the semidiurnal tide from day to day. Some support for this

Fig. 5b. As for Fig. 4a, except for the mean meridional component of the semidiurnal tide.

kind of behaviour is shown in Fig. 6, which shows a time series of the semidiurnal amplitudes and phases for a mean height of 94 km. It is notable that the phases show some stability for periods of a few days before jumping by approximately 6 h to other relatively steady values.
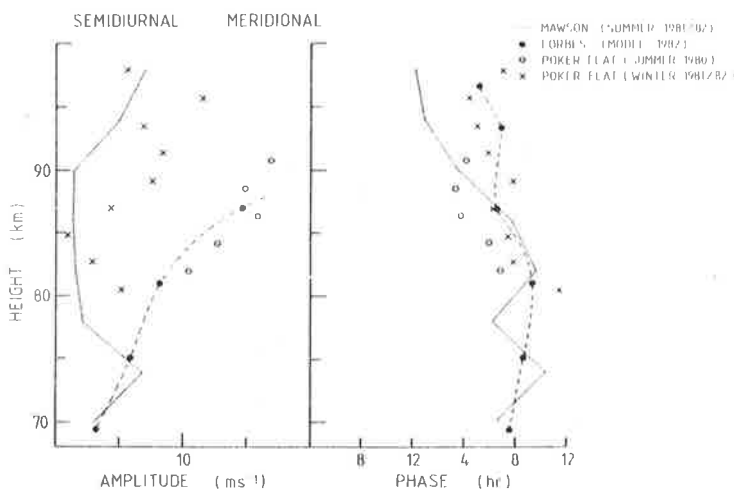
Despite the above remarks, there is, on the whole, good agreement between the model and observed phases. Where the amplitudes are largest, above 90 km, the EW component leads the NS component by about 3 h (i.e. 90°), which is expected in the southern hemisphere. The general in phase behaviour of the Mawson and Poker Flat EW components and the approximate anti-phase (6 h) phase difference (above 90 km) in the NS component, suggests the dominance of symmetric modes.

5. DISCUSSION AND CONCLUSIONS

The observations of mesospheric winds made in the summer of 1981/1982 at Mawson Base in Antarctica
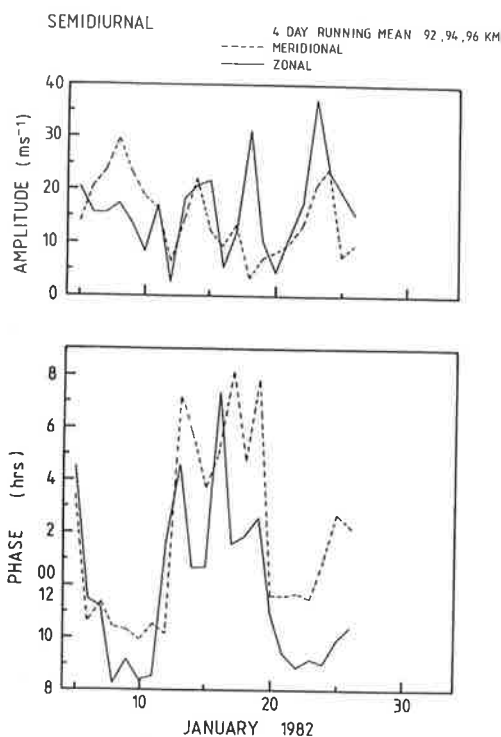
Fig. 6. Four day running means of the amplitudes and phases of the zonal (solid line) and meridional (dotted line) components of the semidiurnal tide at a mean height of 94 km at Mawson.

agree well with recent observations made at other locations. The prevailing westward winds show a peak near 80 km, which is some 10–15 km higher than the location of the summer jet maximum at Adelaide (35°S) (VINCENT, 1984). Similarly, the strong equatorward winds also maximize some 10 km higher than the maximum meridional flow measured at Adelaide. It is believed that breaking gravity waves and the associated momentum deposition play an important role in determining the mean flow in the mesosphere, so it is possible, therefore, that the upward tilt of the westward jet maximum with increasing latitude may indicate changes with latitude in the wave flux and/or their breaking levels.

Comparisons of the atmospheric tides observed at Mawson with those observed at Poker Flat, which is at a similar latitude in the northern hemisphere, show many areas of agreement. The diurnal tide appears to be dominated by symmetric evanescent modes. While there is excellent agreement with the diurnal phase predicted by FORBES (1982a) model, the observed amplitudes tend to be larger than predicted. This may indicate an unresolved in situ heating source.

The semidiurnal tide observed at Mawson does not seem as stable as the diurnal tide. However, the average values indicate some accord with other observations and with the model. The pronounced maxima and minima which appear in the amplitude height profiles suggest interference between several different modes.

It can be expected that further observations with the Mawson partial reflection system will lead to a better understanding of the dynamics of the Antarctic mesosphere. In the light of the experience gained with the first measurements which we have described here, a number of improvements have been made to the system. These include the provision of a minicomputer to make real time wind calculations, which will enable more frequent observations to be taken. This will in turn allow the study of gravity waves, as well as the longer term wind phenomena discussed in this paper.

REFERENCES

Aso T., Nonoyama T. and Kato S.   1981   *J. geophys. Res.* **86,** 388.
Avery S. K., Riddle A. C. and Balsley B. B.   1983   *Radio Sci.* **18,** 1021.
Briggs B. H.   1984   *Handbook for MAP* **13,** 166.
Carter D. A. and Balsley B. B.   1982   *J. atmos. Sci.* **39,** 2905.
CIRA   1972   *COSPAR international reference atmosphere,* Akadmie-
                                                                Verlag, Berlin.
Elford W. G. and Murray E. L.   1960   *Space research,* Kallman Bijl H. Ed., p. 158, North-
                                                                Holland, Amsterdam.
Forbes J. M.   1982a   *J. geophys. Res.* **87,** 5222.
Forbes J. M.   1982b   *J. geophys. Res.* **87,** 5241.
Forbes J. M.   1984   *J. atmos. terr. Phys.* **46,** 1049.
Fraser G. J.   1984   *J. atmos. terr. Phys.* **2,** 143.
Groves G. V.   1969   *J. Br. interplanet. Soc.* **22,** 285.
Koshelkov Yu. P.   1983   *Adv. Space Res.* **3,** 3.
Lysenko I. A., Orlyansky A. D. and   1979   *J. Geomagn. Geoelect.* **31,** 411.
    Portnyagin Yu. I.
Nastrom G. D., Balsley B. B. and Carter D. A.   1982   *Geophys. Res. Lett.* **9,** 139.
Vincent R. A.   1984   *J. atmos. terr. Phys.* **46,** 961.
Vincent R. A. and Ball S. M.   1981   *J. geophys. Res.* **86,** 9189.

Reference is also made to the following published material:

Avery S. K.   1983   Private communication.
Forbes J. M. and Gillette D. F.   1982   Air Force Geophysics Laboratory Environmental
                                                                Research Papers APGL-TR 80-0173(I).

BIBLIOGRAPHY

Ahmed, M.I. and Roper, R.G., "The diurnal and semidiurnal oscillations in meteor winds over Atlanta". J.A.T.P., vol 45, no.4, p 181 - 192, (1983).

Aso, T., and Vincent, R.A., "Some direct comparisons of mesospheric winds observed at Kyoto and Adelaide". J.A.T.P., vol 44, no.3, p 267 - 280, (1982).

Avery, S.K., private communication, (1983).

Ball, S.M., "Upper Atmosphere Tides and Gravity Waves at Mid - Latitudes". Ph.D. thesis, Adelaide University, (1983).

Balsley, B.B., Carter, D.A. and Ecklund, W.L., "On the Relationship between Auroral Electrojet Intensity Fluctuations and the Wind Field Near the Mesospause". Geophys. Res. Letters, vol 9, no.3, p 219 - 222, (1982).

Balsley, B.B., Ecklund, W.L., Carter, D.A. and Johnston, P.E., "The M.S.T. Radar at Poker Flat, Alaska". Radio Science, vol 15, no.2, p 213 - 223, (1980).

Balsley, B.B., Ecklund, W.L. and Fritts, D.C., "V.H.F. Echoes from the High - Latitude Mesosphere and Lower Thermosphere: Observations and Interpretations". J. Atmos. Sci., vol 40, p 2451 - 2466, (1983).

Barnett, J.J. and Corney, M., "Middle Atmosphere Reference Model Derived From Satellite Data". MAP 16, p 47 - 81, (1985).

Belrose, J.S., "Radio wave probing of the ionosphere by the partial reflection of radio waves (from heights below 100km)". J.A.T.P., vol 32, p 567 - 596, (1970).

Bendat, J.S. and Piersol,A.G., "Random Data: Analysis and Measurement Procedures". Wiley, (1971).

Bernard, R., "Seasonal variation in mesospheric semi-diurnal tides. Comparison of meteor radar observations and results from an excitation source model". J.A.T.P., vol 43, p 101 - 109, (1981a).

Bernard, R., "Variability of the semi-diurnal tide in the upper mesosphere". J.A.T.P., vol 43, p 663 - 674, (1981b).

Bolgiano, R.Jr., "The General Theory of Turbulence in the Atmosphere". "Winds and Turbulence in Stratosphere Mesosphere and Ionosphere". North - Holland Publishing Company - Amsterdam, ed. K. Rawer, p 371 - 400, (1968).

Booker, H.G., Ratcliffe, J.A. and Shinn, D.H., "Diffraction from an Irregular Screen with Application to Ionospheric Problems". Royal Society of London Philosophical Transactions, vol A242, p 579 - 607, (1950).

Brekke, A., "Joule Heating and Particle Precipitation". Advances in Space Research, vol 2, no.10, p 45 - 53, (1983).

Briggs, B.H., "Ionospheric Drifts". J.A.T.P., vol. 29, p 1023 - 1031, (1977).

Briggs, B.H., "Radar observations of atmospheric winds and turbulence: a comparison of techniques". J.A.T.P., vol 42, p 823 - 833, (1980).

Briggs, B.H., "The analysis of spaced antenna sensor records by correlation techniques". MAP 13, ed. R.A.Vincent, p 166 - 186, (1984).

Briggs, B.H., Phillips, G.J. and Shinn, D.H., "The Analysis of Observations on Spaced Receivers of the Fading of Radio Signals". Proc. Phys. Soc. London, B63, p 106 -121, (1950).

Briggs, B.H. and Vincent, R.A., "Some Theoretical Considerations on Remote Probing of Weakly Scattering Irregularities". Aust. J. Phys., vol 26, p 805 - 814, (1973).

Carter, B.A. and Balsley, B.B., "The Summer Wind Field Between 80 and 93km Observed by the M.S.T. Radar at Poker Flat, Alaska (65 N)". J. Atmos. Sci., vol 39, no.12, p 2905 - 2915, (1982).

Chapman, S. and Lindzen, R.S., "Atmospheric Tides". D. Reidel Pub. Co., (1970).

CIRA., "COSPAR International Reference Atmosphere". Akadamie-Verlag, Berlin, (1972).

Craig, R.L. and Elford, W.G., "Observations of the quasi 2 - day wave near 90km altitude at Adelaide (35°S)". J.A.T.P., vol 43, no.10, p 1051 - 1056, (1981).

Craig, R.L., Vincent, R.A., Fraser, G.J. and Smith, M.J., "The quasi 2 - day wave in the Southern Hemisphere mesosphere". Nature, vol 287, p 319 - 320, (1980).

Crary, D.J. and Forbes, J.M., "On the Extraction of Tidal Information from Measurements Covering a Fraction of a Day". Geophys. Res. Letters, vol 10, no.7, p 580 - 582, (1983).

Ecklund, W.L. and Balsley, B.B., "Long - Term Observations of the Arctic Mesosphere with the M.S.T. Radar at Poker Flat, Alaska". J.G.R., vol 86, no.A9, p 7775 - 7780, (1981).

Elford, W.G. and Craig,R.L., "Upper atmospheric observations at Adelaide 35°S, August 1974". J.A.T.P., vol. 42, p 61 - 67, (1980).

Elford, W.G. and Murray, E.L., "Upper Atmosphere Wind Measurements in the Antarctic". International Space Research Symposium, Space Research I, Kallmann, H. ed., p 158 - 163, (1960).

Felgate, D.G., "On the point source effect in the measurement of ionospheric drifts". J.A.T.P., vol 32, p 241 - 245, (1970).

Fellous, J.L., Bernard, R., Glass, M., Massebeuf, M. and Spizzichino, A., "A study of the variations of atmospheric tides in the meteor zone". J.A.T.P., vol 37, no.12, p 1511 - 1524, (1975).

Forbes, J.M., "Atmospheric Tides 1: Model Description and Results for the Solar Diurnal Component". J.G.R., vol 87, no.A7, p 5222 - 5240, (1982a).

Forbes, J.M., "Atmospheric Tides 2: The Solar and Lunar Semidiurnal Components". J.G.R., vol 87, no.A7, p 5241 - 5252, (1982b).

Forbes, J.M., "Middle atmosphere tides". J.A.T.P., vol 46, no. 11, p 1049 - 1067, (1984).

Forbes, J.M. and Garrett, H.B., "Thermal Excitation of Atmospheric Tides due to Insolation Absorption by O_3 and H_2O". Geophys. Res. Lett., vol 5, p 1013 - 1016, (1978).

Forbes, J.M. and Garrett, H.B., "Theoretical Studies of Atmospheric Tides". Reviews of Geophysics and Space Physics, vol 17, p 1951 - 1981, (1979).

Forbes, J.M. and Gillette, D.F., Air Force Geophysics Laboratory Environmental Research Papers APGL-TR 80-0173(I), (1982).

Forbes, J.M. and Hagan, M.E., "Tides in the Joint Presence of Friction and Rotation: An f Plane Approximation". J. Geophys. Res., vol 84, p 803 - 810, (1979).

Fraser, G.J., "The Measurement of Atmospheric Winds at Altitudes of 64 - 120 km Using Ground - Based Radio Equipment". J. Atmos. Sci., vol 22, p 217 - 218, (1965).

Fraser, G.J., "Seasonal variation of southern hemisphere mid-latitude winds at altitudes of 70 - 100 km". J.A.T.P., vol 30, p 707 - 719, (1968).

Fraser, G.J., "Summer circulation in the Antarctic middle atmosphere". J.A.T.P., vol 46, no.2, p 143 - 146, (1984a).

Fraser, G.J., "Partial Reflection Spaced Antenna Wind Measurements". MAP 13, Ed. Vincent, p 233 - 247, (1984b).

Fritts, D.C., "The Nonlinear Gravity Wave - Critical Level Interaction". J. Atmos. Sci., vol 35, p 397 - 413, (1978).

Fritts, D.C., "The Excitation of Radiating Waves and Kelvin _ Helmholtz Instabilities by the Gravity Wave - Critical Level Interaction". J. Atmos. Sci., vol 36, p 12 - 23, (1979).

Fritts, D.C., "Shear Excitation of Atmospheric Gravity Waves. Part II: Nonlinear Radiation from a Free Shear Layer". J.Atmos. Sci., vol 41, no.4, p 524 - 537, (1984).

Fukao, S., Sato, T., Harper,R.M. and Kato,S., "Radio wave scattering from the tropical mesosphere observed with the Jicamarca radar". Radio Science, vol 15, no.2, p 447 - 457, (1980).

Gardner, F.F. and Pawsey, J.L., "Study of the ionospheric D - region using partial reflections". J.A.T.P., vol 3, p 321 - 344, (1953).

Geller, M.A., "Dynamics of the Middle Atmosphere". Space Sci. Rev., vol 34, p 359 - 375, (1983).

Gregory, J.B., "Reflections from Heights Below the E Region". Aust. J. Phys., vol 9, p 324 - 342, (1956).

Gregory, J.B., "Radio Wave Reflections from the Mesosphere". J.G.R., vol 33, no. 3, p 429 - 445, (1961).

Gregory, J.B. and Manson, A.H., "Seasonal variations of electron densities below 100km at mid latitudes I". J.A.T.P., vol 31, p 683 - 701, (1969a).

Gregory, J.B. and Manson, A.H., "Seasonal variations of electron densities below 100km at mid latitudes II". J.A.T.P., vol 31, p 702 - 703, (1969b).

Gregory, J.B., Meek, C.E. and Manson, A.H., "An assessment of winds data (60 - 110km) obtained in real - time from a medium frequency radar using the radio wave drifts technique". J.A.T.P., vol 44, no.8, p 649 - 655, (1982).

Gregory, J.B. and Vincent, R.A., "Structure of Partially Reflecting Regions in the Lower Ionosphere". J.G.R., vol 75, no.31, p 6387 - 6389, (1970).

Groves, G.V., "Wind Models From 60 to 130km Altitude for Different Months and Latitudes". Journal of the British Interplanetary Society, vol 22, p 285 - 307, (1969).

Groves, G.V., "The Vertical Structure of Atmospheric Oscillations Formulated by Classical Theory". Planet. Space Sci., vol 30, no 3, p 219 - 244, (1982a).

Groves, G.V., "Hough components of ozone heating". J.A.T.P., vol 44, no.2, p 111 - 121, (1982b).

Groves, G.V., "Hough components of water vapour heating". J.A.T.P., vol 44, no.3, p 281 - 290, (1982c).

Groves, G.V., "Thermospheric Energy Flux of the Semidiurnal Tide". Planet Space Sci., vol 31, no.10, p 1183 - 1186, (1983).

Harper, R.M. and Woodman, R.F., "Preliminary multiheight observations of waves and winds in the mesosphere over Jicamarca". J.A.T.P., vol. 39, p 959 - 963, (1977).

Hines, C.O. and Reddy, C.A., "On the Propagation of Atmospheric Gravity Waves through Regions of Wind Shear". J.G.R., vol 72, no. 3, p 1015 - 1034, (1967).

Hirota, I. et al., "Fifteen - Day Observation of Mesospheric and Lower Thermospheric Motions with the Aid of the Arecibo UHF Radar". J.G.R., vol 88, no.C11, p 6835 - 6842, (1983).

Hocking, W.K., "Angular and Temporal Characteristics of Partial Reflections from the D-Region of the Ionosphere". J.G.R., vol 84, no.A3, p 845 - 850, (1979).

Hocking, W.K., (unpublished), "Investigations of the movement and structure of D-region ionospheric irregularities". PhD thesis, University of Adelaide, (1981).

Hocking, W.K. and Vincent, R.A., "A comparison between HF partial reflection profiles from the D-region and simultaneous Langmuir probe electron density measurements". J.A.T.P., vol. 44, p 843 - 854, (1982a).

Hocking, W.K. and Vincent, R.A., "Comparative Observations of D region HF Partial Reflection at 2 and 6 Mhz". J.G.R., vol 87, no. A9, p 7615 - 7624, (1982b).

Hodges, R.R.Jr., "Generation of Turbulence in the Upper Atmosphere by Internal Gravity Waves". J.G.R., vol 72, no.13, p 3455 - 3458, (1967).

Hodges, R.R.Jr., "Eddy Diffusion Coefficients due to Instabilities in Internal Gravity Waves". J.G.R., vol 74, no.16, p 4087 - 4090, (1969).

Holton, J.R., "The Role of Gravity Wave Induced Drag and Diffusion in the Momentum Budget of the Mesosphere". J. Atmos. Sci., vol 39, p 791 - 799, (1982).

Holton, J.R. and Wehrbein, W.M., "A Numerical Model of the Zonal Mean Circulation of the Middle Atmosphere". Pageoph., vol 118, p 284 - 306, (1980).

Hong, S-S. and Lindzen, R.S., "Solar Semidiurnal Tide in the Thermosphere". J. Atmos. Sci., vol 33, p 135 - 153, (1976).

Hook, J.L., "Winds at the 75-110km Level at College Alaska". Planet. Space Sci., vol 18, p 1623 - 1638, (1970).

Johnson, R.M. and Luhmann, J.G., "Neutral Wind Spectra at the Auroral Zone Mesopause: Geomagnetic Effect?". J.G.R., vol 90, no A2, p 1735 - 1743, (1985).

Kato, S., Tsuda, T, and Watnabe, F., "Thermal excitation of non-migrating tides". J.A.T.P., vol 44, no.2, p 131 - 146, (1982).

Kent, G.S. and Wright, R.W.H., "Movement of ionospheric irregularities and atmospheric winds". J.A.T.P., vol 30, p 657 - 691, (1968).

Kilfoyle, B.F. and Jacka, F., "Geomagnetic L Coordinates". Nature, vol 220, p 773 - 775, (1968).

Koshelkov, Yu.P., "Proposal for a Reference Model of the Middle Atmosphere of the Southern Hemisphere". Advances in Space Research, vol 3, no.1, p 3 - 16, (1983).

Koshelkov, Yu.P., "Climatology of the middle atmosphere of the Southern hemisphere". J.A.T.P., vol 46, no. 9, p 781 - 798, (1984).

Koshelkov, Yu.P., "Observed Winds and Temperatures in the Southern Hemisphere". MAP 16, p 15 - 36, (1985).

Leovy, C., "Simple Models of Thermally Driven Mesospheric Circulation". J. Atmos. Sci., Vol 21, no.4, p 327 - 341, (1964).

Lindner, B.C., "The Nature of D-region Scattering of Vertical Incidence Radio Waves. I. Generalized Statistical Theory of Diversity Effects between Spaced Receiving Antennas". Aust. J. Phys., vol 28, p 163 - 170, (1975a).

Lindner, B.C., "The Nature of D-region Scattering of Vertical Incidence Radio Waves. II. Experimental Observations Using Spaced Antenna Reception". Aust. J. Phys., vol 28, p 171 - 184, (1975b).

Lindzen, R.S., "Thermally Driven Diurnal Tide in the Atmosphere". Q. J. Met. Soc., 93, p 18 - 42, (1967).

Lindzen, R.S., "Internal gravity waves in atmospheres with realistic dissipation and temperature, I, Mathematical development and propagation of waves into the thermosphere". Geophys. Fluid Dyn., vol 1, p 303 - 355, (1970).

Lindzen, R.S., "Effect of Daily Variations of Cumulonimbus Activity on the Atmospheric Semidiurnal Tide". Monthly Weather Review, vol 106, p 526 - 533, (1978).

Lindzen, R.S., "Turbulence and Stress Owing to Gravity Wave and Tidal Breakdown". J.G.R., vol 86, no.C10, p 9707 - 9714, (1981).

Lindzen, R.S. and Blake, D., "Mean heating of the thermosphere by tides". J. Geophys. Res., vol 75, p 6868 - 6871, (1971).

Lindzen, R.S. and Forbes, J., "Turbulence Originating From Convectively Stable Waves". J.G.R., vol 88, no.C11, p 6549 - 6553, (1983).

Lindzen, R.S. and Hong, S-S., "Effects of Mean Winds and Horizontal Temperature Gradients on Solar and Lunar Semidiurnal Tides in the Atmosphere". J. Atmos. Sci., vol 31, p 1421 - 1446, (1974).

Lysenko, I.A., Orlyansky, A.D. and Portnyagin, Yu.I., "Results of Wind Velocity Measurements at Middle and High Latitudes by the Meteor Radar Method". J. Geomag. Geoelectr, vol 31, p 411 - 418, (1979).

MacLeod, R.I. and Vincent, R.A., "Spaced antenna wind measurements in the Antarctic summer mesosphere". J.A.T.P., vol. 47, p 567 - 574, (1985).

Maehlum, B., "Small Scale Structure and Drift in the Sporadic E Layer as Observed in the Auroral Zone". Geophys. Publ. (Norway), vol 23, no 2, pp 19, (1962).

Manson, A.H. and Meek, C.E., "Gravity waves of short period (5 - 90 min) in the lower thermosphere at 52°N (Saskatoon, Canada)". J.A.T.P., vol 42, p 103 - 113, (1980).

Manson, A.H. and Meek, C.E., "Winds and Tidal Oscillations in the Upper Middle Atmosphere at Saskatoon (52°N, 107°W, L=4.3) During the Year June 1982 - May 1983". Planet. Space Sci., vol 32, no 9, p 1087 - 1099, (1984a).

Manson, A.H. and Meek, C.E., "Partial reflection D-region electron densities". MAP 13, p 113 - 123, (1984b).

Manson, A.H., Meek, C.E. and Gregory, J.B., "The Semi - Diurnal Tide at the Equinoxes: MF Radar Observations for 1978 - 1982 at Saskatoon (52°N, 107°W)". J. Atmos. Sci., vol 40, p 969 - 976, (1983).

Manson, A.H., Meek, C.E., Gregory, J.B. and Chakrabarty, D.K., "Fluctuations in tidal (24 - 12 h) characteristics and oscillations (8 h - 5 d) in the mesosphere and lower thermosphere (70 - 110 km): Saskatoon (52°N, 107°W), 1979 - 1981". Planet Space Sci., vol 30, no.12, p 1283 - 1294, (1982).

Manson, A.H. et al. (15 others), "Mean Winds of the Upper Atmosphere (60 - 110km): A Global Distribution from Radar Systems (MF, Meteor, VHF)". MAP 16, p 239 - 268, (1985).

Matsuno, T., "A Quasi One - Dimensional Model of the Middle Atmosphere Circulation Interacting with Internal Gravity Waves". Journal of the Meteorological Society of Japan, vol 60, no.1, p 215 - 226, (1982).

Miller, K.L., Bowhill, S.A., Gibbs, K.P. and Countryman, I.D., "First Measurements of Mesospheric Vertical Velocities by VHF Radar at Temperate Latitudes". Geophysical Research Letters, vol 5, no.11, p 939 - 942, (1978).

Mitra, S.N., "A Radio Method of Measuring Winds in the Ionosphere". Proc. Inst. Elec. Eng., vol 96, part III, p 441 - 446, (1949).

Murgatroyd, R.J. and Singleton, F., "Possible meridional circulations in the stratosphere and mesosphere". Quarterly Journal of the Royal Meteorological Society, vol 87, no.372, p 125 - 135, (1961).

Murphy, D.J., (unpublished), "Vertical Motions in the Mesosphere". MSc thesis, University of Adelaide, (1984).

Nastrom, G.D., Balsley, B.B. and Carter, D.A., "Mean meridional winds in the mid - and high latitude Summer mesosphere". Geophysical Research Letters, vol 9 , no.2, p 139 - 143, (1982).

Phillips, G.J. and Spencer, M., "The effects of anisometric amplitude patterns in the measurement of ionospheric drifts". Proc. Phys. Soc. London, B68, p 481 - 492, (1955).

Ratcliffe, J.A. and Weekes, K., "Physics of the Upper Atmosphere". Ed. Ratcliffe, Academic Press, (1960).

Richmond, A.D., "Energy Relations of Atmospheric Tides and Their Significance to Approximate Methods of Solution for Tides with Dissipative Forces". J. Atmos. Sci., vol 32, p 980 - 987, (1975).

Rossiter, D.E., (unpublished), "Studies of the Lower Ionosphere using a large Antenna Array". PhD thesis, University of Adelaide, (1970).

Rodgers, C.D. and Prata, A.J., "Evidence for a Travelling Two - Day Wave in the Middle Atmosphere". J.G.R., vol 86, no.c10, p 9661 - 9664, (1981).

Rottger, J., "Structure and Dynamics of the Stratosphere and Mesosphere Revealed by Radar Investigations". Pure and Applied Geophysics, vol 118, p 494 - 527, (1980).

Rottger, J., "The MST Radar Technique". MAP 13, ed. Vincent, p 187 - 232, (1984).

Salby, M.L., "The 2-Day Wave in the Middle Atmosphere: Observations and Theory". J.G.R., vol 86, no C10, p 9654 - 9660, (1981).

Salby, M.L., "Survey of Planetary-Scale Traveling Waves: The State of Theory and Observations". Rev. Geophys. Space Phys., vol 22, p 209 - 236, (1984).

Schlegel, K., Brekke, A. and Haug, A., "Some characteristics of the quiet polar D-region and mesosphere obtained with the partial reflection method". J.A.T.P., vol 40, p 205 - 213, (1978).

Schoeberl, M.R. and Strobel, D.F., "The Zonally Averaged Circulation of the Middle Atmosphere". J. Atmos. Sci., vol 35, p 577 - 591, (1978).

Sidi, C. and Tietelbaum, H., "Thin shear turbulent layers within the lower thermosphere induced by non - linear interaction between tides and gravity waves". J.A.T.P., vol 40, p 529 - 540, (1978).

Smith, M.J., "Comparisons of Winds at (44°S, 173°E), 65 - 110km, with CIRA 72". Advances in Space Research, vol 3, no.1, p 25 - 28, (1983).

Teitelbaum, H. and Cot, C., "Antisymmetric tidal modes under equinoctal conditions induced by ozone heating". J.A.T.P., vol 41, p 33 - 41, (1979).

Teitelbaum, H. and Sidi, C., "Formation of discontinuities in atmospheric gravity waves". J.A.T.P., vol 38, p 413 - 421, (1976).

Thrane, E.V. and Grandal, B., "Observations of fine scale structure in the mesosphere and lower thermosphere". J.A.T.P., vol 43, no.3, p 179 - 189, (1981).

Thrane, E.V. and Grandal, B., Fla, T. and Brekke, A., "Fine structure in the ionospheric D-region". Nature, vol. 292, p 221 - 223, (1981).

Vial, F. and Teitelbaum, H. "Some Consequences of Turbulent Dissipation on Diurnal Thermal Tide". Planet Space Sci., vol 32, no. 12, p 1559 - 1565, (1984).

Vincent, R.A., "Gravity - wave motions in the mesosphere". J.A.T.P., vol 46, no.2, p 119 - 128, (1984a).

Vincent, R.A., "MF/HF radar measurements of the dynamics of the mesosphere region - a review". J.A.T.P., vol 46, no. 11, p 961 - 974, (1984b).

Vincent, R.A., "Planetary and Gravity Waves in the Mesosphere and Lower Thermosphere". MAP 16, p 269 - 277, (1985).

Vincent, R.A. and Ball, S.M., "Mesospheric Winds at Low - and Mid - Latitudes in the Southern Hemisphere". J.G.R., vol. 86, p 9159 - 9169, (1981).

Vincent, R.A. and Belrose, J.S., "The angular distribution of radio waves partially reflected from the lower ionosphere". J.A.T.P., vol 40, p 35 - 47, (1978).

Vincent, R.A. and Stubbs, T.J., "A Study of Motions in the Winter Mesosphere Using the P.R.D. Technique". Planet and Space Science, vol 25, p 441 - 455, (1977).

Vincent, R.A., Stubbs, T.J., Pearson, P.H.O., Lloyd, K.H. and Low, C.H., "A comparison of partial reflection drifts with winds determined by rocket techniques - 1". J.A.T.P., vol 39, p 813 - 821, (1977).

Walterscheid, R.L., "Inertio-Gravity Wave Induced Accelerations of Mean Flow Having an Imposed Periodic Component: Implications for Tidal Observations in the Meteor Region". J.G.R., vol 86, no C10, p 9698 - 9706, (1981).

Walterscheid, R.L., DeVore. J.G. and Venkateswaran, S.V., "Influence of Mean Zonal Motion and Meridional Temperature Gradients on the Solar Semidiurnal Atmospheric Tide: A Revised Spectral Study with Improved Heating Rates". J. Atmos. Sci., vol 37, p 455 - 470, (1980).

Walterscheid, R.L. and Venkateswaran, S.V., "Influence of Mean Zonal Motion and Meridional Temperature Gradients on the Solar Semidiurnal Tide: A Spectral Study. Part I: Theory". J. Atmos. Sci., p 1623 - 1635, (1979).

Weinstock, J., "Theoretical Relation Between Momentum Deposition and Diffusion Coefficient Caused by Gravity Waves". Geophysical Research Letters, vol 9, no.8, p 863 - 865, (1982a).

Weinstock, J., "Nonlinear Theory of Gravity Waves: Momentum deposition, Generalized Rayleigh Friction, and Diffusion". J. Atmos. Sci., vol 39, p 1698 - 1710, (1982b).

This addendum to the Ph.D thesis "Dynamics of the Antarctic Mesosphere" by R. I. MacLeod has been included by the author to clarify the various points raised by the examiners in their assessments of this work.

Dr. G. J. Fraser has made the largest number of comments, and his report will be discussed first. The author's response will appear after the page numbers as indicated by Dr. Fraser.

Author's response to Dr. G. J. Fraser's section (a): 'Occasions of inadequate or unclear explanations'.

p.15, para. 3.

In questioning a reference by Hirota et al. (1983), which was cited in relation to the strength of flow in the southern hemisphere, Dr. Fraser is correct, the reference should be: Hirota et al., Quart. J. R. Met. Soc., 109, 443, 1983.

p.47-48, section 3.1 and p.61 bottom.

The points made by Dr. Fraser regarding partial reflection and the abrupt introduction of the random velocity (V_0) are, in the opinion of the author, quite reasonable. In the course of preparing this thesis, several different versions of chapter 3 were produced, some of which included much more detailed accounts of these topics. As the most important parts of the thesis concern the presentation of unique Antarctic wind measurements, the author tried to demonstrate only that the spaced antenna method using partial reflections was most effective for this purpose. In an attempt to keep the thesis simple and as relevent as possible, critical assessment of the methods of partial reflections was avoided.

p.62, para. 1.

The values of pattern scale calculated from Antarctic data were divided by a factor of $\sqrt{2}$ in order to compare them to results obtained by Ball (Upper Atmosphere Tides and Gravity Waves at Mid - Latitudes, Ph.D Thesis, Adelaide University, 1983). This comparison is shown in figure 3.3(a), but no explanation was provided as to why the factor was necessary. This omission will now be corrected.

Drift velocity parameters determined by Full Correlation Analysis are relatively unaffected if correlation functions are calculated from either complex data or amplitude only data. The spatial and temporal characteristics of correlation ellipses do depend on the functional form of the correlation functions as well as the mechanism for scatter. It can be shown (Bramley, E. N., 'Diversity effects in spaced - aerial reception of ionospheric waves', Proc. I.E.E., 98, Part 3, 19, 1951) that for a randomly phased signal,

$$\rho_A(\tau) = |\rho_E(\tau)|^2,$$

where $\rho_A(\tau)$ is the amplitude-modulus correlation function and $\rho_E(\tau)$ is the complex correlation function. If the temporal and spatial correlation functions have an assumed Gaussian form, $\rho_A(\tau)$ is $\sqrt{2}$ times narrower than the complex correlation function $\rho_E(\tau)$. For the purposes of comparison in this thesis, it was assumed that the received signal would be randomly phased rather than specular (for specular reflection the complex and amplitude only correlation functions would be equal) and that the factor of $\sqrt{2}$ was justified.

p.64, para. 3 and p.65, para. 1.

It is the author's opinion that the direction of elongation of ground diffraction patterns does depend on the direction of the local geomagnetic field. The deviation of the horizontal component of the geomagnetic field at Mawson during 1981 was approximately 64° (declination 64°W), and if this correction was included in the figure 3.4, the orientation of the ground diffraction patterns observed at Mawson would appear to be more like those observed at the other latitudes.

The dependence of pattern orientation on collision frequency and therefore altitude is also probable, although the evidence available here is somewhat indirect. That ground diffraction patterns are affected by increases in ionization is indicated in figure 3.5(b), which shows that the pattern scale is significantly larger during the passage of the auroral oval (see p66). Also from figure 3.4, it can be seen that the orientation of the majority of ground diffraction patterns at Mawson is close to geographic east-west in the 88-92km height range, whereas at Townsville the majority of ground diffraction patterns aligned almost north-south are found in the 94-98km height range. Whether this difference in altitude for a majority of patterns to have a particular orientation at Mawson or Townsville is significant or not cannot be determined from the results at hand.

Typical diffraction pattern parameters at Mawson are little different from those observed at Adelaide and Townsville, even though the horizontal component of the geomagnetic field is considerably smaller. If it were possible to examine the 3-dimensional structure of partially reflecting irregularities in detail at Mawson, it might provide a valuable perspective of partially reflecting irregularities in general. A VHF atmospheric sounding system, with a much higher spatial resolution than is available with the PRW system described in this thesis, could be used for such a task.

p.71, para. 3.

Prior to the implementation of incoherent averaging in the data analysis, the results from Full Correlation Analysis of individual 2 minute groups of data were examined in detail. On the whole, the largest number of rejections were found to be due to unsuitable forms of the correlation functions which resulted, and which were not statistically acceptable. Rather than modify the statistical criteria, which may have lead to results that could not easily be compared to other similar experiments, incoherent averaging was applied. The forms of correlation functions which resulted were much more amenable to the standard statistical tests. Short term wind variability was one factor which could have exacerbated the problem of correlation functions of unsuitable form.

p.77-78.

Because so little information is available, the author devoted a good deal of effort in an attempt to find correlations between geomagnetic activity and the observed wind fields, but found nothing conclusive. A chapter was prepared in which the effects of geomagnetic activity on the earth's atmosphere was discussed, but it was deleted because it achieved little more than to review the current literature on magnetospheric processes, and provided no real insight into the effects of geomagnetic activity at the mesospheric level. The author is well aware of the potential significance of a relationship between geomagnetic activity and observed wind fields at this level, but, without real proof, he felt that a discussion of possible mechanisms could have been misleading.

p 81, para. 3.

On re-reading the section in which the phrase "probably accounts" appears, the author agrees with Dr. Fraser that it is an inadequate comment. On reflection, the author would have preferred to remove the "probably" altogether.

Author's response to Dr. G. J. Fraser's section (b): 'The use of experimental uncertainties'.

Without re-writing much of chapter 4, the treatment of the results presented in this thesis cannot be altered now. However, the author acknowledges the honest and conscientious evaluation of the thesis by Dr. Fraser and will bear in mind his comments when presenting scientific results in the future.

Author's response to Dr. G. J. Fraser's section (c): 'Non-significant errors'.

Where applicable, these errors have been corrected in the text of the thesis.

Author's response to Dr. G. J. Fraser's section (d): 'Alternative conclusions from experimental results?'.

The author agrees with Dr. Fraser that the alternative conclusions are valid.

Author's response to the comments of Dr. R. G. Roper.

Dr. Roper expressed a preference for a distribution of the actual number of drift measurements, rather than the presentation of figure 3.8, which shows the diurnal variation of the height distribution of echoes as a percentage of all echoes at a particular height. The percentages indicated in figure 3.7 (for the results of normal Full Correlation Analysis) and figure 3.11 (for incoherently averaged results) were not derived in the same manner as figure 3.8. The percentages indicated in figures 3.7 and 3.11 are percentages of the total number of wind estimates. The total number of wind estimates is identically equal to the number of accepted echoes in the case of figure 3.7 (10573) and the number of results in the case of figure 3.11 (3448). The author accepts full responsibility for not making this clear.